

DECIPHERING POLYMETAMORPHISM BY GARNET GROWTH MODELLING:
AN APPLICATION TO THE AUSTRALPINE CRYSTALLINE BASEMENT EAST
OF THE TAUERN WINDOW

Inauguraldissertation

zur

Erlangung der Würde eines Doktors der Philosophie

vorgelegt der

Philosophisch-Naturwissenschaftlichen Fakultät

der Universität Basel

von

Fred Gaidies

aus Rostock (Deutschland)

Basel, 2007

Genehmigt von der Philosophisch-Naturwissenschaftlichen Fakultät auf
Antrag von

Prof. Dr. Christian de Capitani (Fakultätsverantwortlicher)

Prof. Dr. Rainer Abart (Dissertationsleiter)

Prof. Dr. Sumit Chakraborty (Korreferent)

Prof. Dr. Hans-Peter Hauri (Dekan der Fakultät)

Basel, den 22. Juni 2007

Preface

This thesis is based upon studies conducted between June 2003 and June 2007 at the Institute of Mineralogy and Petrography at Basel University. It was developed under the supervision of Rainer Abart (FU Berlin) and Christian de Capitani (Basel University) and essentially benefited from the guidance of Ralf Schuster (Austrian Geological Survey) in terms of the regional geological framework.

The thesis is divided into six chapters, four of which (Chapter 2 to 5) can be regarded as individual manuscripts:

- Chapter 1 ('Introduction') briefly presents the general background and the aim of the thesis.
- Chapter 2 ('Characterization of polymetamorphism in the Austroalpine basement east of the Tauern Window using garnet isopleth thermobarometry') focuses on the description of the method 'garnet isopleth thermobarometry' and its application to polymetamorphic garnet porphyroblasts from the Austroalpine basement. This method allows to estimate P - T conditions for the formation of pre-existing equilibrium assemblages, employing bulk-rock chemistries and garnet as the only relict mineral phase. This study is published in the *Journal of Metamorphic Geology*.
- Chapter 3 ('THERIA_G: A software program to numerically model prograde garnet growth') contains the description of the software program THERIA_G, which was developed throughout the course of the preparation of this thesis. THERIA_G extends earlier work to simulate the formation of garnet in a given volume of rock to garnet populations. Chapter 3 clearly demonstrates that the chemical composition of garnet porphyroblasts may be influenced by chemical fractionation between garnet and rock matrix during growth, intracrystalline diffusion in garnet, and the nucleation history. This study is under review in *Contributions to Mineralogy and Petrology*.

- Chapter 4 [‘Prograde garnet growth along complex P - T - t paths: Results from numerical experiments on polyphase garnet from the Wölz Complex (Austroalpine basement)’] presents an application of THERIA_G. Due to the application of THERIA_G, essential parts of the P - T - t paths of two different metamorphic events can be obtained from a single polyphase garnet porphyroblast of the Austroalpine basement. This study is under review in Contributions to Mineralogy and Petrology.
- Chapter 5 [‘Coupling garnet growth forward modelling with monazite geochronology: An application to the Rappold Complex (Austroalpine crystalline basement)’] links thermobarometrical information obtained from garnet growth modelling with microprobe monazite ages. As a result, a possible geothermal history is suggested, which indicates the complex metamorphic evolution of the Austroalpine crystalline basement. This study is to be submitted for publication in the Journal of Metamorphic Geology.
- Chapter 6 (‘Overall conclusion’) presents the main summary and conclusion of the entire thesis.

The Appendix, which contains supplementary material to all the chapters, and the enclosed CD, at which the remaining data are stored, complete the thesis.

Contribution of the co-authors

The four chapters, which can be regarded as individual manuscripts (Chapters 2 to 5), benefited from the contributions of various co-authors. In the following, these contributions are briefly described.

- Chapter 2: Gaidies, F., Abart, R., de Capitani, C., Schuster, R., Connolly, J.A.D. and Reusser, E., 2006. Characterization of polymetamorphism in the Austroalpine basement east of the Tauern Window using garnet isopleth thermobarometry. *Journal of Metamorphic Geology*, 24, 451-475.

Together with the second and fourth authors the first author did the field work and the rock sampling. He did all the sample preparation, combustion analyses, X-ray fluorescence analyses and electron probe micro-analyses. In addition, the first author investigated the petrography of all the rock samples and performed the thermodynamic calculations. He prepared the entire manuscript including the figures and tables.

The second author initiated this project and provided essential suggestions throughout the preparation of this study. He carefully reviewed a first draft of the study, which significantly improved it.

The third author gave a lot of good advice regarding the thermodynamic calculations and reviewed the manuscript.

Besides his help with the field work and the rock sampling, the fourth author provided very important discussions on the regional geological framework, contributed a first draft of the text section dealing with the geological setting and carefully reviewed the manuscript.

The fifth author gave an introduction to and some important advice on the thermodynamic modelling with the PERPLEX software. The sixth author kindly helped with some electron probe micro-analyses at ETH Zurich.

- Chapter 3: Gaidies, F., de Capitani, C. and Abart, R., 2007. THERIA_G: A software program to numerically model prograde garnet growth. Under review in *Contributions to Mineralogy and Petrology*.

The first author developed the overall concept of the numerical garnet growth model and programmed the diffusion code. Together with the second author, the first author linked the diffusion module with THERIAK – the Gibbs free energy minimisation algorithm of de Capitani and Brown (1987). The first author did the literature study and prepared the entire manuscript including all the figures and tables.

Besides the implementation of THERIA_G into the THERIAK/DOMINO software package, the second author kindly helped with FORTRAN programming and gave a lot of very important and essential advice. In addition, the second author carefully reviewed the manuscript.

The third author contributed very important suggestions to the general concept of THERIA_G and carefully reviewed the manuscript, which improved the study. Based on his numerous advices, this study strongly benefited from his general interest in and knowledge on diffusion processes.

- Chapter 4: Gaidies, F., de Capitani, C., Abart, R. and Schuster, R., 2007. Prograde garnet growth along complex P - T - t paths: Results from numerical experiments on polyphase garnet from the Wölz Complex (Austroalpine basement). Under review in *Contributions to Mineralogy and Petrology*.

The first author developed the entire concept of this study and performed all the garnet growth calculations. He prepared the manuscript including the figures and tables.

The second and the third authors gave a lot of very important advice and carefully reviewed the manuscript. The fourth author provided important information on the regional geological background and reviewed a first draft of the study.

- Chapter 5: Gaidies, F., Krenn, E., de Capitani, C., and Abart, R. Coupling garnet growth forward modelling with monazite geochronology: An application to the Rappold Complex (Austroalpine crystalline basement). To be submitted for publication in the *Journal of Metamorphic Geology*.

The first author developed the basic concept of this study, did all the garnet growth calculations and wrote the entire manuscript. Together with the second author, the first author performed the chemical analyses of the accessory minerals and the geochronological investigations of monazite.

The second author contributed a first draft of the text sections dealing with monazite dating as well as with monazite and allanite chemical composition. He gave a lot of very important advice.

The third and fourth authors provided essential discussions and carefully reviewed the manuscript.

Acknowledgements

This study benefited from the contribution of many different people. I am indebted to all of them for helping and encouraging me throughout the preparation of this thesis.

First of all, I would like to thank Rainer Abart, who initiated this study. Dear Rainer, it has to be said that you are an expert in creating a highly stimulating and motivating atmosphere for scientific research. This is at least what I have experienced during the entire project and which helped me getting into this – for me almost completely new – topic. Your profound knowledge on and strong enthusiasm in understanding geo-relevant processes was highly inspiring. I enjoyed the various days when I was in Berlin and was quartered at your home. Thank you for your friendliness and the entertaining evenings together with Elli and Lore. You were a great help: Thank you for all of this!

I would like to express my gratitude to Christian de Capitani for all the sleepless nights he had in order to prepare another new computer code for our THERIA_G software. Capi, this software program would definitely not exist without your help. I would like to thank you for giving me the opportunity to implement my diffusion algorithm into your THERIAK/DOMINO software and for the guidance in FORTRAN programming. I thank you for all the discussions on this and other topics. Thank you Capi.

Ralf Schuster accompanied me during my field work in the Eastern Alps, introduced me into the regional geology and guided me to the sample locations. Since these rock samples as well as Ralfs knowledge on the tectono-metamorphic evolution of the Austroalpine basement were crucial for the preparation of this thesis, I am greatly indebted to Ralf. Furthermore, during several stays in Vienna I was accommodated at his place and would like to express my thanks for this again.

Erwin Krenn provided the monazite measurements of the Chapter on garnet growth in the Rappold Complex (Chapter 5 of this thesis) and gave a lot of very good advise during the preparation of this part of the thesis. Thank you Erwin for this essential part of my dissertation

and thank you for the time in Salzburg.

James Connolly helped me in getting into his PERPLEX program in the first study of my thesis. Eric Reusser was helpful in performing X-ray maps and compositional profiles with the microprobe at ETH Zurich, which was of utmost importance for this thesis. Jamie and Eric, I thank you for this.

Willi Tschudin played a major role for the preparation of my thesis. Willi prepared almost uncountable numbers of serial thin-sections for all of my rock samples, which were always of the highest quality. These serial sections were needed to intersect the oldest cores of garnet in my rock samples.

Ralf Milke is thanked for numerous discussions on the kinetics of diffusion and his help with microprobe measurements at FU Berlin.

This thesis benefited from discussions with Tjerk Heijboer at any stage of this project.

For the development of the diffusion model advises from Lukas Keller, Martin Grote, Dani Schmid, and Ralf Dohmen were of significant importance.

Dough Tinkham and Armin Zeh are thanked for their reviews of the garnet isopleth thermobarometry chapter.

Discussions with Holger Stünitz and Stefan Schmid on various topics of this thesis are gratefully acknowledged.

I thank Bernadette Oberlein, Susanne Tobler, Joelle Glanzmann and Verena Scheuring for administrative support and I am indebted to Heinz Hürlimann and Claude Schneider for their help with technical issues. Koni Leu is thanked for computer support.

I would like to thank my colleagues at the department of Basel University for their contribution to this thesis.

Finally, I would like to thank my family for encouragement and support in so many ways to the accomplishment of this thesis.

Elli, mein grösster Dank gebührt dir: Du hast mich die ganzen vier Jahre in der Anfertigung dieser Arbeit unterstützt und mir den zeitlichen Rahmen dafür ermöglicht, du hast mich inspiriert und mir die Kraft gegeben, diese Arbeit zu einem erfolgreichen Abschluss zu bringen. Dafür und für deine Liebe und Geduld möchte ich mich ganz besonders bedanken.

Contents

Preface	iii
Acknowledgements	vii
1 Introduction	1
1.1 General background	1
1.2 Aim of the thesis	3
2 Garnet isopleth thermobarometry	5
2.1 Abstract	5
2.2 Introduction	6
2.3 Geological setting	9
2.4 Methods	13
2.4.1 Sample preparation and EPMA	13
2.4.2 Combustion analyses and WDXRFA	14
2.4.3 Garnet isopleth thermobarometry	14
2.4.4 Calculation of the thermodynamic relevant bulk composition	17
2.5 Sample description	20
2.5.1 Metapelite with polyphase garnet porphyroblasts from the Wölz Complex (sample 12F03)	21
2.5.2 Metapelite with garnet porphyroblasts with only a single growth zone from the Wölz Complex (sample 29F03B)	21
2.5.3 Metapelite with polyphase garnet porphyroblasts from the Rappold Com- plex (sample 35F03)	22
2.6 Results	25

2.6.1	Garnet chemistry	25
2.6.2	Whole-rock chemistry	29
2.6.3	P - T estimates	29
2.7	Discussion	34
2.7.1	P - T estimates for incipient garnet growth	34
2.7.2	Chemical zoning of garnet and estimated P - T paths for progressive garnet growth	39
2.7.3	The influence of Ti-biotite and the composition of the fluid	45
2.7.4	Limitations of garnet isopleth thermobarometry	46
2.8	Conclusions	48
2.9	Acknowledgements	48
3	THERIA_G I: The description	51
3.1	Abstract	51
3.2	Introduction	52
3.3	Simulation of garnet growth	53
3.3.1	Modelling of garnet fractionation	55
3.3.2	Modelling of intracrystalline diffusion	56
3.3.3	Consideration of garnet growth kinetics	60
3.4	Application of THERIA_G	61
3.4.1	Garnet growth along P - T loop A	64
3.4.2	Garnet growth along P - T loop B	68
3.5	Discussion	74
3.6	Conclusions	76
3.7	Acknowledgements	77
4	THERIA_G II: Application to the Austroalpine basement	79
4.1	Abstract	79
4.2	Introduction	80
4.3	Geological background	82
4.3.1	Petrological and geochronological constraints on the geothermal history of the Wölz Complex	83
4.4	Methods	85
4.4.1	Sample preparation, EPMA, combustion analysis, and WDXRFA	85

4.4.2	Numerical modelling of prograde garnet growth	87
4.5	Sample description	88
4.5.1	Petrography	88
4.5.2	Garnet chemistry	89
4.6	Results	89
4.6.1	The original garnet growth zoning	92
4.6.2	Influence of intragranular diffusion on garnet growth zoning	96
4.7	Discussion	99
4.7.1	<i>P-T-t</i> evolution of rock sample 12F03 obtained from garnet growth simulation	101
4.7.2	Limitations of garnet growth simulation	104
4.8	Conclusions	105
4.9	Acknowledgements	106
5	Garnet growth in the Rappold Complex	107
5.1	Introduction	107
5.2	Geological background	109
5.3	Methods	111
5.3.1	Sample preparation, EPMA, and WDXRFA	111
5.3.2	Garnet growth modelling	114
5.3.3	Monazite dating by means of electron-probe micro-analysis	115
5.4	Sample description	116
5.4.1	Petrography	116
5.4.2	Monazite abundance, morphology, and chemical composition	117
5.4.3	Allanite abundance, morphology, and chemical composition	119
5.4.4	Garnet chemistry	121
5.5	Results	124
5.5.1	<i>P-T</i> path of metamorphism	124
5.5.2	Th-U-Pb microprobe ages of monazite	132
5.6	Interpretation and Discussion	134
5.7	Conclusions	139
5.8	Acknowledgements	140
6	Overall conclusions	141

A	Appendix to Chapter 2	143
A.1	EPMA dataset and bulk-rock compositions	143
B	Appendix to Chapter 3	147
B.1	Solution model of Chlorite	147
B.2	Full formalism of the discretized diffusion equation	148
B.2.1	MATLAB [®] -source code for the multi-component diffusion module imple- mented in THERIA_G	153
C	Appendix to Chapter 4	165
C.1	<i>P-T-t</i> paths used for garnet growth simulation	165
	Bibliography	180

Chapter 1

Introduction

1.1 General background

Since the early eighties it has been known that the Austroalpine crystalline basement experienced a polymetamorphic geothermal history (Frank et al., 1982). Thereafter, geochronological investigations on polyphase garnet porphyroblasts by Schuster and Thöni (1996) and Schuster et al. (2001) were performed, revealing that – besides Variscan metamorphism in the Carboniferous (Tollmann, 1977) and Eo-Alpine metamorphism in the Cretaceous (see compilation in Hoinkes et al., 1999) – at least some parts of the Austroalpine basement underwent metamorphism during the Permian as well. However, due to intense overprint of Permian mineral assemblages in the course of metamorphism in the Cretaceous and because of the high number of mineral inclusions in garnet, conventional geothermobarometrical and geochronological methods did not succeed to derive the regional extent of Permian metamorphism.

First estimates for the pressure and temperature (P - T) conditions during Permian metamorphism in the Austroalpine basement were presented by Habler and Thöni (2001) and Schuster et al. (2001) ranging between 570 and 710°C at < 4 kbar. Schuster et al. (2001) argued for lithospheric thinning (Oxburgh, 1992) and magmatic underplating during the Permian to account for the increased geothermal gradient of the high-temperature/low-pressure (HT/LP) metamorphic event. Their model is compatible with the numerous indications of enhanced magmatic activity during the Permian in the Austroalpine basement (e.g. Miller and Thöni, 1997; Thöni and Miller, 2000).

For the reconstruction of the pre-Eo-Alpine metamorphic evolution of the Austroalpine crystalline basement, the chemical zoning patterns of garnet porphyroblasts play a major role. Frequently, the garnet porphyroblasts are the only relics of the polymetamorphic history in the Austroalpine realm. Due to the comparatively slow rates of cation diffusion in garnet at low to medium grade metamorphic conditions (e.g. Loomis, 1982; Chakraborty and Ganguly, 1992; Vielzeuf et al., 2007), the compositional zoning of the garnet porphyroblasts, which reflects parts of the P - T - t evolution of the garnet-bearing rock sample, is preserved in samples from the Austroalpine basement. Therefore, the compositional zoning in garnet may be used for P - T - t path reconstruction.

Estimates for the P - T conditions that prevailed during the incipient stages of garnet formation may be obtained from garnet isopleth thermobarometry (e.g. Vance and Mahar, 1998; Evans, 2004). In order to determine thermobarometrical information on the entire garnet growth history, numerical models may be applied, which simulate the influence of changing P - T conditions on garnet composition during growth (e.g. Cygan and Lasaga, 1982; Spear et al., 1991a).

However, in both cases, the application of garnet isopleth thermobarometry and the numerical simulation of prograde garnet growth, thermodynamic equilibrium has to be established between the rim of garnet and the rock matrix during garnet growth. Only in such a case, the composition of successive garnet growth zones is solely controlled by the P - T conditions as well as fluid composition for any given thermodynamically relevant bulk rock composition.

Garnet growth in previously unmetamorphosed hydrous rocks or in rocks that have only experienced low-grade metamorphism generally occurs by dehydration reactions. During dehydration, an aqueous fluid is likely to be present in excess and, hence, reaction kinetics and material transport are expected to be fast. In such cases, chemical equilibrium is established rapidly and equilibrium domains may develop in the hand specimen or even on a larger scale (Carlson, 1989, 2002; Dohmen and Chakraborty, 2003).

The determination of P - T - t paths from the chemical composition of garnet that grew in a dehydrated rock is considered problematic, because dehydration strongly influences the efficiency of intergranular material transport (Keller et al., 2006). If transport of material is sluggish compared to the rate of interface reactions, the rate of garnet growth may be controlled by intergranular diffusion and, as a consequence, gradients in the chemical potentials of the reacting species evolve and progressively enlarge in the vicinity of the growing garnet (Carlson, 1989; Spear and Daniel, 2001). In such cases, the size of equilibration domains may be so small that a single garnet porphyroblast pertains to different equilibration domains.

In addition, the reconstruction of geothermal histories from the chemical zoning of garnet may be hindered by resorption of garnet during stages of garnet instability. Resorption may significantly modify garnet morphology and composition and may alter the chemical composition of the thermodynamically relevant bulk rock system.

If parts of the P - T path of a garnet-bearing rock are obtained from the investigation of garnet compositional zoning and are linked with garnet age determinations, this may allow to relate metamorphic events in the earth history to their P - T - t trajectories. If intracrystalline diffusion in garnet is taken into consideration, this even may allow to constrain the timing of a specific metamorphic event.

1.2 Aim of the thesis

This thesis was primarily intended to overcome the unsatisfactory situation, that conventional thermobarometry and geochronology could not be used to explore the regional extent of pre-Eo-Alpine metamorphism in the Austroalpine crystalline basement.

In a first study, Faryad and Hoinkes (2003) qualitatively demonstrated a consistent relationship between the core chemistry of garnet from pre-Eo-Alpine metamorphic assemblages, bulk rock composition and metamorphic history of rock samples from different Austroalpine units. Motivated by the study of Faryad and Hoinkes (2003), the idea arose to develop and apply a method, which indirectly discriminates between the different pre-Eo-Alpine metamorphic events based on their geothermal history. In that respect, the prime focus was on garnet, which frequently occurs in several generations forming the only relic of pre-existing metamorphic mineral assemblages.

With the application of the well-founded concepts of equilibrium thermodynamics in complex chemical systems and detailed petrographic and geochemical investigations of garnet-bearing metapelites from the Austroalpine crystalline basement, a widely applicable method should be derived to unravel at least some parts of the polymetamorphic geothermal history of the Eastern Alps.

Chapter 2

Characterization of polymetamorphism in the Austroalpine basement east of the Tauern Window using garnet isopleth thermobarometry

This chapter is published as: **Gaidies, F.**, Abart, R., de Capitani, C., Schuster, R., Connolly, J.A.D. and Reusser, E., 2006. Characterization of polymetamorphism in the Austroalpine basement east of the Tauern Window using garnet isopleth thermobarometry. *Journal of Metamorphic Geology*, **24**, 451-475.

2.1 Abstract

Garnet in metapelites from the Wölz and Rappold Complexes of the Austroalpine basement east of the Tauern Window typically shows two distinct growth zones. A first garnet generation usually forms the cores of garnet porphyroblasts and is separated by a prominent microstructural and chemical discontinuity from a second garnet generation, which forms rims of variable width. Whereas the rims were formed during the Eo-Alpine metamorphic overprint, the garnet cores

represent remnants of at least two pre-Eo-Alpine metamorphic events. The pressure and temperature estimates obtained from garnet isopleth thermobarometry applied to the first growth increments of the pre-Eo-Alpine garnet cores from the Wölz and Rappold Complexes cluster into two distinct domains: (i) in the Wölz Complex, incipient growth of the first-generation garnet occurred at 4 ± 0.5 kbar and $535 \pm 20^\circ\text{C}$, (ii) in the Rappold Complex, incipient growth of the oldest garnet cores took place at 5.3 ± 0.3 kbar and $525 \pm 15^\circ\text{C}$. The Eo-Alpine garnet generation started to grow at 6.5 ± 0.5 kbar and $540 \pm 10^\circ\text{C}$. According to radiometric dating, the low-pressure garnet from the Wölz Complex was formed during a Permian metamorphic event. The first-generation garnet of the Rappold Complex is probably of Variscan age.

2.2 Introduction

The determination of pressure–temperature–time (P – T – t) paths from metamorphic mineral parageneses is an important tool in unravelling the development of orogenic belts (Spear, 1993). Garnet isopleth thermobarometry has been applied to derive P – T estimates from monometamorphic (e.g. Menard and Spear, 1993; Vance and Mahar, 1998; Stowell et al., 2001; Zeh, 2001; Zeh and Holness, 2003; Evans, 2004; Kim and Bell, 2005) and polymetamorphic (e.g. Zeh et al., 2004) rocks.

A prerequisite for the application of garnet isopleth thermobarometry is that thermodynamic equilibrium is maintained between the rim of the garnet and the rock matrix during garnet growth. In this case, the composition of successive garnet growth zones is solely determined by the P – T conditions as well as fluid composition for any given thermodynamically relevant bulk composition. The latter is defined as the volume domain in a rock, over which equilibrium is maintained during garnet growth. Garnet growth in previously unmetamorphosed hydrous rocks or in rocks that have only experienced low-grade metamorphism generally occurs by dehydration reactions. During dehydration, an aqueous fluid is likely to be present in excess and, hence, reaction kinetics and material transport are expected to be fast. In such cases, chemical equilibrium is established rapidly and equilibrium domains may develop in the hand specimen or even on a larger scale (Carlson, 1989, 2002; Dohmen and Chakraborty, 2003). However, rocks that consist of prominent compositional banding may indicate the juxtaposition of different equilibrium domains, which has to be considered if the composition of the thermodynamically relevant bulk composition is to be determined.

Thermodynamic equilibrium between garnet and the rock matrix may be assumed, if garnet

isopleth thermobarometry is applied to the incipient stages of garnet growth, i.e. if only the composition of garnet cores of the oldest garnet generation present in a rock is used. In this case, equilibrium-phase relations that are calculated by free-energy minimization for a system with specified bulk composition (e.g. de Capitani and Brown, 1987; Powell and Holland, 1993; Connolly and Petrini, 2002) and an internally consistent thermodynamic database (e.g. Berman, 1988; Gottschalk, 1997; Holland and Powell, 1998) can be used as theoretical predictions of the equilibrium assemblages that would develop if the corresponding rock maintained equilibrium and the bulk composition is appropriate. The P - T conditions that prevailed during the initial stages of garnet growth can then be derived from comparison of the observed garnet compositions and the equilibrium assemblage diagrams, including contours for garnet composition, calculated for the appropriate bulk-rock composition.

A second prerequisite for the application of garnet isopleth thermobarometry is that the original growth zoning of garnet is preserved in its original state, i.e. that modification of the original chemical zoning pattern by intracrystalline diffusion is negligible. This is a reasonable assumption as long as amphibolite facies conditions are not surpassed, because of the exceedingly slow rates of cation diffusion in garnet (Chakraborty and Ganguly, 1992). Hence, for a persuasive modification of the original chemical pattern at low to moderate temperatures to occur, garnet has to be exposed to these temperatures for extraordinary long durations. In contrast, only the short-term exposure of garnet to temperatures exceeding amphibolite facies conditions prevents them from effective modification of the original zoning pattern. There is general agreement on the presumption that the chemical zoning patterns of garnet porphyroblasts provide reliable records of the P - T evolution up to upper amphibolite facies conditions (e.g. Ayres and Vance, 1997). However, Stowell et al. (1996) demonstrated that in addition to intracrystalline diffusion other processes such as Ca-metasomatism might affect the original growth zoning of garnet.

As a result of the considerably slow intracrystalline diffusion in garnet at low to moderate temperatures, the components which are incorporated into garnet during growth, are effectively removed from the rock matrix (e.g. Vance and Mahar, 1998; Evans, 2004). In general, certain components such as Mn or Fe are preferentially fractionated into garnet. This leads to a successive depletion of these components in the rock matrix and may change the effective bulk-rock composition during garnet growth. This effect is particularly pronounced if the modal amount of newly formed garnet is high. The fractionation effect must be accounted for, if garnet isopleth thermobarometry is used to reconstruct P - T paths from the compositions of successive garnet growth increments. The progressive modification of the thermodynamically relevant bulk-rock

Table 2.1 – Sample locations and GPS coordinates.

Sample	Coordinates ^a		Altitude (m)	Unit
	E	N		
10F03	014°13'15"	47°19'16"	2030	Wölz
11F03	014°13'20"	47°19'20"	2060	Wölz
12F03	014°13'20"	47°19'20"	2060	Wölz
16F03	014°13'00"	47°19'08"	1950	Wölz
28F03	014°15'44"	47°18'39"	2010	Wölz
29F03A+B	014°15'48"	47°18'49"	2020	Wölz
32F03	014°15'52"	47°19'03"	2230	Wölz
37F03	014°24'28"	47°23'17"	2060	Wölz
39F03	014°24'11"	47°23'24"	2040	Wölz
40F03-1	014°24'11"	47°23'25"	2060	Wölz
40F03-2	014°24'11"	47°23'25"	2060	Wölz
41F03	014°24'03"	47°23'29"	2090	Wölz
42F03	014°24'02"	47°23'29"	2100	Wölz
43F03	014°24'02"	47°23'29"	2100	Wölz
44F03	014°23'54"	47°23'33"	2130	Wölz
19F03	014°12'46"	47°18'53"	1790	Rappold
24F03	014°12'46"	47°18'42"	1825	Rappold
31F03	014°15'49"	47°19'00"	2170	Rappold
33F03	014°15'52"	47°19'06"	2265	Rappold
35F03	014°15'46"	47°19'15"	2170	Rappold

^a World Geodetic System 84 (WGS84).

composition during garnet growth may be estimated from a Rayleigh fractionation model (Hollister, 1966; Atherton, 1968; Evans, 2004).

In this study, we present an application of garnet isopleth thermobarometry to polymetamorphic garnet porphyroblasts of metapelites from the Wölz and Rappold Complexes of the Austroalpine crystalline basement east of the Tauern Window (Niedere Tauern, Eastern Alps) (Table 2.1). It will be demonstrated that the application of garnet isopleth thermobarometry allows P – T estimates to be determined for incipient garnet growth of the oldest metamorphic garnet generations preserved, employing bulk-rock chemistries and garnet as the only relic of the preexisting mineral parageneses. Furthermore, it will be shown that the integration of garnet isopleth thermobarometry with the Rayleigh fractionation model of Evans (2004) enables

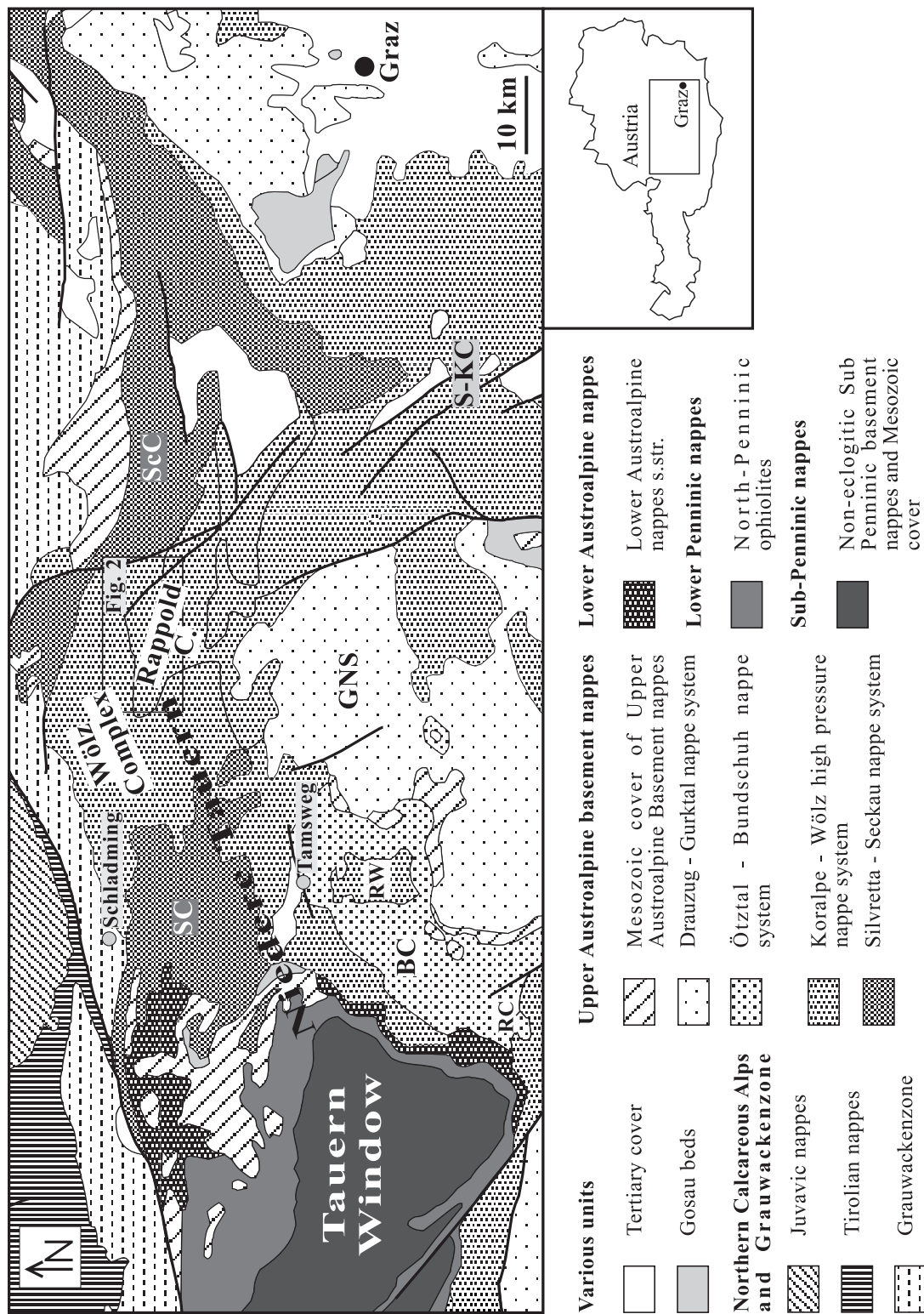
detailed P - T paths to be predicted for garnet growth in the course of different orogenic cycles. The results obtained help to discriminate between distinctive metamorphic events and, hence, provide insights into the polymetamorphic evolution in the Eastern Alps.

2.3 Geological setting

The Eastern Alps form a 500-km-long east–west-trending fold and thrust belt. They developed in the course of two distinct continent–continent collision events during the Cretaceous and Tertiary (Froitzheim et al., 1996). According to Schmid et al. (2004), three major plate-tectonic units can be distinguished in the Eastern Alps: the Helvetic realm and the sub-Penninic nappes are considered to represent one major unit which corresponds to the former southern European margin. The Penninic nappes represent the Jurassic and Cretaceous oceanic crust and microcontinents, and the Austroalpine nappes represent the frontal part of the Apulian continental microplate. In the Cretaceous, the Apulian microplate experienced internal deformation because of a WNW–ESE-directed intracontinental collision event, which is referred to as the Eo-Alpine event. Cretaceous tectonics led to the formation of large décollement nappes in the uppermost crustal levels and substantial shortening and subduction in the deeper basement units. The northern and tectonically deeper units of the Austroalpine basement belong to the lower plate of the Cretaceous intracontinental subduction event and experienced metamorphism ranging from greenschist to eclogite facies conditions at c. 90 Ma (Thöni, 2002).

Conversely, the tectonically higher units in the southern part of the Austroalpine basement units pertain to the upper plate of the Cretaceous intracontinental subduction event. In general, they experienced metamorphic imprints during the Eo-Alpine collision event ranging from greenschist facies conditions at the base to anchizone to diagenetic conditions in the uppermost parts (Schuster et al., 2004). The Penninic nappes and the Austroalpine nappe pile overrode the former southern European margin in the course of the closure of the Penninic Ocean during the Tertiary.

The Austroalpine basement units in the Niedere Tauern (Fig. 2.1), which were part of the tectonic lower plate during Cretaceous orogeny, are primarily composed of paragneisses and metapelites with subordinate intercalations of amphibolites, quartzites, calcsilicate rocks and marbles. Because of widespread greenschist to amphibolite facies metamorphic overprint during the Eo-Alpine metamorphic event, low- to medium-grade parageneses of pre-Cretaceous age have largely been obliterated (e.g. Schuster and Thöni, 1996; Schuster and Frank, 1999; Schuster



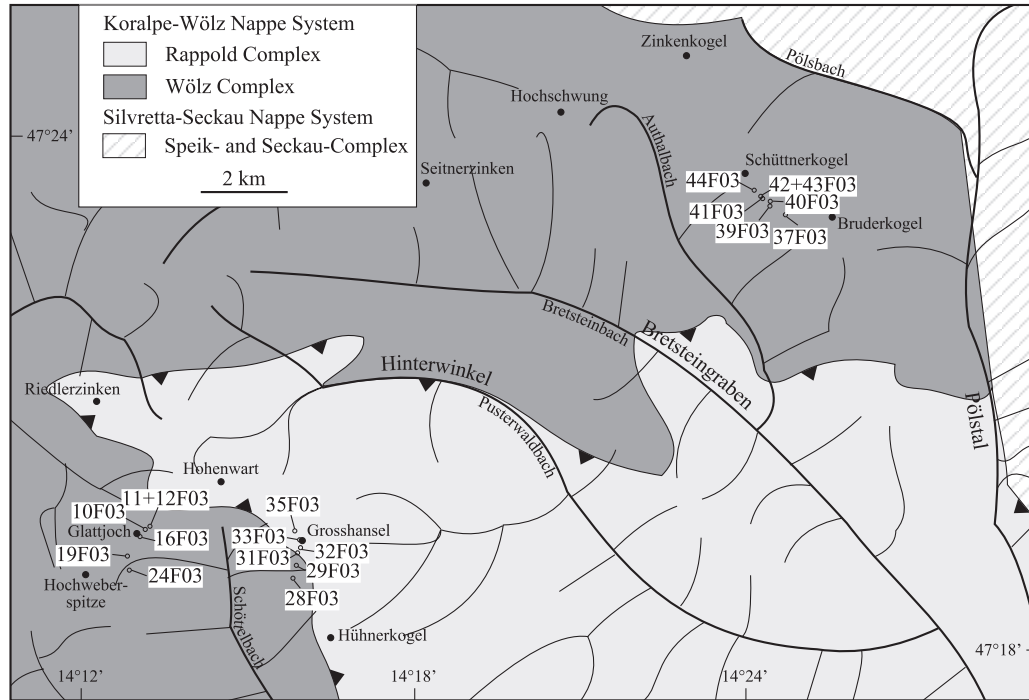


Figure 2.2 – Tectonic map of the study area showing sample locations.

et al., 2001, 2004). The investigation of metamorphic assemblages from those parts of the Austroalpine realm which were less intensely affected during the Cretaceous yielded conditions ranging between 570 and 710°C at < 4 kbar during the Permo-Triassic (e.g. Habler and Thöni, 2001; Schuster et al., 2001).

The Wölz and the tectonically overlying Rappold Complex are prominent lithostratigraphic units in the Niedere Tauern (Figs 2.1 and 2.2). Both complexes are separated from one another by a Cretaceous thrust fault and belong to the Upper Austroalpine basement nappes (Schmid et al., 2004; Schuster et al., 2004). Garnet porphyroblasts with two distinct growth zones in metapelites of the Wölz and Rappold Complexes demonstrate the polymetamorphic history of both units (e.g. Schuster and Thöni, 1996; Bernhard and Hoinkes, 1999; Schuster and Frank, 1999; Schuster et al., 2001; Faryad and Hoinkes, 2003). Based on the microstructural relationship to the main schistosity and on radiometric age determinations it is inferred that the second garnet generation, which commonly constitutes rims enclosing the first-generation garnet, grew synchronously to the formation of the Eo-Alpine foliation (Abart and Martinelli, 1991; Schuster and Frank, 1999) at 550–600°C and 10–12 kbar (e.g. Hoinkes et al., 1999; Schuster and Frank,

Table 2.2 – Garnet core chemistry of samples from the Wölz and Rappold Complex.

Sample	Wölz Complex		Rappold C.
	12F03	29F03	35F03
SiO ₂	37.47	37.59	37.09
TiO ₂	0.05	0.16	0.06
Al ₂ O ₃	21.45	20.32	20.10
FeO	33.83	30.43	33.60
MnO	5.85	3.30	3.67
MgO	1.57	0.97	1.28
CaO	1.59	7.98	4.70
Total	101.81	100.75	100.50
Oxygen	12	12	12
Si	3.00	3.01	3.00
Ti	0.00	0.01	0.00
Al	2.02	1.92	1.92
Fe ³⁺	0.00	0.04	0.08
Fe ²⁺	2.26	2.00	2.19
Mn	0.40	0.22	0.25
Mg	0.19	0.12	0.15
Ca	0.14	0.69	0.41
Fe/(Fe+Mg)	0.92	0.95	0.93
Mg/(Fe+Mg)	0.08	0.06	0.07
X _{alm}	0.76	0.66	0.73
X _{prp}	0.06	0.04	0.05
X _{grs}	0.05	0.23	0.14
X _{sps}	0.13	0.07	0.08

1999; Faryad and Hoinkes, 2003).

In contrast, data on the formation conditions and ages are scarce for the first-generation garnet that forms the core of the garnet porphyroblasts. A garnet core from the Wölz Complex, which was dated to 269 ± 4 Ma using the Sm-Nd garnet–whole-rock method (Schuster and Thöni, 1996; Schuster and Frank, 1999; Thöni, 2002), suggests the formation of the first-generation garnet during Permian times. As the first-generation garnet is the only remnant of Permian metamorphic assemblages in the Wölz Complex and in many cases, quartz and ilmenite are the only mineral inclusions in that garnet, detailed information about the P – T conditions during Permian metamorphism in the Wölz Complex are not known (e.g. Schuster and Frank, 1999; Faryad and Hoinkes, 2003).

From thermobarometry applied to inclusions of biotite, muscovite, plagioclase, quartz, ilmenite and rutile in first-generation garnet of a metapelite from the Rappold Complex, Faryad and Hoinkes (2003) derived P - T conditions of $540 \pm 15^\circ\text{C}$ and 6.6 ± 0.8 kbar. The age of this pre-Eo-Alpine metamorphic event in the Rappold Complex is yet unknown. However, Sm-Nd garnet-whole-rock age determinations of garnet in metapegmatites of the Rappold Complex yielded 262 ± 2 Ma and 288 ± 4 Ma (Schuster and Thöni, 1996; Schuster et al., 2001), indicating an enhanced geothermal gradient during the Permian in the Rappold Complex.

2.4 Methods

2.4.1 Sample preparation and EPMA

To get an insight into the three-dimensional geometrical relationships among garnet porphyroblasts, serial sections with a spacing of 0.6–0.8 mm were made from a representative sample domain of approximately 1 x 2 x 3 cm size of each rock sample. Cross-sections that contain garnet cores were located by selecting the three thin sections with the largest diameters of a single garnet porphyroblast. From these three thin sections, the one which yielded the highest content of X_{sps} [$\text{Mn}/(\text{Fe}^{2+} + \text{Ca} + \text{Mg} + \text{Mn})$] in the central portion of the garnet cross-section, was considered to reflect the entire growth history including the incipient stages of garnet growth.

Electron probe micro-analysis (EPMA) was performed using a JEOL JXA-8600 at the Mineralogical and Petrographical Institute at the University of Basel and with JEOL JXA-8200 at ETH Zurich. The accelerating voltage was 15 kV for a beam current of 10 and 20 nA, respectively. Matrix corrections were performed with a PhiRhoZ routine. The garnet compositions were measured along two profiles that are perpendicular to each other for each of the three selected sections. Furthermore, concentration contour maps were obtained for Ca, Fe, Mg and Mn from calibrated X-ray maps and are shown in Figs 2.5, 2.7 and 2.9. The X_{grs} [$\text{Ca}/(\text{Fe}^{2+} + \text{Ca} + \text{Mg} + \text{Mn})$] and X_{prp} [$\text{Mg}/(\text{Fe}^{2+} + \text{Ca} + \text{Mg} + \text{Mn})$] contents are generally rather constant in the garnet core regions so that the spacing of isopleths is rather wide in these parts of the garnet. Compositional data for the incipient growth increments of three different garnet types are given in Table 2.2. The complete electron probe micro-analysis data set is provided in Appendix A.

Table 2.3 – Representative bulk-rock geochemical data of samples from the Wölz and Rappold Complex (wt%) (average pelite from Symmes and Ferry (1991)).

Sample	Wölz Complex		Rappold C.	Average
	12F03	29F03	35F03	pelite
SiO ₂	57.51	64.04	48.02	59.77
TiO ₂	1.19	0.83	0.97	
Al ₂ O ₃	20.98	18.02	26.21	16.57
Fe ₂ O ₃	9.48	7.70	10.52	6.53
MnO	0.11	0.10	0.06	0.07
MgO	2.28	2.10	2.61	2.62
CaO	0.46	0.52	0.36	2.17
Na ₂ O	1.23	1.06	0.64	1.73
K ₂ O	3.73	3.43	5.84	3.53
H ₂ O	2.75	2.68	3.21	2.49
CO ₂	0.44	0.34	0.60	5.16
Total	100.16	100.82	99.04	100.64

2.4.2 Combustion analyses and WDXRFA

Samples of ~ 1 kg, which were devoid of alteration and macroscopically detectable compositional heterogeneity, were carefully chosen. From these rock volumes, blocks of approximately $1 \times 2 \times 3$ cm in size were extracted for EPMA, and the rest was crushed and ground to a fine powder for combustion analysis using a LECO combustion analyser and to prepare glass pellets for bulk chemical analysis. The major element compositions were obtained by wavelength-dispersive X-ray fluorescence analysis (WDXRFA) using Bruker AXS SRS-3400. Both combustion analysis and WDXRFA were performed at the Mineralogical and Petrographical Institute at University of Basel. Representative whole-rock chemistries of three samples are shown in Table 2.3. The complete data set is provided in Appendix A.

2.4.3 Garnet isopleth thermobarometry

Rock-specific equilibrium assemblage diagrams were calculated in the simplified model system MnO-Na₂O-CaO-K₂O-FeO-MgO-Al₂O₃-SiO₂-H₂O-TiO₂ (MnNCFMASHT). This choice of components ensures that most of the common rock-forming minerals in metapelites can be considered. TiO₂ was chosen as a system component to consider ilmenite. Ilmenite is ubiquitous in metapelites from the Wölz and Rappold Complexes. It may contain significant quantities of manganese and may thus have a strong influence on the low-temperature stability limit of garnet (e.g. Symmes and Ferry, 1991; Mahar et al., 1997). Thermodynamic calculations were performed

using the PERPLEX software (Connolly, 1990; Connolly and Petrini, 2002), adopting a gridded Gibbs free-energy minimization approach (Connolly, 2005), and the internally consistent and updated thermodynamic data set of Holland and Powell (1998) (thermodynamic database of THERMOCALC, version 3.21). The results obtained for three representative samples are presented in that study. Supplementary material, which covers the entire set of P - T phase diagram sections obtained for all the samples studied, is provided in Appendix A.

The following notations, compositions (w, x, y and z are fractions varying between zero and unity and are determined as a function of pressure and temperature by free-energy minimization), and solution models have been employed: Grt [garnet, $\text{Fe}_{3x}\text{Ca}_{3y}\text{Mg}_{3z}\text{Mn}_{3(1-x-y-z)}\text{Al}_2\text{Si}_3\text{O}_{12}$; Holland and Powell (1998)], Chl [chlorite, $(\text{Mg}_x\text{Fe}_w\text{Mn}_{1-x-w})_{5-y+z}\text{Al}_2(1+y-z)\text{Si}_{3-y+z}\text{O}_{10}(\text{OH})_8$; Holland et al. (1998)], AbPl [albite-rich side of the plagioclase solvus, $\text{Na}_x\text{Ca}_{1-x}\text{Al}_{2-x}\text{Si}_{2+x}\text{O}_8$, $x > 1/3$; Newton et al. (1980)], AnPl [anorthite-rich side of the plagioclase solvus, $\text{Na}_x\text{Ca}_{1-x}\text{Al}_{2-x}\text{Si}_{2+x}\text{O}_8$, $x < 1/3$; Newton et al. (1980)], Bt [biotite, $\text{K}(\text{Mg}_x\text{Fe}_y\text{Mn}_{1-x-y})_{3-w}\text{Al}_{1+2w}\text{Si}_{3-w}\text{O}_{10}(\text{OH})_2$; Powell and Holland (1999), extended to cover Fe and Mn solutions], St [stauroilite, $\text{Mg}_{4x}\text{Fe}_{4y}\text{Mn}_{4(1-x-y)}\text{Al}_{18}\text{Si}_{7.5}\text{O}_{48}\text{H}_4$; Holland and Powell (1998), extended to cover Mn-solutions], Cld [chloritoid, $\text{Mg}_x\text{Fe}_y\text{Mn}_{1-x-y}\text{Al}_2\text{SiO}_5(\text{OH})_2$; White et al. (2000), extended to cover Mn-solutions], Pheng [muscovite, $\text{K}_x\text{Na}_{1-x}\text{Mg}_y\text{Fe}_z\text{Al}_{3-2(y+z)}\text{Si}_{3+y+z}\text{O}_{10}(\text{OH})_2$, as described at <http://www.esc.cam.ac.uk/astaff/holland/ds5/muscovites/mu.html>], Camp [clinoamphibole, $\text{Ca}_2\text{Na}_z(\text{Mg}_x\text{Fe}_{1-x})_{3+2y+z}\text{Al}_{3-3y}\text{Si}_{7+y}\text{O}_{22}(\text{OH})_2$; Wei and Powell (2003); White et al. (2003)], Ilm [ilmenite, $\text{Mg}_x\text{Mn}_y\text{Fe}_{1-x-y}\text{TiO}_3$, ideal ilmenite-geikielite-pyrophanite solution], Ky [kyanite, Al_2SiO_5], And [andalusite, Al_2SiO_5], Sil [sillimanite, Al_2SiO_5], Zo [zoisite, $\text{Ca}_2\text{Al}_3\text{Si}_3\text{O}_{12}(\text{OH})$], Rt [rutile, TiO_2], Sa [sanidine, KAlSi_3O_8], Ttn [titanite, CaTiSiO_5], Qtz [quartz, SiO_2], and Mrg [margarite, $\text{CaAl}_4\text{Si}_2\text{O}_{10}(\text{OH})_2$].

To save computational resources, the afchl endmember of chlorite was excluded because its contribution to the total energy of the solution is negligible. The influence of titanium on the stability of biotite (Kleemann and Reinhardt, 1994) was considered using the Ti-biotite solution model of Powell and Holland (1999) to the samples 12F03, 29F03B and 35F03. Both the results obtained by the application of the Ti-bearing and Ti-free biotite solution model (Powell and Holland, 1999) were compared. H_2O and SiO_2 were considered as excess phases implying the presence of quartz and an aqueous fluid throughout the entire P - T range of interest. To consider the influence of changing H_2O and CO_2 activities during garnet growth, a graphite-buffered and carbon-, oxygen-, and hydrogen-bearing (GCOH-) fluid (Connolly and Cesare, 1993) was applied and compared with a P - T phase diagram section obtained with pure H_2O .

Table 2.4 – Garnet composition at points (1) to (4) of a garnet from the Wölz Complex with two growth zones (sample 12F03) and composition of the bulk chemistries corrected for chemical fractionation during garnet growth (M = weight fraction of crystallized garnet; $k_d=55$).

Normalized composition of garnet point (in wt.%)				
	(1)	(2)	(3)	(4)
SiO ₂	36.80	36.73	36.85	36.99
TiO ₂	0.05	0.05	0.02	0.07
Al ₂ O ₃	21.07	21.13	21.14	21.31
FeO	33.23	33.77	35.03	30.71
MnO	5.75	5.16	3.75	2.98
MgO	1.55	1.66	1.73	1.25
CaO	1.56	1.51	1.48	6.70
Total	100.00	100.00	100.00	100.00
Oxygen	12	12	12	12
Si	3.00	2.99	3.00	2.98
Ti	0.00	0.00	0.00	0.00
Al	2.02	2.03	2.03	2.02
Fe ³⁺	0.00	0.00	0.00	0.02
Fe ²⁺	2.26	2.30	2.38	2.05
Mn	0.40	0.36	0.26	0.20
Mg	0.19	0.20	0.21	0.15
Ca	0.14	0.13	0.13	0.58
Fe/(Fe+Mg)	0.92	0.92	0.92	0.93
Mg/(Fe+Mg)	0.08	0.08	0.08	0.07
X_{alm}	0.76	0.77	0.80	0.69
X_{prp}	0.06	0.07	0.07	0.05
X_{grs}	0.05	0.04	0.04	0.19
X_{sps}	0.13	0.12	0.09	0.07
M	0.001	0.003	0.009	0.013

Normalized effective bulk chemistry for the growth of garnet (in wt.%)			
	(1)	(2)	(3)
SiO ₂	59.89	59.93	60.07
TiO ₂	1.24	1.24	1.25
Al ₂ O ₃	21.85	21.85	21.85
FeO	8.89	8.84	8.69
MnO	0.11	0.10	0.08
MgO	2.37	2.38	2.38
CaO	0.48	0.48	0.47
Na ₂ O	1.28	1.28	1.29
K ₂ O	3.88	3.89	3.91
Total	100.00	100.00	100.00

Although it is known that Zn strongly partitions into staurolite (e.g. Griffen, 1981; Proyer and Dachs, 2000), this feature could not be considered in our calculations because of the lack of thermodynamic data on Zn-staurolite. In the garnet analysed by EPMA, the recalculated $\text{Fe}^{3+}/\text{Fe}^{tot}$ varies between 0.00 and 0.04 (see Table 2.2), indicating that iron is predominantly present in the ferrous state. Thus, Fe^{3+} was not considered in our calculations.

The algorithm used in PERPLEX involves discretization of solid-solution compositions by series of so-called pseudocompounds with a fixed composition. For garnet solid solution, the spacing of the pseudocompounds was set to 0.2–0.3 mol.% for the respective garnet endmembers. For practical purposes, a pseudocompound spacing of 1–2.5 mol.% was chosen for chlorite and biotite solid solution. The database file, one solution-model file, and one input file used with PERPLEX is provided in Appendix A.

The X_{sps} , X_{grs} and X_{alm} [$\text{Fe}^{2+}/(\text{Fe}^{2+} + \text{Ca} + \text{Mg} + \text{Mn})$] isopleths were used as the three independent thermodynamic variables to describe the compositional variation of garnet in P – T space. The intersections of the isopleths that represent the observed garnet compositions are used to estimate the P – T conditions of the respective increment of garnet growth.

2.4.4 Calculation of the thermodynamic relevant bulk composition

To adequately predict the order of magnitude of the effect of chemical fractionation during garnet growth on garnet stability and composition, the method described by Evans (2004) is applied. According to Hollister (1966), the following relation is used to account for chemical fractionation:

$$C_{MnO}^{Grt} = C_{MnO}^{rock} \cdot k_d(1 - M)^{k_d - 1},$$

where C_{MnO}^{Grt} is the weight fraction of MnO in garnet, C_{MnO}^{rock} is the initial weight fraction of MnO in the rock, k_d is the distribution coefficient by weight of MnO between garnet and the rock matrix, and M corresponds to the weight fraction of garnet that has already crystallized in the rock. The amount of garnet crystallized from the above relation was calculated for several compositions along the microprobe traverses presented in this study. The garnet–matrix distribution coefficient for Mn, k_d , was assumed constant during garnet growth and was approximated by the ratio between C_{MnO}^{Grt} in the oldest garnet portion and C_{MnO}^{rock} of the unfractionated bulk-rock chemistry. This is justified by the notion that neither temperature nor equilibrium-phase relations change drastically during the stage of incipient garnet growth. The bulk fractionation is obtained from integration over the successive growth increments (Fig. 2.11). The chemical

Table 2.5 – Garnet composition at points (1) to (3) of a garnet from the Rappold Complex with two growth zones (sample 35F03) and composition of the bulk chemistries corrected for chemical fractionation during garnet growth (M = weight fraction of crystallized garnet; $k_d=61$).

	Normalized composition of		
	garnet point (in wt.%)		
	(1)	(2)	(3)
SiO ₂	36.91	36.98	36.91
TiO ₂	0.05	0.18	0.06
Al ₂ O ₃	20.00	20.17	20.24
FeO	33.44	33.48	36.76
MnO	3.65	3.21	1.07
MgO	1.28	1.35	1.73
CaO	4.68	4.63	3.24
Total	100.00	100.00	100.00
Oxygen	12	12	12
Si	3.00	3.00	3.00
Ti	0.00	0.01	0.00
Al	1.92	1.93	1.94
Fe ³⁺	0.08	0.05	0.06
Fe ²⁺	2.19	2.23	2.44
Mn	0.25	0.22	0.07
Mg	0.15	0.16	0.21
Ca	0.41	0.40	0.28
Fe/(Fe+Mg)	0.93	0.93	0.92
Mg/(Fe+Mg)	0.07	0.07	0.08
X_{alm}	0.73	0.74	0.81
X_{prp}	0.05	0.05	0.07
X_{grs}	0.14	0.13	0.09
X_{sps}	0.08	0.07	0.03
M	0.000	0.002	0.020

	Normalised effective bulk chemistry for		
	the growth of garnet (in wt.%)		
	(1)	(2)	(3)
SiO ₂	50.98	51.01	51.27
TiO ₂	1.03	1.03	1.05
Al ₂ O ₃	27.83	27.84	27.98
FeO	10.06	10.01	9.54
MnO	0.06	0.06	0.02
MgO	2.77	2.77	2.80
CaO	0.38	0.37	0.31
Na ₂ O	0.68	0.68	0.69
K ₂ O	6.20	6.21	6.33
Total	100.00	100.00	100.00

Normalized composition of garnet point (in wt.%)			
	(1)	(2)	(3)
SiO ₂	37.31	37.33	37.45
TiO ₂	0.16	0.21	0.12
Al ₂ O ₃	20.17	20.25	20.34
FeO	30.20	30.54	32.25
MnO	3.28	2.38	0.90
MgO	0.96	1.05	1.50
CaO	7.92	8.23	7.44
Total	100.00	100.00	100.00
Oxygen	12	12	12
Si	3.01	3.01	3.01
Ti	0.01	0.01	0.01
Al	1.92	1.92	1.93
Fe ³⁺	0.04	0.03	0.04
Fe ²⁺	2.00	2.03	2.13
Mn	0.22	0.16	0.06
Mg	0.12	0.13	0.18
Ca	0.69	0.71	0.64
Fe/(Fe+Mg)	0.95	0.94	0.92
Mg/(Fe+Mg)	0.06	0.06	0.08
X _{alm}	0.66	0.67	0.71
X _{prp}	0.04	0.04	0.06
X _{grs}	0.23	0.24	0.21
X _{sps}	0.07	0.05	0.02
M	0.001	0.011	0.039

Table 2.6 – Garnet composition at points (1) to (3) of a garnet from the Wölz Complex with a single growth zone (sample 29F03) and composition of the bulk chemistries corrected for chemical fractionation during garnet growth (M = weight fraction of crystallized garnet; $k_d=34$).

Normalised effective bulk chemistry for the growth of garnet (in wt.%)			
	(1)	(2)	(3)
SiO ₂	66.00	66.33	67.16
TiO ₂	0.86	0.86	0.88
Al ₂ O ₃	18.57	18.55	18.50
FeO	7.15	6.87	6.16
MnO	0.10	0.07	0.03
MgO	2.16	2.18	2.20
CaO	0.54	0.45	0.25
Na ₂ O	1.09	1.11	1.14
K ₂ O	3.53	3.58	3.68
Total	100.00	100.00	100.00

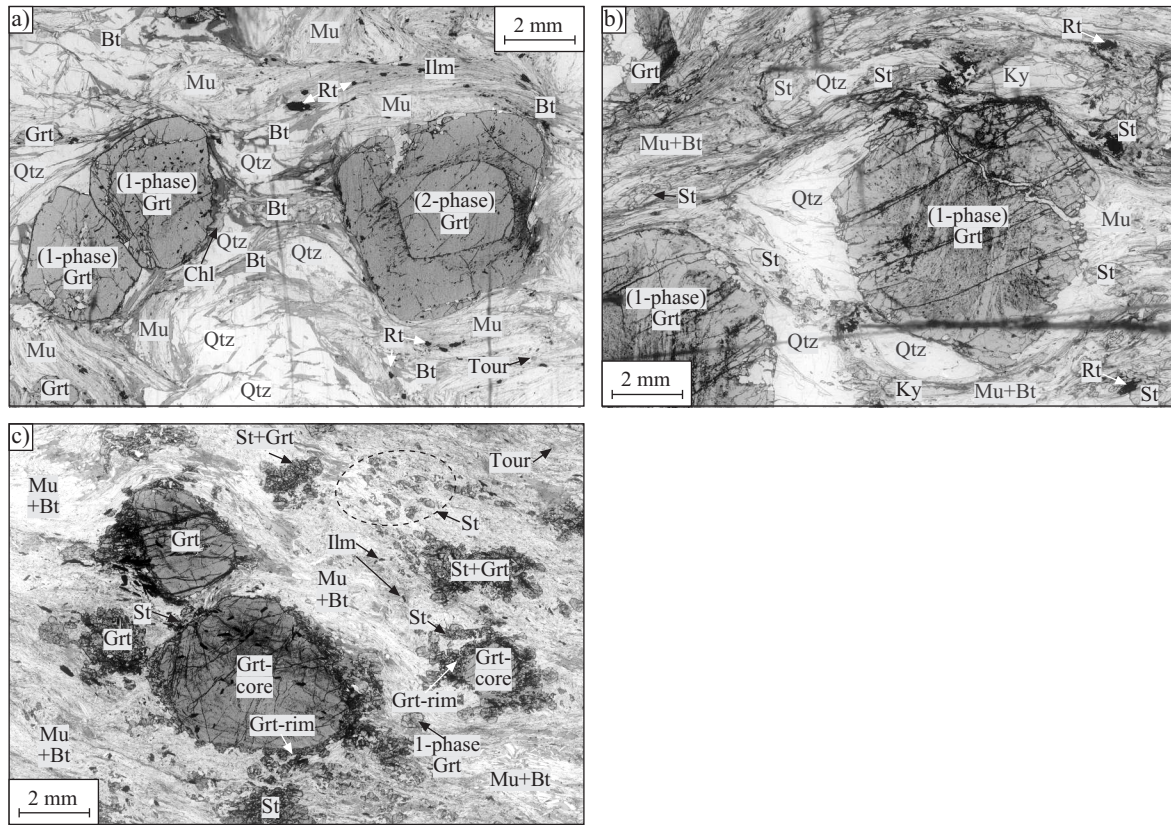


Figure 2.3 – Metapelites with (a) garnet porphyroblasts from the Wölz Complex with one and two distinct growth zones (sample 12F03), (b) garnet porphyroblasts from the Wölz Complex with one growth zone (sample 29F03B) and (c) garnet porphyroblasts from the Rappold Complex with one and two distinct growth zones (sample 35F03). Mu, muscovite; Grt, garnet; Bt, biotite; Chl, chlorite; Qtz, quartz; Tour, tourmaline; Rt, rutile; St, staurolite; Ky, kyanite; Ilm, ilmenite.

shift of the thermodynamically relevant bulk composition of the rock matrix is finally obtained by subtraction of the material that is fractionated into garnet from the respective bulk-rock composition. The M values calculated for different points within the garnet porphyroblasts, as well as the corresponding garnet and matrix compositions are given in Tables 2.4, 2.5 and 2.6.

2.5 Sample description

Twenty-one samples are discussed in this study and were taken from both the Wölz and the Rappold Complexes. Their geographical locations are given in Table 2.1 and Fig. 2.2. Three samples, which are considered as being representative of the entire set of samples, are described

in some detail. Samples 12F03 (Fig. 2.3a) and 29F03B (Fig. 2.3b) are micaschists of the Wölz Complex with garnet grains containing two distinct growth zones and one growth zone, respectively. The sample 35F03 is a garnet-bearing metapelite of the Rappold Complex with polyphase garnet porphyroblasts (Fig. 2.3c).

2.5.1 Metapelite with polyphase garnet porphyroblasts from the Wölz Complex (sample 12F03)

The rock-matrix is composed of quartz, biotite, muscovite, tourmaline, ilmenite, rutile, retrograde chlorite and plagioclase. Biotite, muscovite and ilmenite define the pervasive foliation of the rock. The garnet porphyroblasts, which are up to 6 mm in diameter, are composed of two distinct growth zones. Abundant inclusions of finely dispersed graphite and ilmenite are concentrated along the boundaries between the two growth zones, which makes it easy to discern them even macroscopically.

The first-generation garnet is 4 mm in diameter and contains inclusions of quartz, ilmenite, tourmaline and small muscovite grains. The second-generation garnet is 1.5 mm in size and forms rims enclosing the first-generation garnet. Mineral inclusions of ilmenite, rutile, tourmaline, muscovite and quartz are perceived in the second-generation garnet. Additionally, an intense graphitic pigmentation is observed in the inner portions, which decreases towards the outer portions of the rim. Similarly, the abundance of ilmenite decreases outwards whereas the abundance of rutile increases (Fig. 2.5).

2.5.2 Metapelite with garnet porphyroblasts with only a single growth zone from the Wölz Complex (sample 29F03B)

The typical matrix mineral assemblage is quartz, muscovite, rutile, plagioclase and biotite. Kyanite porphyroblasts with undulatory extinction are commonly observed. They are up to 8 mm long and are often intergrown with staurolite porphyroblasts. They contain abundant inclusions of rutile and graphite. The garnet porphyroblasts are up to 8 mm in diameter and only show a single growth zone (Fig. 2.3b). Garnet inclusion suites are dominated by graphite, ilmenite, rutile, quartz, tourmaline, clinozoisite and allanite. The inclusions of ilmenite display, when elongate, a pre-existing foliation but are not found when rutile inclusions appear in the garnet rim. In few cases, inclusions of kyanite are observed in the outermost parts of garnet.

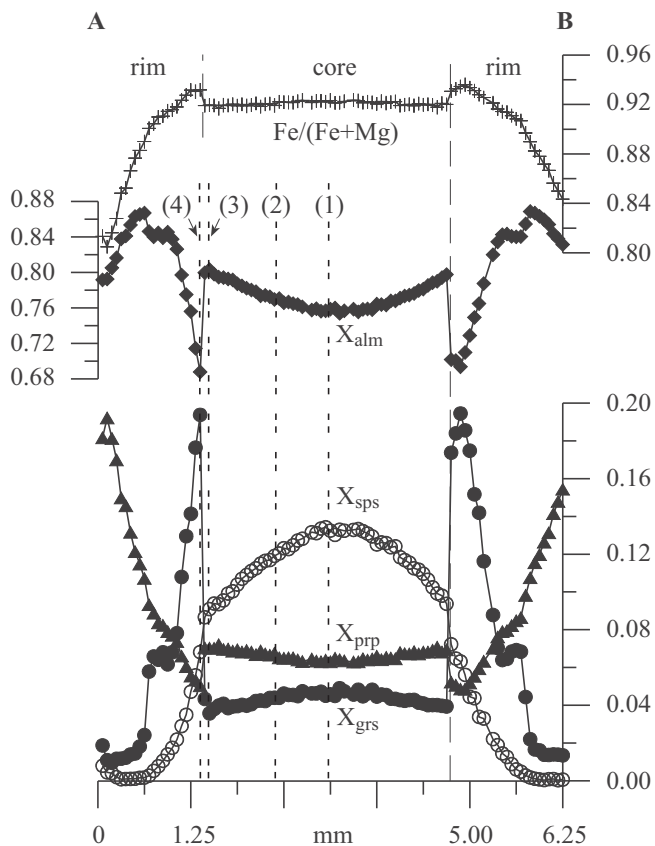


Figure 2.4 – Compositional profile across a garnet porphyroblast with two growth zones (sample 12F03, Wölz Complex). Note the sharp increase of grossular and concomitant decrease of almandine contents at the transition from the first to the second growth zone. P – T estimates for points (1) to (4) are given in Fig. 2.12.

Graphite inclusions are elongated and aligned, which together with ilmenite presumably represent a foliation that existed during garnet growth. Based on their microstructural relationship to the main schistosity, it is deduced that the garnet porphyroblasts grew at the same time as the Eo-Alpine foliation.

2.5.3 Metapelite with polyphase garnet porphyroblasts from the Rappold Complex (sample 35F03)

Biotite and muscovite, which trace the main foliation of the rock, as well as ilmenite, tourmaline, quartz and minor plagioclase, are the most abundant minerals of the matrix. Furthermore, up to 1-mm-size strongly resorbed staurolite blasts with abundant finely dispersed graphitic inclusions are observed, which occasionally rim the first growth zone of garnet porphyroblasts. Equilibrium textures are observed between staurolite and the first-generation garnet including straight interphase boundaries.

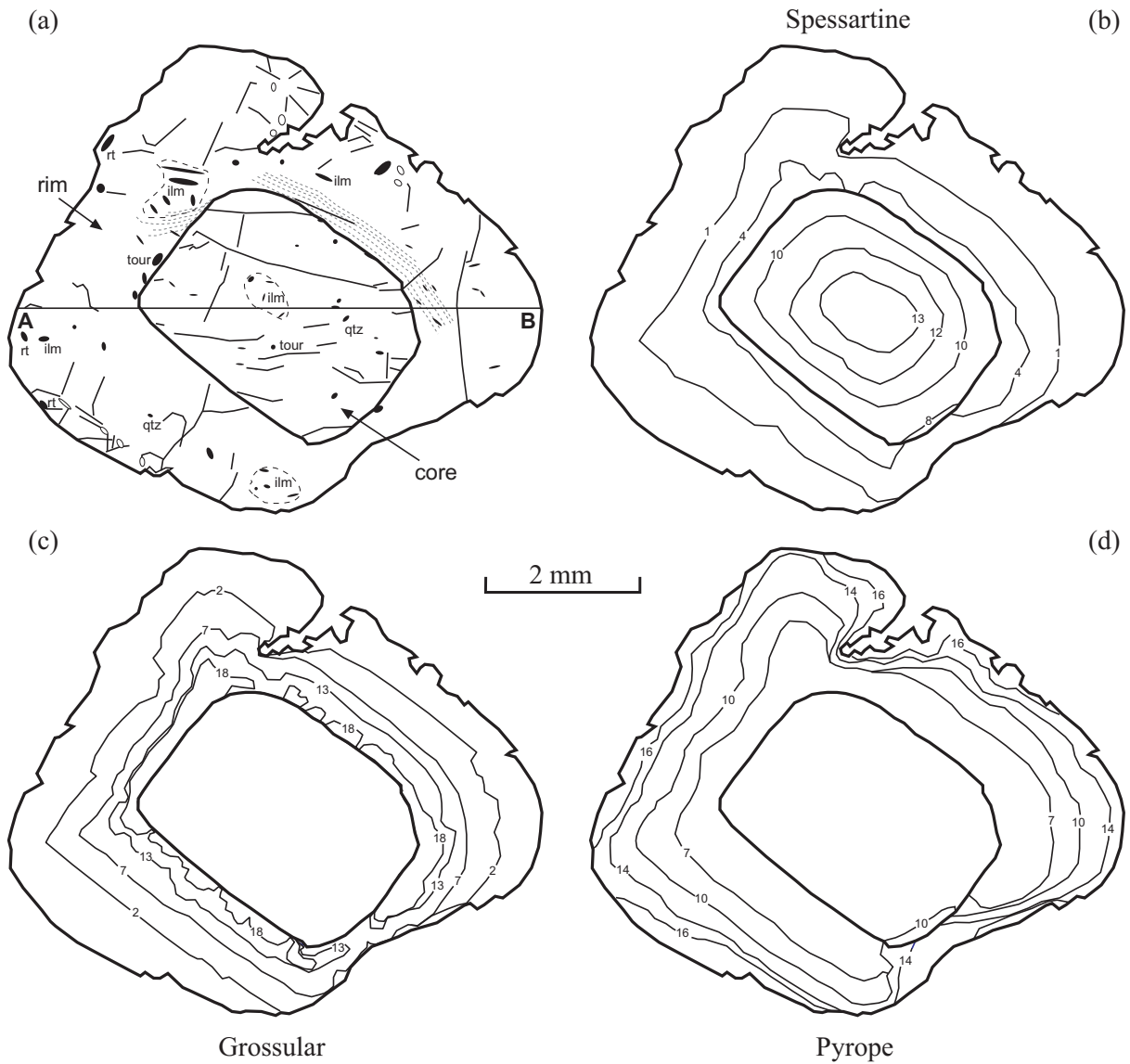


Figure 2.5 – (a) Textural and (b-d) compositional maps (in mol.%) of a garnet porphyroblast from the Wölz Complex with two growth zones (sample 12F03). Rutile appears at the outermost rim of the second-generation garnet, and ilmenite disappears at the same time. Small dashed lines represent graphitic pigmentation, which is restricted to the inner part of the second-generation garnet. The location of the profile A–B as shown in Fig. 2.4 is indicated.

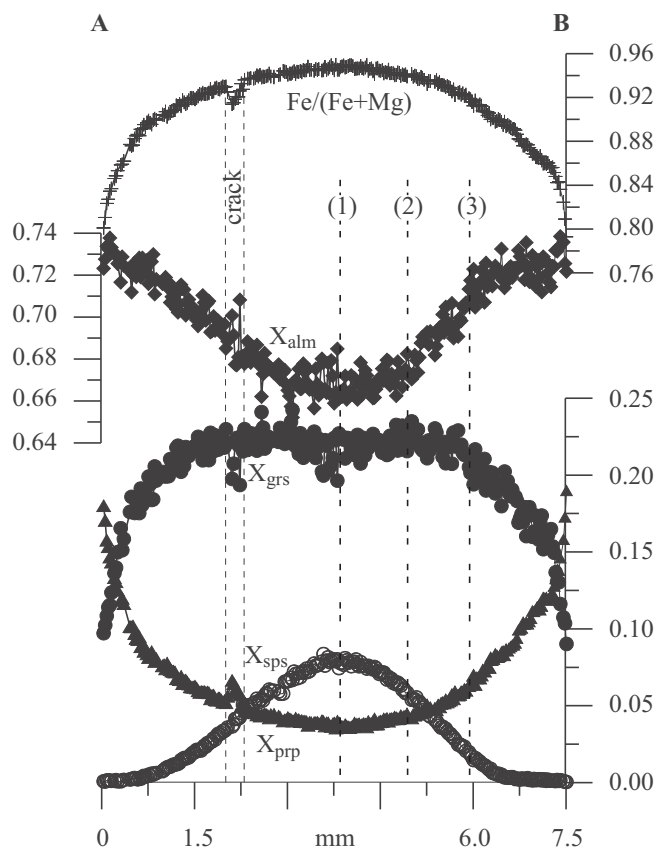


Figure 2.6 – Compositional profile across a garnet porphyroblast from the Wölz Complex with one growth zone (sample 29F03B). P – T estimates for points (1), (2) and (3) are given in Fig. 2.14.

The two growth zones of garnet porphyroblasts differ significantly in size (Figs 2.8 and 2.9). The first generation is strongly graphitic and up to 7 mm in diameter (Fig. 2.3c). Ilmenite (up to 0.5 mm in size), quartz, muscovite, small chloritoid grains, tourmaline, as well as biotite in the outermost portions were observed as mineral inclusions in the first-generation garnet. The needle-shaped tourmaline grains and the graphite inclusions, when elongate, are generally parallel or sub-parallel to the included fabric.

The second-generation garnet is present as single-phase individual crystals and as a < 1-mm-wide overgrowth on the large garnet cores enclosing quartz, tourmaline, ilmenite, biotite and muscovite (Fig. 2.9). In several cases, indications of the replacement of staurolite by the second-generation garnet are observed.

2.6 Results

2.6.1 Garnet chemistry

Polyphase garnet porphyroblasts from the Wözl Complex (sample 12F03)

The chemical composition of the first-generation garnet is characterized by a shallow continuous increase of X_{alm} and X_{prp} from the centre towards the rim, whereas $Fe/(Fe + Mg)$, X_{sps} and X_{grs} decrease (Fig. 2.4). The X_{sps} isopleths in Fig. 2.5 document the almost euhedral growth zoning pattern and only the 0.08 X_{sps} isopleth shows a local irregularity.

The transition between the first- and the second-generation garnet is characterized by a rapid increase of X_{grs} from 0.04 at the outermost part of the core to more than 0.17 at the innermost portion of the rim (Fig. 2.4). Furthermore, X_{alm} and X_{prp} drop off sharply from 0.80 to 0.70 and from 0.07 to 0.05, respectively. $Fe/(Fe + Mg)$ increases from 0.92 to 0.93 at the transition between the inner and outer garnet growth zone.

The compositional gradients of the second-generation garnet are much larger than in the first-generation garnet. X_{grs} shows a sharp outward decrease to values of 0.01 to 0.02 at the outer edge. X_{prp} is somewhat lower in the innermost portion of the second-generation garnet (0.05) compared with that in the outermost portion of the first-generation garnet (0.07) and it shows a continuous outward increase to 0.16 to 0.20 at the outer edge of the rim. In places, the innermost portion of the second-generation garnet is characterized by a short stage with increasing $Fe/(Fe + Mg)$ and X_{grs} and a concomitant decrease in X_{alm} , X_{prp} and X_{sps} (see right-hand side of the profile in Fig. 2.4). In the central portion of the garnet rim, a shoulder in the X_{grs} profile, which interrupts the general trend of outward falling X_{grs} , is observed. X_{alm} is relatively low in the innermost and outermost portions of the second-generation garnet and passes through a maximum in the central portion. A decrease in X_{prp} and a concomitant increase in $Fe/(Fe + Mg)$ is commonly observed in the outermost, several tens of micrometres wide zone of the rim (see left-hand side of the profile in Fig. 2.4).

Garnet porphyroblasts from the Wözl Complex with only a single growth zone (sample 29F03B)

In the core region of the garnet, the concentration of X_{grs} is substantially higher and X_{alm} and X_{prp} are lower than in the central portion of the first-generation garnet of polyphase garnet from the Wözl Complex (Figs 2.4 and 2.6). Furthermore, X_{grs} and $Fe/(Fe + Mg)$ decrease more

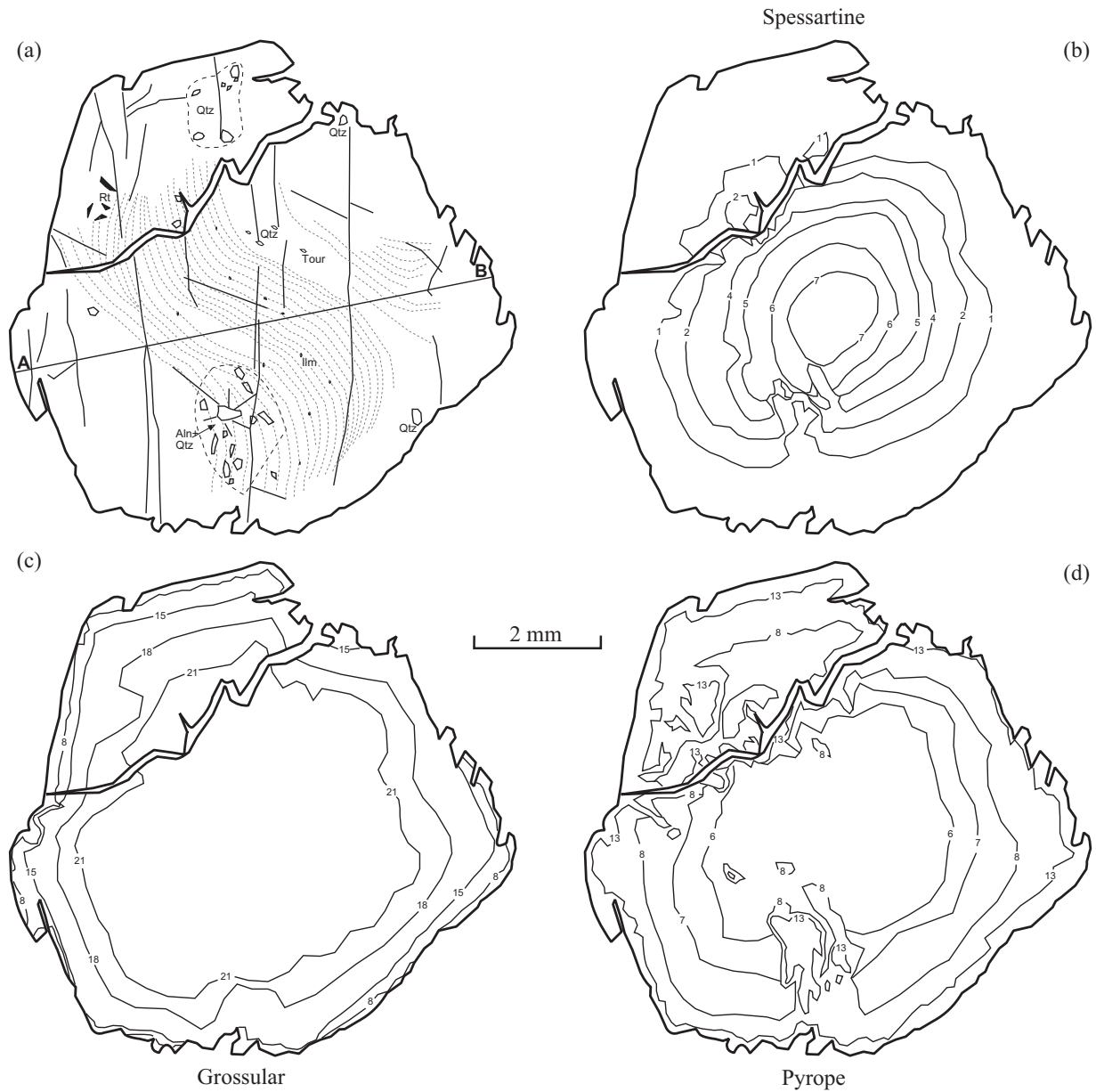


Figure 2.7 – (a) Textural and (b–d) compositional maps (in mol.%) of a garnet porphyroblast from the Wölz Complex with one growth zone (sample 29F03B). The location of the profile A–B as shown in Fig. 2.6 is indicated. The original growth zoning is modified along cracks and around mineral inclusions. Note the presence of allanite and the radial cracks surrounding it. The small dashed lines indicate an intense s-shaped graphitic pigmentation, which disappears in the outermost portion of the garnet.

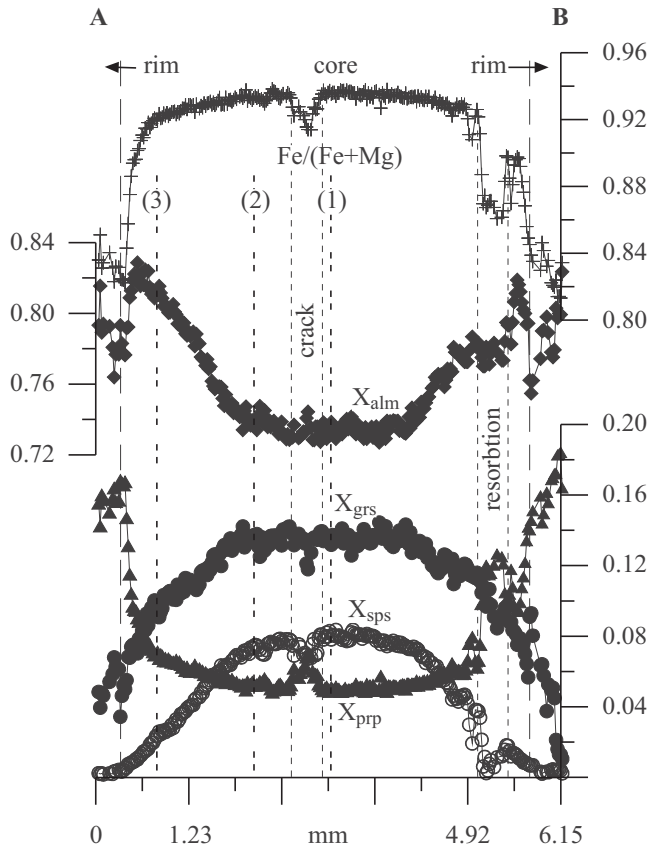


Figure 2.8 – Compositional profile across a garnet porphyroblast from the Rappold Complex with two growth zones (sample 35F03). The increase in the grossular content at the outer parts of the garnet marks the transition between the two growth zones. P – T estimates for points (1), (2) and (3) are given in Fig. 2.13.

steeply and X_{alm} as well as X_{prp} rise more rapidly from core to rim. Qualitatively, the zoning pattern of the one-phase garnet is similar to the zoning pattern of the second-generation garnet of polyphase garnet porphyroblasts of the Wölz Complex. The composition of the innermost portion of the one-phase garnet (Fig. 2.6) closely resembles the composition of the earliest portion of the second-generation garnet (Fig. 2.4). The number of mineral inclusions (Fig. 2.7) and the fluctuations in X_{grs} and X_{alm} (Fig. 2.6) are, however, higher in the one-phase garnet than in the second-generation garnet of the polyphase garnet.

Polyphase garnet porphyroblasts from the Rappold Complex (sample 35F03)

The X_{grs} , X_{sps} and $Fe/(Fe + Mg)$ of the first-generation garnet decrease, whereas X_{alm} and X_{prp} increase from the centre outwards (Fig. 2.8). In their outermost growth increments, the first-generation garnet shows a local maximum in X_{alm} . In this respect, it is similar to the

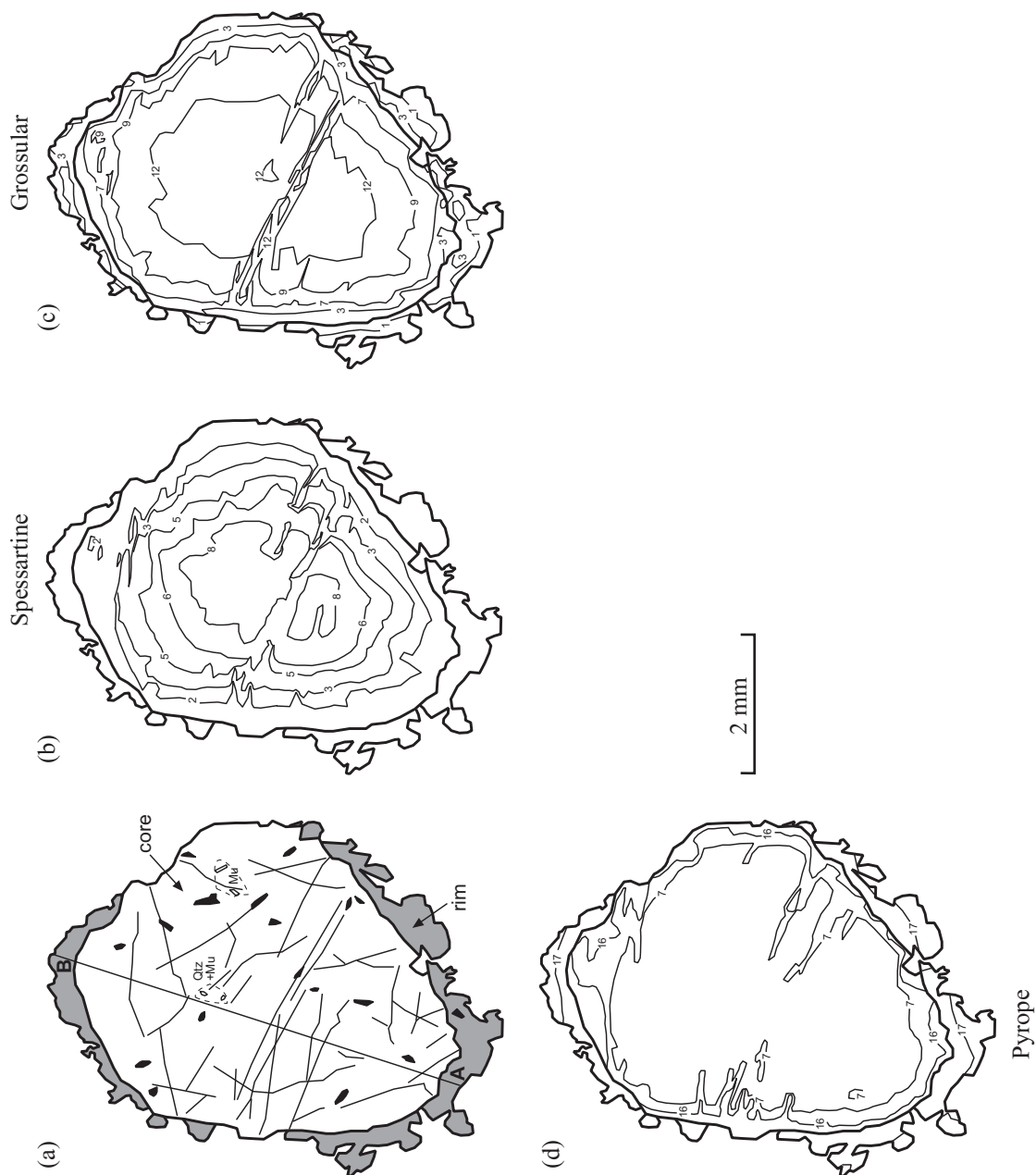


Figure 2.9 – (a) Textural and (b–d) compositional maps (in mol.%) of a strongly fractured and resorbed garnet porphyroblast from the Rappold Complex with two growth zones (sample 35F03). Both garnet generations are characterised by an intense graphitic pigmentation. The location of the profile A–B as shown in Fig. 2.8 is indicated.

second-generation garnet of the polyphase garnet from the Wölz Complex (Fig. 2.4). The first-generation garnet from the Rappold Complex is markedly more compositionally heterogeneous than the garnet core phase from the Wölz Complex. A condensation of the X_{sps} isopleths in the upper right portion (Fig. 2.9) is observed. In its innermost growth increment, the second-generation garnet shows higher values of X_{grs} than the first-generation garnet. The higher values of X_{grs} mark the transition between garnet core and rim. Within the garnet rim, X_{alm} shows a substantial outward increase. In the outermost 10–20 μm , $\text{Fe}/(\text{Fe} + \text{Mg})$ increases sharply, with a concomitant decrease in X_{prp} .

2.6.2 Whole-rock chemistry

The bulk-rock compositions and the compositions of the garnet cores, which were used for garnet isopleth thermobarometry, are plotted in AFM and ACF diagrams in Fig. 2.10. The composition of the average pelite of Symmes and Ferry (1991) (Table 2.3), which is very similar to the composition of the average low-grade pelite of Shaw (1956), is shown for reference. Although there is some scatter in the data, on average, the garnet-bearing metapelites of the Wölz and Rappold Complexes are similar in terms of their compositions. In the AFM diagram, all samples show distinctively lower relative concentrations of MgO than the average pelite of Symmes and Ferry (1991), and in the ACF diagram, they generally plot at somewhat higher A-values than the reference sample (Fig. 2.10). The compositions of garnet cores differ significantly from the average bulk-rock compositions. In the AFM projection, the compositions of garnet cores are at higher X_{Fe} than the respective bulk rock and they are at lower A-values in the ACF diagram. It is interesting to note that the compositions of garnet cores from the Wölz Complex define a linear trend in the ACF diagram, which represents variable C/F ratios at constant A-value. This indicates that the values of X_{grs} are highly variable in garnet cores from the Wölz Complex (Fig. 2.10b). In contrast, garnet cores from the Rappold Complex do not show any variation in their C/F ratios.

2.6.3 P – T estimates

The first-generation garnet of polyphase garnet from the Wölz Complex

Figure 2.12a–c illustrates the variation of garnet composition with pressure and temperature. Compositional isopleths were calculated for the original bulk-rock composition of sample 12F03 obtained from XRF analysis without correction for the effect of chemical fractionation associated

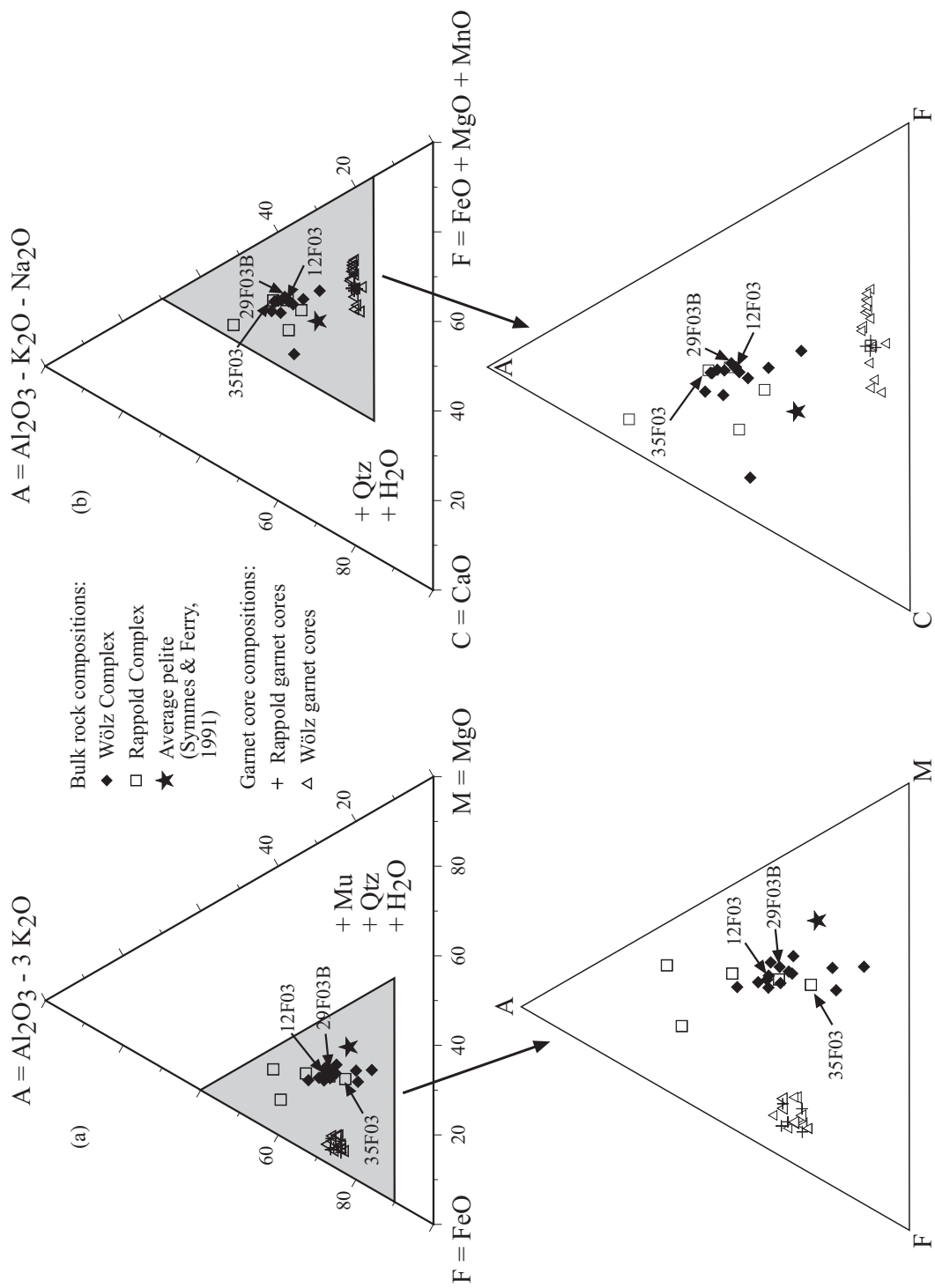


Figure 2.10 – Bulk-rock XRF geochemical data and garnet core compositions of all the samples used for garnet isopleth thermobarometry plotted in an (a) AFM projection from muscovite, quartz and H₂O (Thompson, 1957) and (b) ACF projection from quartz and H₂O. Total iron in all samples is assumed to be FeO.

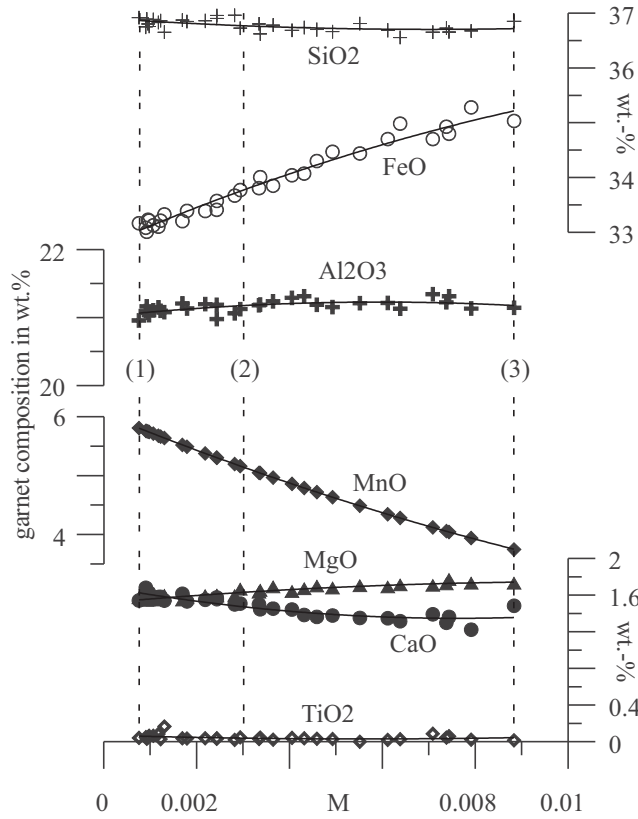


Figure 2.11 – Relationship between M (weight fraction of crystallized garnet) and the chemical composition of the successive growth increments of first-generation garnet from the Wölz Complex (sample 12F03). Points (1), (2) and (3) correspond to the garnet points in Fig. 2.4. For k_d (distribution coefficient of MnO) a value of 55 was used.

with garnet growth (solid lines) and for the effective bulk composition that corresponds to the garnet growth stage represented by point (3) in Fig. 2.4 (dashed lines). The shift of the garnet stability field and of the compositional isopleths produced by chemical fractionation is minute for this specific sample. The effect of chemical fractionation at point (2) of Fig. 2.4 is not shown in Fig. 2.12a–c for the sake of legibility, but it is given in Table 2.4.

The isopleths corresponding to the garnet compositions of the growth stages represented by points (1), (2) and (3) of Fig. 2.4 are shown in Fig. 2.12d. For the incipient stages of garnet growth (point 1), the isopleths intersect close to the low-temperature stability limit of garnet. The centre of the area of isopleth intersection is at 4 kbar and 540°C; this reflects the conditions during incipient garnet growth. As the influence of chemical fractionation during the growth stages (1) to (3) (Fig. 2.4) on garnet stability and composition is negligible for this particular rock sample, equilibrium-phase relations calculated for the bulk-rock composition of sample 12F03 (Table 2.3) are valid for the three garnet growth stages studied (Fig. 2.12e). The area of isopleth intersection that corresponds to incipient garnet growth in sample 12F03 [point (1) in Fig. 2.4]

occurs in the stability field of the assemblage garnet, staurolite, chlorite, albite-rich plagioclase, quartz, ilmenite and muscovite. The P - T estimates obtained for incipient garnet growth of other first-generation garnet from the Wölz Complex yield conditions of 4 ± 0.5 kbar and $535 \pm 20^\circ\text{C}$ (Fig. 2.15). The P - T conditions derived from the composition of the outermost portion of the first-generation garnet [point (3)] are 4.3 kbar and 550°C . The equilibrium assemblage remained unchanged during garnet growth from point (1) to point (3) (Figs 2.4 and 2.12e).

The second-generation garnet of polyphase garnet from the Wölz Complex (sample 12F03)

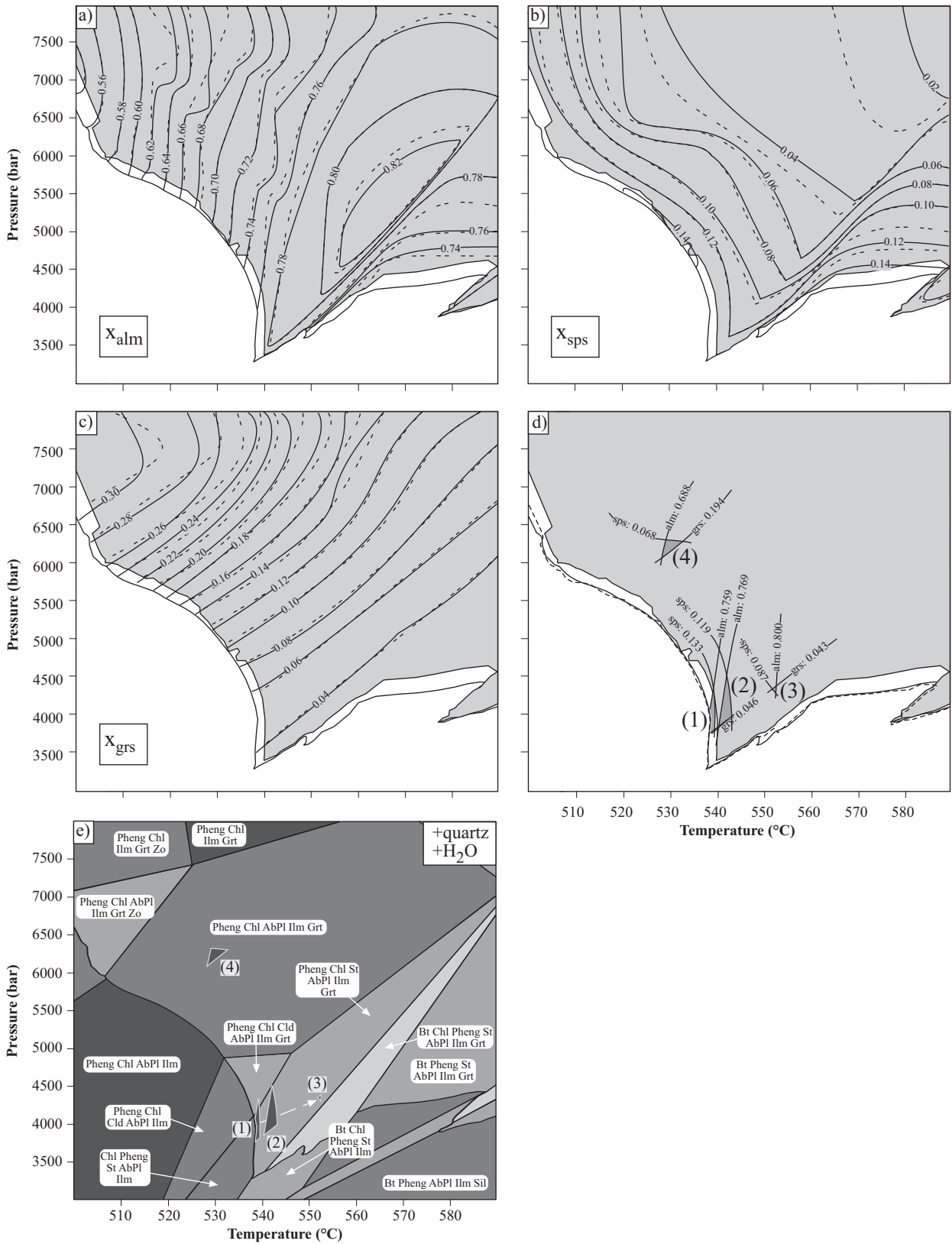
Point (4) of the compositional profile depicted in Fig. 2.4 pertains to the second-generation garnet in the Wölz Complex. The effects on the effective bulk composition of partial resorption of the garnet core and of successive fractionation during rim growth cannot be quantified. This is why the effective bulk composition that was calculated for point (3) (Table 2.4) was used for garnet isopleth thermobarometry. The resulting P - T estimates are at 6.25 kbar and 530°C for the growth stage represented by point (4) (Fig. 2.12e) and occur in the assemblage garnet, chlorite, muscovite, albite-rich plagioclase, quartz and ilmenite.

The one-phase garnet from the Wölz Complex (sample 29F03B)

Garnet isopleth thermobarometry yielded 7.0 kbar and 530°C as the conditions during incipient growth (Fig. 2.14). Calculated phase relations indicate that incipient garnet growth occurred in the assemblage garnet, chlorite, muscovite, albite-rich plagioclase, quartz and ilmenite. On average, conditions of 6.5 ± 0.5 kbar and $540 \pm 10^\circ\text{C}$ are obtained from the central portions of other one-phase garnet from the Wölz Complex (Fig. 2.15).

Taking into account the effect of chemical fractionation during garnet growth, conditions

Figure 2.12 (facing page) – Calculated garnet composition (a-c), compositional contours corresponding to the observed garnet compositions (d), and P - T phase diagram section (e) for a metapelite from the Wölz Complex containing garnet with two growth zones (sample 12F03). The grey-shaded area and stippled lines in (a-c) show the stability field and composition of garnet considering chemical fractionation during the growth from point (1) to the outermost rim of the first-generation garnet [point (3) in Fig. 2.4]. Unbroken lines refer to the garnet, which grew before fractionation started [point (1) in Fig. 2.4]. The dark-grey-shaded areas in (d) mark the areas of isopleth intersection for points (1), (2), (3) and (4) in Fig. 2.4. The stippled line in (d) corresponds to the lower stability limit of garnet predicted for the growth of point (2); (e) was calculated using the bulk-rock composition.



of 7.2 kbar and 535°C and 8.7 kbar and 550°C have been derived for the growth stages represented by the points (2) and (3), respectively (see compositional profile illustrated in Fig. 2.6). The predicted equilibrium assemblage of point (3) is composed of muscovite, biotite, chlorite, ilmenite, garnet and quartz.

The first-generation garnet of polyphase garnet from the Rappold Complex (sample 35F03)

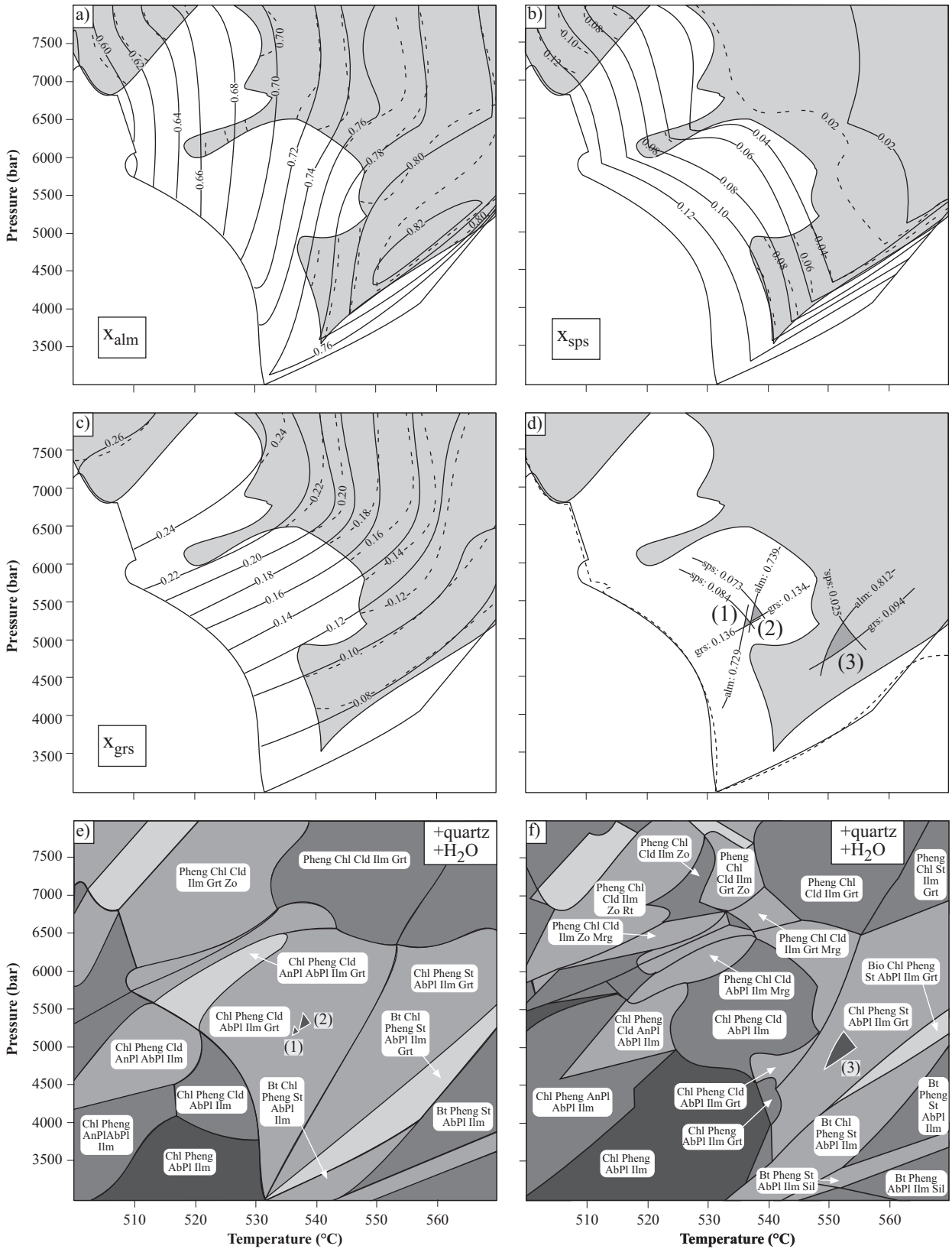
From the composition of the oldest growth increment conditions of 5.2 kbar and 535°C have been derived (Fig. 2.13). The corresponding equilibrium assemblage consists of garnet, chloritoid, chlorite, muscovite, albite-rich plagioclase, quartz and ilmenite. As shown in Fig. 15, the cores of other first-generation garnet from the Rappold Complex yield P - T conditions of 5.3 ± 0.3 kbar and $525 \pm 15^\circ\text{C}$. The P - T conditions calculated for the growth stage represented by point (2) are 5.4 kbar and 535°C; this is within uncertainties identical to the conditions obtained for incipient garnet growth. For point (3), P - T conditions of 5 kbar and 550°C and the assemblage garnet, chlorite, muscovite, staurolite, albite-rich plagioclase, ilmenite and quartz are derived. The area of isopleth intersection is comparatively large for this growth stage, and the uncertainties are accordingly large.

2.7 Discussion

2.7.1 P - T estimates for incipient garnet growth

In medium grade metamorphic schists and gneisses, X_{grs} is sensitive to pressure during garnet growth (e.g. Kretz, 1964; Koziol and Newton, 1988, 1989). From the observation that the

Figure 2.13 (facing page) – Calculated garnet composition (a-c), compositional contours corresponding to the observed garnet compositions (d), and P - T phase diagram sections (e-f) for a metapelite from the Rappold Complex containing garnet with two growth zones (sample 35F03). The grey-shaded area and stippled lines in (a-c) show the stability field and composition of garnet considering chemical fractionation during the growth from point (1) to point (3) in Fig. 2.8. Unbroken lines refer to the garnet, which grew before fractionation started [point (1) in Fig. 2.8]. The dark-grey-shaded areas in (d) mark the areas of isopleth intersection for points (1), (2) and (3) in Fig. 2.8. The stippled line in (d) corresponds to the lower stability limit of garnet predicted for the growth of point (2); (e) and (f) were calculated using the bulk-rock chemistry as the composition of the thermodynamic system at the initial stage of garnet growth and the calculated effective composition for garnet growth stage (3), respectively.



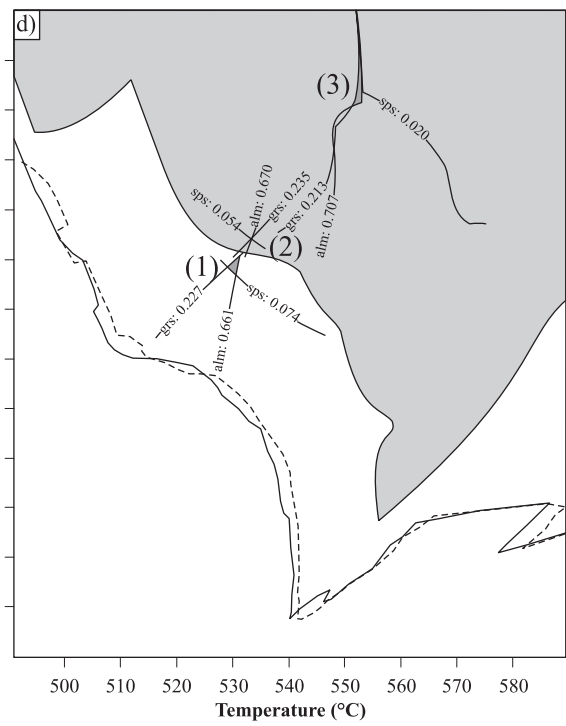
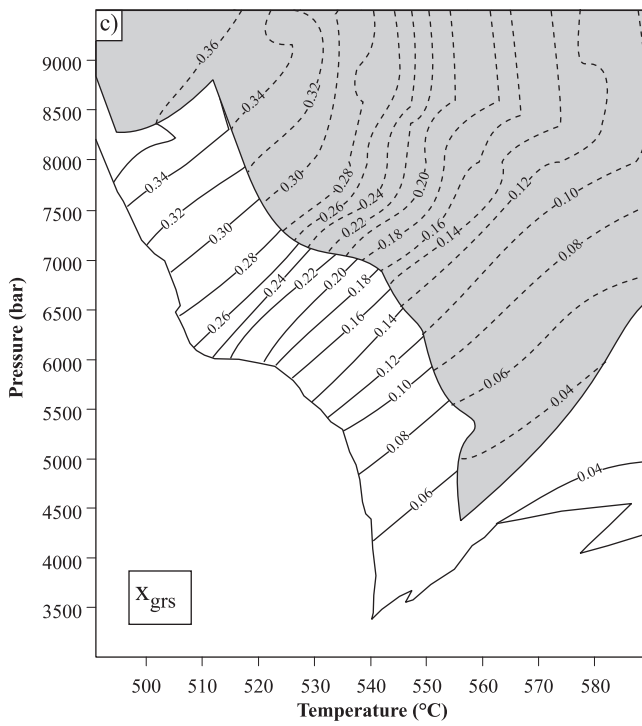
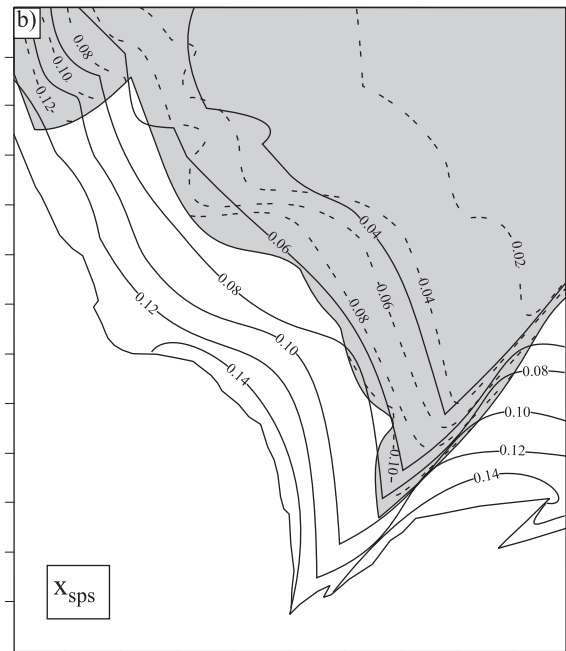
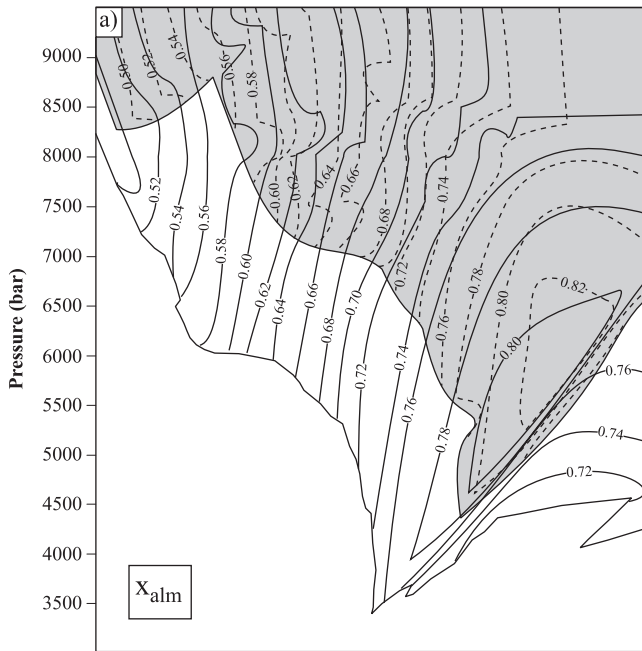
CaO/(CaO + FeO + MgO + MnO) ratios of first growth increments of the first- and the second-generation garnet from the Wölz Complex vary systematically despite relatively constant bulk-rock compositions (Fig. 2.10), it may be inferred that these garnet portions were formed at several stages with different pressure conditions in the Wölz Complex. It must be noted, however, that reactions with a Ca-bearing accessory phase and/or pre-existing chemical heterogeneities may also influence the grossular content of the first garnet growth increments. In contrast, all garnet cores appear to have been formed at a single stage of their polymetamorphic evolution in the Rappold Complex.

Garnet from the Wölz Complex

The application of garnet isopleth thermobarometry to the central portions of all the first-generation garnet studied (Fig. 2.15) testifies to garnet growth at relatively low pressures during the Permian metamorphic event with a geotherm of $40^{\circ}\text{C km}^{-1}$.

The Cretaceous second-generation garnet is considered problematic in the context of garnet isopleth thermobarometry because it forms overgrowths on pre-existing garnet, i.e. it grew in rocks, which already contained garnet that was formed during pre-Eo-Alpine stages. These rocks underwent substantial dehydration during pre-Eo-Alpine times and the extent of chemical equilibration, i.e. the size of equilibration domains that developed during the Eo-Alpine event is not known. However, the area of isopleth intersection obtained for the first-growth increments of the second-generation garnet considering garnet fractionation is small (Fig. 2.12). In addition, the calculated equilibrium-phase assemblage is observed as mineral inclusions in the second-generation garnet with the exception of chlorite and plagioclase, which might have been part of the matrix. Hence, the pronounced difference in the composition of the oldest growth

Figure 2.14 (facing page) – Calculated garnet composition (a–c), compositional contours corresponding to the observed garnet compositions (d), and P – T phase diagram sections (e–f) for a metapelite from the Wölz Complex containing garnet with a single growth zone (sample 29F03B). The grey-shaded area and stippled lines in (a–c) show the stability field and composition of garnet considering chemical fractionation during the growth from point (1) to point (3) as shown in Fig. 2.6. Unbroken lines refer to the garnet which grew before fractionation started [point (1) in Fig. 2.6]. The dark-grey-shaded areas in (d) mark the areas of isopleth intersection for points (1), (2) and (3) in Fig. 2.6. The stippled line in (d) corresponds to the lower stability limit of garnet predicted for the growth of point (2); (e) and (f) were calculated using the bulk-rock chemistry as the composition of the thermodynamic system at the initial stage of garnet growth and the calculated effective chemical composition at garnet growth stage (3), respectively.



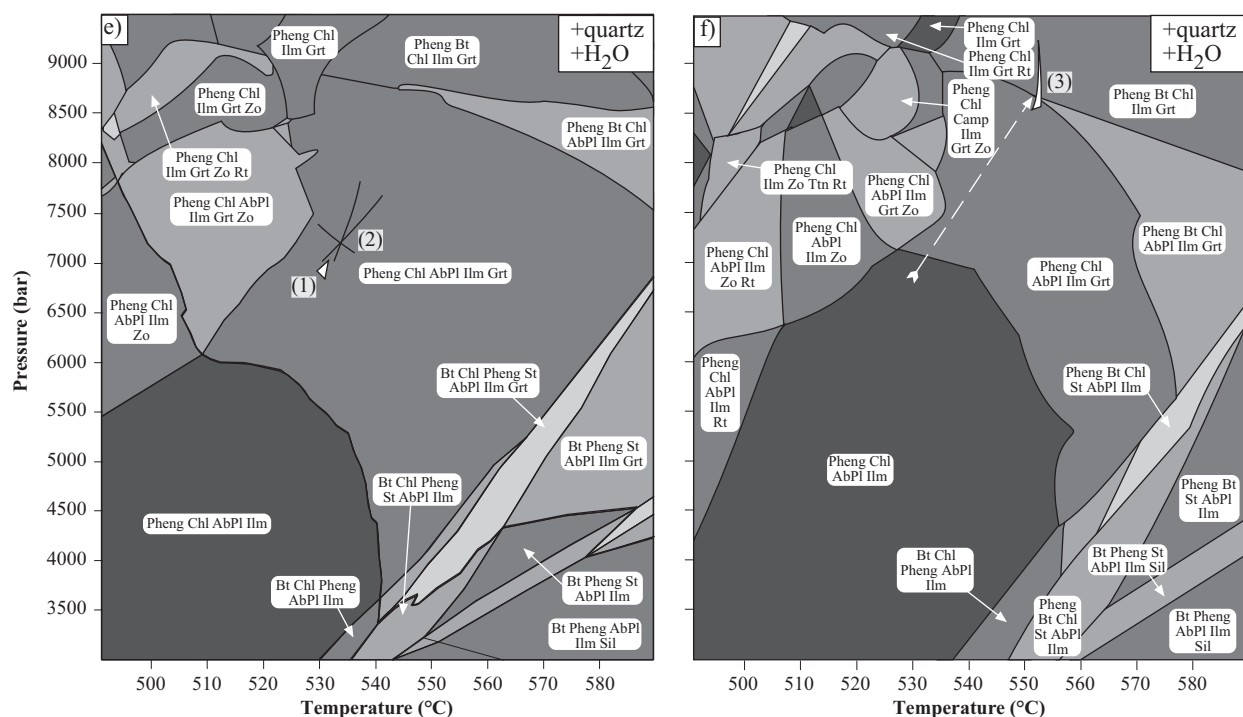


Figure 2.14 – Cont'd.

increment of the Permian first-generation garnet and of the Eo-Alpine second-generation garnet is interpreted to reflect a pressure difference of 2 kbar between the Permian and Eo-Alpine metamorphic events, at least during the stages of incipient garnet growth.

The most promising candidate for garnet isopleth thermobarometry on Eo-Alpine paragneeses is garnet from the Wölz Complex with a single growth zone. As shown in Fig. 2.15, conditions of 6.5 ± 0.5 kbar and $540 \pm 10^\circ\text{C}$ are obtained for their incipient formation.

The similarities of the P - T conditions indicated for incipient growth of garnet with a single growth zone and those indicated for the earliest growth stages of the second-generation garnet confirm that both were formed during the same Eo-Alpine metamorphic event. During the incipient growth stages of Eo-Alpine garnet, the geothermal gradient was at 20°C km^{-1} . This is markedly lower than a thermally relaxed continental geotherm and indicates that Eo-Alpine garnet started to grow during a fast subduction process, where thermal relaxation could not keep up with rapid pressure increase.

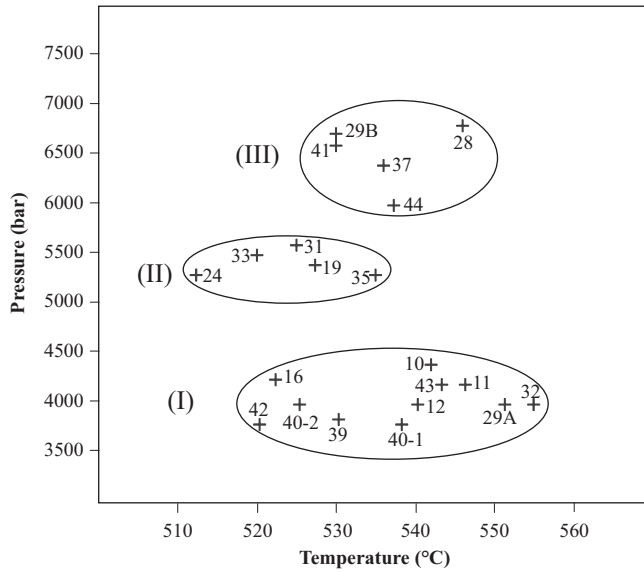


Figure 2.15 – Summary of the P – T estimates obtained for the incipient stages of garnet growth in metapelites from the Wölz and Rappold Complexes. (i) First-generation garnet of Permian age from the Wölz Complex; (ii) first-generation garnet of unknown age from the Rappold Complex; (iii) garnet with a single growth zone of Cretaceous age from the Wölz Complex. Geographical position of the samples is given in Table 2.1 and Fig. 2.2. The respective areas of isopleth intersection are provided in Appendix A for the entire set of samples.

Garnet from the Rappold Complex

Garnet isopleth thermobarometry applied to the oldest growth increments of first-generation garnet yields P – T conditions of 5.3 ± 0.3 kbar and $525 \pm 15^\circ\text{C}$ (Fig. 2.15). These temperatures are within uncertainties identical to those obtained by Faryad and Hoinkes (2003). The pressures, however, are lower by 1.3 kbar. The fact, that this garnet constitutes a group, which is clearly separated in P – T space from the first-generation, low-pressure garnet from the Wölz Complex, suggests that they pertain to a different metamorphic event, possibly of Variscan age. Alternatively, the garnet cores of the Rappold Complex may also have formed during the Permian but in a different crustal segment than the first-generation garnet of the Wölz Complex. According to our P – T estimates, the geothermal gradient was at 30°C km^{-1} during this pre-Eo-Alpine event.

2.7.2 Chemical zoning of garnet and estimated P – T paths for progressive garnet growth

The general zoning patterns observed in garnet porphyroblasts from the Rappold and Wölz Complexes, in particular, the bell-shaped distribution of X_{sps} , (Figs 2.4, 2.6 and 2.8) are typical for garnet growth under greenschist and amphibolite facies conditions during a prograde P – T path (e.g. Hollister, 1966; Tracy et al., 1976; Spear, 1993). The successive outward decrease of X_{sps} reflects the progressive Mn depletion of the matrix caused by fractionation of Mn into

garnet. Depending on the P - T path, certain components such as Mg or Fe tend to be preferentially fractionated into garnet as well. By this mechanism, the thermodynamically relevant bulk composition can substantially change during garnet growth. As shown in Fig. 2.10, the compositions of the garnet cores from the Wölz and Rappold Complexes differ significantly from the average bulk-rock compositions. This implies that the composition of the equilibrium domain was progressively changed by chemical fractionation during garnet growth especially if the modal percentage of newly formed garnet was high.

To account for the effects of chemical fractionation during garnet growth, the fractionation model of Evans (2004) was employed to estimate the P - T conditions during garnet growth although the distribution coefficient of MnO between garnet and the rock matrix cannot be assumed constant as the temperature changes and the composition of the garnet-bearing phase assemblage is possibly modified during garnet evolution. In spite of this insufficiency, the obtained areas of isopleth intersection are small (Figs 2.12d, 2.13d and 2.14d). This indicates that the fractionation model correctly describes the modification of the thermodynamically relevant bulk composition associated with garnet growth for the samples studied.

Two-phase garnet from the Wölz Complex

The almost euhedral growth zoning pattern of the Permian first-generation garnet documented by the spessartine isopleths (Fig. 2.5) indicates the preservation of the primary zoning pattern. Only the 0.08 X_{sps} isopleth shows a local irregularity, which is probably caused by a late-stage alteration along a crack. The smooth zoning of the major components (Fig. 2.4) reflects growth in the course of temporally continuous reactions, where the nutrients for garnet formation were continuously liberated by the breakdown of the precursor phases and transported to the sites of garnet formation.

The P - T path for the formation of the entire first-generation garnet obtained by garnet isopleth thermobarometry and the fractionation model of Evans (2004) is relatively flat [points (1) to (3) in Fig. 2.12d]. The areas of isopleth intersection are comparatively small and the predicted influence of garnet fractionation on garnet stability and composition is almost negligible even for the last growth stage of garnet growth. It is interesting to note that garnet growth along such a P - T path produces a successive decrease in X_{grs} despite growth during slightly increasing pressure.

The equilibrium phase assemblage predicted for the three garnet growth stages [points (1) to (3) in Fig. 2.12e] is not completely preserved as inclusions in the first-generation garnet.

Only ilmenite, quartz, muscovite and tourmaline inclusions are observed. Chlorite, staurolite and albite-rich plagioclase are interpreted to have been part of the Permian matrix assemblage. The P - T estimates for incipient and progressive growth increments of the first-generation garnet support the hypothesis of a Permian extensional event for this part of the Austroalpine Basement (e.g. Miller and Thöni, 1997; Schuster and Thöni, 1996; Schuster et al., 2001).

The innermost portions of the Cretaceous second-generation garnet are characterized by a continuous increase of $\text{Fe}/(\text{Fe} + \text{Mg})$ from 0.93 to 0.94 and simultaneous decrease of X_{alm} , X_{prp} , and X_{sps} and concomitant increase of X_{grs} (see right-hand side of the profile in Fig. 2.4). According to Spear et al. (1991a), this may be interpreted as a result of garnet growth during increasing pressure and decreasing temperature conditions. Such a P - T trajectory would, however, imply a very special tectonic evolution, which is not known for the Eo-Alpine orogenic event in the Eastern Alps. Alternatively, the peculiar zoning pattern may be explained by modification through diffusional exchange across the interface between first and second growth stage of garnet porphyroblasts. The shoulder in the X_{grs} trend (Fig. 2.4) defines a separate stage of second-generation garnet growth. This feature is observed in almost every second-generation garnet from polyphase garnet of the Wölz Complex. It reflects a period of enhanced availability of calcium, which may be due to the breakdown of a Ca-bearing phase such as epidote rather than large changes in P - T conditions. The decrease in X_{prp} and concomitant increase in $\text{Fe}/(\text{Fe} + \text{Mg})$, which is observed in the outermost portions of the second-generation garnet, is ascribed to diffusive Fe-Mg exchange between garnet and matrix phases during retrogression. Hence, the compositions of the outermost garnet rims cannot be considered as equilibrium relations at peak metamorphic conditions. They reflect the element partitioning between garnet and matrix phases at some stage during cooling, which makes it difficult to apply conventional thermobarometry to these rocks.

Quantitative information about the P - T conditions during progressive growth of the Cretaceous second-generation garnet, which rims the Permian first-generation garnet, could not be obtained employing garnet isopleth thermobarometry and the fractionation model. The areas of isopleth intersection are large and the uncertainties in P - T estimates are accordingly large for the outermost portions of Eo-Alpine garnet. This is, at least in part, due to the fact that the X_{alm} -, X_{sps} - and X_{grs} -isopleths tend to become parallel to each other and become pressure-independent at pressures in excess of 7 kbar (Fig. 2.12). In addition, as mentioned above, the size of equilibration domains may have been rather limited during the Eo-Alpine metamorphic overprint in the rocks, which already had experienced earlier medium-grade metamorphism.

This is why bulk-rock compositions combined with a simple fractionation model are no longer an adequate description of the thermodynamically relevant bulk composition. Disequilibrium between the garnet rim and the matrix phases at later stages of garnet growth can also be invoked.

Nevertheless, qualitative information on the P - T conditions during the growth of the second-generation garnet can be deduced from the calculated phase relations in Fig. 2.12. The local maximum in X_{alm} in the outer part of the second-generation garnet (Fig. 2.4) indicates that the rocks followed a P - T path, which passes through the predicted maximum in X_{alm} (Fig. 2.12a). The existence of a local maximum in X_{alm} in P - T space is predicted for all bulk-rock compositions investigated in this study. It generally falls into the chlorite stability field and approximately coincides with the low-temperature stability limit of biotite (Figs 2.12, 2.13 and 2.14). A chemical zoning pattern similar to that of the second-generation garnet from the Wölz Complex (Fig. 2.4), in particular, a maximum in X_{alm} combined with a concomitant decrease of X_{grs} and $Fe/(Fe + Mg)$ was obtained by Spear et al. (1991a) from numerical simulations that implied increasing pressures and temperatures during garnet growth. Such zoning patterns have also been reported from several other prograde garnet growth stages by Vance and Holland (1993) and by Vance and Mahar (1998) and interpreted as a primary, reaction-controlled feature. From a simulation of garnet growth at the expense of chlorite, Inui and Toriumi (2004) suggest that the rapid rise of X_{Mg} and the concomitant decrease in X_{alm} is due to an increase in the relative amounts of clinocllore $[Mg_5Al_2Si_3O_{10}(OH)_8]$ and amesite $[Mg_4Al_4Si_2O_{10}(OH)_8]$ and a decrease of daphnite $[Fe_5Al_2Si_3O_{10}(OH)_8]$ in chlorite with increasing temperature.

The position of the high-pressure limit of the X_{alm} -maximum is slightly shifted to higher pressures because of chemical fractionation associated with garnet growth (Figs 2.12a, 2.13a and 2.14a). In contrast, the position of the low-pressure limit is not affected. Garnet, which grew in a similar chemical system but at higher pressure than the second-generation garnet from the Wölz Complex may pass by the predicted maximum in X_{alm} and thus lack the local X_{alm} -maximum in their chemical zoning pattern.

One-phase garnet from the Wölz Complex

The X-ray maps of the Cretaceous one-phase garnet show the modifying influence of crack formation and mineral inclusions on the original garnet growth zoning (Fig. 2.7). The relatively high number of mineral inclusions compared with those in the Cretaceous second-generation garnet of the Wölz Complex and the fluctuations of X_{alm} and X_{grs} may be due to a slightly

different mineralogical composition of the pre-existing matrix at the site of garnet formation or to a higher rate of garnet growth. Assuming similar values of volume garnet growth, the extent of radial garnet growth strongly depends on the size of the grain, which is overgrown. Hence, the rate of radial garnet growth would be faster for the formation of the one-phase garnet than for the formation of the second-generation garnet of the polyphase garnet porphyroblasts, which forms rims around pre-existing garnet grains.

Considering garnet fractionation (Evans, 2004), a P - T path for the core formation of the Cretaceous one-phase garnet [points (1) to (3) in Fig. 2.6] is obtained, which passes by the predicted maximum in X_{alm} (Fig. 2.14). Therefore, the garnet lacks a local maximum in X_{alm} in its zoning pattern. The P - T path is comparatively steep, which is in line with the hypothesis of garnet growth during an Eo-Alpine subduction process.

The modelled equilibrium-phase assemblage for the oldest garnet portion [point (1) in Figs 2.6 and 2.14e] agrees exactly with the paragenesis predicted for the formation of point (2) (Figs 2.6 and 2.14e), and the influence of garnet fractionation on garnet composition and stability during this garnet growth stage is insignificant. In contrast, fractionation throughout the last growth stage [point (2) to (3) in Figs 2.6 and 2.14f] results in a remarkable change of the phase diagram topology.

Allanite and clinozoisite inclusions are observed in central parts of garnet but are not predicted as stable phases employing garnet isopleth thermobarometry and garnet fractionation [points (1) to (3) in Fig. 2.14]. Both phases are members of the epidote group, which is approximated as zoisite in the calculations. The areas of isopleth intersection for points (1), (2) and (3) are positioned at somewhat lower pressures or slightly higher temperatures than the stability limit of zoisite-bearing assemblages (Fig. 2.14f). We attribute this discrepancy to reflect differences in the thermodynamic properties of clinozoisite and allanite compared with zoisite. Kyanite and rutile inclusions are noticed in the outermost garnet rim, which grew subsequently to the formation of the youngest garnet growth stage considered [point (3) in Figs 2.6 and 2.14e]. Therefore, we suggest the formation of rutile and kyanite as well as staurolite, which is commonly intergrown with kyanite in the matrix, during and following the latest periods of Cretaceous garnet growth accounting for their absence in the phase assemblages modelled.

The P - T conditions obtained for the growth of the second-generation garnet from the Wölz Complex represent parts of a Cretaceous prograde P - T path in the course of Eo-Alpine metamorphism. However, peak metamorphic conditions for the Eo-Alpine event could not be obtained. They are expected to exceed the maximum conditions achieved for the growth of the one-phase

garnet from the Wölz Complex. In this respect, they would be in accordance with thermo-barometrical estimates of 10–11 kbar and 600–650°C obtained for peak metamorphic conditions during Eo-Alpine metamorphism in the Wölz Complex by Faryad and Hoinkes (2003). Koroknai et al. (1999) obtained conditions of 10 kbar and 600°C for metapelites from the southernmost section of the Wölz Complex (Radenthein Complex; Fig. 2.1). In contrast, peak metamorphic conditions for the central parts of the Wölz Complex (Ramingstein Window; Fig. 2.1) were estimated at 7 kbar and 570°C by Schuster and Frank (1999).

Polyphase garnet from the Rappold Complex

The compositional heterogeneity of the first-generation garnet (Fig. 2.8) may be due to the inheritance of pre-existing chemical heterogeneities, or to late-stage diffusional modification of the chemical composition of garnet adjacent to cracks and mineral inclusions (Fig. 2.9). A condensation of the X_{sps} isopleths in the upper right portion of the garnet core is observed, which probably reflects a period of garnet resorption (Fig. 2.9). The sharp increase of $Fe/(Fe + Mg)$ and concomitant decrease in X_{prp} in the outermost 10–20 μm is supposed to indicate retrograde diffusional exchange with matrix phases.

It is interesting to note that Mn is not entirely depleted from the rock matrix even during the latest growth increments of the first-generation garnet (Fig. 2.8). This points to the presence of an additional Mn-bearing phase, which acted as a source of Mn even after chlorite has been entirely consumed in the course of garnet growth.

The resulting P – T path for the growth of the central part of the first-generation garnet proposes garnet formation at increasing temperature and constant or even decreasing pressure (Fig. 2.13d). The estimated P – T path is aimed at the local maximum in X_{alm} that is predicted for the respective bulk-rock composition (see Fig. 2.13a). The reversal trend of X_{alm} in the compositional profile (Fig. 2.8) implies that this feature is passed through at later growth stages.

With the exception of chlorite and plagioclase, all the predicted minerals are perceived as inclusions in early portions of the first-generation garnet. Chemical fractionation in the course of garnet growth noticeably changes the topology of the predicted-phase assemblage relations (Fig. 2.13e,f). At point (3), staurolite instead of chloritoid is calculated to be stable (Fig. 2.13f) and probably corresponds to the strongly resorbed staurolite porphyroblasts noticed in thin sections, which enclose first-generation garnet and form equilibrium textures with them (Fig. 2.3c). Biotite, which is observed in the outermost portions of the first-generation garnet, was not predicted as part of the paragenesis at point (3). However, the position of the lower

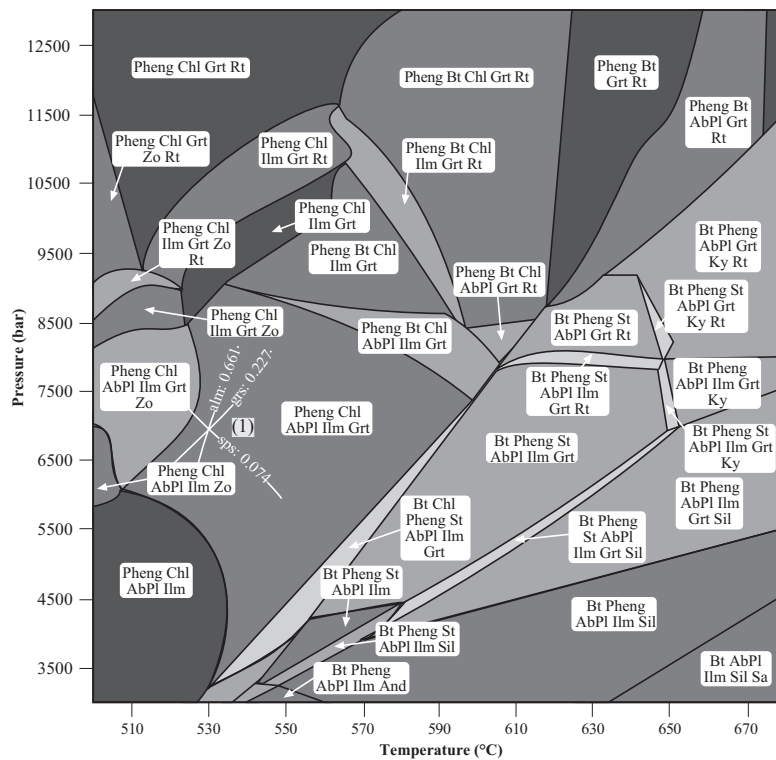


Figure 2.16 – P – T phase diagram section for incipient garnet growth in a metapelite from the Wölz Complex containing garnet porphyroblasts with a single growth zone (sample 29F03B) considering a GCOH-fluid (Connolly and Cesare, 1993) (for further explanation see text).

stability limit of biotite is located at slightly higher temperatures as calculated for the formation of point (3) (Fig. 2.13f). Hence, biotite might be part of an equilibrium assemblage at later stages of garnet growth, which evolves, if the rock follows a P – T path proceeding through the maximum in X_{alm} .

2.7.3 The influence of Ti-biotite and the composition of the fluid

The comparison of P – T phase diagram sections obtained by the implementation of the Ti-free and Ti-bearing solution model of biotite (Powell and Holland, 1999) yields a slightly increased stability of garnet in equilibrium assemblages with Ti-biotite, e.g. consideration of Ti in biotite shifts the garnet-in curve to slightly lower pressures at temperatures exceeding the lower stability limit of biotite. However, the chemical composition of garnet is not affected. As incipient garnet growth is assumed to occur at the expense of chlorite, the influence of Ti-biotite on the stability of garnet can be ignored in this case.

To assess the influence of changing H_2O and CO_2 activities during garnet growth on garnet composition and phase diagram topology and to account for the remarkable amount of graphite observed in the garnet porphyroblasts studied, a P – T phase diagram section was calculated

(Fig. 2.16) considering a graphite-buffered carbon-, oxygen- and hydrogen-bearing (GCOH-) fluid (Connolly and Cesare, 1993). At pressures of 3.5 kbar, the lower stability limit of garnet is shifted to lower temperatures by 10°C compared with the respective equilibrium-phase assemblage diagram calculated with pure H₂O (Fig. 2.14e) whereas the composition of garnet was not changed. However, the influence of fluid composition on garnet stability decreases as the pressure increases. At pressures exceeding 6 kbar, the phase diagram topologies illustrated in Figs 2.14e and 2.16 match exactly. Figure 2.16 also shows the area of isopleth intersection for incipient garnet growth in sample 29F03B. The P - T conditions obtained correspond to the P - T estimates acquired using pure H₂O.

2.7.4 Limitations of garnet isopleth thermobarometry

The P - T conditions predicted for the growth of the most primitive garnet in samples 35F03 and 29F03B are not exactly located at the low-temperature, low-pressure stability limit of the garnet stability field (Figs 2.13f and 2.14f). Several possible mechanisms may be invoked to explain this apparent discrepancy: the position of the lower limit of the stability field of garnet strongly depends on the amount of Mn available for garnet growth. Thus, Mn-bearing phases that may coexist with garnet must be taken into account during thermodynamic modelling. If such phases are ignored or inadequately described thermodynamically, this may have a strong influence on the stability field of garnet. The application of different solution models for solid solution in feldspar (Newton et al., 1980; Baldwin et al., 2005) clearly reflects that the quantity of Ca available for garnet growth strongly influences the position of the garnet-in curve. However, the choice of the feldspar model does not significantly alter the position and shape of the garnet isopleths, e.g. the predicted composition of garnet is only slightly affected by the thermodynamic properties of feldspar solid solution. Furthermore, errors in experimentally obtained thermodynamic properties of minerals, which are introduced via the thermodynamic database used, have to be taken into account. Alternatively, reaction overstepping due to kinetically impeded nucleation and/or volume diffusion of Mn may be invoked. At the stage of incipient growth, the garnet individuals were supposedly very small, and the modal proportion of garnet in the rock can be neglected (Tables 2.5 and 2.6). It may be hypothesized that, despite the low temperatures, volume diffusion of Mn was fast enough to homogenize any growth zoning in garnet effectively, so that the entire grains could maintain an equilibrium distribution with the rock matrix in terms of their Mn concentrations. In this case, garnet isopleth thermobarometry yields valid P - T estimates for an early growth stage.

Of more than 40 samples investigated from both lithostratigraphic units, about 20 have not been deemed successful. In these cases, the areas of isopleth intersection cover more than 1.5 kbar and 20°C, and are too large to obtain well-founded P - T estimates. The failure of garnet isopleth thermobarometry may be due to several reasons.

If the method is applied to late increments of garnet growth without consideration of the effect of chemical fractionation produced during preceding garnet growth, i.e. if bulk-rock chemistries are used for phase equilibrium calculations, this may result in enlarged areas of isopleth intersection and unsatisfactory precision of the method. In the case of garnet that grew under greenschist to amphibolite facies conditions, this may even lead to systematic underestimation of pressure and to overestimation of temperature, because of the characteristic growth zoning of such garnet.

Furthermore, the positions of the isopleths may tend to become parallel at high pressures as shown for the Cretaceous second-generation garnet of sample 12F03. This results in strongly extended areas of isopleth intersection and unsatisfactorily large P - T uncertainties for garnet grown at relatively high pressures.

In garnet isopleth thermobarometry, the bulk-rock composition or the effective bulk-rock composition is usually employed as the thermodynamically relevant system composition. This is valid as long as thermodynamic equilibrium is maintained over the entire rock volume considered at any time of garnet growth. In general, equilibration volumes will be of finite size, depending on the efficiency of mass transport in the rock matrix. Mass transfer in rocks may be slow so that a single rock specimen may contain several equilibration domains. Garnet cores in a rock sample which grew at the same metamorphic event and nucleate at similar times but differ strongly with respect to their chemical composition may be considered indicators for the juxtaposition of different equilibration domains. In this case, the chemical composition of the rock sample averages out over the neighbouring equilibration domains and differs from the composition that is thermodynamically relevant for the growth of garnet within an individual equilibration domain.

The large number of fractures and mineral inclusions especially in garnet from the Rappold Complex are assumed to be responsible for secondary diffusional relaxation and modification of the original garnet composition. Moreover, garnet isopleth thermobarometry could not be applied to samples containing significant quantities of Fe^{3+} -bearing phases such as epidote or the garnet endmember andradite. An estimation of the original amounts of Fe_2O_3 at the time of incipient garnet growth could lead to more realistic models of rock-specific equilibrium-phase relations.

2.8 Conclusions

Estimates for the P - T conditions during incipient garnet growth and P - T trajectories representative for garnet growth in the course of pre-Eo-Alpine and Eo-Alpine metamorphic events in the Austroalpine basement are deduced from the investigation of bulk-rock chemistries and compositions of zoned metamorphic garnet porphyroblasts. The comparison of calculated garnet chemistries obtained from P - T phase diagram sections and garnet fractionation modelling with observed garnet compositions suggests different pre-Eo-Alpine metamorphic histories in the Wölz and Rappold Complexes. Whereas the Permian garnet from the Wölz Complex started to grow at 4 ± 0.5 kbar and $535 \pm 20^\circ\text{C}$ incipient garnet growth of garnet from the Rappold Complex occurred at 5.3 ± 0.3 kbar and $525 \pm 15^\circ\text{C}$. The P - T estimates for the earliest growth zones of garnet from the Wölz Complex are in line with the presumed high temperature/low pressure conditions of the Permian metamorphic event. The P - T estimates for garnet from the Rappold Complex reflect a Barrow-type P - T path typical of Variscan metamorphism in the Eastern Alps. Investigations of Eo-Alpine garnet from the Wölz Complex yielded P - T conditions of 6.5 ± 0.5 kbar at $540 \pm 10^\circ\text{C}$ during incipient garnet growth.

The typical growth zoning patterns observed in garnet of the Wölz and Rappold Complexes reflect changing component availabilities at the time of garnet growth. Besides garnet fractionation, component availability is controlled by several poorly constrained factors such as transport pathways and rates, the kinetics of decomposition reactions of precursor phases and garnet nucleation and growth, as well as diffusional relaxation. Therefore, the potential of garnet isopleth thermobarometry to derive P - T paths from zoning patterns is limited. In contrast, application of this technique to the first increments of garnet growth is reliable (e.g. Vance and Mahar, 1998; Stowell et al., 2001; Zeh, 2001; Zeh and Holness, 2003; Evans, 2004).

The application of garnet isopleth thermobarometry together with garnet age determinations is suggested to be an efficient approach to obtain P - T - t information for the first metamorphic event of rocks that underwent a polymetamorphic evolution. In particular, it sheds light on pre-Eo-Alpine metamorphic events in the Austroalpine realm.

2.9 Acknowledgements

The authors thank W. Tschudin for the sample preparation, appreciate the editorial handling by M. Brown and D. Robinson and are grateful to D. K. Tinkham and A. Zeh for their thorough

reviews. J. MacKenzie is thanked for language improvements.

Chapter 3

THERIA_G: A software program to numerically model prograde garnet growth

This chapter is under review as: **Gaidies, F.**, de Capitani, C. and Abart, R., 2007. THERIA_G: A software program to numerically model prograde garnet growth. *Contributions to Mineralogy and Petrology*.

3.1 Abstract

We present the software program THERIA_G, which allows for numerical simulation of garnet growth in a given volume of rock along any pressure-temperature-time (P - T - t) path. THERIA_G assumes thermodynamic equilibrium between the garnet rim and the rock matrix during growth and accounts for component fractionation associated with garnet formation as well as for intracrystalline diffusion within garnet. In addition, THERIA_G keeps track of changes in the equilibrium phase relations, which occur during garnet growth along the specified P - T - t trajectory. This is accomplished by the combination of two major modules: A Gibbs free energy minimization routine is used to calculate equilibrium phase relations including the volume and composition of successive garnet growth increments as P and T and the effective bulk rock composition change. With the second module intragranular multi-component diffusion is modelled for spherical garnet geometry.

THERIA_G allows to simulate the formation of an entire garnet population, the nucleation and growth history of which is specified via the garnet crystal size frequency distribution (CSD). Garnet growth simulations with THERIA_G produce compositional profiles for the garnet porphyroblasts of each size class of a population and full information on equilibrium phase assemblages for any point along the specified P - T - t trajectory. The results of garnet growth simulation can be used to infer the P - T - t path of metamorphism from the chemical zoning of garnet porphyroblasts. With a hypothetical example of garnet growth in a pelitic rock we demonstrate that it is essential for the interpretation of the chemical zoning of garnet to account for the combined effects of the thermodynamic conditions of garnet growth, the nucleation history and intracrystalline diffusion.

3.2 Introduction

The chemical zoning patterns of garnet porphyroblasts play a key role in reconstructing the pressure-temperature (P - T) history of metamorphic rocks (e.g. Spear, 1993). Due to the comparatively slow rates of cation diffusion in garnet (e.g. Loomis, 1982; Chakraborty and Ganguly, 1992), garnet compositional zoning, which reflects parts of the P - T - t evolution of the rock, may be preserved over geological time spans even at medium to high grade metamorphic conditions.

To extract geothermobarometric information from garnet composition, numerical models, which simulate the influence of changing P - T conditions on garnet composition during growth, can be employed (e.g. Cygan and Lasaga, 1982; Spear et al., 1991a). In combination with petrographic, geochemical, and microstructural investigations this approach may provide essential information on the metamorphic evolution of the garnet-bearing rock sample.

The DiffGibbs computer program (Florence and Spear, 1991; Spear and Florence, 1992; Spear et al., 1991b) was the first numerical model, which was designed to predict the chemical zoning pattern of garnet that grows in equilibrium with a given set of phases along a specific P - T - t path. The DiffGibbs program accounts for chemical fractionation during garnet growth as well as for intragranular diffusion in garnet. DiffGibbs modelling requires knowledge of the compositions and modal abundance of all phases that pertain to the equilibrium assemblage in a given rock sample at specified P - T conditions. It does not test for the stability of this assemblage and, as a consequence, does not update phase relations along the P - T - t trajectory. In addition, the DiffGibbs model does not allow for simulation of formation of an entire garnet population, i.e. in DiffGibbs modelling all garnet crystals nucleate at the same time, so that

the influence of the nucleation history on the chemical zoning of garnet can not be addressed adequately.

In this communication we present the THERIA_G¹ software program. Similarly to DiffGibbs, it simulates garnet growth and accounts for chemical fractionation due to the formation of garnet, intracrystalline diffusion within garnet and diffusional fluxes between garnet porphyroblasts and the matrix. However, THERIA_G implements the THERIAK code (de Capitani and Brown, 1987), which is based on Gibbs Free energy minimisation. Therefore, the configuration of the thermodynamically stable metamorphic mineral assemblages as well as the chemical compositions and modal abundances of all phases that evolve as the external conditions and bulk rock composition change during garnet growth, can be taken into account.

In addition, THERIA_G allows to simulate the formation of an entire garnet population, which comprises several classes of garnet individuals, i.e. porphyroblasts of different size that nucleate and start to grow at different times along the P - T - t trajectory. If component diffusion in the matrix is fast, i.e. not rate limiting, the final sizes of the garnet individuals reflect their time of nucleation. THERIA_G can be used to simulate the formation of garnet crystals of progressively smaller size so that any prescribed rock specific crystal size frequency distributions (CSD) can be reproduced. This offers the possibility to evaluate the influences of the growth history of garnet on its chemical zoning pattern.

The aim of the current communication is to describe the software program in detail and to discuss an application of THERIA_G to the average garnet bearing metapelite of Shaw (1956) using different scenarios for garnet growth kinetics and P - T - t trajectories. Applications to polymetamorphic garnet-bearing metapelites from the Austroalpine basement are presented in a companion paper (Gaidies et al., *subm.b*).

3.3 Simulation of garnet growth

The THERIA_G program consists of two major parts: (1) THERIAK (de Capitani and Brown, 1987) computes the equilibrium phase relations for given P and T conditions and a specific effective bulk rock composition² using an internally consistent thermodynamic database (e.g. Berman, 1988; Holland and Powell, 1998). This allows to predict the amount and composition

¹THERIA_G is coded in Fortran77. The code as well as executable files for Mac, UNIX, and PC are available from the enclosed CD (see Appendix B.2).

²We refer to the composition of the volume domain in a rock over which thermodynamic equilibrium is established during each increment of garnet growth as the “thermodynamically relevant” or “effective bulk rock composition”

of garnet that is formed after an incremental change in P and T . The calculated amount of garnet is added by THERIA_G to pre-existing garnet porphyroblasts as successive spherical shells. In general, for such calculations, thermodynamic equilibrium is assumed to be maintained between the garnet rims and the rock matrix at any time during garnet growth. (2) The diffusion module calculates the effects of intracrystalline multicomponent diffusional transport between successive garnet shells, the initial compositions of which represent garnet growth zoning. Furthermore, the diffusion module calculates the component fluxes between garnet and the matrix.

The two basic components of THERIA_G communicate via an interface, which is also used for data input. The input parameters comprise the initial thermodynamically relevant bulk rock composition, the P - T - t trajectory over which garnet growth is to be modelled as well as the relative garnet crystal size frequency distribution (CSD) of the respective garnet population. In addition, the thickness of successive garnet shells needs to be chosen. Finally, the thermodynamic database and the kinetic parameters for intragranular diffusion in garnet need to be specified.

As the thermodynamically relevant composition, the bulk rock composition of an unaltered rock volume of hand specimen size that is devoid of macroscopically detectable compositional heterogeneity may be chosen. For THERIA_G modelling it is essential to choose a P - T - t path, which begins outside the garnet stability field. For practical purposes it is expedient to first delineate the garnet stability field by constructing an equilibrium assemblage diagram. This can be done by using the program DOMINO, which is part of the THERIAK-DOMINO software package (de Capitani, 1994) and is available online at: <http://titan.minpet.unibas.ch/minpet/theriak/theruser.html>.

The different individuals of a garnet population are assigned to radius classes via the CSD, which gives the relative abundance of garnet individuals of a specified size range. An example of a relative CSD is illustrated in Figure 3.1.

THERIA_G simulates garnet growth as a succession of spherical shells. The resolution of growth increments is determined by the choice of a fixed thickness, Δr_{shell} , for the successive garnet shells. For each growth increment, Δr_{shell} and the CSD data are used to calculate the volume of garnet, which is searched for along the pre-defined P - T - t path. That is, if P and T are incremented within the garnet stability field, THERIA_G varies P and T along the prescribed P - T trajectory until the volume of newly formed garnet is such that it may be distributed to form spherical shells of thickness Δr_{shell} on all garnet individuals and, if applicable to newly formed garnets of size $2\Delta r_{shell}$. For conditions outside the garnet stability field, P and T are incremented along the P - T path with regular steps of at least 0.5 °C or 20 bar. For conditions

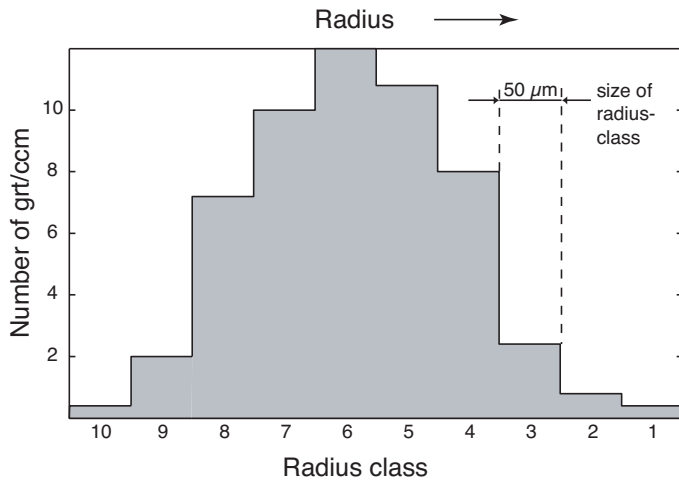


Figure 3.1 – Relative garnet crystal size frequency distribution (CSD1) used for garnet growth simulations.

within the garnet stability field this procedure yields irregular P - T steps that largely depend on the chosen shell thickness and, in general, increase with garnet growth. In contrast, the thickness of successive garnet shells is constant. This technique is motivated by the fact that the regular spacing of successive garnet shells renders interpolation methods during diffusion modelling unnecessary. Such interpolation would have been indispensable to keep numerical errors small, if the successive garnet shells were irregularly spaced (see below).

The choice of Δr_{shell} is guided by finding a compromise between computational efficiency, which is highest for large values of Δr_{shell} and high accuracy, which requires small Δr_{shell} . The calculation of chemical fractionation associated with garnet growth is particularly sensitive to the choice of Δr_{shell} . It turned out that a $\Delta r_{shell} < 10 \mu\text{m}$ ensures satisfactory accuracy when modelling the formation of a garnet population where the largest individuals have a diameter of 2 mm.

The present version of THERIA_G offers calculations with the dataset of Holland and Powell (1998) (thermodynamic database of THERMOCALC, version 3.21). For the kinetic parameters, the data acquired by Chakraborty and Ganguly (1992) or Loomis et al. (1985) can be chosen.

3.3.1 Modelling of garnet fractionation

When the garnet stability field is hit for the first time in a simulation, THERIA_G calculates the initial garnet volume from the thickness of the first shell and the CSD information, i.e. number of garnet individuals per unit volume of the rock that pertain to the first radius class of the specified CSD. It starts to iteratively search for the P - T conditions along the given P - T - t trajectory, at which the corresponding garnet volume is grown. The solution is accepted, as

soon as the differences in T and P after successive iteration loops is smaller than 10^{-4}°C or 20 bar, respectively. As a result, the initial garnet growth increment is formed, which has uniform chemical composition.

To account for chemical fractionation during garnet growth, the material, which is used to produce garnet, is numerically removed from the bulk rock composition. In general, this leads to chemical fractionation. The new effective composition of the matrix is then used for the next garnet volume search. In contrast to isothermal fractionation models (Atherton, 1968; Hollister, 1966), this approach accounts for the progressive modification of the distribution coefficients with T and P . If the steps in P and T become infinitesimally small, our model approaches Raleigh fractionation.

During the search for the P - T increment, which is needed to create the next garnet shell, the program keeps track of changes in the equilibrium assemblage. If a phase disappears from the garnet bearing assemblage or a new phase comes in before the P - T conditions are reached, at which the next garnet shell can be produced, THERIA_G finds the conditions at which the paragenesis changes to within $\pm 10^{-4}\text{°C}$ or ± 20 bar, respectively. It stops the growth of the current shell at these conditions. In such a situation the resulting thickness of the garnet shell is smaller than Δr_{shell} . The effective bulk rock composition is adjusted accordingly and the respective P - T conditions are used as the starting point for the search of the next garnet shell.

3.3.2 Modelling of intracrystalline diffusion

In general, as garnet forms at changing P - T conditions, successive garnet shells have different chemical compositions. This gives rise to garnet growth zoning, which may be modified subsequently by intracrystalline diffusion. To investigate these effects the relaxation of compositional gradients by intracrystalline diffusion in garnet is modelled after each growth increment.

In general, for multicomponent diffusion, Fick's Second Law (Onsager, 1945) takes the form of a parabolic partial differential equation

$$\frac{\partial C_i}{\partial t} = \frac{\partial}{\partial x} \sum_{j=1}^{n-1} D_{ij} \left(\frac{\partial C_j}{\partial x} \right) \quad (3.1)$$

where C_i is the concentration of a component in an n -component system, t is time, the D_{ij} s are the interdiffusion coefficients, and x is distance. In an n -component system, only $n - 1$ components can diffuse independently.

The interdiffusion coefficients, D_{ij} , are calculated following the method suggested by Lasaga

(1979) for multicomponent ideal ionic solutions

$$D_{ij} = D_i^* \delta_{ij} - \left(\frac{D_i^* z_i z_j X_i}{\sum_{k=1}^n z_k^2 X_k D_k^*} \right) (D_j^* - D_n^*) \quad (3.2)$$

where δ_{ij} is the Kronecker delta ($\delta_{ij} = 0$ at $i \neq j$ and $\delta_{ij} = 1$ at $i = j$), z is the charge of the diffusing species, X is the mole fraction of the component. D_i^* is the tracer diffusion coefficient of component i and can be calculated from the Arrhenius relation

$$D_i^* = D_0 \exp \left(\frac{-E_a - (P - 1) \Delta V^+}{RT} \right) \quad (3.3)$$

with the pre-exponential constant, D_0 , the activation energy of diffusion, E_a , at 1 bar, the activation volume of diffusion, ΔV^+ , the universal gas constant, R , and the temperature, T .

For multicomponent diffusion in a spherical geometry equation (3.1) takes the form (Crank, 1975)

$$\frac{\partial C_i}{\partial t} = \frac{1}{r^2} \frac{\partial}{\partial r} \sum_j^{n-1} D_{ij} r^2 \left(\frac{\partial C_j}{\partial r} \right) \quad (3.4)$$

where r corresponds to the radius of the sphere. Neglecting the concentration dependence of the interdiffusion coefficients, D_{ij} , expression (3.4) takes the form

$$\frac{\partial C_i}{\partial t} = \sum_i^{n-1} D_{ij} \left(\frac{\partial^2 C_j}{\partial r^2} + \frac{2\partial C_j}{r\partial r} \right). \quad (3.5)$$

THERIA_G calculates diffusion of Mn, Mg, Fe, and Ca, whereby Ca is treated as the dependent component. Thus, a system of three equations may be written

$$\frac{\partial C_{Mn}}{\partial t} = D_{MnMn} \left(\frac{\partial^2 C_{Mn}}{\partial r^2} + \frac{2\partial C_{Mn}}{r\partial r} \right) \quad (3.6a)$$

$$+ D_{MnFe} \left(\frac{\partial^2 C_{Fe}}{\partial r^2} + \frac{2\partial C_{Fe}}{r\partial r} \right) \quad (3.6b)$$

$$+ D_{MnMg} \left(\frac{\partial^2 C_{Mg}}{\partial r^2} + \frac{2\partial C_{Mg}}{r\partial r} \right) \quad (3.6c)$$

$$\frac{\partial C_{Fe}}{\partial t} = D_{FeMn} \left(\frac{\partial^2 C_{Mn}}{\partial r^2} + \frac{2\partial C_{Mn}}{r\partial r} \right) \quad (3.7a)$$

$$+ D_{FeFe} \left(\frac{\partial^2 C_{Fe}}{\partial r^2} + \frac{2\partial C_{Fe}}{r\partial r} \right) \quad (3.7b)$$

$$+ D_{FeMg} \left(\frac{\partial^2 C_{Mg}}{\partial r^2} + \frac{2\partial C_{Mg}}{r\partial r} \right) \quad (3.7c)$$

$$\frac{\partial C_{Mg}}{\partial t} = D_{MgMn} \left(\frac{\partial^2 C_{Mn}}{\partial r^2} + \frac{2\partial C_{Mn}}{r\partial r} \right) \quad (3.8a)$$

$$+ D_{MgFe} \left(\frac{\partial^2 C_{Fe}}{\partial r^2} + \frac{2\partial C_{Fe}}{r\partial r} \right) \quad (3.8b)$$

$$+ D_{MgMg} \left(\frac{\partial^2 C_{Mg}}{\partial r^2} + \frac{2\partial C_{Mg}}{r\partial r} \right) \quad (3.8c)$$

which THERIA_G solves numerically using a Finite Difference Method (FDM). The Crank-Nicolson scheme (Crank and Nicolson, 1947) is used as the discretization algorithm, whereby an irregular spatial grid is considered. As a result, (3.6a) can be expressed as

$$\begin{aligned} \frac{D_{MnMn}}{r\Delta r_2\Delta r_1} \times & \left(\frac{r\Delta r_1 C_{Mn,n+1}^{m+1} - r\Delta r_1 C_{Mn,n}^{m+1}}{(\Delta r_2 + \Delta r_1)} \right. \\ & \frac{-r\Delta r_2 C_{Mn,n}^{m+1} + r\Delta r_2 C_{Mn,n-1}^{m+1}}{(\Delta r_2 + \Delta r_1)} \\ & + \frac{(\Delta r_1)^2 C_{Mn,n+1}^{m+1} - (\Delta r_1)^2 C_{Mn,n}^{m+1}}{(\Delta r_2 + \Delta r_1)} \\ & \left. + \frac{(\Delta r_2)^2 C_{Mn,n}^{m+1} - (\Delta r_2)^2 C_{Mn,n-1}^{m+1}}{(\Delta r_2 + \Delta r_1)} \right) \end{aligned}$$

$$\begin{aligned}
& + \frac{D_{MnMn}}{r\Delta r_2\Delta r_1} \times \left(\frac{r\Delta r_1 C_{Mn,n+1}^m - r\Delta r_1 C_{Mn,n}^m}{(\Delta r_2 + \Delta r_1)} \right. \\
& \quad \left. \frac{-r\Delta r_2 C_{Mn,n}^m + r\Delta r_2 C_{Mn,n-1}^m}{(\Delta r_2 + \Delta r_1)} \right. \\
& \quad \left. \frac{+(\Delta r_1)^2 C_{Mn,n+1}^m - (\Delta r_1)^2 C_{Mn,n}^m}{(\Delta r_2 + \Delta r_1)} \right. \\
& \quad \left. \frac{+(\Delta r_2)^2 C_{Mn,n}^m - (\Delta r_2)^2 C_{Mn,n-1}^m}{(\Delta r_2 + \Delta r_1)} \right),
\end{aligned}$$

where n and m are nodes of a radius–time (r - t) grid, respectively. The terms Δr_1 and Δr_2 correspond to the spatial steps at both sides of a specific grid node. To account for thin shells that may result from changes in the garnet-bearing assemblages during an incremental step in P and T , the spatial grid is treated as irregular. In principle, the irregularity of the r - t grid contributes to the numerical error that stems from discretization of (3.5). Since the majority of the spatial steps Δr_1 and Δr_2 have the predefined size of Δr_{shell} , the numerical error is kept at a minimum. Nevertheless, the number of shells plays an essential role: The more shells a garnet contains, the smaller is the numerical imprecision that results from discretization.

If (3.7) - (3.8) are treated accordingly, the discretized form of (3.5) is obtained. Solution of this equation requires specification of initial and boundary conditions.

At the inner boundary, $n = 0$, equation (3.5) is replaced by

$$\frac{\partial C_i}{\partial t} = \sum_i^{n-1} 3D_{ij} \frac{\partial^2 C_j}{\partial r^2} \quad (3.9)$$

(Evans et al., 1999). In order to close the inner boundary symmetrically, a fictitious node $n_{f1} = -1$ is introduced, which matches node $n = 1$ with respect to its chemical composition and distance to $n = 0$. Hence, at $n = 0$

$$\begin{aligned}
\Delta r_1 &= \Delta r_2 \\
C_{i,n-1}^m &= C_{i,n+1}^m \\
C_{i,n-1}^{m+1} &= C_{i,n+1}^{m+1}.
\end{aligned}$$

The composition of garnet at the outer boundary is calculated by THERIAK for the current thermodynamically relevant bulk rock composition. This composition as well as the external

conditions are held constant during the diffusion step. Therefore, a flux across the garnet/matrix boundary is initiated, which is monitored to adjust the bulk rock composition accordingly after each diffusion step. If the quantity of a component i that should enter garnet exceeds the size of the respective matrix reservoir, the garnet is closed for diffusional exchange with the matrix. Consequently, – in this specific situation – chemical fractionation during garnet growth will be the only process that changes the composition of the thermodynamically relevant bulk rock composition.

For a complete formulation of the system of equations (3.6) – (3.8) considering the boundary conditions and employing the Crank-Nicolson scheme, see Appendix B.2. The system of equations is simultaneously solved after each time step, Δt , for $C_{Mn,n}^{m+1}$, $C_{Fe,n}^{m+1}$, and $C_{Mg,n}^{m+1}$ by Gaussian elimination. To account for appropriate accuracy, Δt is calculated by

$$\Delta t = \frac{\Delta r_{shell}}{10D_L}, \quad (3.10)$$

where D_L corresponds to the largest of the interdiffusion coefficients, D_{ij} , that are recalculated employing relation (3.2) and (3.3) after each time step. If Δt is larger than the period of time that is related to the change of the external conditions P and T as defined in the P - T - t path, a value, which is about 10-times smaller than this period, is used.

3.3.3 Consideration of garnet growth kinetics

In THERIA_G modeling the garnet growth rate is solely controlled by the rate at which the rock evolves along its P - T path. At any time during garnet growth thermodynamic equilibrium is assumed to be maintained between the rim of the garnet crystals and the rock matrix. Therefore, the implementation of the THERIAK code (de Capitani and Brown, 1987) to determine the garnet rim composition is well-founded. As a consequence, THERIA_G considers component transport in the rock matrix and interface reactions to be fast relative to garnet growth. In distributing the newly formed garnet it is assumed that the radial growth rate during a specific growth increment is constant for all garnet porphyroblasts. This assumption is motivated by theoretical considerations (Kretz, 1974) and by empirical evidence (Kretz, 1993; Chernoff and Carlson, 1997; Spear and Daniel, 1998). Hence, for a given relative CSD of garnet and at the respective point in P - T - t space, THERIA_G distributes the newly formed volume of garnet onto the surfaces of the existing garnet crystals such that the radial increase is the same for each individual. As a result, the Mn content at the centres of garnet crystals of progressively smaller

Table 3.1 – Bulk rock composition of the average metapelite of Shaw (1956) (wt%).

SiO ₂	Al ₂ O ₃	Fe ₂ O ₃	MnO	MgO	CaO	Na ₂ O	K ₂ O	H ₂ O	CO ₂	Σ
59.77	16.57	6.53	0.07	2.62	2.17	1.73	3.53	2.49	5.16	100.64

size decreases. Moreover, because the growth of all garnet crystals finishes at the same time, all garnet rims have the same composition.

To simulate the formation of progressively smaller garnet crystals as part of a garnet population, THERIA_G repeatedly initiates nucleation of garnet. Nucleation of a group of garnet crystals occurs as soon as the garnet individuals that originate from the former nucleation event exceed the size of their radius class as defined by the relative CSD (Fig. 3.1). The required input parameters to model the formation of a garnet population are the number of garnet radius classes, the corresponding nucleation densities as well as the size range of the radius classes. It should be noted that only a relative CSD is used as an input; the actual size ranges of the individual radius classes result from the garnet growth simulation.

In general, THERIA_G considers garnet nucleation as an episodic process, the recurrence of which can be controlled by the choice of the number and the size of the garnet radius classes that are to be formed. That is, in contrast to Cashman and Ferry (1988), garnet CSDs are not interpreted as the result of the growth of larger individuals on the expense of smaller ones but they are treated as resulting from variations in garnet nucleation rates during garnet growth. If – theoretically – an infinite number of garnet size classes and an infinitesimally small value for the size of the radius classes is used, garnet nucleation can be seen as a continuous process with rate fluctuations.

3.4 Application of THERIA_G

To exemplify the capabilities of THERIA_G, garnet growth simulations are done for the average metapelite of Shaw (1956) (Table 3.1). The calculated equilibrium phase relations are shown in Fig. 3.2. For phase diagram calculations the bulk rock composition was taken as the effective composition, i.e. the calculated phase relations represent a situation before or at the incipient stage of garnet growth. Fig. 3.2 also shows the P - T loops along which garnet growth is simulated.

SiO₂ and H₂O were considered as excess components, implying saturation of the system with respect to quartz and an aqueous fluid along the entire P - T path. To ensure that most of the

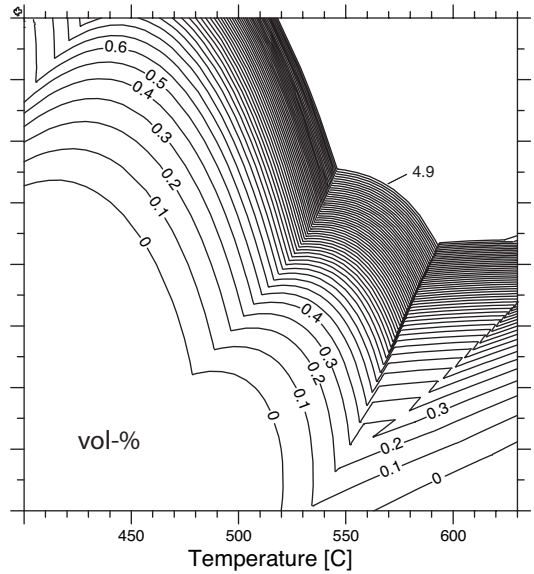
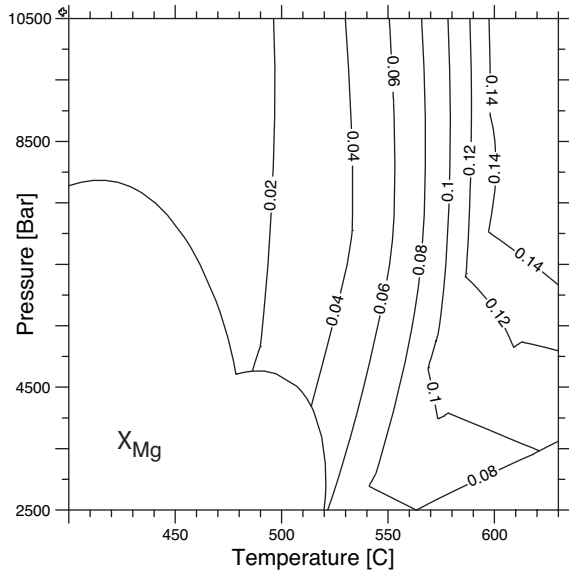
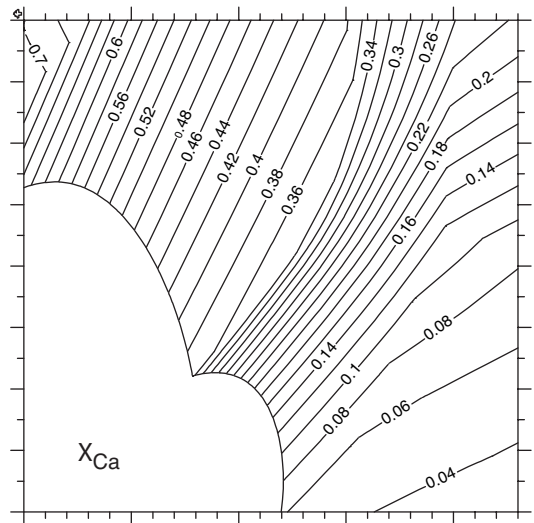
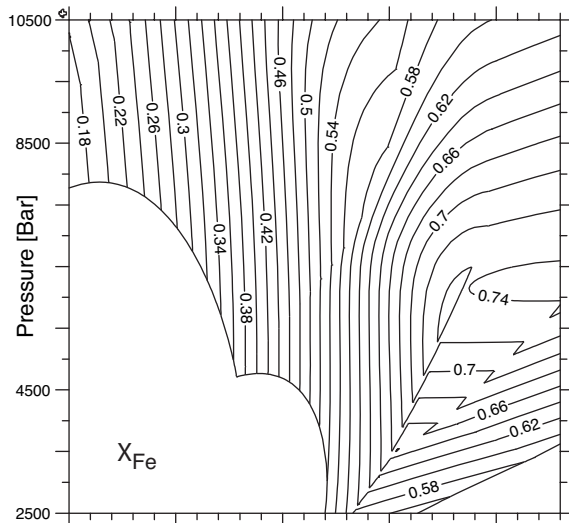
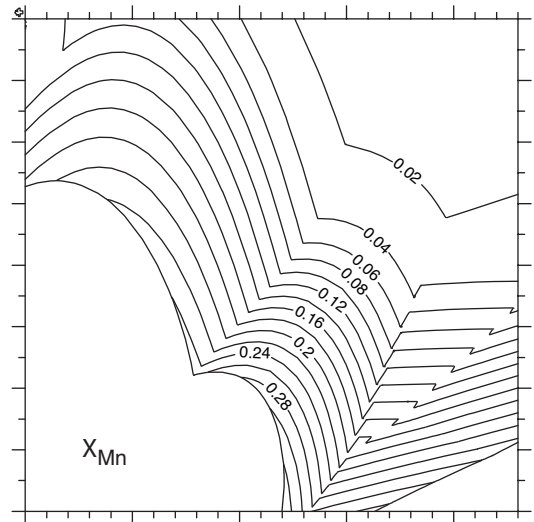
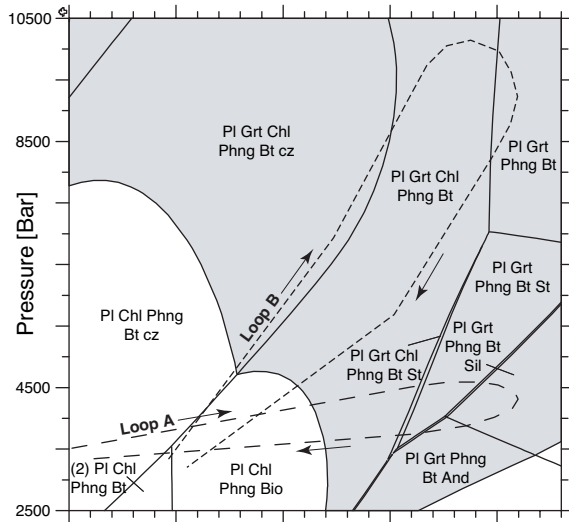
Table 3.2 – P - T - t paths for loop A (Fig. 3.2).

T (°C)	P (bar)	t (My) for a heating rate of		
		50 °C My ⁻¹	20 °C My ⁻¹	5 °C My ⁻¹
400.00000	3500.00000	0.00000	0.00000	0.00000
560.00000	4500.00000	3.20000	8.00000	32.00000
577.25424	4576.92308	3.54508	8.86271	35.45085
592.20339	4576.92308	3.84407	9.61017	38.44068
600.74576	4532.05128	4.01492	10.03729	40.14915
608.57627	4403.84615	4.17153	10.42881	41.71525
610.00000	4307.69231	4.20000	10.50000	42.00000
610.10000	4300.00000	4.20200	10.50500	42.02000
607.50847	4153.84615	4.25383	10.63458	42.53831
598.96610	4006.41026	4.42468	11.06169	44.24678
585.79661	3865.38462	4.68807	11.72017	46.88068
560.88136	3730.76923	5.18637	12.96593	51.86373
404.67359	3316.40625	8.31053	20.77632	83.10528

common rock-forming minerals in a metapelite can be considered adequately, calculations were done in the simplified model system MnO-Na₂O-CaO-K₂O-FeO-MgO-Al₂O₃-SiO₂-H₂O-TiO₂ (MnNCFMASHT) using thermodynamic data of Holland and Powell (1998) (thermodynamic database of THERMOCALC, version 3.21). The following mixing models and notations were applied: Grt [garnet; Holland and Powell (1998)], Pl [plagioclase; Newton et al. (1980)], Bt [biotite; Powell and Holland (1999), extended to cover Fe and Mn solutions], St [staurolite; Holland and Powell (1998), extended to cover Mn solutions], Phng (phengite, following the description at <http://www.esc.cam.ac.uk/astaff/holland/ds5/muscovites/mu.html>), Ilm (ilmenite, ideal ilmenite-geikiellite-pyrophanite solution), ky (kyanite), and (andalusite), sill (sillimanite), cz (clinozoisite), and qtz (quartz). For the description of the solution model for Chl (chlorite) the reader is referred to Appendix B.1. For modelling intragranular diffusion of Fe, Mg and Mn in garnet the diffusion coefficients of Chakraborty and Ganguly (1992) were used. Following the approach of Loomis et al. (1985) and Florence and Spear (1991), D_{Ca}^* was set equal to $D_{Fe}^*/2$.

To assess the influence of time on the degree of homogenization of garnet growth zoning

Figure 3.2 (facing page) – P - T phase diagram section with the garnet stability field shaded in grey and calculated garnet compositions and total vol-% of garnet for the average metapelite of Shaw (1956) (Table 3.1); the dashed lines indicate the P - T loops along which garnet growth is simulated (see Table 3.2 and Table 3.3 for detailed P - T values); SiO₂ and H₂O were considered as excess components; the calculations were done with the DOMINO software (de Capitani, 1994), which – similarly to THERIA_G – employs the THERIAK code for Gibbs free energy minimization.



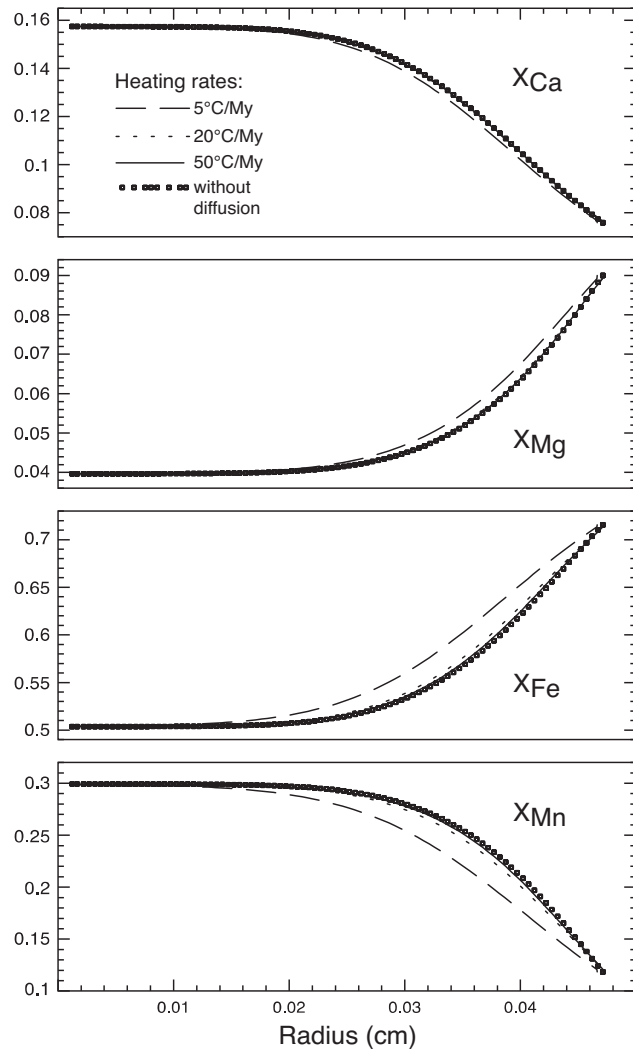


Figure 3.3 – Influence of the heating rate on the chemical composition of the largest garnet crystal (garnet of radius class 1) illustrated in Fig. 3.1. The P - T - t paths shown in Table 3.2 are used. Δr_{shell} is ca. $5 \mu\text{m}$. The compositional profile, which illustrates growth zoning, is marked with symbols.

through intragranular diffusion, different heating rates were used for two P - T paths (loop A and loop B in Fig. 3.2 as well as Table 3.2 and Table 3.3).

3.4.1 Garnet growth along P - T loop A

Fig. 3.3 shows the influence of the heating rate on the chemical composition of the largest garnet crystal that grew along P - T loop A (Fig. 3.2) for the theoretical relative CSD shown in Fig. 3.1 (CSD1). Similar crystal size frequency relations are reported by several authors (e.g. Kretz, 1966, 1993; Cashman and Ferry, 1988) for a number of metamorphic minerals. Fig. 3.3 clearly shows that the growth zoning of the largest garnet in the corresponding rock volume

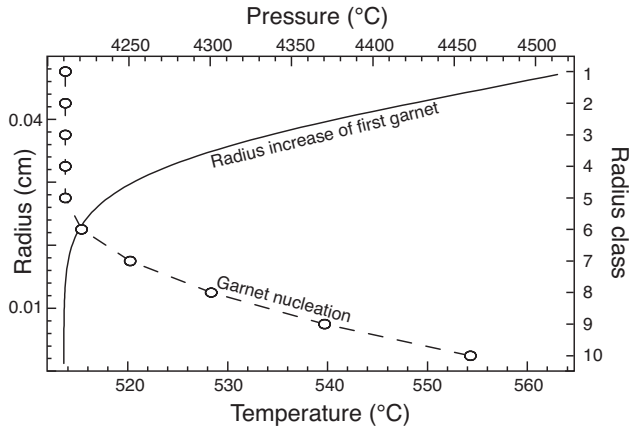


Figure 3.4 – Relation between changes of the P - T conditions and the size of the oldest garnet crystal (solid line) calculated for P - T loop A (Fig. 3.2 and Table 3.2) and CSD1 (Fig. 3.1). In addition, the P - T conditions at the time of nucleation of garnet from the different size classes are displayed (open circles along the dashed line).

is significantly modified at a heating rate of $5\text{ }^{\circ}\text{C My}^{-1}$. In garnet, diffusion of Mn and Fe is substantially faster than diffusion of Ca and Mg (Chakraborty and Ganguly, 1992). In Fig. 3.3 the modification of garnet growth zoning is more pronounced for Mn and Fe than for Mg and Ca, accordingly. At heating rates larger than $20\text{ }^{\circ}\text{C My}^{-1}$ modification of the growth zoning by intracrystalline diffusion becomes negligible.

The original composition of the core regions of the oldest garnet individuals is largely preserved even at slow heating rates. This is due to the fact that during the incipient stages of garnet growth the increments in P and T needed to produce a shell of thickness Δr_{shell} are relatively small. As a consequence the innermost portions of the garnets form over a small range of P - T conditions, and core compositions are rather homogeneous. Therefore compositional gradients and diffusional fluxes are small (Fig. 3.4).

During later stages of garnet growth the P and T increments needed to produce successive shells of thickness Δr_{shell} increase. This is why compositional gradients and the resulting diffusional fluxes are higher in small garnet crystals that originate at later stages in the nucleation interval than in garnet individuals, which nucleated earlier. Hence, modification of the growth zoning becomes successively more pronounced for younger garnet crystals (Figs. 3.5).

In our example, garnet crystals that pertain to radius class 3 are the first garnet individuals, where modification of the growth zoning in the core region is readily detected for a heating rate of $5\text{ }^{\circ}\text{C My}^{-1}$ (Figs. 3.5 and 3.6). For all garnet porphyroblasts, which started to grow subsequent to garnet from radius class 3, the growth zoning was modified substantially by intragranular diffusion. For crystals of radius class 10 intragranular diffusion even lead to a complete obliteration of the Ca and Mg growth zoning.

In this scenario, the initial compositions of all contemporaneously growing garnet shells

Figure 3.5 – Influence of diffusional relaxation in garnet (lines) on garnet growth zoning (symbols) illustrated for X_{Mn} considering CSD1 and a heating rate of $5\text{ }^{\circ}\text{C My}^{-1}$ along loop A. Numbers correspond to the labels of the radius classes denoted in Fig. 3.1. Δr_{shell} is ca. $5\text{ }\mu\text{m}$.

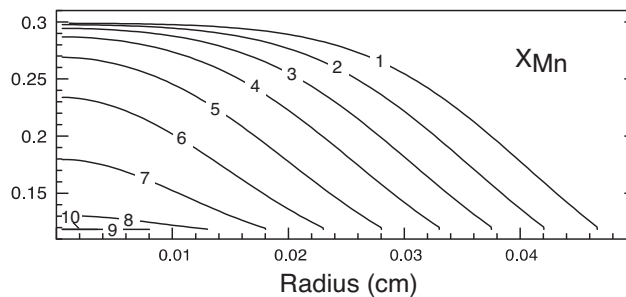
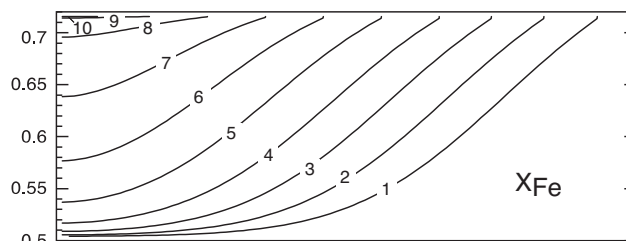
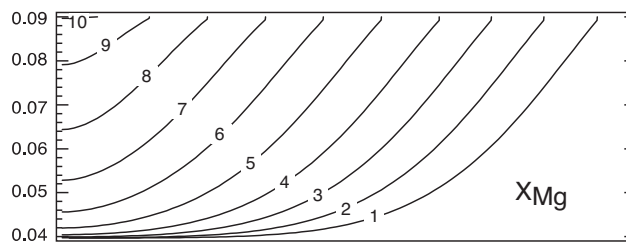
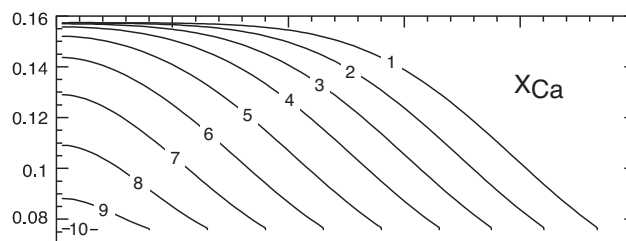
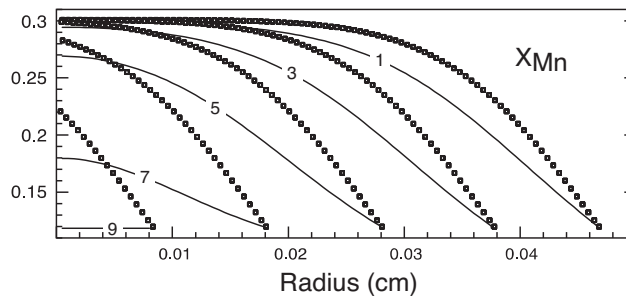


Figure 3.6 – Compositional profiles of the garnet porphyroblasts computed for CSD1 (Fig. 3.1) and a heating rate of $5\text{ }^{\circ}\text{C My}^{-1}$ along loop A. Numbers correspond to the labels of the radius classes denoted in Fig. 3.1. Δr_{shell} is ca. $5\text{ }\mu\text{m}$.

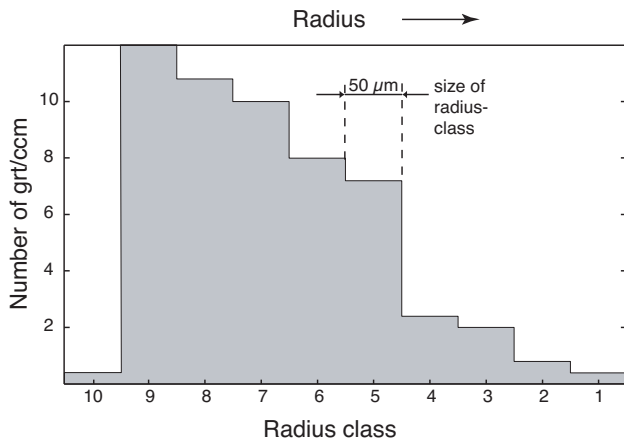


Figure 3.7 – Relative garnet crystal size frequency distribution (CSD2) used for the calculation of garnet chemical composition illustrated in Fig. 3.8.

and the compositional gradients between successive shells are similar for all garnets (compare Carlson, 1989; Kretz, 1993; Spear and Daniel, 1998). As a consequence, the initial composition of a given succession of growth shells that represents the core region of a garnet that grew at a late stage in the thermal history may correspond to the growth zoning of a peripheral region in a previously formed garnet (Fig. 3.5).

In general, the number of garnet crystals per rock volume, which grew early in the thermal history, is markedly smaller than the amount of younger crystals in the rock for similar garnet crystal size frequency relations (Fig. 3.1). This needs to be taken into account, if P - T estimates for the incipient stages of garnet growth are to be determined from primary core chemistries of garnet that grew in a bulk rock chemistry similar to the average metapelite of Shaw (1956) and experienced a comparable geothermal history.

Garnet growth simulation along P - T loop A, which were forced to develop a theoretical relative CSD as illustrated in Fig. 3.7 (CSD2), produces bigger garnet individuals than the calculations for CSD1 (Fig. 3.1). Even though the total amount of garnet per rock volume is the same for both CSDs, the simulation that is based on CSD2 results in slightly different garnet compositions (Fig. 3.8). The most conspicuous difference is the Mg and Ca zoning of the youngest garnet crystals, which is not completely homogenized.

Garnet growth along loop A ceases when staurolite becomes stable. From this point on, the P - T path passes below the low pressure limit of the garnet stability field (see Fig. 3.9). Note that the garnet stability field in Fig. 3.9 is substantially smaller than in Fig. 3.2. This is due to changes in the effective bulk rock composition through chemical fractionation during garnet growth and through diffusional fluxes between garnet and the matrix. The latter strongly depends on the extent of relaxation of compositional gradients through intragranular diffusion

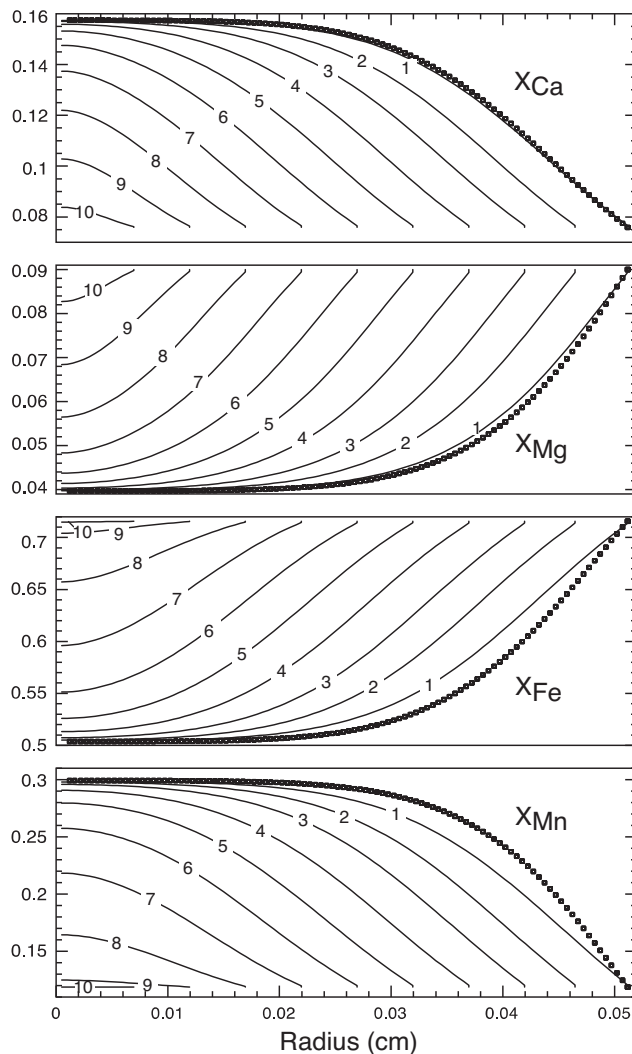


Figure 3.8 – Compositional profiles of the garnet porphyroblasts computed for CSD2 (Fig. 3.7) and a heating rate of $5\text{ }^{\circ}\text{C My}^{-1}$ along P - T loop A. The compositional profile of the oldest garnet crystal, which illustrates garnet growth zoning, is marked with symbols. Numbers correspond to the labels of the radius classes denoted in Fig. 3.7. Δr_{shell} is ca. $5\text{ }\mu\text{m}$.

and, hence, on CSD and heating rate. Both parameters were specified for constructing Fig. 3.9.

3.4.2 Garnet growth along P - T loop B

To simulate the growth of garnet along P - T loop B (Fig. 3.2 and Table 3.3), a relative garnet crystal size frequency relation is used which exactly matches CSD1 (Fig. 3.1) but differs with respect to the size of the radius classes. In order to limit the number of different radius classes to a maximum of 10, a size of $150\text{ }\mu\text{m}$ is used for each radius class.

The calculated initial compositional profile of garnet from radius class 4 and the influence

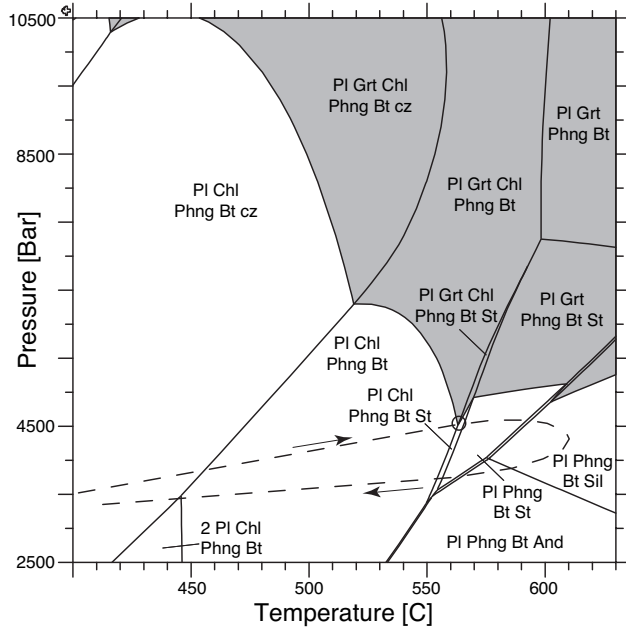


Figure 3.9 – P - T phase diagram section illustrating the equilibrium phase relations and P - T conditions at which garnet growth ceases along P - T loop A for a heating rate of $5\text{ }^{\circ}\text{C My}^{-1}$ and CSD1 (Fig. 3.1). The conditions where garnet first becomes unstable are marked with an open circle.

T ($^{\circ}\text{C}$)	P (bar)	t (My) for a heating rate of		
		$50\text{ }^{\circ}\text{C My}^{-1}$	$20\text{ }^{\circ}\text{C My}^{-1}$	$5\text{ }^{\circ}\text{C My}^{-1}$
446.17989	3345.11121	0.00000	0.00000	0.00000
523.58062	6935.51254	1.54801	3.87004	15.48015
560.04451	9270.83333	2.27729	5.69323	22.77292
567.55193	9739.58333	2.42744	6.06860	24.27441
577.10682	10062.50000	2.61854	6.54635	26.18539
588.02671	10145.83333	2.83694	7.09234	28.36936
601.33531	9968.75000	3.10311	7.75777	31.03108
607.13650	9625.00000	3.21913	8.04783	32.19132
610.10000	9229.16667	3.27840	8.19601	32.78402
606.79525	8781.25000	3.34450	8.36124	33.44497
598.26409	8250.00000	3.51512	8.78780	35.15120
551.91482	5687.51208	4.44211	11.10526	44.42106
454.81836	3210.71116	6.38403	15.96009	63.84035

Table 3.3 – P - T - t paths for loop B (Fig. 3.2).

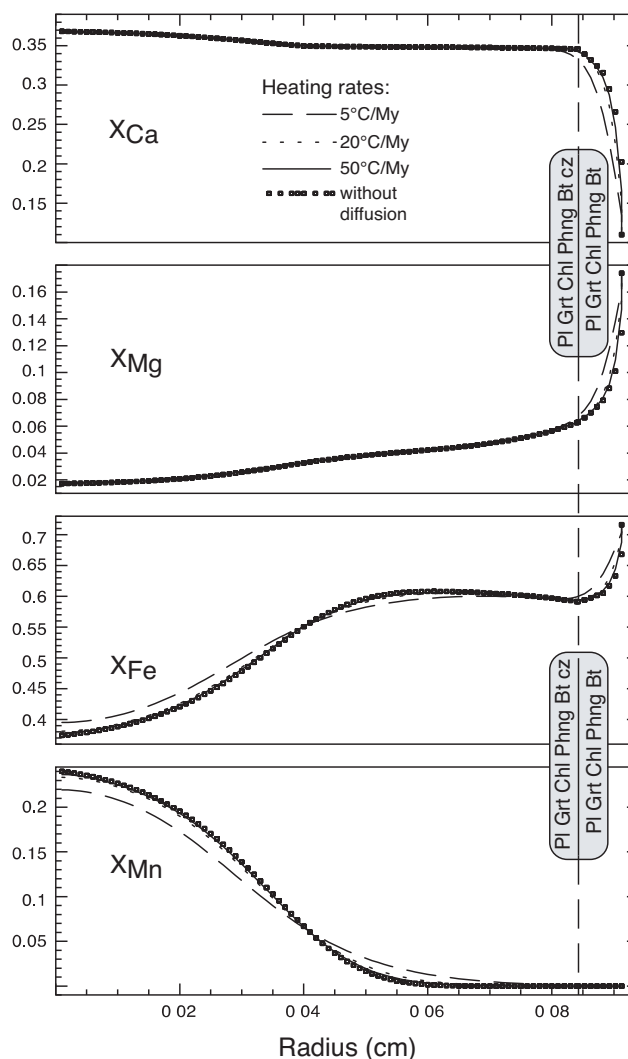


Figure 3.10 – Influence of different heating rates on the chemical composition of garnet that pertains to the fourth radius class and grew along P - T loop B (Fig. 3.2). Δr_{shell} is ca. $10 \mu\text{m}$. One change of the equilibrium assemblage is marked. The CSD encountered along loop B corresponds to the one displayed in Fig. 3.1, where a value of $150 \mu\text{m}$ is used as the size of the radius class. The symbols mark growth zoning.

of intragranular diffusion for different heating rates on garnet growth zoning is illustrated in Fig. 3.10. At a heating rate of $5 \text{ }^\circ\text{C My}^{-1}$ the Fe and Mn concentrations in the garnet core are substantially reduced as compared to the initial composition.

The number of garnet porphyroblasts that pertain to radius class 4 is substantially larger than the number of older crystals, which – in the course of petrographic investigations – may lead to an overestimation of the relative age of individuals from this size class.

In addition, the point along loop B where clinozoisite becomes unstable is indicated in Fig. 3.10. Clinozoisite as well as plagioclase are the main suppliers of Ca for the formation of the grossular component of garnet. When clinozoisite disappears the Ca supply decreases

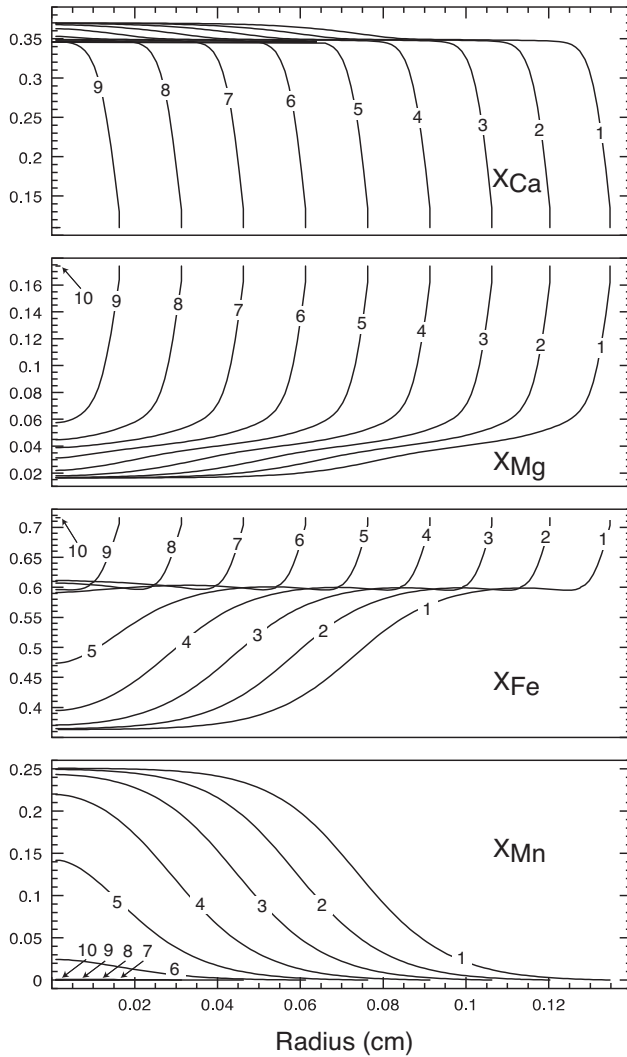


Figure 3.11 – Compositional profiles of the garnet porphyroblasts computed for CSD1 (Fig. 3.1) with $150\ \mu\text{m}$ as the size of the radius class and a heating rate of $5\ ^\circ\text{C}\ \text{My}^{-1}$ along P - T loop B. Numbers correspond to the labels of the radius classes denoted in Fig. 3.1. Δr_{shell} is ca. $10\ \mu\text{m}$.

substantially. As a consequence the grossular content of garnet decreases rapidly whereas X_{Mg} and X_{Fe} increase concomitantly.

The calculated compositional profiles of all the garnet crystals that grew along P - T loop B at a heating rate of $5\ ^\circ\text{C}\ \text{My}^{-1}$ are shown in Fig. 3.11. Garnet porphyroblasts that pertain to the radius classes 7 to 10 are completely homogenized with respect to their Mn zoning. It is interesting to note that garnet from radius class 7 is approximately as big as the first garnet that grew along P - T loop A for both CSD1 and CSD2 (Figs. 3.1, 3.7). However, the zoning pattern of garnet that grew along loop A is only slightly modified by intragranular diffusion even though it grew at the same heating rate and experienced exactly the same maximum temperature during

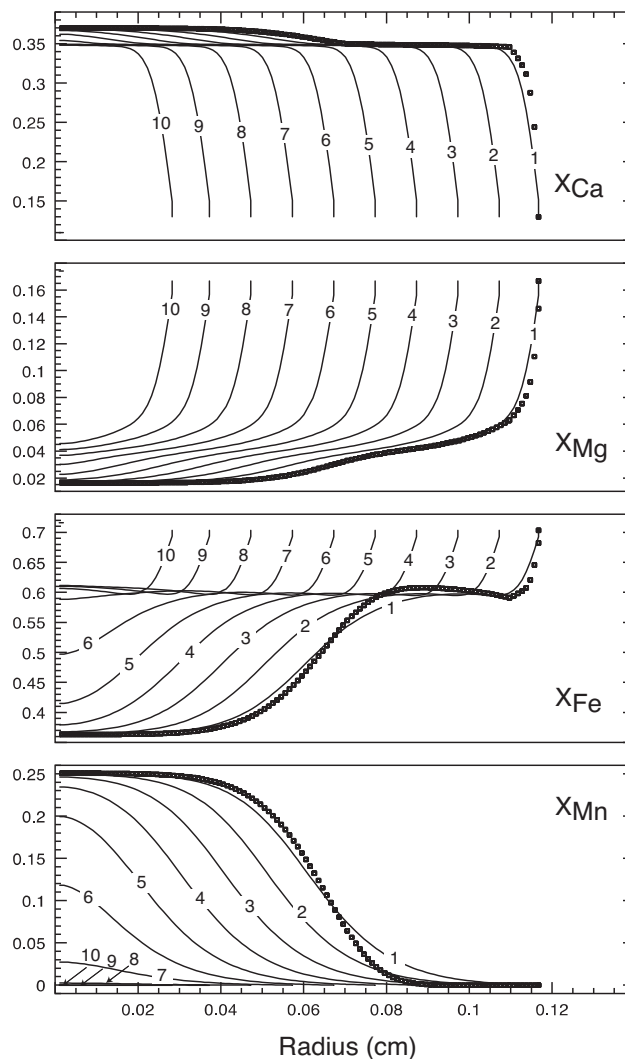


Figure 3.12 – Compositional profiles of the garnet porphyroblasts calculated for the case that garnet nucleation ceases prior to garnet growth (see text for explanation). Garnet is forced to produce CSD1 (Fig. 3.1) with $100\ \mu\text{m}$ as the size of the radius class along P - T loop B. The heating rate is $5\ \text{°C My}^{-1}$. For Δr_{shell} a value of $10\ \mu\text{m}$ was chosen.

its geothermal history (Tables 3.2, 3.3). This difference can be explained by the fact that the Mn concentrations show notably larger gradients for garnets that grow along P - T loop B than for those which grow along loop A.

Furthermore, due to the fact that the amount of garnet produced along P - T loop B is larger than the amount of garnet that is formed along P - T loop A, the oldest garnet individuals originating along P - T loop B are significantly larger than those, which grew along P - T loop A. Because of the garnet growth model implemented in THERIA_G, the steep chemical gradient is shifted into the core regions of garnet, which nucleated late in the nucleation interval. Therefore, the effectiveness of homogenisation by diffusion is substantially enhanced and may lead to

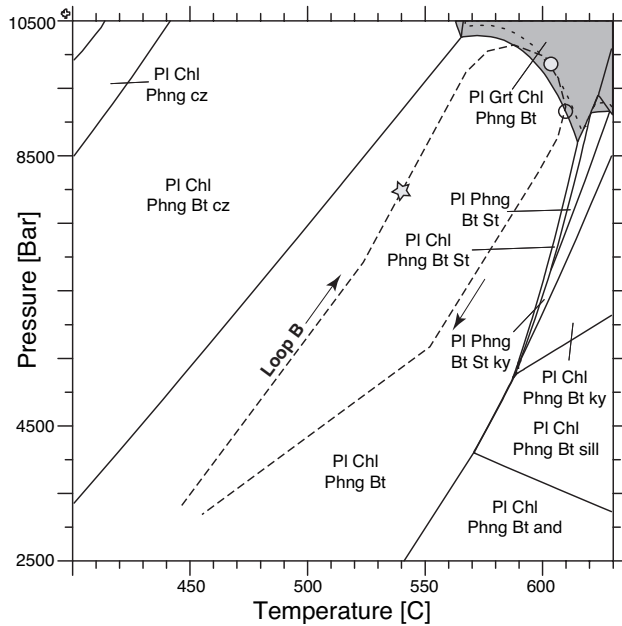


Figure 3.13 – P - T phase diagram section illustrating the equilibrium phase relations and P - T conditions at which garnet nucleation and growth finish along P - T loop B for a heating rate of $5\text{ }^{\circ}\text{C My}^{-1}$ (open circle). Garnet growth was forced to develop CSD1 (Fig. 3.1) with a value of $150\text{ }\mu\text{m}$ as the size of the radius class. In addition, the filled circle marks the P - T conditions, at which garnet growth ceases, if nucleation stops prior to garnet growth (star). For this simulation, CSD1 (Fig. 3.1) was used with a value of $100\text{ }\mu\text{m}$ as the size of the radius class (see text for explanations).

complete homogenisation in garnet of radius classes 7-10.

To account for a scenario where garnet nucleation ceases before garnet growth ends, the theoretical relative CSD1 (Fig. 3.1) is used and a value of $100\text{ }\mu\text{m}$ is employed for the size of the radius class. This approach terminates in the decrease of the size of garnet grains from radius classes 1 to 4 and leads to the enlargement of younger grains if compared with the former results (Fig. 3.11 and Fig. 3.12). The P - T conditions, at which garnet nucleation stops, are marked in Fig. 3.13.

A further consequence of the condensed period of garnet nucleation is the reduction of the garnet stability field. In contrast to concomitant garnet nucleation and growth, the formation of garnet ceases at conditions before the prograde part of the P - T path ends (filled circle in Fig. 3.13). This may be explained by remarkable intragranular diffusional fluxes in garnet crystals, which originated from late stages of the geothermal history. In such cases, the chemical composition of the matrix changes, if the diffusion module implemented in THERIA.G regards the outer boundary of the garnet crystals as open. That is, both processes, chemical fractionation associated with garnet growth as well as effective diffusional relaxation in garnet, modify the thermodynamically relevant bulk rock composition, but both processes operate in opposite directions.

3.5 Discussion

The main assumption behind THERIA_G modelling is that the garnet crystal, which is treated as an undeformed sphere, devoid of any mineral inclusions and cracks, has a rim that is always in thermodynamic equilibrium with the matrix during growth. For a thermodynamical homogeneous matrix intergranular diffusion of the reacting species has to be faster than the rates of precursor decomposition and garnet precipitation. This is likely as long as garnet grows along a prograde P - T path in a hydrous rock, which experienced only low grade metamorphic conditions prior to garnet formation. In such a case, gradients in the chemical potential of each reacting species that form at the garnet/matrix interface are small and thermodynamic equilibrium can be considered to be maintained over volume domains of hand specimen size or even on a larger scale.

In general, the rate of garnet crystallisation is effected by the rates of material transport in the rock matrix and by the rates of interface reactions at the surfaces of precursor phases and the evolving garnet porphyroblast. If the growth rate of a garnet porphyroblast is controlled by reactions at the surface of the growing crystal the growth rate law follows the form

$$\frac{dV}{dt} \approx Ak\Delta_r G \quad (3.11)$$

where V and A correspond to volume and surface of the growing crystal, respectively, k is a rate constant and $\Delta_r G$ is the driving force for the reaction (compare Kretz, 1974, 1993; Carlson, 1989).

For spherical geometry (3.11) takes the form

$$\frac{dr}{dt} \approx k\Delta_r G, \quad (3.12)$$

which indicates, that for interface-controlled growth crystals of all sizes grow with the same radial rate. Simulations performed by Spear and Daniel (1998) using the geometric limitations of (3.12) and varying nucleation densities during garnet growth yielded compositional profiles, which are parallel at all concentrations for the crystals of different size. Such a geometric relation was repeatedly observed for MnO, FeO, and MgO in garnet of metapelites (e.g. Kretz, 1993; Chernoff and Carlson, 1997; Spear and Daniel, 1998; Zeh, 2006). As described above, THERIA_G considers this relation for the distribution of newly formed garnet on pre-existing crystals during each growth increment. However, due to the lack of information on interface

kinetics the variations of the chemical potentials of the reacting species around garnet, which stem from the reactions at the surface of garnet, can not be taken into account sufficiently.

THERIA.G modelling to simulate garnet growth in dehydrated rocks is considered problematic, because dehydration strongly influences the efficiency of intergranular material transport (Keller et al., 2007). If transport of material is sluggish compared to the rate of interface reactions, the rate of garnet growth may be controlled by intergranular diffusion and, as a consequence, gradients in the chemical potentials of the reacting species evolve and progressively enlarge in the vicinity of the growing garnet (Carlson, 1989; Spear and Daniel, 2001). In such cases the size of equilibration domains may be so small that a single garnet porphyroblast pertains to different equilibration domains. Systematic variations of garnet rim compositions give evidence for such behavior and have been reported from retrograde reactions in high grade rocks (Hauzenberger et al., 2005; Keller et al., 2007) and from garnet rim growth at eclogite facies conditions (Keller et al., 2006). In addition, competitive growth of several neighbouring garnet grains may occur (Carlson, 1991).

The radial growth-rate law for intergranular diffusion-controlled growth takes the form

$$\frac{dr}{d\sqrt{t}} \approx k\Delta_r G \quad (3.13)$$

(compare Christian, 1975). Reformulation of (3.13) yields

$$\frac{dr}{dt} \approx \frac{k}{r} \Delta_r G, \quad (3.14)$$

which indicates that for diffusion-controlled garnet growth the radial rate depends on the size of the garnet crystals, i.e. smaller garnet crystals will grow faster than large porphyroblasts.

The radius-rate relation illustrated in Fig. 3.4 directly results from the quasi-linear increase of garnet volume with time assuming a constant heating rate and following the principles of equilibrium thermodynamics. Departure from the linear relationship between garnet volume and temperature only occurs at conditions, at which the composition of the equilibrium phase assemblage changes. These findings strongly conflict with the suggestion of Kretz (1974, 1993), where the garnet production rate is highly acceleratory.

Because in our model the matrix is assumed to be thermodynamical homogeneous with fast component diffusion, the simulation of retrograde exchange reactions between the rim of garnet and specific matrix phases (e.g. Florence and Spear, 1995; Keller et al., 2007) is not implemented. However, since this process is commonly restricted to the outermost few 10 – 50

μm , its contribution to the principle compositional configuration of garnet is small.

It is important to note, that resorption processes may strongly modify garnet chemical composition and morphology. Even along the prograde part of a P - T path, periods of garnet instability may occur framed by stages of garnet stability (Gaidies et al., *subm.b*). However, since information on the kinetics of garnet resorption is scarce, the influence of resorption during periods of garnet instability is not considered in our model.

Our simulations predict compositional profiles for the oldest garnet in a given volume of rock to be marked with a flat chemical pattern for all the major components in the core region. Progressively younger grains show steeper gradients in their cores. Steep compositional gradients in garnet cores are, however, rarely reported. We suggest, that the typical bell-shaped Mn-curves, which are frequently observed in greenschist to amphibolite facies rocks, result from diffusional relaxation of steep compositional gradients in younger garnet. It should be noticed that this effect is only relevant for sections that crosscut the core of a garnet crystal. Sections, which do not intersect the core, will always produce bell-shaped Mn-gradients.

Moreover, it can be hypothesised, that in the case of substantial reaction overstepping, the rate of garnet nucleation may be high already for the first stages in the nucleation interval. In this case, the number of comparatively large garnet grains with a flat chemical gradient in their cores will increase.

3.6 Conclusions

With the development of the software program THERIA_G earlier work to simulate the formation of compositional profiles in garnet (e.g. Cygan and Lasaga, 1982; Loomis, 1982; Spear, 1988; Spear et al., 1991a; Florence and Spear, 1991) is extended to garnet populations. Garnet growth can now be modelled based on the well-founded concepts of equilibrium thermodynamics in complex chemical systems and multicomponent diffusional transport in simple geometries. Based on the assumption that the radial growth rate is similar for all garnet porphyroblasts at a given point in time any predefined garnet crystal size frequency distribution can be produced. This offers the opportunity to compare garnet chemistries as well as garnet crystal size frequency distributions that are simulated for predefined conditions with field observations.

Garnet growth simulation with THERIA_G clearly demonstrates that the chemical zoning of garnet porphyroblasts may be influenced by chemical fractionation between matrix and garnet during growth, intracrystalline diffusion in garnet and the nucleation history. In particular it is

shown that the sensitivity of garnet growth zoning to modification by intracrystalline diffusion is different for garnet crystals that nucleated at different stages of the nucleation history. Whereas early nucleated garnet individuals tend to have relatively flat chemical zoning patterns in their cores, garnet crystals that nucleated late may have sharp compositional gradients in their growth zoning, which are prone to modification through intracrystalline diffusion.

Finally, the software program THERIA_G is suggested as a powerful tool for unravelling the metamorphic history of garnet bearing rocks from the investigation of garnet chemical zoning. Furthermore, it may allow for testing models for the kinetics of garnet nucleation and growth.

3.7 Acknowledgements

The current study was strongly inspired by the CUSO short course on "Diffusion in geological materials", held in 2005 at Basel University. In addition, the study benefited from discussions with M. Grote, L. Keller, T. Heijboer and R. Dohmen.

Chapter 4

Prograde garnet growth along complex P - T - t paths: Results from numerical experiments on polyphase garnet from the Wölz Complex (Austroalpine basement)

This chapter is under review as: **Gaidies, F.**, de Capitani, C., Abart, R. and Schuster, R., 2007. Prograde garnet growth along complex P - T - t paths: Results from numerical experiments on polyphase garnet from the Wölz Complex (Austroalpine basement). *Contributions to Mineralogy and Petrology*.

4.1 Abstract

Garnet in metapelites from the Wölz Complex of the Austroalpine crystalline basement east of the Tauern Window characteristically consists of two growth phases, which preserve a comprehensive record of the geothermal history during polymetamorphism. From numerical modelling of garnet formation, detailed information on the pressure-temperature-time (P - T - t) evolution during prograde metamorphism are obtained. In that respect, the combined influences of chemical fractionation associated with garnet growth, modification of the original growth zoning

through intragranular diffusion and the nucleation history on the chemical zoning of garnet as P and T change during growth are considered. The concentric chemical zoning observed in garnet and the homogenous rock matrix, which is devoid of chemical segregation, render the simulation of garnet growth through successive equilibrium states reliable.

Whereas the first growth phase of garnet was formed at isobaric conditions of ~ 3.8 kbar at low heating/cooling rates the second growth phase grew along a Barrovian P - T path marked with a thermal peak of ~ 625 °C at ~ 10 kbar and a maximum in P of ~ 10.4 kbar at ~ 610 °C. For the heating rate during the growth of the second phase of garnet, rates faster than 50 °C Ma^{-1} are obtained. From geochronological investigations the first growth phase of garnet from the Wölz Complex pertains to the Permian metamorphic event. The second growth phase grew in the course of Eo-Alpine metamorphism during the Cretaceous.

4.2 Introduction

Due to slow diffusion within garnet at conditions of low to medium grade metamorphism (e.g. Loomis et al., 1985; Chakraborty and Ganguly, 1992; Vielzeuf et al., 2007), the compositions that a garnet acquires during growth have high potential to be preserved as chemical zoning. If chemical transport in the rock matrix is fast relative to the rate of garnet growth, successive growth increments may form in thermodynamic equilibrium with the remainder of the phases present in the rock matrix. In this case, the growth zoning of garnet reflects the equilibrium partitioning of the chemical components between the growing garnet and the rock matrix. As the equilibrium partitioning varies with pressure (P) and temperature (T), the chemical zoning of garnet bears thermobarometric information on the portion of the P - T trajectory, over which it was formed (Spear, 1993).

Estimates for the P - T conditions that prevailed during garnet growth may be obtained from garnet isopleth thermobarometry (Evans, 2004; Gaidies et al., 2006; Stowell et al., 2001; Vance and Mahar, 1998; Zeh, 2001; Zeh and Holness, 2003). This technique is based on equilibrium thermodynamic concepts and makes use of the compositional relations between the matrix and the garnet porphyroblast. In garnet isopleth thermobarometry, observed chemical compositions of garnet growth increments in a given volume of rock are compared with garnet compositions that are calculated from phase equilibria for the respective bulk rock composition. Given that mass transport in the rock matrix is fast compared to garnet growth, the composition of the matrix is the thermodynamically relevant bulk composition. Because of the limited efficiency

of diffusion within garnet, the chemical components that are incorporated into garnet during growth are effectively removed from the rock matrix. This process is commonly referred to as chemical fractionation (e.g. Hollister, 1966; Atherton, 1968) and may substantially change the chemical composition of the rock matrix. Therefore, chemical fractionation must be accounted for, if garnet isopleth thermobarometry is to be applied to successive growth increments of a garnet porphyroblast (e.g. Gaidies et al., 2006; Evans, 2004).

Garnet isopleth thermobarometry applied to successive garnet growth increments yields information on the P - T conditions over the entire interval of garnet growth (Evans, 2004; Gaidies et al., 2006). In garnet isopleth thermobarometry it is commonly assumed that diffusion within garnet is infinitely slow so that the original chemical zoning is preserved without modification. In this study we drop the assumption of infinitely slow diffusion within garnet, and we investigate the potential effects of intracrystalline diffusion on the chemical zoning pattern of garnet porphyroblasts.

The efficiency of intragranular diffusion depends on component mobility and the gradients of the respective chemical potentials, where the latter are related to compositional gradients in the growth zoning of garnet. It has been argued by Gaidies et al. (subm.a) that sharp maxima in manganese concentration may develop in the cores of garnet porphyroblasts that nucleate late during a metamorphic event. Such sharp maxima are effectively degraded by the diffusive loss of manganese from the core region. If garnet isopleth thermobarometry is applied to such regions of a garnet this may systematically overestimate T , because – for a given bulk rock composition – the spessartine content of garnet is very sensitive to T .

Large compositional gradients in garnet also occur at those growth increments that coincide with changes in the thermodynamically stable mineral assemblage (Gaidies et al., subm.a). Such changes in paragenesis may occur repeatedly throughout the entire garnet growth history so that modification of the original growth zoning by intragranular diffusion needs to be considered all over a garnet porphyroblast. As envisaged by Spear (1988), although rather inefficient, intragranular diffusion may lead to a flux of components between garnet and the rock matrix. Similar to garnet fractionation but in a complementary fashion, this may modify the thermodynamically relevant bulk rock composition. This effect was referred to as "internal metasomatism" by Spear (1988).

We use the software program THERIA_G (Gaidies et al., subm.a) for forward modelling of garnet growth. This tool allows to account simultaneously for the requirements of thermodynamic equilibrium between garnet rim and the rock matrix, chemical fractionation during garnet

growth, modification of the original growth zoning through intragranular diffusion, as well as the nucleation history. We apply this technique to unravel the polymetamorphic history of garnet from the Austroalpine crystalline basement. We obtain constraints on the P - T - t trajectories of a Permian and a Cretaceous metamorphic event from modelling the chemical zoning of two distinct growth phases of garnet. The model P - T - t paths are compared with information on the geothermal history constrained by independent petrological and geochronological data. Finally, an often perceived feature of the growth zoning of polymetamorphic garnet from the Austroalpine crystalline basement is presented, which may be used as a rock specific geothermobarometer.

4.3 Geological background

The rock sample, which is investigated in the present study, was taken from the Wölz Complex, a prominent lithostratigraphic unit of the Upper Austroalpine basement nappes in the Eastern Alps (Schmid et al., 2004). The Austroalpine nappe system represents the frontal part of the Apulian continental microplate, which underwent internal deformation due to an intracontinental collision event during the Cretaceous. The Wölz Complex was part of the tectonic lower plate and experienced a greenschist to amphibolite facies metamorphic overprint during the Cretaceous subduction event. Because of Cretaceous metamorphism, which is referred to as Eo-Alpine metamorphism, low- to medium grade metamorphic assemblages of pre-Cretaceous origin have been largely obliterated (Gaidies et al., 2006; Schuster and Frank, 1999; Schuster et al., 2004, 2001; Schuster and Thöni, 1996).

The polymetamorphic history of the Wölz Complex is documented by garnet porphyroblasts with two distinct growth phases (Abart and Martinelli, 1991; Bernhard and Hoinkes, 1999; Faryad and Chakraborty, 2005; Faryad and Hoinkes, 2003; Gaidies et al., 2006; Schuster and Frank, 1999; Schuster et al., 2001; Schuster and Thöni, 1996). The oldest garnet growth phase forms the cores of the garnet porphyroblasts and is separated from the younger garnet growth phase by a microstructural and compositional discontinuity. From radiometric dating of garnet from the Wölz Complex it is known that the first growth phase grew during a Permian metamorphic event and the second growth phase was formed in the course of Cretaceous metamorphism (Schuster and Frank, 1999; Schuster and Thöni, 1996; Thöni, 2002; Sölva et al., 2001).

The studied rock sample is a garnet bearing metapelite from the Schöttelbach area. For a detailed description of the geographical position and more information on the regional geology, the reader is referred to a previous study (Gaidies et al., 2006).

4.3.1 Petrological and geochronological constraints on the geothermal history of the Wölz Complex

The cores of the oldest garnets represent the earliest testimony of metamorphism in the rocks from the Wölz Complex. They were subject to several geochronological and thermobarometrical studies. Using the Sm–Nd garnet–whole-rock method, an age of 269 ± 4 Ma was obtained for garnet that forms the cores of polyphase garnet porphyroblasts (Schuster and Thöni, 1996; Schuster and Frank, 1999; Thöni, 2002). Permian metamorphism in the Austroalpine basement occurred in an extensional tectonic regime. This is indicated by magmatic activity as well as high-temperature/low-pressure (*HT/LP*) metamorphic assemblages and the continuous penetration of the surface topography as inferred from the sedimentary record (Schuster et al., 2001). Lithospheric extension probably started at ~ 290 Ma and the thermal peak was reached at ca. ~ 260 Ma.

Phengite thermobarometry (Feenstra, 1996; Franz et al., 1977) applied to monomineralic inclusions of margarite, paragonite, and muscovite in the Permian growth phase of garnet from the Wölz Complex (Schuster and Frank, 1999) yielded *T* conditions of lower greenschist facies at low *P* (Schuster et al., 2001). According to Gaidies et al. (2006) incipient garnet growth during the Permian occurred at 535 ± 20 °C and 4.0 ± 0.5 kbar in rock samples from the Schöttelbach area [*P-T-t* point (1) in Fig. 4.1]. From the observed *P-T* conditions a geothermal gradient of ~ 40 °C km⁻¹ can be calculated supporting the hypothesis of a Permian extensional event for this part of the Austroalpine basement. However, the heating rate associated with the respective pre-Eo-Alpine metamorphic event as well as the peak conditions of Permian metamorphism in the Wölz Complex are yet unknown.

From the Late Permian to the Early Jurassic more than 3000 m of shallow water sediments were deposited on the slowly subsiding Austroalpine crust (Mandl, 2000; Tollmann, 1985). Due to intense overprint in the course of Eo-Alpine metamorphism, this part of the geothermal history is not documented in metapelites of the Wölz Complex. However, for Austroalpine units which reached similar metamorphic conditions during the Permian metamorphic event but were less intensely affected during the Cretaceous, K-Ar muscovite ages (reflecting cooling below ~ 420 °C) in the range of 240–210 Ma [*P-T-t* point (2) in Fig. 4.1] are characteristic (Schuster et al., 2001). Therefore, a geothermal gradient of ~ 25 °C km⁻¹ can be assumed for the respective period in the geothermal history.

In the Valanginian (~ 137 Ma) the Permomesozoic sediments were sheared off from the

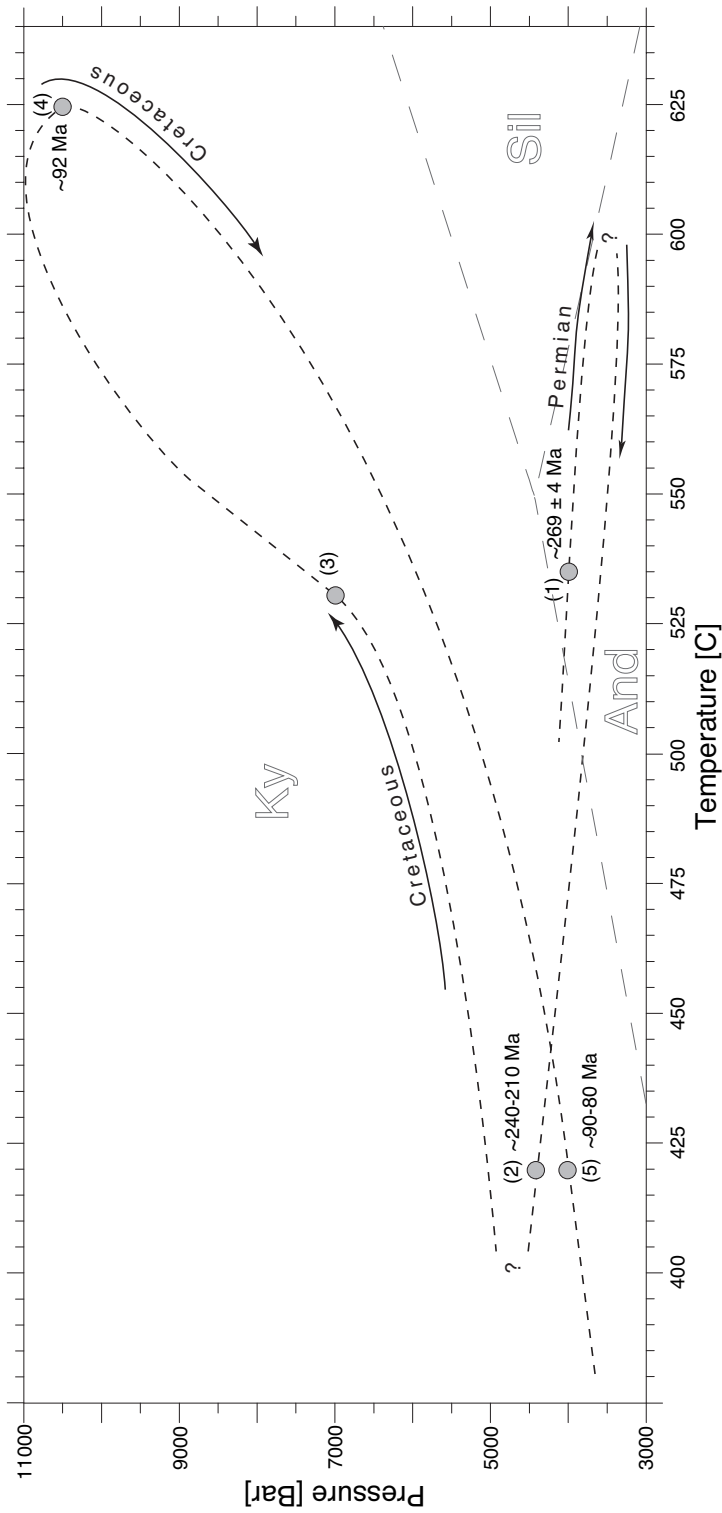


Figure 4.1 – Compilation of geochronological and thermobarometrical data (marked with points) obtained from rocks of the Wölz Complex (Schuster and Thöni, 1996; Schuster and Frank, 1999; Thöni, 2002; Schuster et al., 2001; Sölvä et al., 2001; Faryad and Hoinkes, 2003; Thöni, 2006; Hejl, 1984; Gaidies et al., 2006). For explanation see text.

future Koralpe-Wölz nappe system and the subduction of basement rocks started within the Eo-Alpine intracontinental subduction zone (Schmid et al., 2004). The application of isopleth thermobarometry to garnet, which grew during the Eo-Alpine metamorphic event, yielded 540 ± 10 °C and 6.5 ± 0.5 kbar for the stage of incipient garnet growth [P - T point (3) in Fig. 4.1] in metapelites from the Schöttelbach region (Gaidies et al., 2006).

For samples from similar geographical positions conditions of 600–650 °C at 10–11 kbar were determined by Faryad and Hoinkes (2003) for the metamorphic peak at ~ 92 Ma (Thöni, 2006) [P - T - t point (4) in Fig. 4.1]. From these P - T estimates, a geothermal gradient of ~ 20 °C km^{-1} is calculated. The markedly low geothermal gradient points to fast subduction during the Cretaceous, where thermal relaxation could not keep up with rapid P increase. After the metamorphic peak the rocks of the Koralpe-Wölz nappe system were exhumed in a metamorphic extrusion wedge (Schmid et al., 2004) and typical K-Ar and Rb-Sr cooling ages on micas are 90–80 Ma (Hejl, 1984) [P - T - t point (5) in Fig. 4.1]. From diffusion modelling in polyphase garnet porphyroblasts of the Wölz Complex Faryad and Chakraborty (2005) suggest a duration of ~ 0.8 – 0.9 Ma from P - T conditions similar to point (3) in Fig. 4.1 to P - T conditions of ~ 540 °C and 4 kbar along the retrograde part of the Cretaceous P - T - t trajectory. For the metamorphic peak of Eo-Alpine metamorphism in the Wölz Complex Faryad and Chakraborty (2005) considered conditions of ~ 590 °C at 10 kbar. According to apatite fission track ages obtained by Hejl (1998), final cooling below ~ 100 °C occurred in the Miocene at 15–20 Ma.

4.4 Methods

4.4.1 Sample preparation, EPMA, combustion analysis, and WDXRFA

The rock sample 12F03, which is investigated in the present study, was also subject to previous research (Gaidies et al., 2006). Serial sections with a spacing of ~ 0.6 – 0.8 mm were prepared from the largest garnet in a representative sample domain of $\sim 1 \times 2 \times 3$ cm. The aim of this procedure was, to obtain a cross-section of garnet, which contains the entire garnet growth history.

Electron probe micro-analysis (EPMA) was done on a JEOL JXA-8200 at ETH Zurich. The accelerating voltage was 15 kV for a beam current of 10 nA. X-ray maps and the compositional profiles of garnet were produced for Mn, Fe, Mg, and Ca. The X-ray maps as well as the respective compositional profile, which intersects the garnet core and thus contains the most information on garnet growth history, are shown in Figs. 4.3 and 4.2.

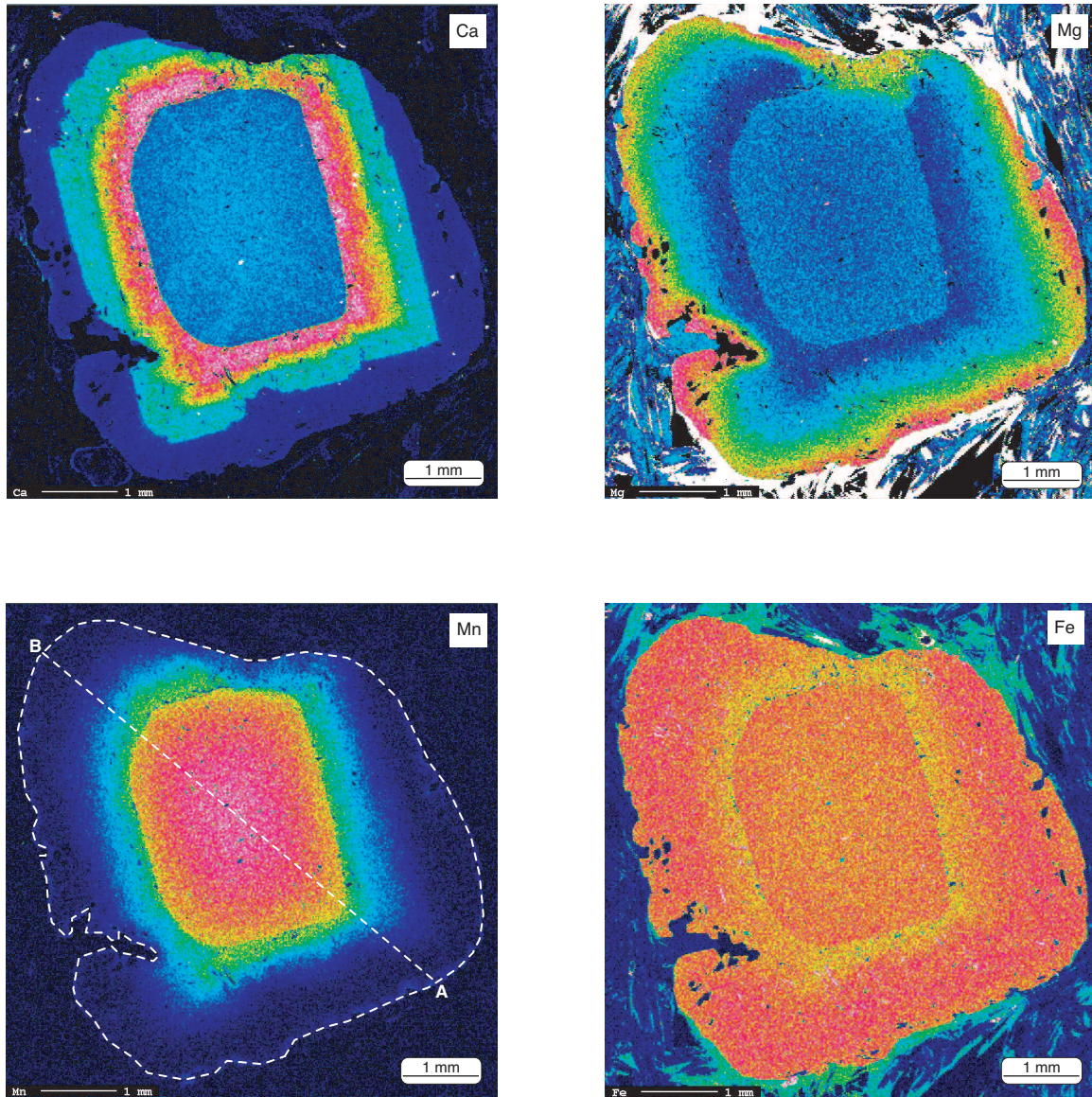


Figure 4.2 – X-ray maps of a garnet porphyroblast of a representative domain of rock sample 12F03. The location of the compositional profile A-B as illustrated in Fig. 4.3 is shown.

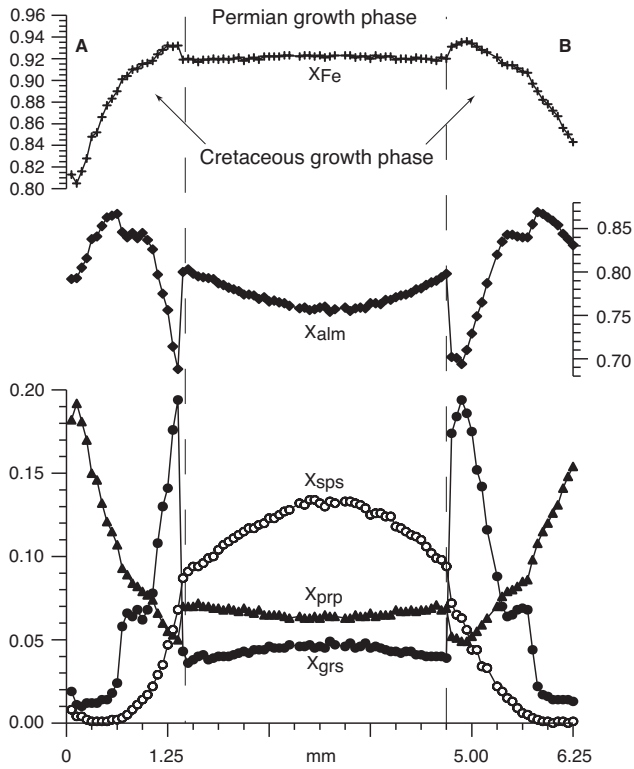


Figure 4.3 – Compositional profile intersecting the centre of the largest garnet porphyroblast in a representative domain of rock sample 12F03.

Table 4.1 – Bulk rock composition of sample 12F03 (wt%).

SiO ₂	TiO ₂	Al ₂ O ₃	Fe ₂ O ₃	MnO	MgO	CaO	Na ₂ O	K ₂ O	H ₂ O	CO ₂	Σ
57.51	1.19	20.98	9.48	0.11	2.28	0.46	1.23	3.73	2.75	0.44	100.16

Combustion analysis and wavelength-dispersive X-ray fluorescence analysis (WDXRFA) were done to obtain the major element composition of the rock sample. For the combustion analysis, a LECO combustion analyser was used. WDXRFA was carried out on a glass pellet prepared from a rock sample of ~ 1 kg employing a Bruker AXS SRS-3400 at Basel University. The bulk rock composition obtained for the sample investigated in the present study is given in Table 4.1.

4.4.2 Numerical modelling of prograde garnet growth

The bulk rock composition of sample 12F03 (Table 4.1) was used as the thermodynamically relevant bulk composition for the stage of incipient garnet growth. For thermodynamic calculations in the simplified model system MnO-Na₂O-CaO-K₂O-FeO-MgO-Al₂O₃-SiO₂-H₂O-TiO₂, the database of Holland and Powell (1998) (thermodynamic database of THERMOCALC, version 3.21) was used [for detailed information on the solution models and notations used in the

current study, the reader is referred to the companion paper (Gaidies et al., *subm.a*)]. Rock specific equilibrium assemblage diagrams were calculated with program DOMINO (de Capitani, 1994, see also: <http://titan.minpet.unibas.ch/minpet/theriak/theruser.html>). In garnet growth simulations, H₂O and SiO₂ are considered as excess components to account for the presence of quartz and an aqueous fluid throughout the entire *P-T* range of interest.

The kinetic parameters of Chakraborty and Ganguly (1992) were applied to model intragranular diffusion in garnet. Small graphite inclusions are very abundant in the garnet porphyroblast investigated in this study indicating coexistence with a graphite saturated fluid. This is why the kinetic data of Chakraborty and Ganguly (1992), which were obtained with graphite present, could be employed without modification. In a previous study (Gaidies et al., 2006) it was shown that the influence of changing H₂O and CO₂ activities on garnet composition and stability is minor for the sample studied and decreases with increasing *P*. Therefore, in the present study, pure H₂O was considered as fluid phase.

4.5 Sample description

A detailed description of the petrography and garnet chemistry of sample 12F03 can be found in Gaidies et al. (2006). In the following only a brief summary is given.

4.5.1 Petrography

The rock sample investigated in the present study is a metapelite with garnet porphyroblasts, which consist of two distinct growth phases. A first growth phase, which forms the cores of the porphyroblasts, can easily be distinguished from the rim-forming second phase based on abundant ilmenite and graphite inclusions that are concentrated at the boundary between both zones. From the microstructural relationship to the main schistosity it is inferred that the second garnet growth phase grew synchronously to the formation of the foliation.

The rim of garnet of sample 12F03 is marked by inclusions of quartz, muscovite, ilmenite, rutile and tourmaline and is strongly pigmented with graphite. It is interesting to note that the abundance of rutile inclusions rises towards the outer portions of the rim, whereas the abundance of ilmenite decreases. In a similar fashion, the intensity of graphite pigmentation decreases from the inner portions of the rim outwards. Whereas the rim of the garnet porphyroblast investigated in the present study is approximately 1.5 mm wide, the first growth phase is about 4 mm in diameter. It contains ilmenite, quartz, tourmaline as well as small muscovite grains as mineral

inclusions. The polyphase garnet porphyroblasts are enclosed by a fine-grained matrix composed of muscovite, quartz, tourmaline, biotite, ilmenite, rutile as well as plagioclase and retrograde chlorite. The foliation of the rock is formed by muscovite, biotite, tourmaline, and ilmenite.

4.5.2 Garnet chemistry

The garnet porphyroblasts of rock sample 12F03 are strongly zoned with respect to $X_{sps} [= Mn/(Fe^{2+} + Ca + Mg + Mn)]$, $X_{alm} [= Fe^{2+}/(Fe^{2+} + Ca + Mg + Mn)]$, $X_{prp} [= Mg/(Fe^{2+} + Ca + Mg + Mn)]$, and $X_{grs} [= Ca/(Fe^{2+} + Ca + Mg + Mn)]$ (Figs. 4.2, 4.3). The chemical zoning patterns (Fig. 4.2) exhibit an almost euhedral shape indicating that the original zoning was preserved and resorption did not occur to any detectable extent. The boundary between first and second growth phase can easily be discerned from a sharp increase of X_{grs} by ~ 13.5 mol% and a concomitant decrease of X_{alm} by ~ 9.5 mol%. The boundary between first and second growth phase is also marked by a sudden decrease of X_{sps} by ~ 2.5 mol-% (Fig. 4.3).

The first growth phase is characterized by a continuous outwards decrease of X_{sps} and X_{grs} and a concomitant increase of X_{alm} and X_{prp} . A 'shoulder' in the X_{grs} profile forms a conspicuous feature in the central part of the second growth phase. X_{grs} decreases sharply from this shoulder outwards and, finally, reaches a constant value of ~ 0.015 in the outermost 0.3 mm of the garnet rim. In a similar fashion, a 'step' in the X_{alm} profile is observed. Whereas X_{grs} decreases sharply from the shoulder outwards, X_{alm} increases and reaches a maximum of ~ 0.87 within the garnet of the second growth phase. From the location of maximum X_{alm} outwards the almandine content decreases continuously.

In the outermost tens of micrometers of the garnet rim X_{grs} , X_{sps} , and $X_{Fe} [= Fe/(Fe + Mg)]$ increase, and the X_{prp} decreases concomitantly. This feature is only locally developed.

4.6 Results

To extract geothermobarometric information from the chemical zoning pattern of the entire garnet porphyroblast garnet growth was simulated for various P - T - t trajectories and different theoretical garnet crystal size frequency distributions (CSD). In this communication, the most successful results of the garnet growth simulations are presented. In that respect, firstly the P - T path and garnet CSD was determined, along which the garnet growth simulations yield the best fit with the observed garnet chemical patterns. In a second step, the influence of intragranular diffusion on garnet and effective bulk rock composition was considered linking the P - T trajectory

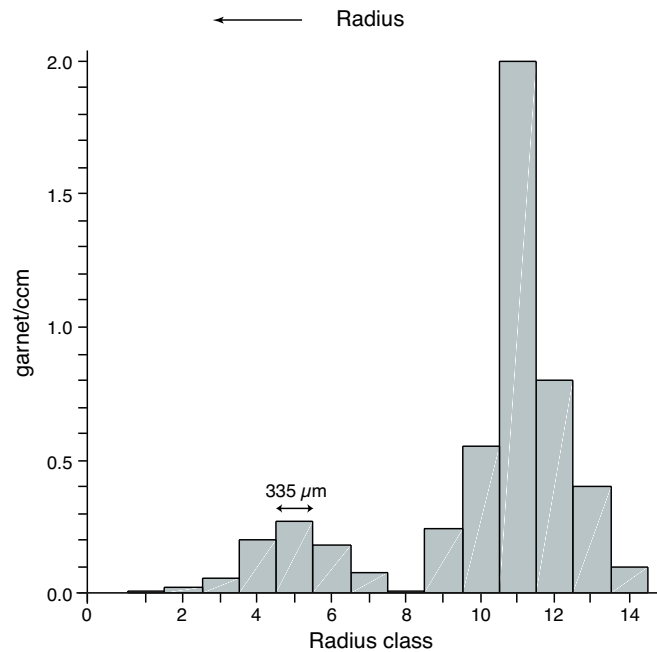


Figure 4.4 – Theoretical relative garnet crystal size frequency distribution used for garnet growth simulation.

to different heating and cooling scenarios.

Because the garnet porphyroblasts of rock sample 12F03 are very coarse-grained, an enormous preparational effort would have to be undertaken to obtain a garnet CSD-analysis with sufficient statistical significance. This could not be done in our study. For practical purposes, a theoretical CSD with a polymodal size-frequency distribution was applied (Fig. 4.4) that accounts for crystallization during the Permian and the Cretaceous metamorphic events.

For the Permian event the CSD (radius classes 1 to 8 in Fig. 4.4) was chosen in such a way, that the garnet individuals of radius class 4 have similar size as the first garnet growth phase of sample 12F03. This is motivated by the notion that the garnet investigated probably pertains to a relatively large size class but almost certainly is not the largest individual of the first growth phase that was formed in a larger rock volume with similar composition as the investigated sample. The specific size-frequency distribution of garnet crystals that originate from the second metamorphic cycle (radius classes 9 to 14 in Fig. 4.4) was chosen so that the simulated size of the second growth phase on individuals of radius class 4 (of the first growth phase) matches the size of the respective individual in sample 12F03. Garnet individuals of radius classes 9–14 are single-phase porphyroblasts, the nucleation and growth of which entirely pertains to Cretaceous metamorphism.

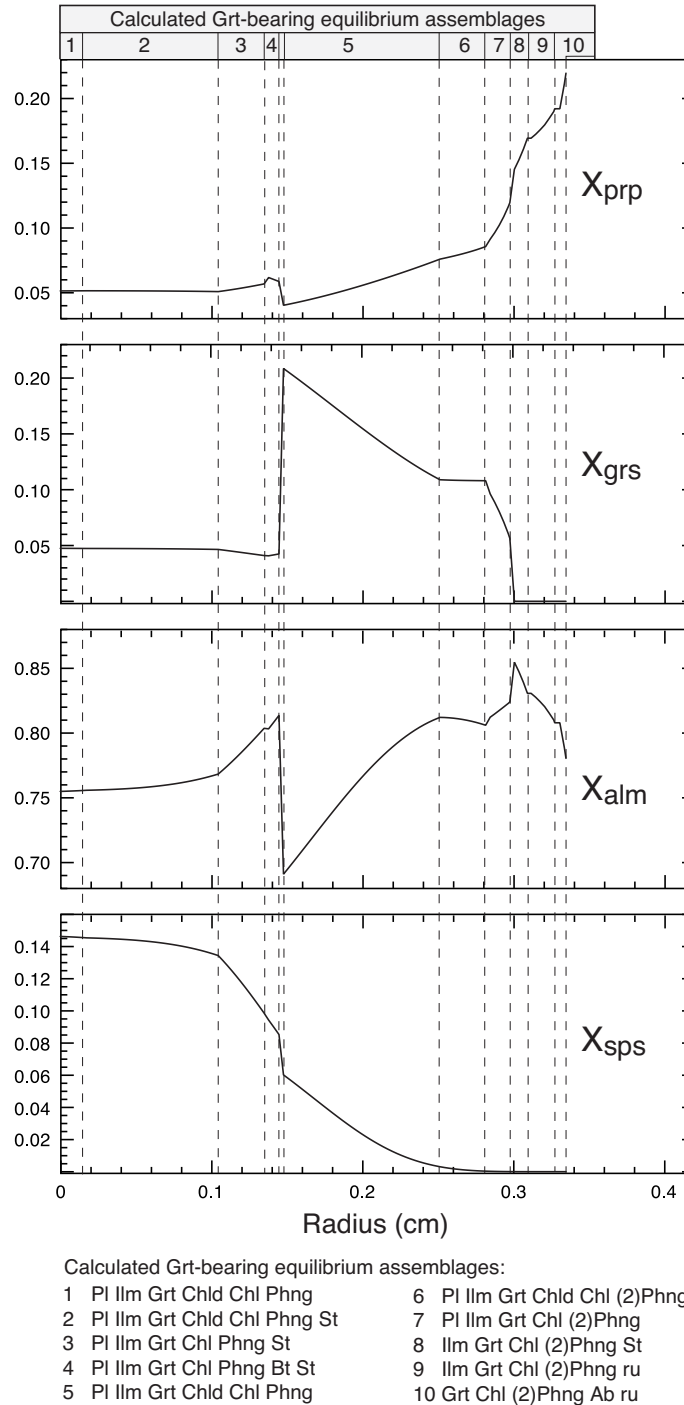


Figure 4.5 – Calculated compositional profile of garnet in rock sample 12F03 neglecting the influence of intragranular diffusion on garnet and effective bulk rock composition. Garnet growth simulation was performed along P - T path A (Fig. 4.7, Appendix C) using a bimodal CSD (Fig. 4.4). The profile was calculated for garnet of radius class 4. All equilibrium assemblages contain H_2O and Qtz. ((2)Phng corresponds to unmixing of Phng into a paragonite- and muscovite-rich phase)

4.6.1 The original garnet growth zoning

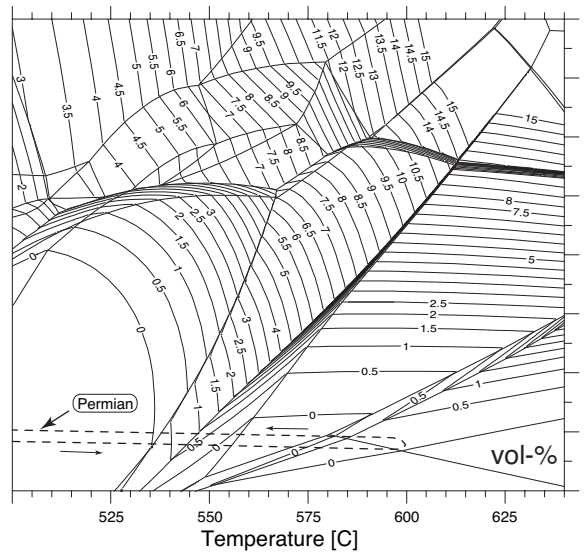
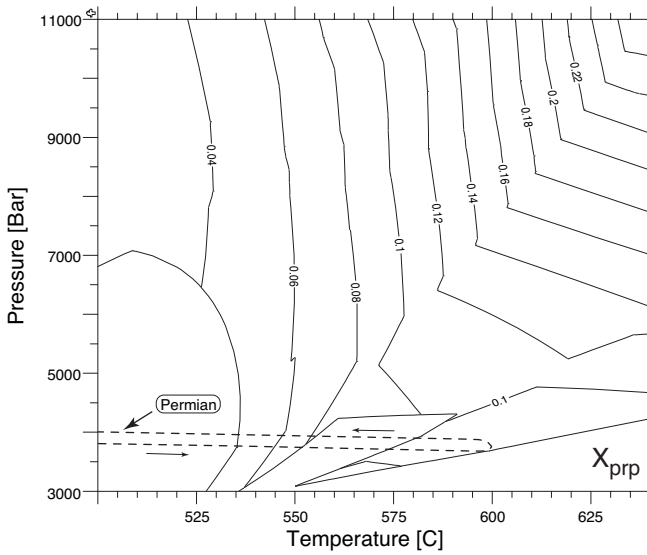
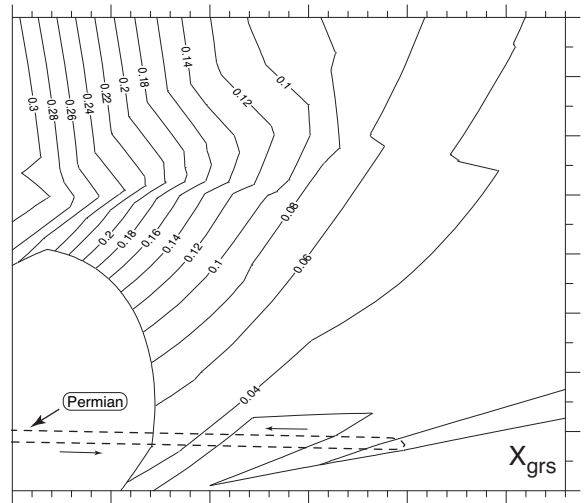
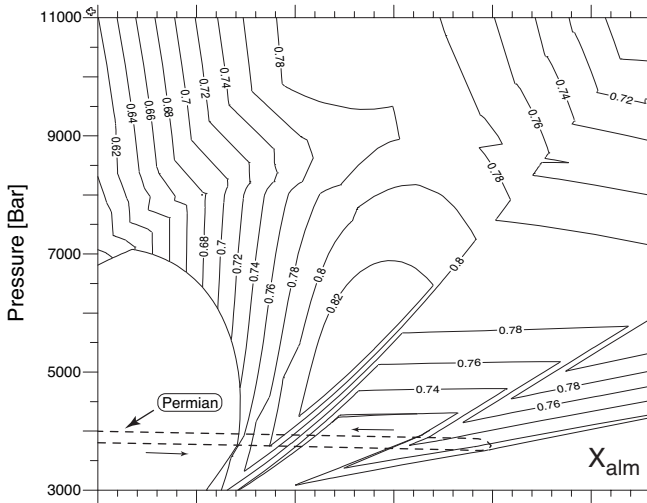
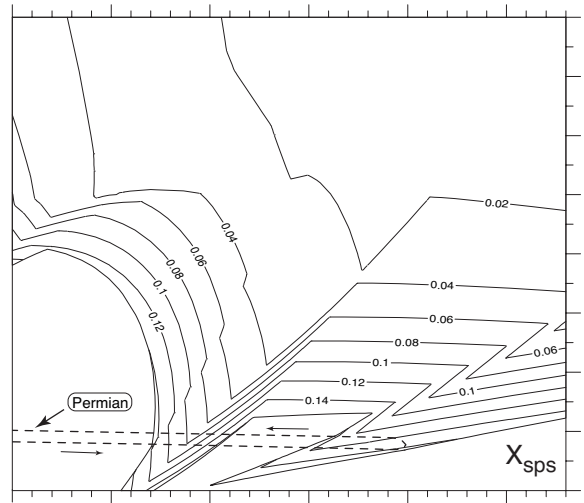
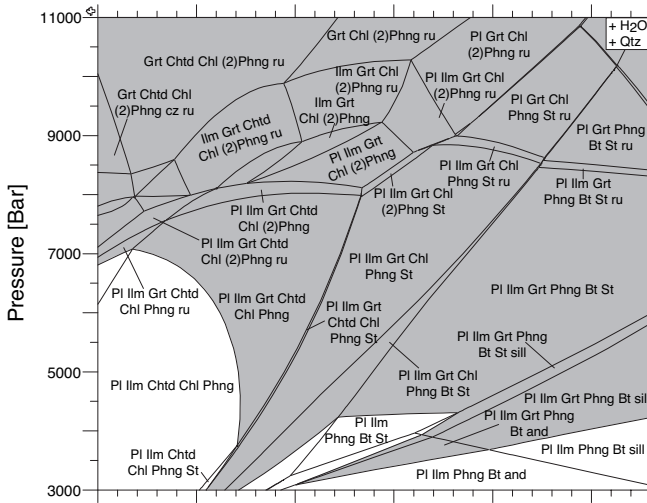
Fig. 4.5 illustrates the calculated compositional profile of garnet from size class 4 (Fig. 4.4), which results from growth along P - T path A (Fig. 4.7). The chemical patterns shown in Fig. 4.5 were calculated from equilibrium phase relations taking into account the effect of chemical fractionation during garnet growth. Intragranular diffusion was not considered so that the calculated compositional profile represents pure garnet growth zoning. In addition, Fig. 4.5 shows the equilibrium assemblages that correspond to the respective garnet growth increments. The calculated equilibrium phase relations for the time of incipient garnet growth in rock sample 12F03 are illustrated in Fig. 4.6.

The garnet growth simulation clearly shows that changes in the thermodynamically stable equilibrium assemblage during garnet growth produce marked changes in the chemical gradients within the growth zoning of garnet (Fig. 4.5). Our calculations indicate that most of the first garnet growth phase grew in equilibrium with plagioclase, ilmenite, chloritoid, chlorite, phengite, as well as staurolite, quartz, and H_2O (assemblage 2 in Fig. 4.5). It is interesting to note that this assemblage is stable only over a fairly small P - T range (Fig. 4.6).

In general, the compositional profiles obtained from garnet growth modelling are very sensitive to the choice of the P - T path. In particular, for the bulk rock composition of sample 12F03, X_{grs} of the first garnet growth increment is strongly contingent on P . X_{grs} observed in garnet of rock sample 12F03 (Fig. 4.3) constrains P to ~ 3.8 kbar during the incipient stages of Permian garnet growth. If a P - T path were chosen that exceeds the applied trajectory by ~ 1 kbar, this would lead to an increase in X_{grs} by ~ 0.03 during initial garnet growth. This is beyond the analytical uncertainty.

The first P - T loop was chosen to represent the HT - LP Permian metamorphic event. In the garnet growth simulation, garnet growth during the Permian event ceases at the P - T conditions where biotite enters the stable equilibrium assemblage. The position of the isopleths that represent P - T conditions of constant garnet modes drastically change as the biotite-bearing equilibrium assemblage becomes thermodynamically stable (Fig. 4.6). Consequently, for this specific HT - LP trajectory, garnet growth ceases when biotite becomes stable. However, for

Figure 4.6 (facing page) – Initial equilibrium phase relations and dependency of garnet chemistry and garnet volume on P - T for the bulk rock chemistry of sample 12F03 (Table 4.1). H_2O and SiO_2 are considered as excess components throughout the respective P - T space. In addition, the Permian part of P - T path A, which is used for garnet growth simulation, is shown (for the detailed P - T values see Appendix C).



the retrograde part of the Permian P - T path, THERIA_G modelling predicts garnet growth in equilibrium with biotite and staurolite (assemblage 4 in Fig. 4.5). It is interesting to note that such an equilibrium assemblage would not form if garnet grew along a clockwise P - T path.

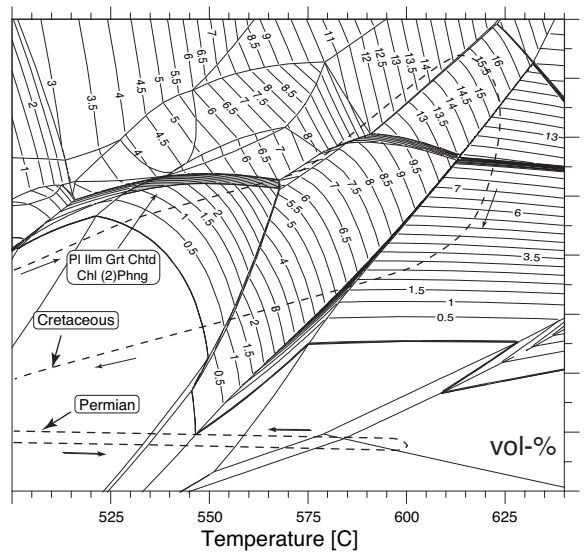
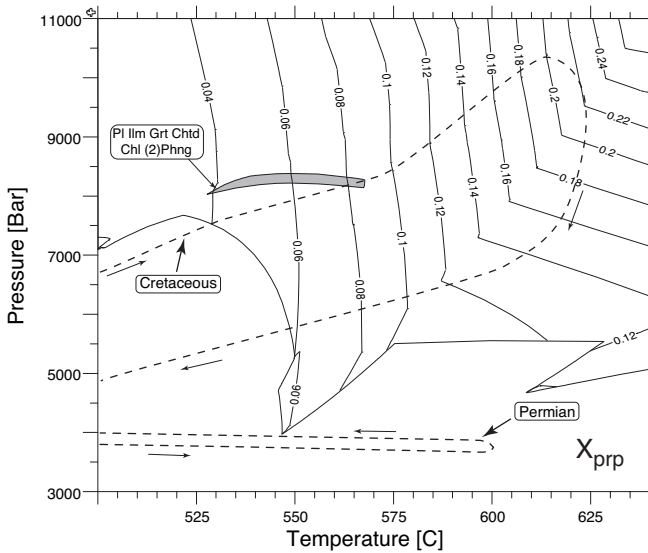
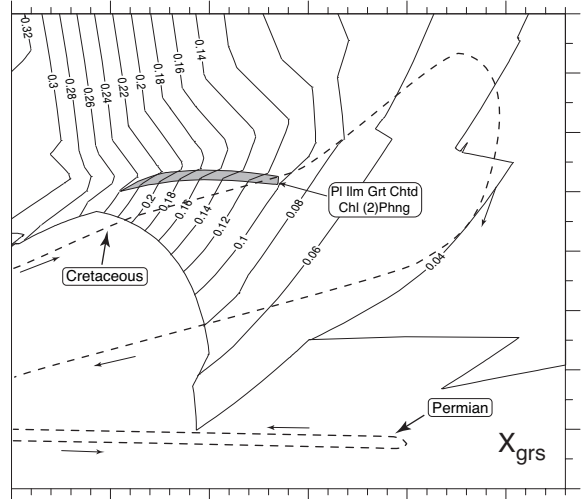
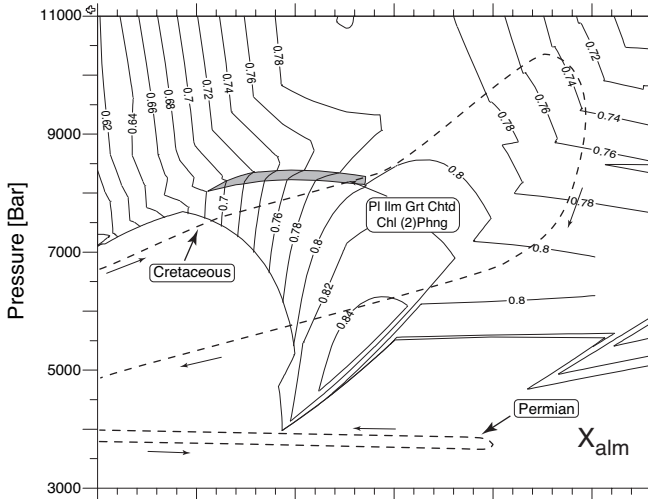
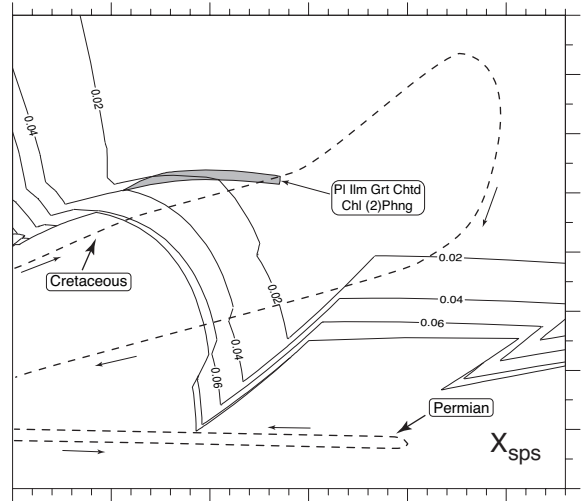
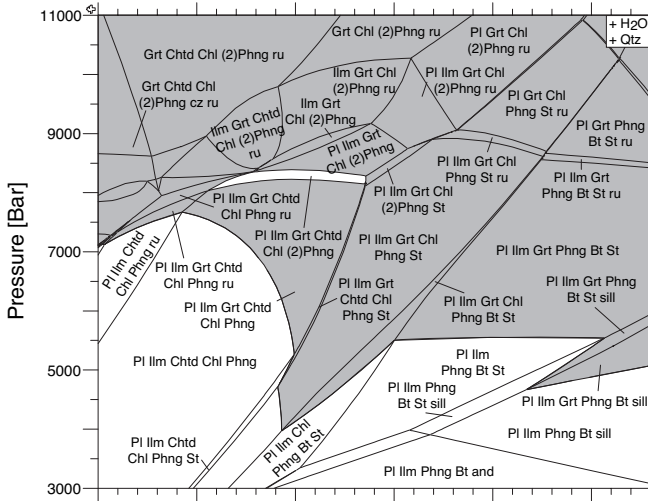
The equilibrium phase relations and the garnet chemistry calculated for incipient garnet growth in the Cretaceous applying P - T path A and neglecting the influences of intragranular diffusion on garnet and effective bulk rock composition are illustrated in Fig. 4.7. The size of the garnet stability field is reduced in comparison with the initial equilibrium phase relations prior to garnet growth (Fig. 4.6). This is due to the influence of chemical fractionation associated with garnet growth during the first metamorphic cycle on thermodynamic effective bulk rock composition.

The second P - T cycle is modelled to exemplify the geothermal history of the Cretaceous Eo-Alpine metamorphic event. Incipient garnet growth in the course of the Cretaceous event occurs at ~ 530 °C and ~ 7.6 kbar. As a result, at the boundary between first and second growth phase of garnet an increase of X_{grs} by ~ 15 mol-% is produced as well as a decrease of X_{sps} , X_{alm} , and X_{prp} by ~ 2 , 12, and 2 mol-%, respectively.

From garnet growth simulations with THERIA_G it is evident that during the Cretaceous metamorphic cycle the metapelite followed a P - T trajectory, which intersects the stability field of the equilibrium assemblage plagioclase, ilmenite, garnet, chloritoid, chlorite, (2)phengite (muscovite and paragonite), quartz, and an aqueous fluid (marked in Fig. 4.7). The position and shape of the X_{grs} and X_{alm} isopleths in the corresponding P - T field are such that during the growth along such a P - T trajectory a shoulder in X_{grs} and a local maximum in X_{alm} are formed. For the bulk rock composition at hand, this is a unique feature. There is no alternative assemblage, in which the garnet chemistry changes similarly with P - T . Garnet growth simulations along P - T paths, which intersect the same assemblage but correspond to smaller geothermal gradients as illustrated in Fig. 4.7 result in a broader X_{grs} shoulder with significantly higher values of X_{grs} .

Whereas at P - T conditions of ~ 586 °C and 9.1 kbar garnet disappears from the equilibrium

Figure 4.7 (facing page) – Equilibrium phase relations and dependency of garnet chemistry and garnet volume on P - T for the time of incipient garnet growth during the Cretaceous. The influence of diffusional relaxation in garnet on effective chemical composition is not taken into account. H_2O and SiO_2 are considered as excess components throughout the respective P - T space. In addition, P - T path A that was used for garnet growth simulation is shown (for the detailed P - T values see Appendix C). The equilibrium assemblage is marked, which has to be intersected by the P - T path to form a shoulder in X_{grs} and a local maximum in X_{alm} .



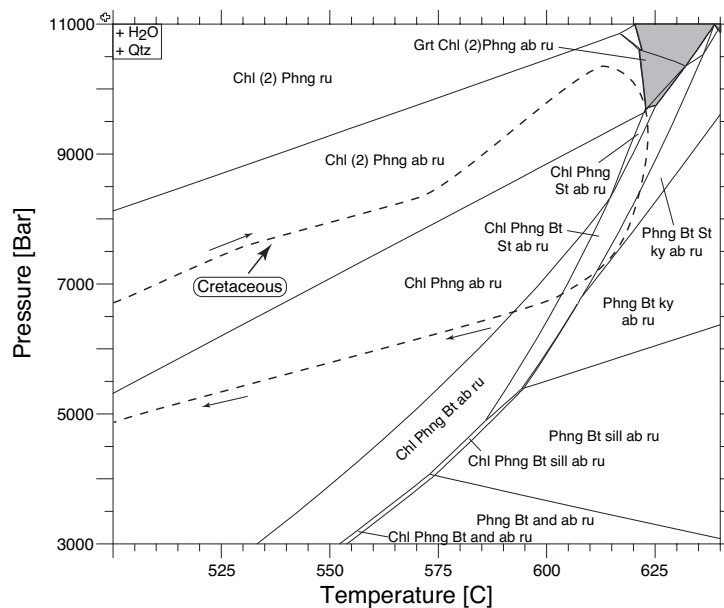


Figure 4.8 – Equilibrium phase relations subsequent to garnet growth. The influence of intragranular diffusion in garnet on thermodynamic effective bulk rock composition is not considered.

assemblage, which consists of plagioclase, ilmenite, garnet, chlorite, (2)phengite, quartz, and H_2O (assemblage 7 in Fig. 4.5), at conditions of $\sim 595^\circ\text{C}$ and 9.6 kbar the equilibrium assemblage ilmenite, garnet, chlorite, (2)phengite, staurolite, quartz, and H_2O (assemblage 8 in Fig. 4.5) and a maximum in X_{alm} is formed at a later stage along the P - T trajectory. That is, along the prograde part of the Cretaceous P - T path, a period of garnet instability is calculated spanning $\sim 10^\circ\text{C}$ and 0.5 kbar. During the last stages of garnet formation, THERIA_G modelling yields an outermost rim of ~ 0.4 mm width, where the second garnet growth phase has extremely low X_{sps} and X_{grs} .

The equilibrium phase relations calculated for a thermodynamically relevant bulk composition that is representative for the stage subsequent to garnet growth are displayed in Fig. 4.8. From Fig. 4.8 it is evident that for further growth of garnet the rock would have to follow a P - T path that reaches at least upper amphibolite facies conditions. Because Mn and Ca have been completely fractionated into garnet during earlier growth stages, the equilibrium phase assemblages are devoid of ilmenite and plagioclase.

4.6.2 Influence of intragranular diffusion on garnet growth zoning

The P - T conditions, at which garnet growth ceases along the prograde part of the Permian P - T path (Fig. 4.6), do not necessarily correspond to the peak conditions of Permian metamorphism. In order to evaluate the influence of the possible peak conditions during Permian metamorphism

on garnet composition, garnet growth is modelled along different P - T - t loops while the influence of intragranular diffusion in garnet on garnet and on effective bulk rock composition is taken into account. The P - T - t loops employed differ with respect to the thermal maximum reached during the Permian. Whereas for P - T - t path A* (Table C.1) a thermal maximum of 600 °C is considered, for P - T - t path B (Table C.2) 650 °C and for loop C (Table C.3) 675 °C are applied.

In all cases, garnet growth is modelled with 3 °C Ma⁻¹ and 100 °C Ma⁻¹ for the Permian and Cretaceous heating rates, respectively. For the cooling rates -3 °C Ma⁻¹ and -100 °C Ma⁻¹ were used for Permian and Cretaceous metamorphism. A prolonged residence of the rock at elevated P - T conditions has a similar effect as slow heating/cooling rates. It is impossible to discern between these two alternative scenarios from the compositional zoning of garnet. This is why the potential effects of prolonged residence at the thermal maximum is not investigated separately.

The compositional profile of garnet from radius class 4 (Fig. 4.4) calculated for garnet growth along P - T - t loop A* largely resembles the chemical composition of garnet computed for the growth along P - T - t path B and C (Fig. 4.9). Garnet growth up to 650 °C (loop B) results in more shallow compositional gradients in the first growth phase of the polyphase garnet crystal than for the growth up to 600 °C (loop A*). However, the calculated chemical gradients of all components for both, P - T - t trajectories A* and B, are somewhat gentler in the core region and steeper in the outer portions of the Permian growth phase compared with the observed compositional gradients (Fig. 4.9). This feature is more pronounced for X_{sps} and X_{alm} than for X_{grs} and X_{prp} . The systematic discrepancy between observed and modelled compositional gradients suggests that the original growth zoning was degraded by intracrystalline diffusion to a larger extent than accounted for in the model.

The garnet growth simulation applying a maximum T of 675 °C during the Permian (loop C) yields a compositional pattern for the first garnet growth phase that matches the observed chemical gradients fairly well (Fig. 4.9). In that case, the only difference between predicted and observed garnet composition is in the calculated contents of X_{alm} and X_{prp} which differ from the observed quantities by an almost uniform value of ~ 0.01 and ~ -0.01 , respectively.

Results that are obtained, if P - T path A (Fig. 4.6) is linked to a heating rate of 1 °C Ma⁻¹ for the Permian metamorphic cycle, where during the retrograde part of the P - T path the rate increases to ~ -150 °C Ma⁻¹ (Table C.4) yield a compositional profile of garnet from radius class 4, which is rather similar to the chemical pattern acquired for growth along P - T - t loop A* (Fig. 4.9).

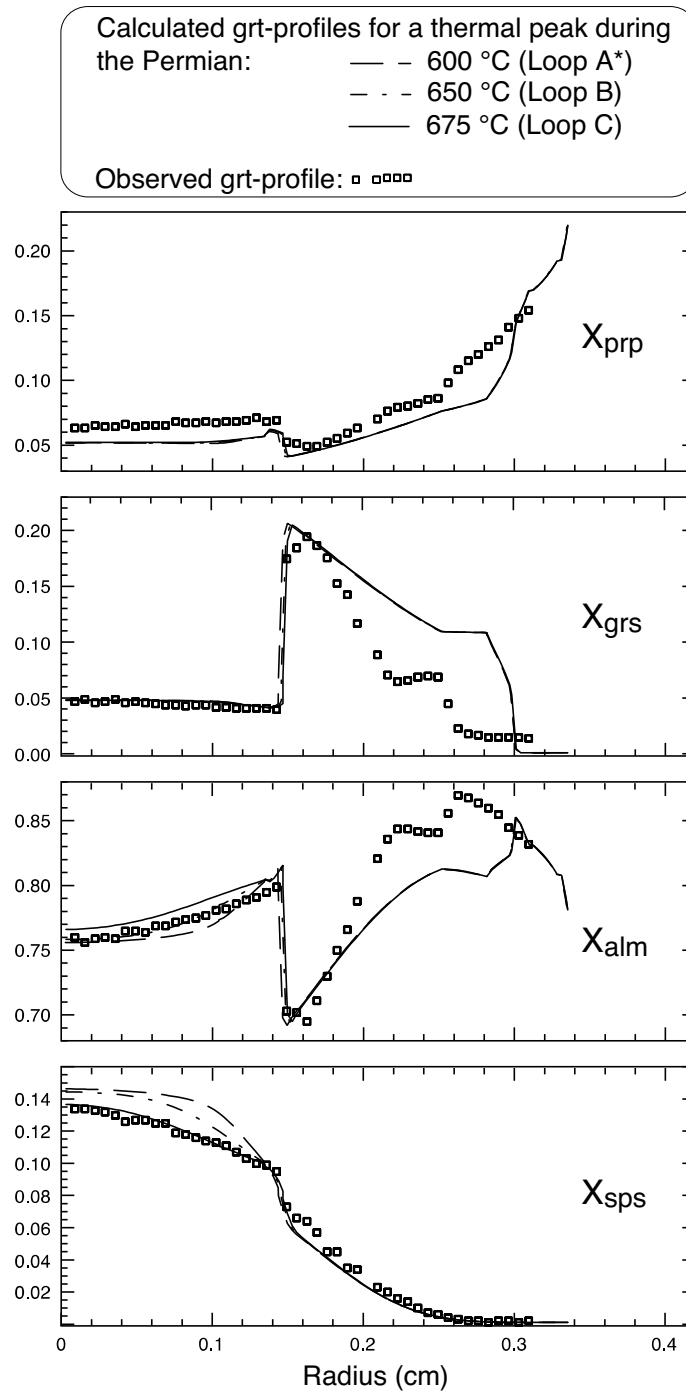


Figure 4.9 – Compositional profiles of garnet from radius class 4 (Fig. 4.4) calculated for different peak conditions during the Permian metamorphic event. For the Permian heating rate 3 °C Ma^{-1} and for Eo-Alpine metamorphism 100 °C Ma^{-1} are considered. The symbols correspond to the observed compositional profile to the right-hand side of the core in Fig. 4.3.

For modeling the chemical zoning of the Cretaceous garnet growth phase, P - T path A (Fig. 4.7) was applied. The results obtained for different heating rates are illustrated in Fig. 4.10. The most prominent features of the chemical zoning are nicely reproduced, at least in a qualitative sense. Nevertheless, remarkable differences between calculated and observed garnet composition can be perceived.

Even though a shoulder in X_{grs} as well as a concomitant local maximum in X_{alm} are simulated, their specific positions in garnet differ from the positions, at which they are observed in garnet of sample 12F03 (Fig. 4.10). Furthermore, the calculated contents of X_{grs} and X_{alm} that form the X_{grs} shoulder and the step in X_{alm} differ from the observed quantities by ~ 0.04 and 0.03 , respectively. In contrast to the observed garnet porphyroblast, the calculated rim of the second growth phase of garnet does not contain X_{grs} . The predicted absolute maximum in X_{alm} differs from the observed X_{alm} maximum by $\sim 0.03 - 0.04$ depending on the heating rate applied for the simulation of garnet growth during the Cretaceous (Fig. 4.10). Except for the case, where the Cretaceous P - T - t loop is modelled with a heating rate of $5 \text{ }^\circ\text{C Ma}^{-1}$, the garnet growth simulations predict a significant X_{alm} peak, which is not discerned in the investigated porphyroblast of rock sample 12F03 (Fig. 4.10).

Significant differences in the compositional gradients that result from variations of the heating rate applied for the Eo-Alpine metamorphic event can also be perceived at the transition between first and second garnet growth phase (Fig. 4.10). Whereas for simulations applying a heating rate of $100 \text{ }^\circ\text{C Ma}^{-1}$ a sharp compositional step is obtained even for X_{sps} between first and second garnet growth phase, garnet growth modelling with heating rates smaller than $20 \text{ }^\circ\text{C Ma}^{-1}$ yields significantly smoothed compositional gradients.

4.7 Discussion

The concentric chemical zoning and the homogeneous matrix that is devoid of chemical segregation in rock sample 12F03 are characteristic for the garnetiferous metapelites of the Wölz Complex. Both features indicate that chemical transport in the rock matrix was fast compared to the rates of garnet growth during the Permian and Cretaceous metamorphic events. In addition, the chemical zoning indicates that resorption of garnet that may potentially have occurred during phases of instability along the prograde part of the P - T path or during retrogression was minute and can be neglected when analyzing the compositional zoning pattern. Based on these notions, the rocks from the Wölz Complex lend themselves to the forward modelling of garnet

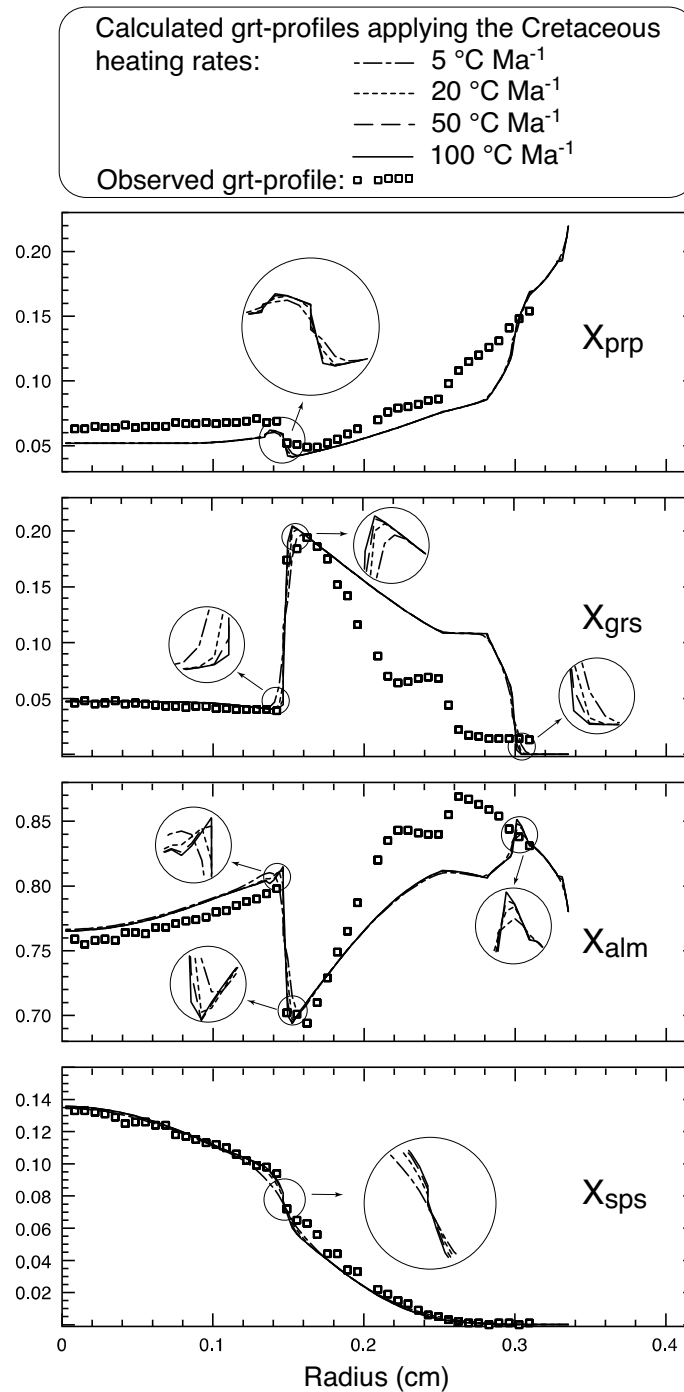


Figure 4.10 – Compositional profiles of garnet from radius class 4 (Fig. 4.4) calculated for different heating rates during the Eo-Alpine metamorphic event in the Cretaceous. For the geothermal history during the Permian a heating rate of 3 °C Ma⁻¹ and a maximum T of 675 °C are considered.

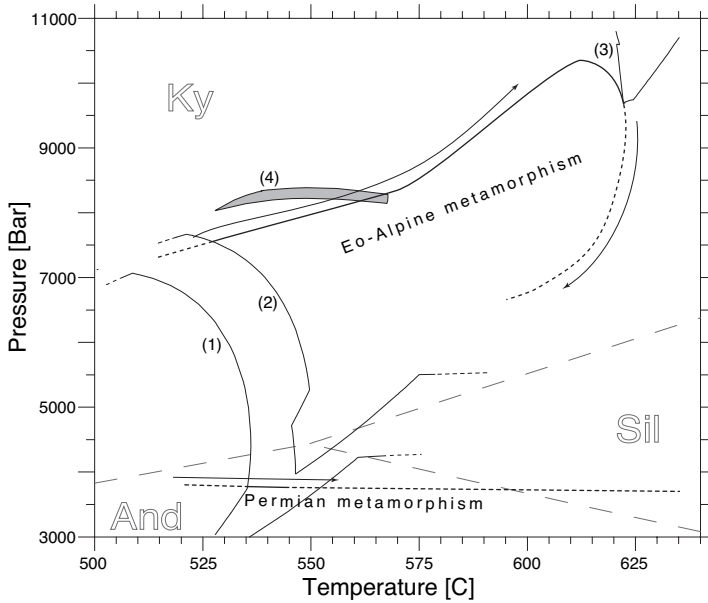


Figure 4.11 – Polymetamorph P - T evolution of rock sample 12F03 obtained from garnet growth simulation (unbroken lines). (1) P - T conditions of incipient garnet growth during the Permian; (2) P - T conditions of incipient garnet growth during the Cretaceous considering an anti-clockwise Permian P - T loop; (3) low- P - T conditions of garnet stability subsequent to garnet growth in the Cretaceous; (4) P - T conditions of the critical equilibrium assemblage, which have to be reached by the Eo-Alpine P - T trajectory (see text).

growth zoning with THERIA_G (Gaidies et al., this volume).

4.7.1 P - T - t evolution of rock sample 12F03 obtained from garnet growth simulation

Even though the first garnet growth phase of the investigated garnet porphyroblast is 4 mm in diameter, garnet growth in the course of Permian metamorphism occurred over a comparatively small P - T - t range. This is explained by the large radial growth rate of garnet during the incipient stages of garnet growth (Gaidies et al., subm.a). For the garnet growth simulation along P - T - t loop A*, this may lead to a garnet population density of ~ 0.85 grt/cm³ after a period of ~ 2.8 Ma. Garnet crystals that originate from the fourth nucleation event are ~ 3 mm in diameter. At the same time, garnet porphyroblasts that stem from the first nucleation event during the nucleation interval are ~ 5 mm in diameter.

Simulation of garnet growth from ~ 535 °C up to 545 °C (Fig. 4.11) at isobaric conditions of ~ 3.8 kbar using a thermal maximum of 675 °C and a heating and cooling rate of 3 °C Ma⁻¹ and -3 °C Ma⁻¹ during the Permian metamorphic cycle yields the best fit with the chemical zoning observed in the first garnet growth phase (Fig. 4.9). These results match the P - T conditions for the incipient stages of garnet growth in the Wölz Complex obtained in a previous study (Gaidies et al., 2006). From application of the isothermal fractionation model of Evans (2004) Gaidies et al. (2006) suggested a relatively flat P - T path for the formation of the first garnet growth

phase, where P slightly increases with T .

Mineral inclusions of ilmenite, quartz, and muscovite are observed in the first growth phase of garnet from rock sample 12F03 and are considered as parts of the equilibrium assemblages during Permian garnet growth. The first garnet growth phase and its inclusions represent the only remnants of Permian metamorphism in the rock sample. This assemblage is not diagnostic for the peak metamorphic conditions of the Permian event, and the question arises, whether the peak conditions can be constrained from garnet growth modelling.

A thermal maximum of 675 °C for the Permian metamorphic event seems to conflict with the fine-grained rock matrix of sample 12F03. We hypothesise that the comparatively short-termed Eo-Alpine metamorphic event (Faryad and Chakraborty, 2005) with peak conditions of ~625 °C at ~10 kbar (Fig. 4.11) would not be able to reduce the size of all the coarse-grained matrix grains, which would have been formed in response to a previous metamorphic event with a thermal maximum of ~675 °C and a total duration of ~150 My (Table C.3). Coarse-grained minerals in addition to garnet are expected to be preserved as remnants of former HT metamorphic assemblages. Furthermore, pegmatite dykes, which are likely to be associated with such high-grade metamorphic rocks in the Austroalpine basement (e.g. Habler and Thöni, 2001), are not known from the Wölz Complex. These findings contradict a thermal maximum of 675 °C and rather point to a significantly lower maximum T for the Permian metamorphic event in the Wölz Complex.

A possible explanation for the discrepancy is the large uncertainty in the thermodynamic model and/or kinetic dataset. At this point, it must be noted that the requirements with respect to the accuracy of thermodynamic data are higher for garnet growth modelling than for conventional geo-thermobarometric methods and garnet isopleth thermobarometry. This is due to the fact that errors in the determination of the composition of the first garnet growth increment are propagated and possibly even amplified via the fractionation calculation. This may be problematic in particular for modelling of the late stages of garnet growth (Fig. 4.12).

Garnet isopleth thermobarometry applied to the early growth increments of garnet often yields P - T conditions that lie well above the calculated LP/LT stability limit of garnet (e.g. Gaidies et al., 2006; Stowell et al., 2001). This conspicuous discrepancy may either be due to reaction overstepping or it may simply be an effect of insufficient accuracy of the thermodynamic data. Yet an alternative explanation invokes modification of the original growth zoning through intragranular diffusion. Garnet isopleth thermobarometry is very sensitive to X_{sps} . According to thermodynamic modelling, X_{sps} should be highest in the first garnet growth increments and

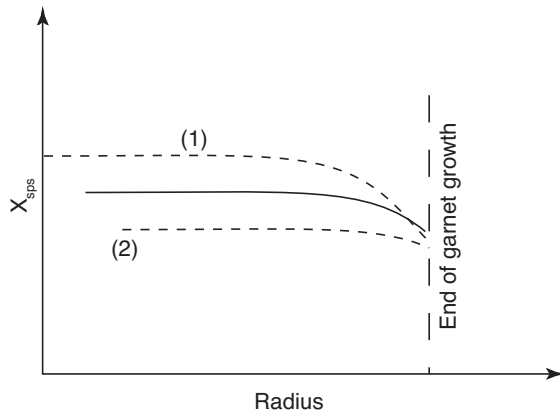


Figure 4.12 – Influence of (1) underestimation and (2) overestimation of the P - T conditions of incipient garnet growth on the primary chemical gradient of X_{sps} caused by the application of different solution models of Mn-bearing phases. The P - T conditions, at which garnet growth ceases, are only slightly affected.

it should decrease rapidly from the garnet-in curve into the garnet stability field. Manganese is the fastest diffusing component in garnet and it was shown by Gaidies et al. (subm.a) that it may effectively diffuse out of the garnet core and by this mechanism modify the original growth zoning.

Since the Permian garnet growth phase of rock sample 12F03 lacks inclusions of biotite, a possible anti-clockwise P - T trajectory during the Permian is merely hypothetically at this juncture. However, because enhanced gradients in X_{prp} and X_{alm} at the outermost rim of the first garnet growth phase are not observed in garnet of sample 12F03 (Fig. 4.9), a clockwise P - T loop seems more likely.

The complex compositional pattern of the second garnet growth phase allows a detailed reconstruction of the geothermal history during Eo-Alpine metamorphism. In that respect, the shoulder in the X_{grs} profile and the concomitant local maximum in X_{alm} , which are frequently observed in the central portion of the second growth phase of garnet porphyroblasts from the Wölz Complex, can be seen as rock specific geothermobarometer. From THERIA_G modelling, we infer that garnet growth started at ~ 530 °C and ~ 7.6 kbar and ceased at ~ 623 °C and ~ 9.7 kbar, which corresponds to the thermal maximum of the Cretaceous P - T - t trajectory (Fig. 4.11). Whereas the T calculated for incipient garnet growth during the Cretaceous matches estimates obtained by Gaidies et al. (2006) the P differs from what is proposed by the latter authors by ~ 0.7 kbar. Between ~ 586 °C at ~ 9.1 kbar and ~ 595 °C at ~ 9.6 kbar a period of garnet instability is found by THERIA_G modelling, at which garnet may have been subject to resorption. For the barometrical maximum of Eo-Alpine metamorphism a P of ~ 10.4 kbar is computed (Fig. 4.11).

Quartz, muscovite, ilmenite, rutile, plagioclase, and chlorite are calculated to have grown during the second metamorphic cycle. This is in agreement with petrographical observations.

Furthermore, the growth simulations are consistent with a decrease of ilmenite and an increase of the modal amount of rutile towards the garnet rim. THERIA_G modelling predicts equilibrium assemblages with chloritoid between ~ 530 °C at ~ 7.6 kbar to ~ 568 °C at ~ 8.3 kbar (assemblages 5 and 6 in Fig. 4.5) and a staurolite-bearing assemblage for the range between ~ 595 °C at ~ 9.6 kbar and ~ 605 °C at ~ 10.1 kbar (assemblage 8 in Fig. 4.5). Chloritoid and staurolite are, however, not discerned in rock sample 12F03. Chloritoid should have been formed relatively early during the growth of the second garnet growth phase and it is indeed frequently observed in the innermost portion of the Cretaceous growth phase of garnet porphyroblasts from the Wölz Complex. The lack of chloritoid at the respective position within the second growth phase of garnet from sample 12F03 may be explained by resorption of chloritoid in the course of garnet growth.

Although predicted from calculated equilibrium phase relations staurolite probably was never present during Cretaceous garnet growth. For the stage where staurolite and garnet were in equilibrium with ilmenite, chlorite, (2)phengite, quartz, and H₂O (assemblage 8 in Fig. 4.5) a significant maximum in X_{alm} is predicted in the corresponding garnet growth increment for any feasible heating rates, i.e. for heating rates in excess of 5 °C Ma⁻¹ (Fig. 4.10). However, such a feature is not perceived in the compositional profile of garnet.

From garnet growth modelling, heating rates larger than 50 °C Ma⁻¹ for the Eo-Alpine metamorphic event are likely. Only for such cases, the steep chemical gradients observed at the boundary between first and second garnet growth phase and particularly the sharp decrease of X_{sps} can be reproduced numerically (Fig. 4.10). Hence, our results are compatible with the findings of Faryad and Chakraborty (2005) who obtained a heating rate of 100 - 260 °C Ma⁻¹ for the Eo-Alpine metamorphic event.

Biotite, which is often observed as matrix mineral in rock sample 12F03 is not calculated to occur in garnet-bearing assemblages. The numerical simulations suggest its formation during decompression and retrogression subsequent to garnet growth (Fig. 4.8).

4.7.2 Limitations of garnet growth simulation

In principle, THERIA_G modelling may provide detailed information on the primary compositional gradients at the transition between the Permian and the Cretaceous garnet growth phase, which may be used as initial conditions for diffusion modelling. However, since the initial conditions are strongly contingent on the accuracy of the thermodynamic data, information on the temporal aspects of prograde metamorphism can yet only approximately be determined.

Besides inaccuracies in the thermodynamic and kinetic databases, the departure of the calculated compositional profile of the second garnet growth phase from the observed chemical patterns may be explained by sluggish mass transport in the rock matrix. Such a scenario may be expected for the Cretaceous metamorphic event because the rocks were dehydrated significantly during Permian metamorphism. As a consequence, Cretaceous garnet growth may rather be seen as a competitive process between neighbouring garnet individuals (Carlson, 1991).

In our growth modelling, all calcium-bearing matrix phases are exhausted during late stages of garnet growth, and the outermost portion of the second garnet growth phase is predicted to be free in X_{grs} . The fact that the outermost portions of the garnet porphyroblast of rock sample 12F03 have a low but readily detectable X_{grs} content suggests that another calcium-bearing phase was present in the matrix also during the latest stages of garnet growth. Epidote and allanite are obvious candidates which have not been considered in the thermodynamic model.

It may be hypothesised that during the period of garnet instability between the Permian and the Cretaceous, the composition of the thermodynamically relevant bulk rock composition was changed. As possible mechanisms, resorption of garnet or fluid infiltration may be considered. However, because of the euhedral shape of the garnet grain and the satisfactory reconstruction of the oldest garnet growth increments that occurred during the Cretaceous, substantial resorption of the outermost portion of the first garnet growth phase are very unlikely.

4.8 Conclusions

If local equilibrium can be demonstrated between the rim of a growing garnet and the rock matrix, the chemical zoning patterns of the garnet porphyroblast may provide thermobarometric information on the entire garnet growth history. This information may be extracted from the observed zoning pattern by forward modelling of garnet growth with the THERIA_G software. For a given bulk rock composition the calculated zoning pattern is highly sensitive to the P - T trajectory, along which garnet growth is simulated. If intracrystalline diffusion is taken into consideration, this even may allow to constrain the timing of a specific metamorphic event. Both, slow heating and cooling rates as well as prolonged residence of the rock at elevated T tend to degrade compositional gradients that may be present in the original growth zoning. It is generally not possible to unravel detailed rate information from the zoning pattern of a garnet porphyroblast, but the integrated effects of T and t may be constrained.

With THERIA_G modelling many of the features of the complex compositional zoning observed in a garnet porphyroblast of rock sample 12F03 from the polymetamorphic Wölz Complex can be reproduced numerically. For this sample our garnet growth modelling yields an isobaric prograde P - T path at ~ 3.8 kbar for the first garnet growth phase at low heating/cooling rates. This confirms the presumed HT/LP metamorphic event associated with lithospheric extension during the Permian. From the chemical zoning of the second garnet growth phase, constraints can be obtained on the geothermal history during Cretaceous garnet growth. Whereas for Permian metamorphism in the Wölz Complex a Buchan-type geothermal history is inferred, a Barrovian metamorphic event is documented for the Cretaceous. For the thermal maximum of Eo-Alpine metamorphism T conditions of ~ 625 °C at ~ 10 kbar are calculated. The maximum P yielded ~ 10.4 kbar at ~ 610 °C, and heating/cooling rates are estimated to have been larger than 50 °C Ma^{-1} during the Cretaceous event.

The full potential of THERIA_G modelling can only be exploited, if detailed information on garnet CSD and mineral chemistry of the respective rock sample is available. In such case, the specific investigation of garnet grains that nucleated late in the geothermal history may provide well-founded estimates for the temporal aspects of prograde metamorphism. Furthermore, the improvement of thermodynamic data and further information on the kinetics of intragranular diffusion in garnet will essentially enhance the applicability of THERIA_G to natural rocks.

4.9 Acknowledgements

We thank E. Reusser and R. Milke for their help with EMPA of garnet and are grateful to W. Tschudin for the sample preparation.

Chapter 5

Coupling garnet growth forward modelling with monazite geochronology: An application to the Rappold Complex (Austroalpine crystalline basement)

This chapter is to be submitted for publication as: **Gaidies, F.**, Krenn, E., de Capitani, C., and Abart, R. Coupling garnet growth forward modelling with monazite geochronology: An application to the Rappold Complex (Austroalpine crystalline basement). *Journal of Metamorphic Geology*.

5.1 Introduction

Monazite is a light rare earth element (LREE)-bearing phosphate, which is found in many rock types, especially in those with metagranitic to metapelitic composition. In such rocks, it can be formed over a wide range of metamorphic conditions (Cocherie et al., 2005; Spear and Pyle, 2002). Since Th and U preferentially partition into monazite during growth compared with other common accessory minerals and the major silicates (e.g. Kohn and Malloy, 2004) and because the accessory mineral is nearly unaffected by the loss of Pb up to high crustal

temperatures (e.g. Montel et al., 2000; Smith and Giletti, 1997), monazite plays a key role in dating igneous and metamorphic rocks. Monazite chemical composition and abundance in metamorphic rocks depend on the reaction history of REE-bearing accessory phases such as allanite, xenotime, and apatite and are contingent on major phase relations. In that respect, the extent of thermodynamic stability of garnet is of remarkable importance. Garnet may host considerable amounts of P and REE and thus influences the element budget available for the growth of refractory mineral phases during its growth and dissolution.

In the current communication the modal abundance and chemical composition of each major phase is calculated that evolves along a predefined metamorphic P - T - t trajectory in a specific metapelitic system. The formation of a garnet population in a given volume of rock is simulated and stages of garnet instability are determined, during which resorption of garnet may have occurred. For this purpose, the software program THERIA_G (Gaidies et al., *subm.a*) is used, which calculates the influence of changing P - T conditions on the rock-specific equilibrium phase relations. The model accounts for chemical fractionation associated with garnet growth and intragranular diffusion in garnet and considers their influence on effective bulk rock composition.

The coupling of THERIA_G modelling with monazite chemical Th-U-Pb microprobe ages offers the chance to link the trajectory of metamorphic P - T evolution with geochronological information. Based on compositional and textural relations between monazite and the major silicates in the rock volume under study, this may allow to relate metamorphic events in the earth history to their P - T evolution.

The rock samples investigated in this study are garnet-bearing metapelites from the Rappold Complex of the Austroalpine crystalline basement east of the Tauern Window. Even though, estimates for the P - T conditions of incipient garnet growth in the Rappold Complex (Gaidies et al., 2006) and for the thermal maximum of metamorphism (Faryad and Hoinkes, 2003) are known, information is scarce on the complete P - T evolution. Due to the high number of mineral inclusions in garnet, Sm-Nd garnet-whole rock geochronology could not be applied and ages for the time of garnet growth are yet unknown. However, Sm-Nd garnet-whole rock ages obtained for garnet in metapegmatites of the Rappold Complex yielded 262 ± 2 Ma and 288 ± 4 Ma (Schuster and Thöni, 1996; Schuster et al., 2001) suggesting an elevated geothermal gradient during the Permian.

5.2 Geological background

The Rappold Complex is a prominent lithostratigraphic unit of the Upper Austroalpine basement nappes east of the Tauern Window (Schmid et al., 2004). It is tectonically positioned between the Wölz and the overlying Saualpe-Koralpe Complexes and is separated from these units by Cretaceous thrust faults.

The Austroalpine nappe system represents the frontal part of the Apulian continental microplate, which in the Cretaceous was subject to internal deformation in the course of intra-continental collision. The Wölz, Rappold, and Saualpe-Koralpe Complexes formed parts of the tectonic lower plate during Cretaceous deformation and underwent greenschist to eclogite facies conditions. The intra-continental collision event in the Cretaceous is referred to as the Eo-Alpine event. Eo-Alpine metamorphism with maximum conditions of $\sim 550\text{-}625^\circ\text{C}$ and 10-12 kbar in the Wölz and Rappold Complexes (Gaidies et al., *subm.b*; Hoinkes et al., 1999; Schuster and Frank, 1999; Faryad and Hoinkes, 2003) and $700\text{-}740^\circ\text{C}$ and 22-25 kbar in the Saualpe-Koralpe Complex (Miller et al., 2005; Thöni, 2006) largely obliterated pre-Cretaceous metamorphic assemblages of low to medium metamorphic grade.

Garnet porphyroblasts from the Wölz Complex consist of two distinct growth zones (Abart and Martinelli, 1991; Bernhard and Hoinkes, 1999; Faryad and Chakraborty, 2005; Gaidies et al., 2006; Schuster and Frank, 1999; Schuster et al., 2001; Schuster and Thöni, 1996; Gaidies et al., *subm.b*). A first garnet generation commonly forms the cores of the garnet porphyroblasts and is separated from the rim-forming second generation by a microstructural and compositional discontinuity. According to geochronological investigations the garnet core of porphyroblasts from the Wölz Complex is related to Permian metamorphism whereas the rim was formed during the Eo-Alpine metamorphic overprint (Schuster and Thöni, 1996; Schuster and Frank, 1999; Thöni, 2002).

Based on garnet isopleth thermobarometry and the numerical simulation of garnet formation in the Wölz Complex Gaidies et al. (2006) and Gaidies et al. (*subm.b*) derived metamorphic temperatures of ~ 535 to 545°C at isobaric conditions of ~ 4.0 kbar at low heating/cooling rates for the Permian stage of garnet growth. These estimates confirm the assumption of an extensional tectonic regime during Permian metamorphism in the Wölz Complex, which is indicated by enhanced magmatic activity and high-temperature/low-pressure metamorphic assemblages (Schuster et al., 2001).

From parts of the Saualpe crystalline basement, which were less intensely affected during

the Cretaceous, Habler and Thöni (2001) derived conditions ranging between 600 to 700°C at ~ 4 kbar for assemblages of Permo-Triassic origin.

The morphological and compositional variety of garnet in metapelites from the Rappold Complex, which is tectonically positioned between Wölz and Saualpe-Koralpe Complex, is commonly taken as evidence for their polymetamorphic geothermal history (e.g. Gaidies et al., 2006; Bernhard and Hoinkes, 1999; Hoinkes et al., 1999; Schuster et al., 2001). In that respect, large garnet porphyroblasts of up to 1.5 cm in size are considered as pre-Eo-Alpine garnet generation, which was partly overgrown by individual garnet grains of < 1 mm in size. From the textural relation between the garnet generations and the rock matrix, it is inferred that the younger generation grew during a metamorphic overprint in the course of Eo-Alpine metamorphism. However, geological ages for the different garnet generations are yet unknown.

Gaidies et al. (2006) determined $525^{\circ}\text{C} \pm 15^{\circ}\text{C}$ and 5.3 ± 0.3 kbar for the stage of incipient garnet growth in the Rappold Complex, which yields a geothermal gradient of $\sim 30^{\circ}\text{C km}^{-1}$ for the respective metamorphic event. Faryad and Hoinkes (2003) derived P - T conditions of $\sim 540^{\circ}\text{C} \pm \sim 15^{\circ}\text{C}$ and 6.6 ± 0.8 kbar from the assemblage biotite, muscovite, plagioclase, quartz, ilmenite, and rutile. These P - T estimates are interpreted to reflect a different metamorphic event compared with garnet cores from the Wölz Complex, possibly of Variscan age. As an alternative explanation, Gaidies et al. (2006) suggest garnet formation in the Rappold Complex during the Permian as well but in a different crustal segment than the garnet cores of the Wölz Complex. Based on garnet-biotite thermometry and rutile-ilmenite equilibria Bernhard and Hoinkes (1999) derived 600-650°C and > 8 kbar for the growth of the second garnet generation, which they attribute to be the result of Eo-Alpine metamorphism.

Sm-Nd garnet-whole-rock ages obtained from garnet in metapegmatites of the Rappold Complex yielded 262 ± 2 Ma and 288 ± 4 Ma (Schuster and Thöni, 1996; Schuster et al., 2001). These results indicate an enhanced geothermal gradient during the Permian in the Rappold Complex.

For a detailed description of the geographical and tectonic position of the rock samples from the Rappold Complex investigated in this study, the reader is referred to a previous study (rock samples 31F03 and 35F03 in Table 1 and Fig. 2 of Gaidies et al., 2006).

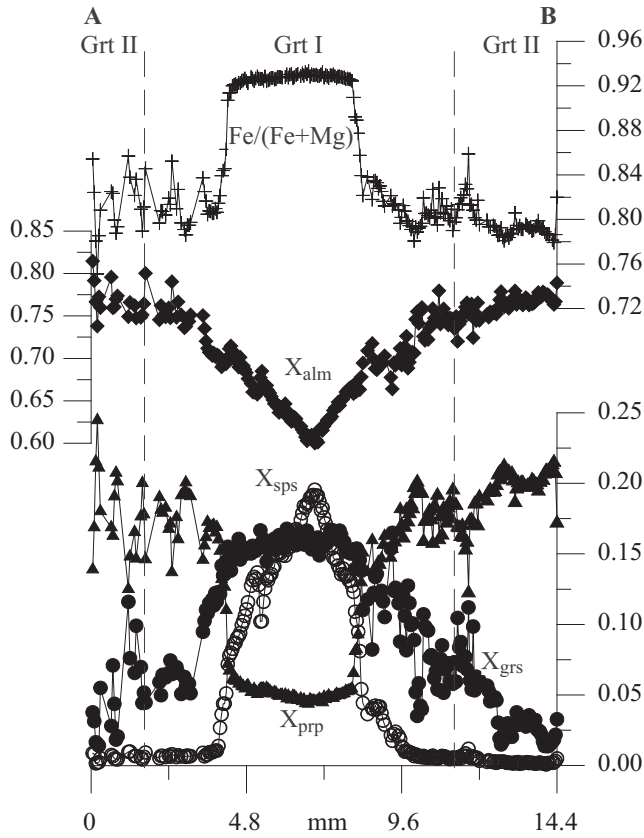


Figure 5.1 – Compositional profile of a garnet porphyroblast of rock sample 31F03. The transition between Grt I and Grt II is marked by an increase in X_{grs} and a concomitant decrease in X_{prp} and X_{alm} .

5.3 Methods

5.3.1 Sample preparation, EPMA, and WDXRFA

In order to investigate the entire geothermal history that a garnet may have been exposed to during metamorphism, serial sections with a distance of $\sim 0.6 - 0.8$ mm were prepared from a rock volume of $1 \times 2 \times 3$ cm size. The section of garnet with the largest diameter and with the highest content of X_{sps} [= $Mn / (Fe^{2+} + Ca + Mg + Mn)$] was carefully chosen to represent a traverse through the oldest garnet portion, thus containing the most compositional information of garnet available in the respective rock volume.

Electron-probe micro-analyses (EPMA) were performed with JEOL JXA-8200 at ETH Zurich to prepare compositional profiles (Figs 5.1, 5.2) of the garnet porphyroblasts under study. The garnet core compositions are listed in Table 5.1. X-ray maps for X_{grs} [= $Ca / (Fe^{2+} + Ca + Mg + Mn)$],

Table 5.1 – Garnet core chemistry of samples from the Rappold Complex.

Sample	31F03	35F03
SiO ₂	35.10	37.09
TiO ₂	0.08	0.06
Al ₂ O ₃	21.28	20.10
FeO	28.39	33.60
MnO	7.94	3.67
MgO	1.08	1.28
CaO	5.03	4.70
Total	98.90	100.50
Oxygen	12	12
Si	2.87	3.00
Ti	0.01	0.00
Al	2.05	1.92
Fe ³⁺	0.19	0.08
Fe ²⁺	1.76	2.19
Mn	0.55	0.25
Mg	0.13	0.15
Ca	0.44	0.41
Fe/(Fe+Mg)	0.93	0.93
X _{prp}	0.05	0.05
X _{alm}	0.61	0.73
X _{grs}	0.15	0.14
X _{sps}	0.19	0.08

$X_{alm} [=Fe^{2+}/(Fe^{2+}+Ca+Mg+Mn)]$, $X_{prp} [=Mg/(Fe^{2+}+Ca+Mg+Mn)]$, and X_{sps} are shown in Figs 5.6 and 5.7. The accelerating voltage was 15 kV for a beam current of 20 nA. Raw data were corrected using a PhiRhoZ routine. In a previous study (Gaidies et al., 2006), compositional maps of the garnet porphyroblast of sample 35F03 were prepared (their Fig. 9).

Accessory phase compositions and selected compositional profiles of garnet in the vicinity of monazite inclusions were investigated using JEOL JXA-8600 at Salzburg University. The microprobe is equipped with a backscattered-electron (BSE) imaging facility, an energy-dispersive analytical system (EDS) as well as four wavelength-dispersive (WD) spectrometers. At an accelerating voltage of 15 kV, different analytical routines were used: (1) Apatite and plagioclase were analysed with a 40 nA beam current and with a beam diameter of 5-15 μ m. (2) In order to obtain appropriate analytical accuracy, analyses of allanite were done using a beam diameter of 1-10 μ m at 50-100 nA in dependence on the size of the respective allanite domain under study and contingent on the H₂O content of allanite. (3) Garnet was analysed with 200 nA and

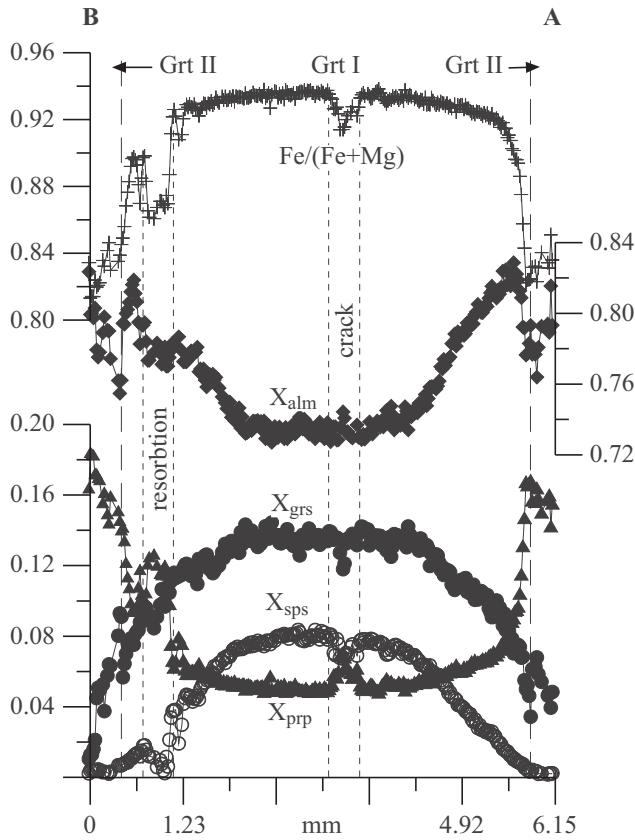


Figure 5.2 – Compositional profile of a garnet porphyroblast of rock sample 35F03. The transition between Grt I and Grt II is marked by an increase in X_{grs} and a concomitant decrease in X_{prp} and X_{alm} .

5-10 μm beam diameter. At such conditions and with a counting time of 60 s at the Y peak and 30 s at the background, detection limits and two sigma errors are in the range of 200-300 ppm. Element lines, analysing crystals, counting times, errors and detection limits for a beam current of 40 nA are given in Krenn and Finger (2004). Detection limits and errors for allanite analyses are somewhat better than those for plagioclase and apatite, which in turn are roughly two times higher than for garnet analyses. (4) For chemical dating, a beam current of 200 nA was used with a slightly defocused beam. Counting times for Pb, U, and Th were 240 s, 50 s, and 30 s, respectively. At such conditions, the one sigma errors for Th, U, and Pb were typically 0.02, 0.01, and 0.006 wt.-%, respectively. Except for Y (necessary for line overlap correction on Pb $M\alpha$), no other trace element (< 0.5 wt.-%) was analysed in this routine to keep the overall analysis time per point as short as possible and avoid beam irradiation effects (Jercinovic and William, 2005). In order to control the analytical results, a monazite standard of known age (341 Ma) was measured several times.

To obtain the bulk composition of the rock samples, wavelength-dispersive X-ray fluorescence

analyses (WDXRFA) on glass and powder pellets were performed with Bruker AXS SRS-3400. In that respect, ~ 1 kg of each sample that are devoid of macroscopically detectable chemical in-homogeneity were carefully chosen and crushed and ground to prepare rock powders for combustion analyses and fused pellets as well as powder pellets for XRFA. H_2O and CO_2 contents were determined by combustion analysis using a LECO combustion analyser. WDXRFA and combustion analysis were performed at the Mineralogical and Petrographical Institute at Basel University. The bulk rock compositions are given in Table 5.2.

5.3.2 Garnet growth modelling

To simulate the growth of a garnet population in a given volume of rock the software program THERIA_G (Gaidies et al., *subm.a*) was used. Based on Gibbs free energy minimisation, THERIA_G calculates the rock-specific equilibrium phase relations for any point along a predefined P - T - t path and considers the influence of chemical fractionation associated with garnet growth on effective bulk rock composition. In addition, the model accounts for intragranular diffusion in garnet and considers the influence on garnet chemical composition of the garnet nucleation history. As a result, THERIA_G modelling yields compositional profiles for each size class of a garnet population as well as all relevant information on the corresponding equilibrium phase assemblages such as equilibrium assemblage composition and chemical composition and modal abundance of all stable phases.

In the current study, the thermodynamic data of Holland and Powell (1998) (thermodynamic database of THERMOCALC, version 3.21) were used and calculations were done in the simplified model system MnNCFMASHT. To imply saturation of the system with respect to quartz and an aqueous fluid, SiO_2 and H_2O are considered as excess components throughout the entire P - T range studied. The following mixing models and notations are applied: Grt [garnet; Holland and Powell (1998)], Pl [plagioclase; Newton et al. (1980)], Bt [biotite; Powell and Holland (1999), extended to cover Fe and Mn solutions], St [staurolite; Holland and Powell (1998), extended to cover Mn solutions], Phng (phengite, following the description at <http://www.esc.cam.ac.uk/astaff/holland/ds5/muscovites/mu.html>), Ilm (ilmenite, ideal ilmenite-geikiellite-pyrophanite solution), ky (kyanite), and (andalusite), sill (sillimanite), cz (clinozoisite), ru (rutile), san (sanidine), and qtz (quartz). For the description of the solution model of Chl (chlorite) the reader is referred to the Appendix of Gaidies et al. (*subm.a*).

For the kinetic data of intragranular diffusion in garnet, the dataset of Chakraborty and Ganguly (1992) is employed.

Sample	31F03	35F03
SiO ₂	44.52	48.02
TiO ₂	1.30	0.97
Al ₂ O ₃	27.78	26.21
Fe ₂ O ₃	12.41	10.52
MnO	0.25	0.06
MgO	3.05	2.61
CaO	0.92	0.36
Na ₂ O	1.57	0.64
K ₂ O	5.24	5.84
P ₂ O ₅	0.17	0.16
H ₂ O	3.21	3.21
CO ₂	0.03	0.6
Total	100.45	99.20
Ce	78.0	148.3
La	34.7	65.7
Pb	47.7	20.8
Th	24.8	23.9
U	2.7	2.4
Y	29.1	31.3
Zr	171.3	109.8
Cr	157.6	146.9
Rb	250.8	248.5
Sr	287.2	131.8

Table 5.2 – Representative bulk-rock compositions of samples from the Rappold Complex (major elements in wt%, trace elements in ppm).

5.3.3 Monazite dating by means of electron-probe micro-analysis

Due to radioactive decay of ²³²Th, ²³⁸U, and ²³⁵U in monazite to ²⁰⁸Pb, ²⁰⁷Pb, and ²⁰⁶Pb, a chemical age, τ , can be calculated after measuring the Th, U, and Pb contents in the monazite grain. According to the relation

$$\begin{aligned}
 Pb = & \frac{Th}{232} \left(e^{\tau\lambda^{232}} - 1 \right) 208 \\
 & + \frac{U}{238} 0.9928 \left(e^{\tau\lambda^{238}} - 1 \right) 206 \\
 & + \frac{U}{238} 0.0072 \left(e^{\tau\lambda^{235}} - 1 \right) 207,
 \end{aligned} \tag{5.1}$$

presented by Montel et al. (1996) a chemical age may be calculated through mathematical iteration. In relation (5.1) λ^{232} , λ^{238} , and λ^{235} are the radioactive decay constants of ²³²Th,

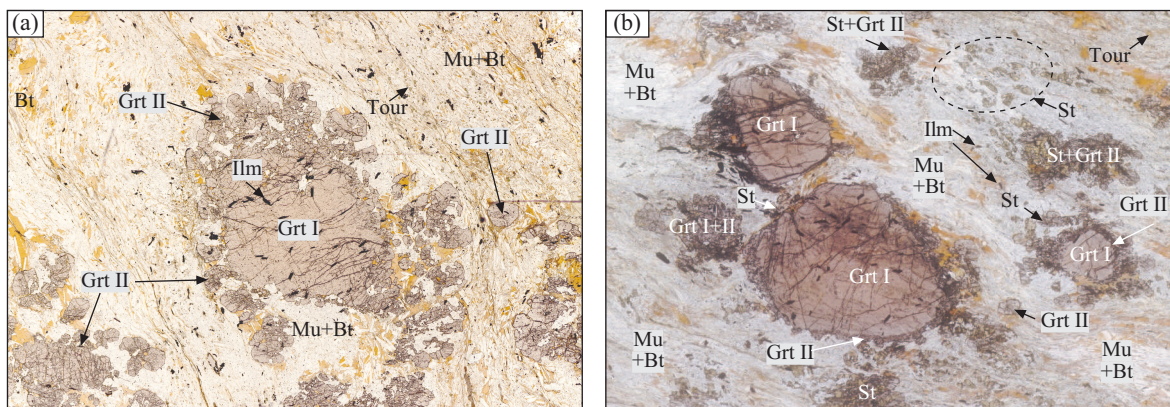


Figure 5.3 – Photomicrographs showing garnet porphyroblasts with two generations (Grt I and Grt II) of (a) rock sample 31F03 and (b) rock sample 35F03. In sample 35F03, Grt II rims St and indications are found for the growth of Grt II at the expense of St. In rock sample 31F03 St is scarce.

^{238}U , and ^{235}U , respectively, and Pb, Th, and U are the chemical concentrations in ppm as analysed with the electron microprobe. Assuming low amounts of common Pb (Parrish, 1990) and slow diffusion rates for Th, U, and Pb in monazite (Cherniak et al., 2004), the chemical age is expected to closely reflect the formation age of a monazite crystal (or a monazite domain), thus providing a geological meaningful age information.

If several monazite grains tend to be of the same age, the overall error can be minimised by calculating a weighted average age (Montel et al., 1996) considering the errors of single monazite ages. As a test for data consistency and the absence of common Pb, Th* vs. Pb isochron diagrams after Suzuki et al. (1991) are prepared in the present study.

5.4 Sample description

5.4.1 Petrography

Biotite, muscovite, tourmaline, and rutile, which form the main foliation of the rock samples from the Rappold Complex, as well as minor sericitic plagioclase, quartz, secondary chlorite and ilmenite are the most abundant minerals of the rock matrix. Biotite is found as two different generations, where the older one forms strongly resorbed and recrystallised blasts of 1 - 2 mm in size. The younger biotite generation is < 1 mm in size and represents an essential part of the foliation. Furthermore, numerous staurolite blasts are observed in rock sample 35F03, but are scarce in sample 31F03 (Fig. 5.3). Staurolite typically includes abundant finely dispersed

graphite particles and – similar to the first biotite generation – is intensely resorbed. Occasionally, staurolite rims a first garnet generation. Equilibrium textures are found between staurolite and the first garnet generation including straight interphase boundaries.

The first garnet generation (Grt I) is up to 15 mm in size and strongly graphitic. Inclusions of ilmenite and tourmaline, which trace a former foliation without indication of porphyroblast rotation during garnet growth, as well as small chloritoid grains and muscovite are observed. Grt I is subhedral and strongly fractured.

The second garnet generation (Grt II) differs from Grt I with respect to the number and size of mineral inclusions and its wart-like texture. Grt II forms $\sim < 1$ -mm-wide overgrowths on Grt I and is observed as separate individuals in the rock matrix as well. In such cases, Grt II commonly rims staurolite (but in sample 31F03) and indications for the growth of Grt II at the expense of staurolite are noticed. Small mineral inclusions are abundant in Grt II and are rutile, biotite, tourmaline, minor ilmenite and muscovite. From the textural relation to the main foliation it is concluded that Grt II was formed concomitantly to the main foliation of the rock. An increased number of mineral inclusions along the boundary between Grt I and Grt II could not be perceived. Some inclusions in Grt II individuals trace a former foliation and indicate garnet rotation during growth.

5.4.2 Monazite abundance, morphology, and chemical composition

Monazite grains are abundant in rock samples 31F03 and 35F03 and are up to 50 μm in size (Fig. 5.4). It is important to note, that monazite is restricted to Grt II and the rock matrix. Monazite inclusions in Grt I are scarce and are related to alteration zones. In such cases, monazite forms clusters in sample 35F03 closely associated with quartz, \pm muscovite, \pm biotite, \pm plagioclase [Fig. 5.4(d)]. Single microscopic monazite individuals are observed in Grt I of rock sample 31F03 as well and are clearly related to alteration and infiltration of garnet along cracks.

Whereas in both, Grt II and the rock matrix, single monazite grains are observed in sample 31F03, clusters of monazite are present in rock sample 35F03 [Fig. 5.4(a-d)]. In most cases, the clustered monazite is euhedral to subhedral, $\sim 20 \mu\text{m}$ in size and lacks evidence of marginal resorption. Occasionally, tiny allanite relicts are found adjacent to these clusters.

Whereas the monazite grains in rock sample 35F03 are similar in morphology irrespective of their textural position, the situation is different for rock sample 31F03. In sample 31F03, monazite inclusions are idiomorphic to hypidiomorphic and poorly embayed if enclosed in Grt II. On the contrary, monazite observed in the rock matrix is highly irregular in shape, deeply

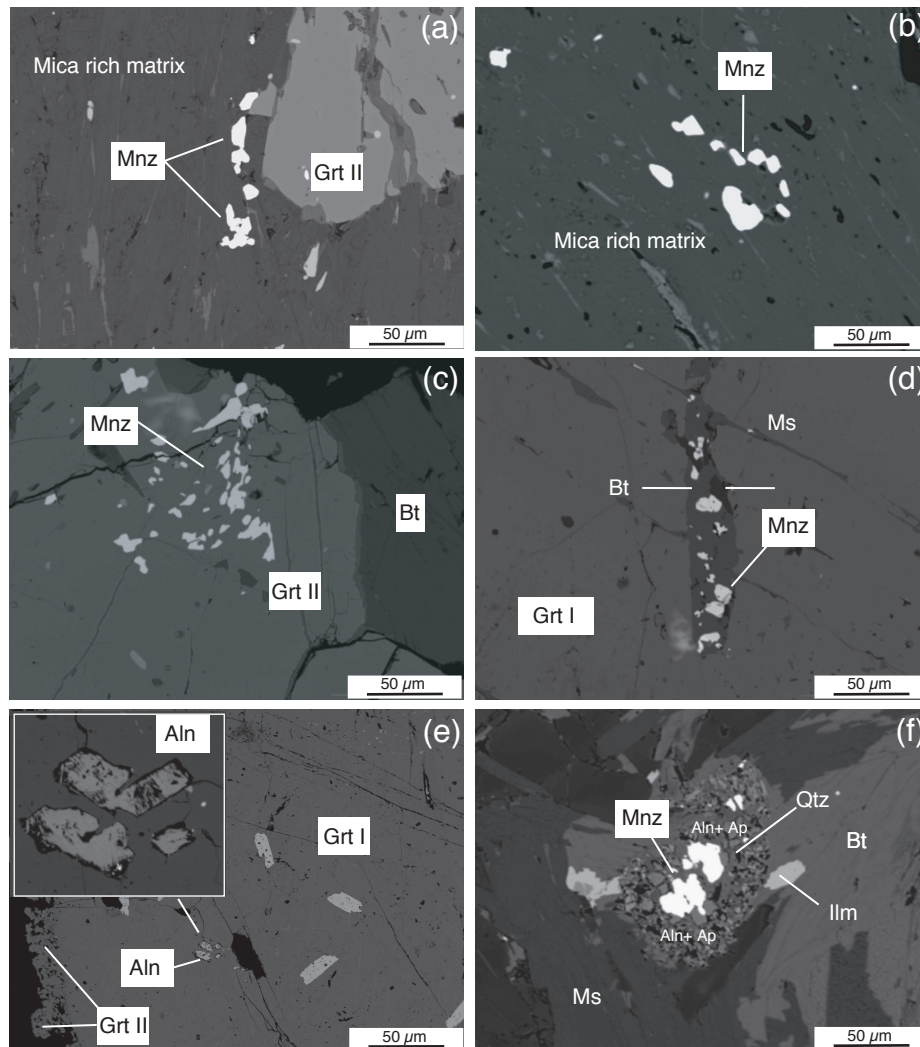


Figure 5.4 – Back-scattered electron (BSE) photomicrographs of monazite and allanite in garnet-bearing metapelites of the Rappold Complex. In rock sample 35F03 clusters of monazite are observed in the rock matrix (a+b) as well as within Grt II (c) and Grt I (d). Monazite in Grt I is considered as secondary (see text for explanation). Allanite is restricted to Grt I in both samples studied (e) and was observed in the rock matrix (f). (f) illustrates an allanite-apatite corona surrounding monazite in sample 31F03.

Position	Grt II	Grt II	Grt II	Grt II
Y	1.46	1.30	1.65	1.39
Th	2.31	3.50	2.70	3.55
U	0.34	0.59	0.31	0.48
Pb	0.04	0.06	0.04	0.06
Th*	3.42	5.39	3.71	5.11
Age	266	250	254	270
Error	40	34	49	31
La	11.02	9.84	9.95	9.97
Nd	9.38	10.01	10.07	9.30
Oxide Σ	98.91	100.13	98.92	98.23
tetr.	1.00	0.98	0.99	1.01
oct.	1.00	1.04	1.04	0.99
Br%	4.50	7.18	5.27	8.18
Hu%	1.09	0.61	0.44	0.46

Table 5.3 – Representative age analyses of monazite from rock sample 31F03.

indented and always surrounded by allanite - apatite seams [Fig. 5.4(f)].

Monazite grains, which form clusters in sample 35F03, are uniform with respect to their Y content but contain variable amounts of Th. However, the Y content significantly varies between monazite of different clusters [Fig. 5.5(a)]. In general, Y in different monazite grains of rock sample 31F03 display similar high Y contents.

5.4.3 Allanite abundance, morphology, and chemical composition

Allanite is observed as part of the rock matrix and as mineral inclusion in Grt I in both, rock sample 31F03 and 35F03 [Fig. 5.4(e-f)]. Allanite is not found as inclusion in Grt II. Allanite inclusions remarkably differ from allanite grains observed in the matrix with respect to their morphology and chemical composition.

Matrix allanite solely occurs closely intergrown with microscopic apatite, monazite, quartz, \pm chlorite, \pm biotite, \pm ilmenite. Monazite commonly forms the cores of these mineral aggregates. In most cases, the allanite grains are fractured and perforated [Fig. 5.4(f)]. Furthermore, the BSE intensities are variable across a single grain, indicating irregularly distributed domains with heterogeneous chemical composition. Dark zones in BSE images correspond to higher contents in Y and M+HREE as well as lower contents in Th and LREE compared with bright zones in BSE intensity.

In contrast to allanite grains of the rock matrix, inclusions of allanite in Grt I are by far less

Table 5.4 – Representative age analyses of monazite from rock sample 35F03.

Position	Gr I	Grt II	Matrix	Grt II	Grt II	Grt II	Grt II	Grt II
Y	0.62	0.97	0.79	1.12	1.01	1.23	1.36	1.05
Th	2.62	3.37	0.91	0.91	1.25	3.37	3.71	1.64
U	0.07	0.36	0.45	0.20	0.40	0.36	0.30	0.23
Pb	0.04	0.06	0.03	0.02	0.03	0.06	0.06	0.04
Th*	2.83	4.55	2.38	1.55	2.54	4.56	4.69	2.40
Age	283	297	250	284	243	277	298	346
Error	45	28	62	127	109	124	133	155
La	10.93	10.87	13.11	11.59	10.98	10.21	9.94	10.77
Nd	9.99	10.04	9.77	9.92	10.13	9.67	9.87	9.80
Oxide Σ	98.15	97.94	98.65	99.31	98.86	97.81	98.99	97.21
tetr.	1.03	1.00	1.02	0.99	0.99	1.00	0.98	1.00
oct.	0.96	1.00	0.97	1.02	1.02	1.01	1.04	1.02
Br%	0.85	6.49	1.91	1.68	2.69	5.99	6.19	2.99
Hu%	5.96	0.60	0.55	0.57	0.33	0.62	0.89	0.53

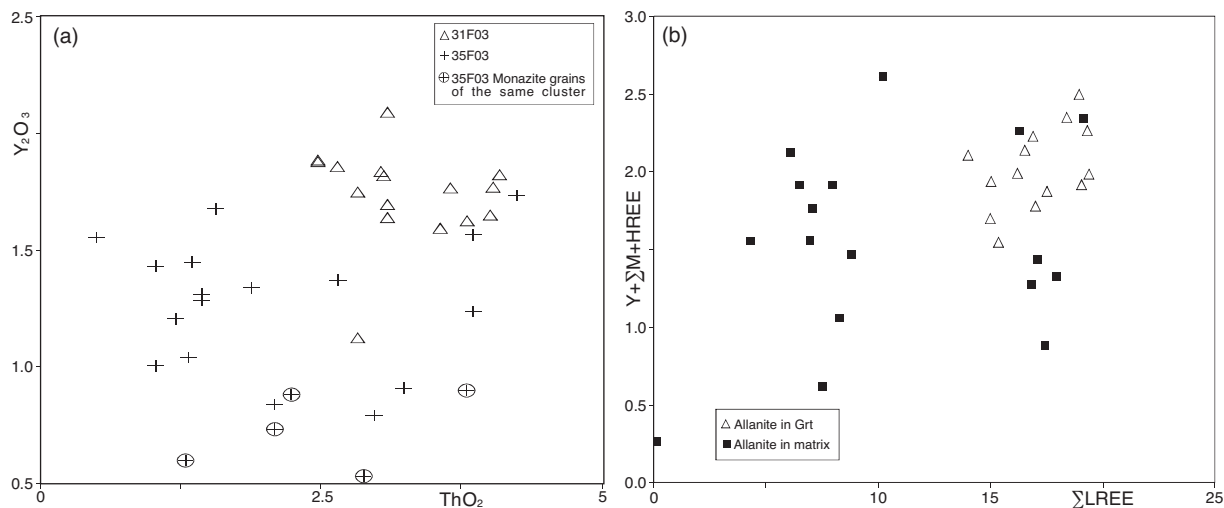


Figure 5.5 – Variation of chemical composition of (a) monazite with respect to the Y_2O_3 and ThO_2 contents and (b) allanite with respect to the contents of LREE and $Y + (HREE, MREE)$. Note that high quantities of Y are common in rock sample 31F03 but were observed in sample 35F03 as well. Allanite is homogeneous when present as inclusion in garnet but displays a certain spread in LREE vs. $Y + (HREE, MREE)$ when observed in the rock matrix.

Table 5.5 – Chemical composition of allanite.

Sample	31F03	35F03	35F03	31F03	31F03
Position	Gr I	Gr I	Gr I	Matrix	Matrix
SiO ₂	34.33	35.13	35.11	35.46	38.93
Al ₂ O ₃	19.76	21.23	21.47	21.18	26.31
CaO	9.48	11.62	11.86	10.40	18.83
FeO	11.46	11.27	10.49	10.34	7.29
MgO	0.18	0.25	0.28	0.83	0.37
TiO ₂	0.09	0.03	0.01	0.14	0.24
MNIO	1.31	0.12	0.10	0.00	0.00
∑LREE	19.33	16.88	17.01	17.06	6.92
∑M+HREE	1.91	1.68	1.11	1.31	0.99
Total	97.84	98.22	97.44	96.72	99.88

fractured and more homogeneous in BSE intensity and chemical composition [Figs 5.4(e), 5.5(b)]. Allanite is observed all over the entire volume of Grt I in both rock samples. Whereas allanite in Grt I of rock sample 35F03 is up to several 100 μm in size and euhedral, allanite in garnet of sample 31F03 is somewhat smaller and in most cases subhedral. Despite the differences in size and morphology of allanite grains in rock samples 31F03 and 35F03, their chemical compositions are relatively uniform with high contents of LREE and $\sum\text{REE}$ contents of up to 20 % (Table 5.5). In general, allanite in Grt I lacks indications of alteration, and intergrowths with other minerals are not observed [Fig. 5.4].

5.4.4 Garnet chemistry

The compositional profiles across the core of the garnet porphyroblasts of rock samples 31F03 and 35F03 are illustrated in Figs 5.1 and 5.2. The respective X-ray maps and BSE images are shown in Figs 5.6 and 5.7. From the information on garnet chemical composition of both samples an increase of X_{alm} and X_{prp} as well as a decrease of X_{sps} , X_{grs} , and $\text{Fe}/(\text{Fe}+\text{Mg})$ from the core to the rim of Grt I are discernible. However, the gradient of X_{sps} and X_{alm} in the core of garnet from rock sample 31F03 is much steeper compared with garnet from rock sample 35F03. In addition, the X_{sps} content is noticeably larger and X_{alm} is remarkable smaller in the core of sample 31F03 than in garnet of rock sample 35F03 (Table 5.1).

Whereas the compositional profile of Grt I in rock sample 35F03 may be considered symmetrical, the profile of Grt I in the porphyroblast of sample 31F03 is rather disproportionate. Furthermore, the compositional trends in Grt I of 31F03 are discontinuous indicating periodic garnet growth and resorption.

The transition between Grt I and Grt II can be identified according to the distinct increase of

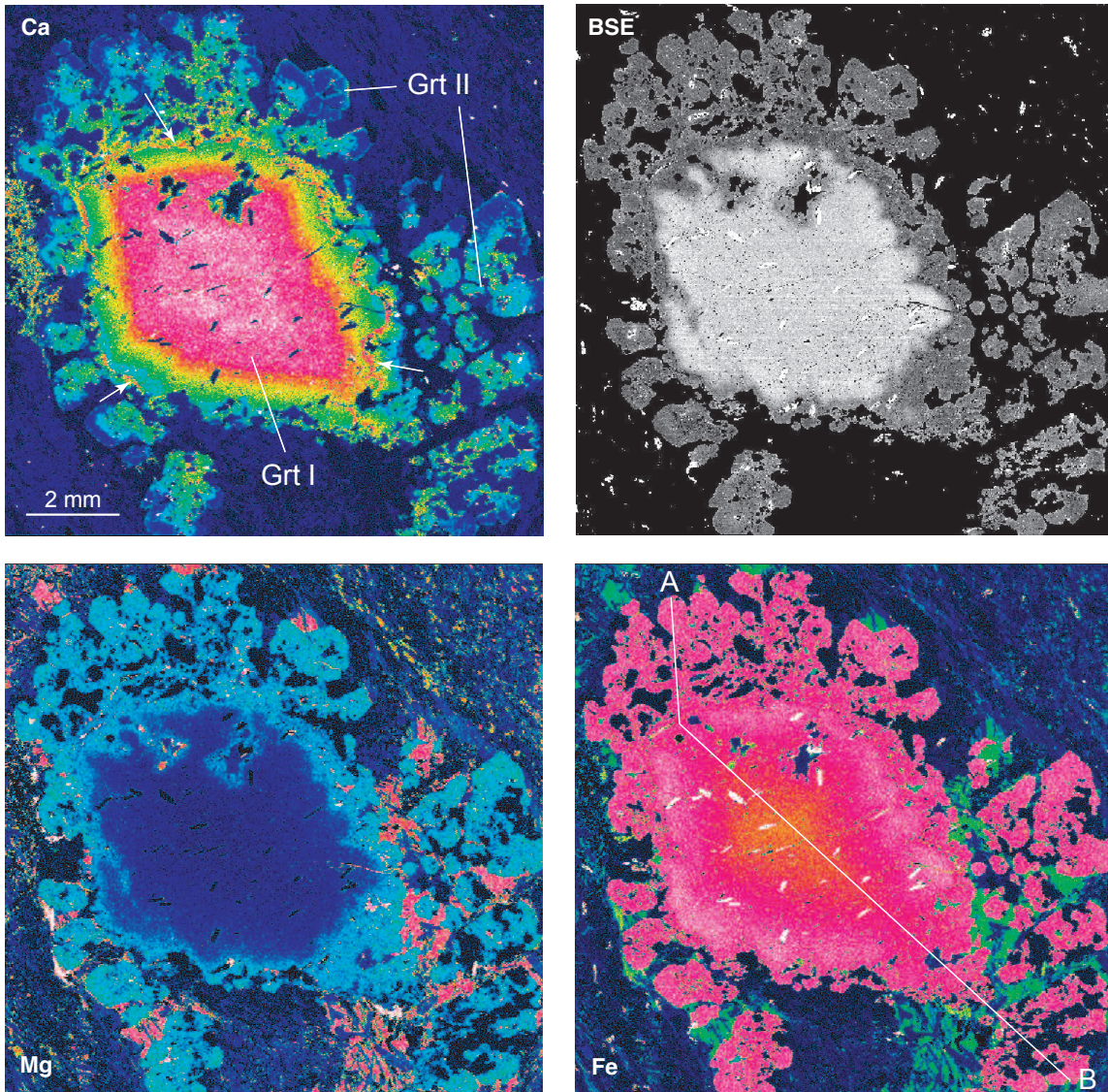


Figure 5.6 – X-ray maps for Ca, Mg, and Fe and BSE image of a garnet porphyroblast of rock sample 31F03. Grt I and Grt II are marked. The arrows in the Ca-map denote the Ca-annulus in the innermost portion of Grt II. Note the undulating outline of the Ca-annulus, which may indicate significant resorption of Grt I prior to the formation of Grt II. Profile A-B of Fig. 5.1 is indicated.

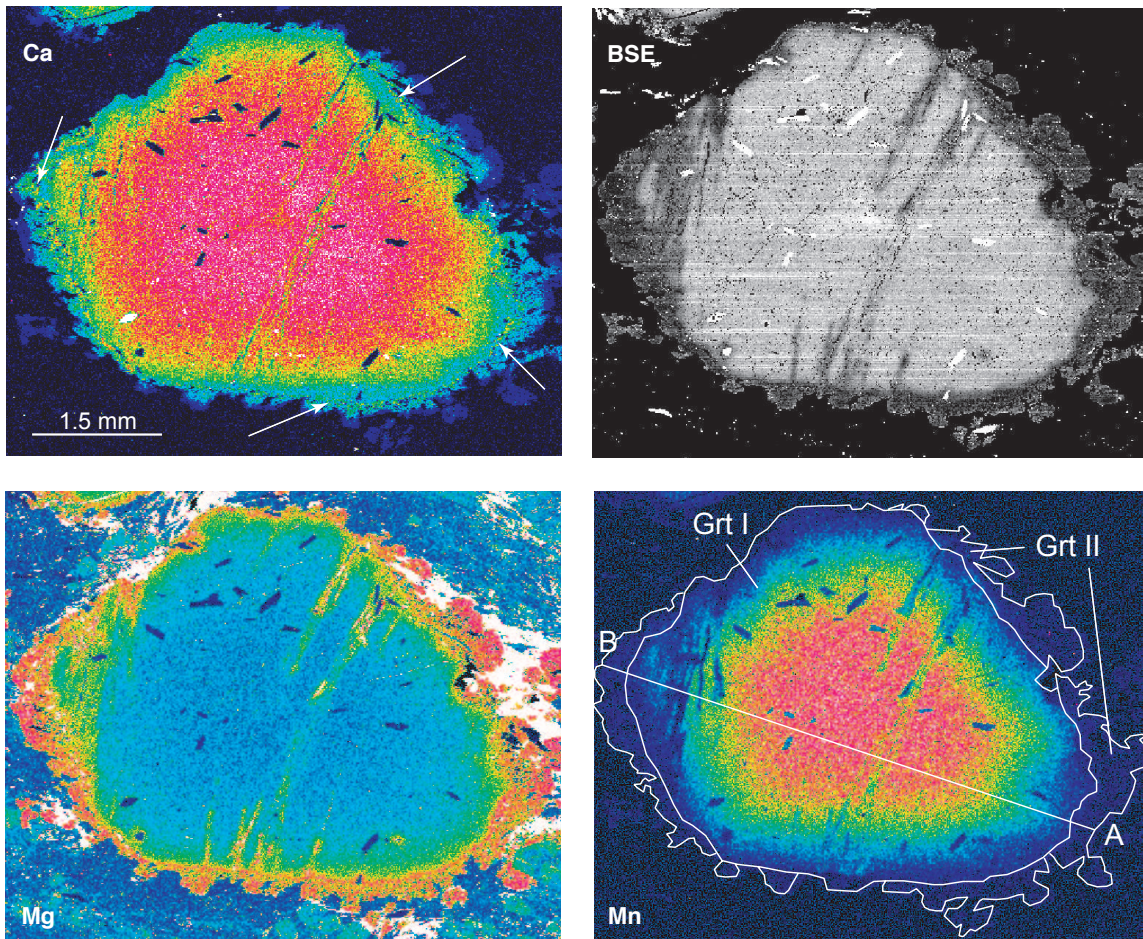


Figure 5.7 – X-ray maps for Ca, Mg, and Mn and BSE image of a garnet porphyroblast of rock sample 35F03. The transition between Grt I and Grt II is marked. The arrows in the Ca-map denote the Ca-peak in the innermost portion of Grt II. Line A-B of the compositional profile in Fig. 5.2 is illustrated.

X_{grs} and concomitant decrease of X_{alm} and X_{prp} (Figs 5.1, 5.2, 5.6, 5.7, and 5.8). The increase in X_{grs} is steeper in 31F03 compared with the garnet porphyroblast of 35F03. The sharp increase of X_{prp} in Grt I of both samples is responsible for the distinct feature in their BSE images.

Fig. 5.6 displays the undulating shape of the X_{grs} annulus in Grt II of rock sample 31F03, indicating remarkable resorption of Grt I prior to the growth of Grt II. The wavy outline of the X_{grs} annulus is less striking in garnet of rock sample 35F03 which may point to a rather moderate impact of resorption on garnet morphology (Fig. 5.7). However, in both samples remarkable garnet resorption subsequent to the formation of Grt II is indicated.

5.5 Results

5.5.1 P-T path of metamorphism

The P - T conditions during the incipient stages of garnet formation in rock samples 31F03 and 35F03 are obtained by the application of garnet isopleth thermobarometry. A description of that method as well as applications to garnet-bearing metapelites of the Austroalpine basement are given in Gaidies et al. (2006). The equilibrium phase relations prior to and at the initial stage of garnet growth as well as the corresponding areas of isopleth intersection are illustrated in Figs 5.9, 5.10, and 5.11. Whereas the area of isopleth intersection for sample 35F03 is directly positioned at the lower limit of the garnet stability field at $\sim 533^\circ\text{C}$ and ~ 5.2 kbar, isopleth intersection for sample 31F03 occurs at P - T conditions of $\sim 512^\circ\text{C}$ and ~ 5.5 kbar. The obtained P - T conditions for incipient garnet growth in sample 31F03 exceed the calculated lower limit of garnet stability by $\sim 25^\circ\text{C}$.

In a previous study (Gaidies et al., 2006) the bulk rock composition of rock sample 35F03 was already used for garnet isopleth thermobarometry and an area of isopleth intersection was obtained that – in contrast to the calculations presented here but similar to sample 31F03 – exceeds the lower limit of the garnet stability field. The discrepancy between the calculations presented in the current study compared with the results of Gaidies et al. (2006) may be due to the different models used for the solid solution of chlorite [see Appendix in Gaidies et al. (subm.a)] or due to the different algorithms for Gibbs free energy minimisation implemented in the THERIAK/DOMINO (de Capitani and Brown, 1987; de Capitani, 1994) and PERPLEX (Connolly, 1990; Connolly and Petrini, 2002; Connolly, 2005) software. It is interesting to note that in both cases the calculations result in an area of isopleth intersection that is positioned at exactly the same P - T conditions. However, the P - T conditions of the lower limit of the garnet

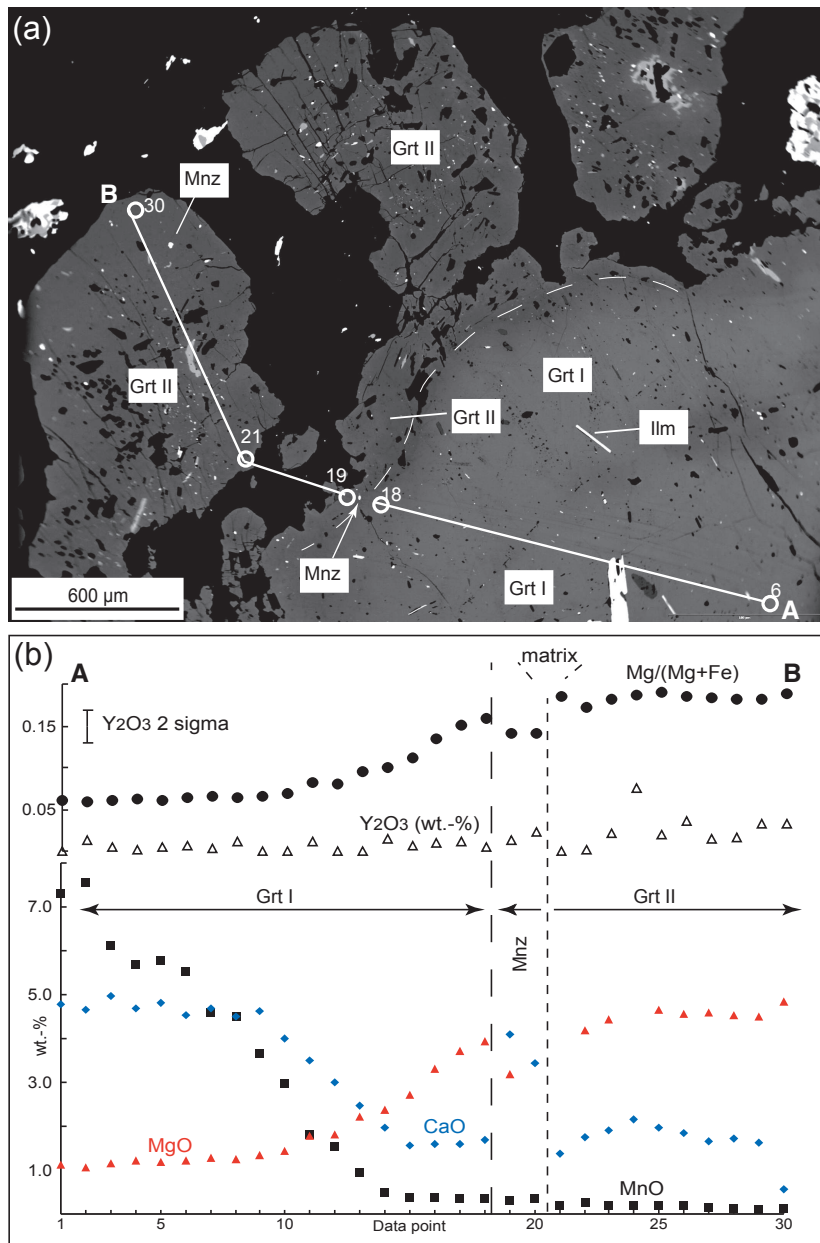


Figure 5.8 – Compositional profile A-B across the transition between Grt I to Grt II in rock sample 31F03. (a) BSE image illustrating the position of the profile as displayed in (b). Note the monazite inclusion at the innermost portions of Grt II and its textural relation to the sharp increase of CaO in garnet.

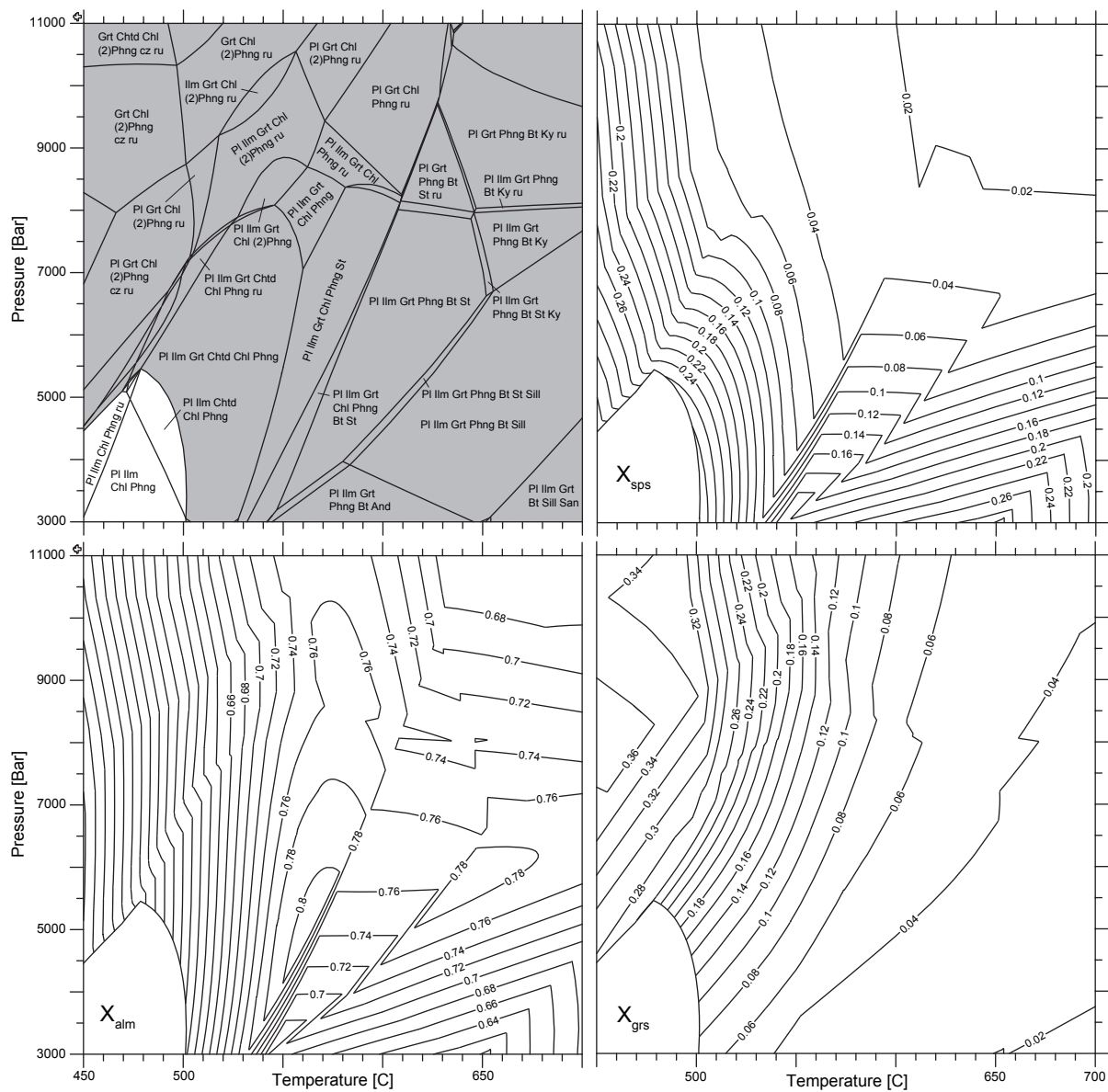


Figure 5.9 – Equilibrium phase relations and P - T dependency of garnet chemical composition and modal abundance prior to garnet formation calculated for rock sample 31F03. H_2O and SiO_2 are considered as excess components throughout the entire P - T range.

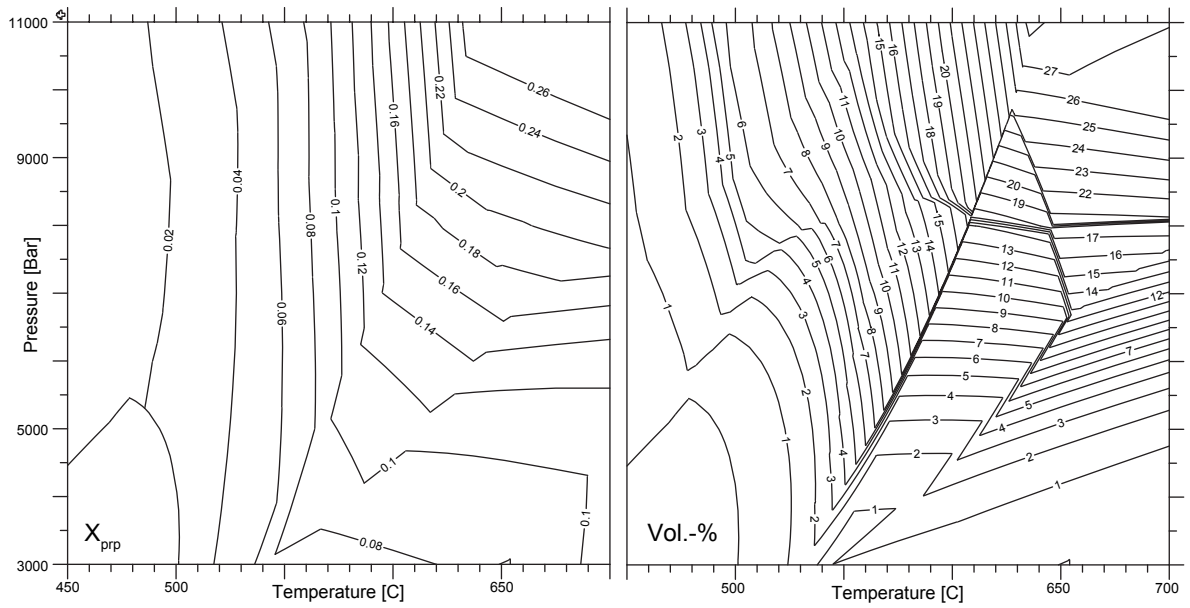


Figure 5.9 – Cont'd.

stability field differ by $\sim 25^{\circ}\text{C}$.

The symmetrical compositional pattern of garnet in rock sample 35F03 and the comparatively few indications of garnet resorption during growth (Figs 5.2 and 5.7) lend this sample to the reconstruction of the possible P - T - t path of metamorphism by THERIA_G modelling. Due to the irregular compositional zoning of garnet in rock sample 31F03 and indications for periodic garnet growth and resorption (Figs 5.1 and 5.6), garnet growth modelling applied to sample 31F03 is deemed problematic.

From the results of garnet isopleth thermobarometry applied to garnet of rock sample 35F03 (Fig. 5.11) it can be assumed that the garnet porphyroblast under study is one of the oldest individuals of the garnet population in the respective equilibrium volume. Therefore, a theoretical garnet crystal size frequency distribution (CSD) is used for garnet growth modelling, which results in size ranges for the largest porphyroblasts that are similar to the size of garnet in sample 35F03.

The most successful result of garnet growth modelling is presented in Fig. 5.12(a). The predicted chemical composition of Grt I greatly resembles the observed garnet chemistry with the exception of the chemical gradients of X_{grs} and the absolute concentrations of X_{prp} . The observed X_{grs} trend shows an irregularity in the central portions of Grt I, which could not be recreated numerically. The calculated absolute concentrations of X_{prp} underestimate the

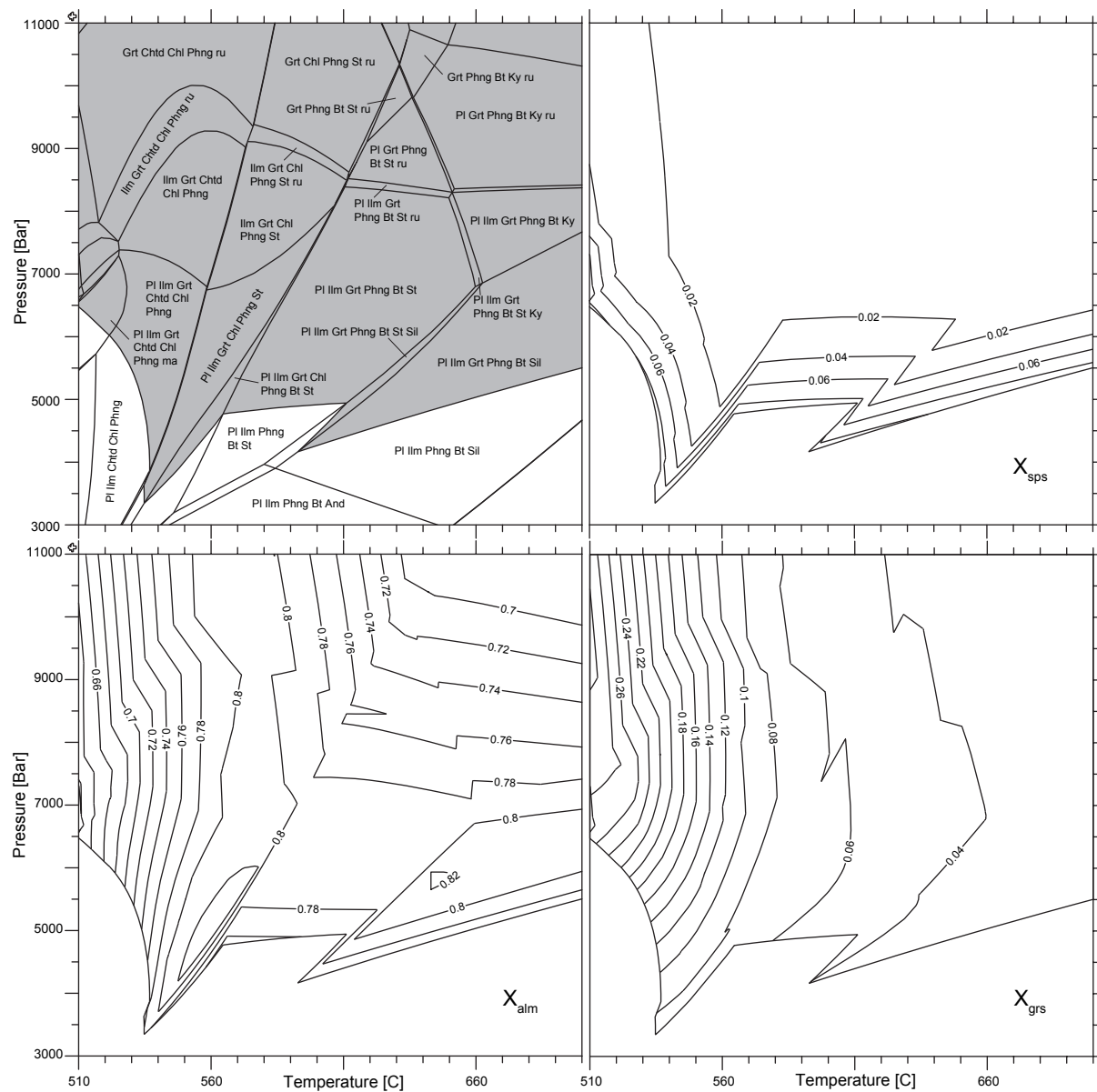


Figure 5.10 – Equilibrium phase relations and P - T dependency of garnet chemical composition and modal abundance prior to garnet formation calculated for rock sample 35F03. H_2O and SiO_2 are considered as excess components throughout the entire P - T range.

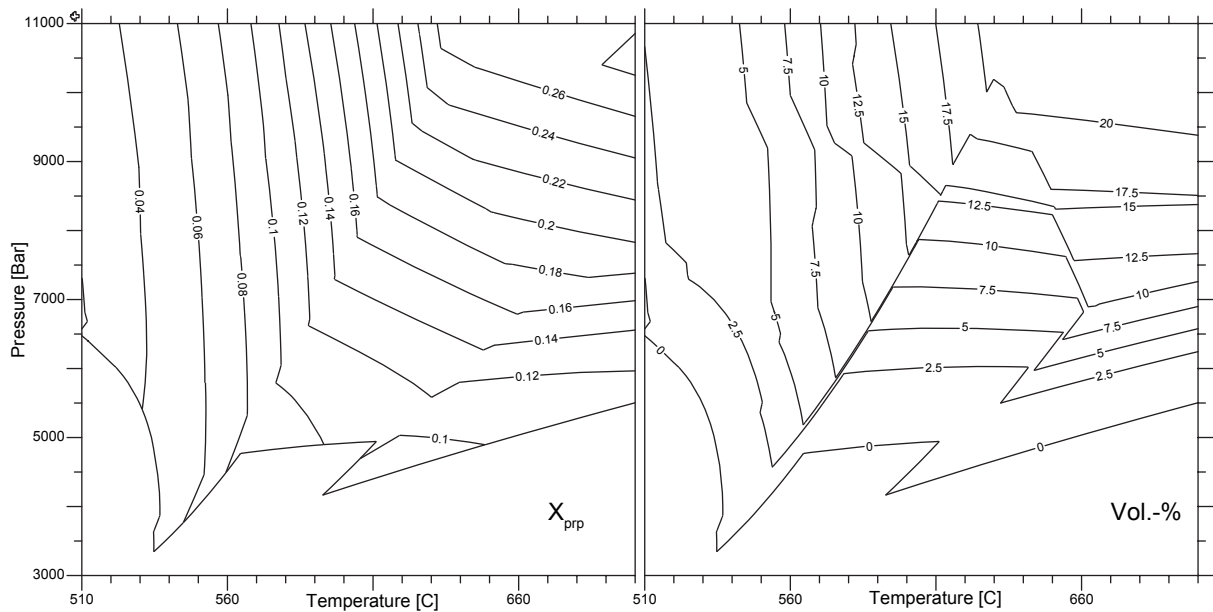


Figure 5.10 – Cont'd.

observed values by <1 mol-%.

The most significant differences between the observed and calculated compositional profiles can be perceived especially for Grt II. The increase in X_{grs} , which typically marks the transition between Grt I and Grt II (Figs 5.1, 5.2, 5.6, 5.7, and 5.8), could not be predicted. In our calculations, plagioclase is the only mineral phase, which provides Ca for garnet growth [see assemblages in Fig. 5.12(b)]. However, since during growth of Grt I crucial amounts of Ca were fractionated into garnet, the Ca-activity of the thermodynamic relevant bulk rock composition is strongly reduced and the modal abundance of plagioclase remarkably decreases during growth of Grt II. This is the reason, why the calculations yield values for $X_{grs} < 0.001$. As a consequence, the predicted X_{prp} exceeds the observed quantities by ~ 0.05 .

The compositional profiles and garnet-bearing equilibrium assemblages illustrated in Fig. 5.12 were obtained by THERIA_G modelling along the P - T - t path shown in Fig. 5.13. The calculations indicate that growth of Grt I started at P - T conditions of $\sim 533^\circ\text{C}$ and ~ 5.2 kbar [point (1) in Fig. 5.13] and ended at $\sim 580^\circ\text{C}$ and ~ 6.4 kbar [point (2) in Fig. 5.13]. Between points (1) and (2) garnet growth was continuous and occurred in the equilibrium assemblages 1-3 given in Fig. 5.12(b).

To account for a possible polymetamorphic history of the rock samples from the Rappold

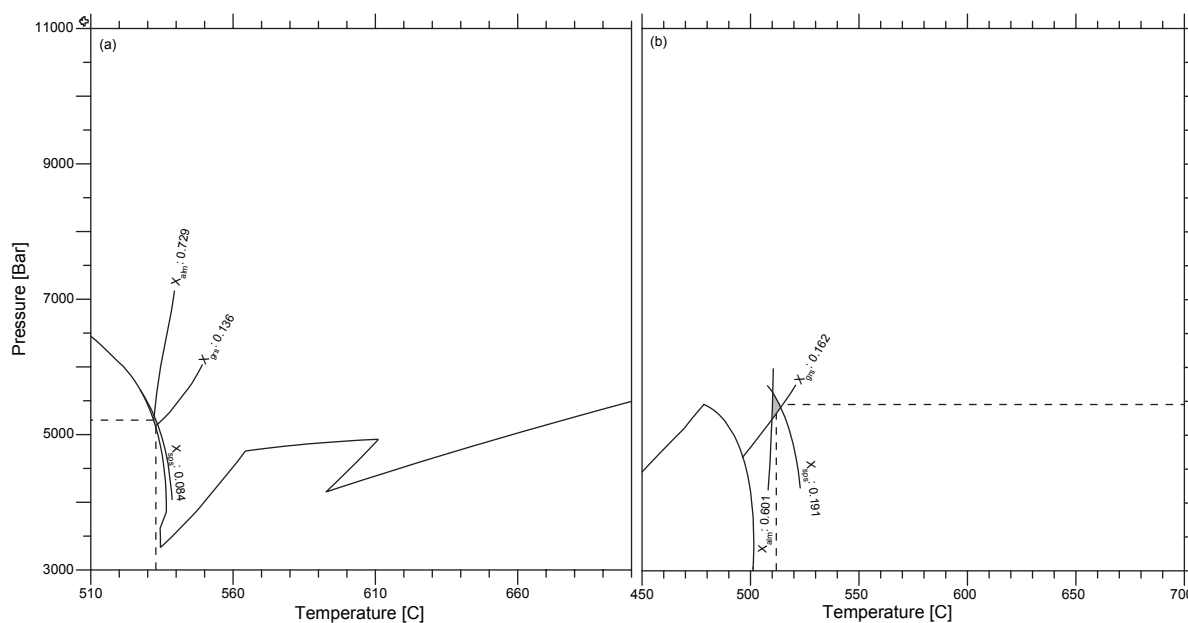


Figure 5.11 – P - T conditions during incipient growth of Grt I for (a) rock sample 35F03 and (b) rock sample 31F03 obtained by garnet isopleth thermobarometry (Gaidies et al., 2006). Note the distinct difference between the P - T conditions obtained for incipient garnet growth in sample 31F03 and the lower limit of the garnet stability field.

Complex, different geothermal histories are considered in our calculations (Fig. 5.13). In every case, a metamorphic evolution is modelled, which consists of three different metamorphic cycles. During the first cycle, Grt I grows between P - T points (1) and (2) (Fig. 5.13) and the thermal maximum of the cycle is at $\sim 660^\circ\text{C}/6.5$ kbar. Garnet growth along other possible P - T trajectories is modelled as well but resulted in completely different compositional profiles for garnet compared with the observed trends.

A second metamorphic cycle follows, which is modelled as a high-temperature/low-pressure (HT/LP) metamorphic event typical for Permian metamorphism in the Austroalpine crystalline basement. The equilibrium phase relations subsequent to the formation of Grt I are illustrated in Fig. 5.14. Because the P - T path of the second cycle does not intersect the lower limit of the garnet stability field, equilibrium assemblages with garnet do not occur.

The increased gradients in chemical compositions, which followed from the changes of the garnet-bearing equilibrium assemblages during growth of Grt I, were relaxed by intragranular diffusion during the second metamorphic cycle. The possible influence of different thermal maxima during the HT/LP event on the efficiency of intragranular diffusion in garnet is given

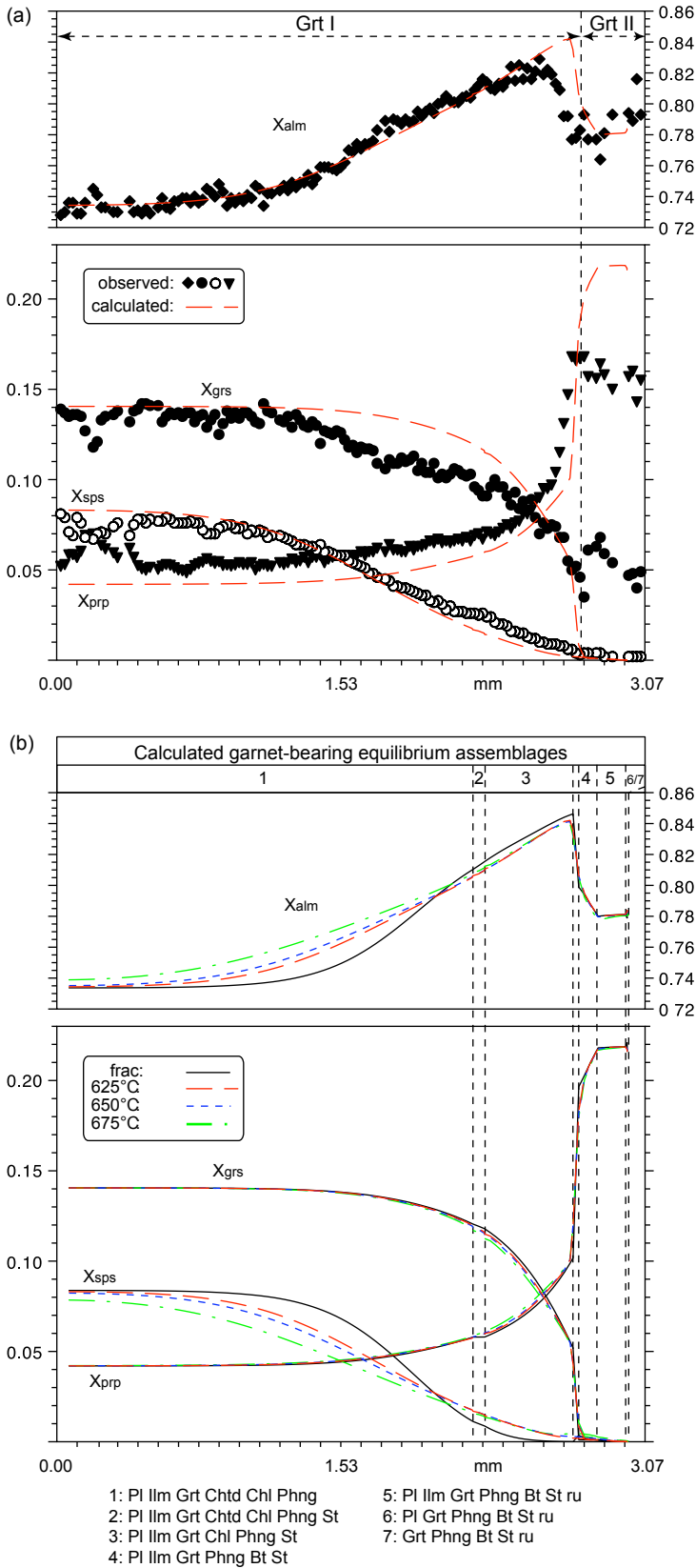


Figure 5.12 – Observed and calculated compositional profiles of garnet in rock sample 35F03. (a) illustrates the best result obtained from garnet growth modelling. The P - T - t conditions during garnet growth are shown in Fig. 5.13. For the thermal maximum of the second P - T loop, 625°C are used. (b) focuses on the influence of the thermal maximum during the second metamorphic cycle (Fig. 5.13) on garnet chemical composition. For comparison, the compositional profile is shown, which results, if only chemical fractionation during growth is considered and intragranular diffusion is neglected [profile ‘frac’ in (b)]. All assemblages with Qtz and H₂O.

in Fig. 5.12(b). The most successful result is obtained by considering a thermal maximum of $\sim 625^\circ\text{C}$ for the second metamorphic event. A possible prolonged residence of the rock samples at the thermal maximum of metamorphism is not considered in our calculations. In general, this would lead to an enhanced efficiency of diffusion.

In our modelling, a significant period of garnet instability occurred between the growth of Grt I and Grt II, which spans $\sim 60^\circ\text{C}$ and 2 kbar [points (2) and (3) in Fig. 5.13]. Resorption of garnet, which may have happened during such a period, especially if the rock sample experienced elevated T conditions, is not modelled. It can be assumed that resorption would modify the compositional gradients of the outermost portions of Grt I and may result in changes of the effective bulk rock composition.

Metamorphism along the third metamorphic cycle considered in our calculations may result in the growth of Grt II between the points (3) and (4) in Fig. 5.13. It is interesting to note that the P - T conditions needed to create the chemical composition of the first growth increments of Grt II are a continuation of the P - T trajectory during formation of Grt I. Whereas during growth of Grt I biotite is not calculated as part of the thermodynamic stable garnet-bearing equilibrium assemblage, biotite is predicted to be stable together with plagioclase, ilmenite, phengite, and staurolite during the formation of Grt II [assemblage 4 in Fig. 5.12(b)].

The phase relations of equilibrium assemblage 4 in Fig. 5.12(b) document the thermal maximum along the metamorphic P - T evolution. Garnet growth in the same assemblage proceeds along retrograde conditions. Retrograde growth of Grt II occurs between $\sim 644^\circ\text{C}$ at 9.0 kbar and $\sim 631^\circ\text{C}$ at 9.4 kbar and finishes as soon as plagioclase leaves the stable equilibrium assemblage.

5.5.2 Th-U-Pb microprobe ages of monazite

Despite the chemical variation of various monazite grains [Fig. 5.5(a)] and their different textural positions in rock samples 31F03 and 35F03 (Fig. 5.4) almost all analyses yield a Permian age. The weighted mean ages, which have been calculated using the software Isoplot/Ex (Ludwig, 2001), are 267 ± 12 Ma for rock sample 31F03 and 274 ± 17 Ma for rock sample 35F03. Weighted average ages are in good agreement with Th^* vs. Pb isochron ages, which have been obtained using the Th^* vs. Pb diagram after Suzuki et al. (1991) (Fig. 5.15). Since the isochrons trend towards the origin of the diagram, the Th-U-P system can be deemed undisturbed. That is, the Permian ages are likely to be of geological relevance.

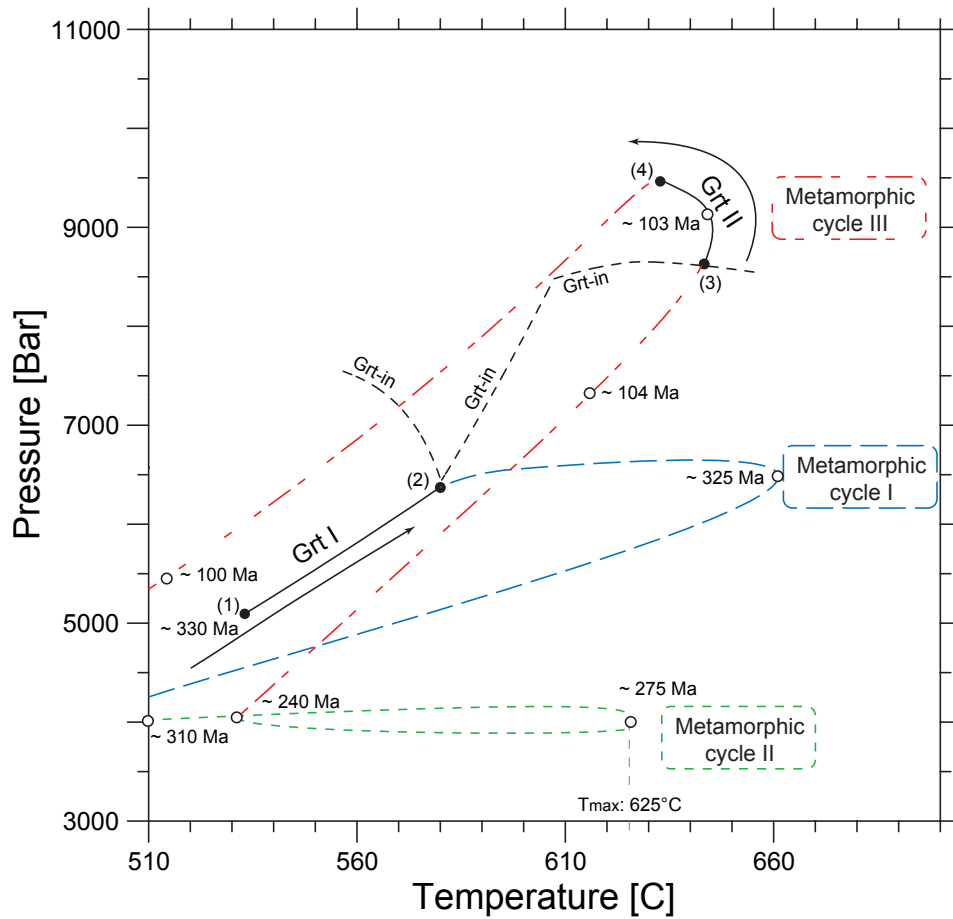


Figure 5.13 – P - T - t trajectory (stippled line) used for the calculation of the compositional profile of garnet illustrated in Fig. 5.12(a). Growth of Grt I occurs between points (1) and (2) as part of the first possible metamorphic cycle (metamorphic cycle I). During the second metamorphic event (metamorphic cycle II) garnet does not grow because the lower limit of the garnet stability field is not intersected by the HT/LP path (the Grt-in curve for the stage subsequent to formation of Grt I is shown for reference). In Fig. 5.12, the influence of different thermal maximum conditions during the second cycle on garnet composition is shown. Grt II is formed between points (3) and (4) in the course of the third metamorphic cycle (possible metamorphic cycle III).

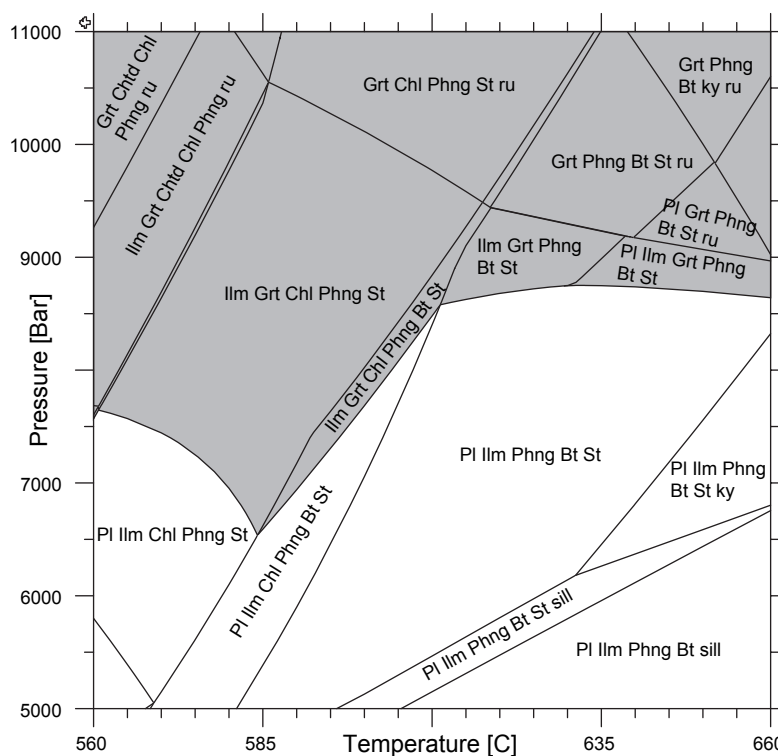


Figure 5.14 – P - T phase diagram section showing the equilibrium phase relations subsequent to the growth of Grt I [P - T point (2) in Fig. 5.13]. The grey area marks the stability field of garnet. All assemblages with Qtz and H_2O .

5.6 Interpretation and Discussion

Despite similar P - T conditions during incipient growth of Grt I in the rock samples 31F03 and 35F03 (Fig. 5.11), both rocks differ significantly in terms of the X_{sps} contents of their first growth increments (Table 5.1). This can be explained by the remarkable difference in MnO in the bulk-rock chemistries (Table 5.2). From the steep gradients in X_{alm} and X_{sps} in sample 31F03 (Fig. 5.1) and the shift between the lower limit of garnet stability and the area of isopleth intersection (Fig. 5.11), we conclude that this garnet porphyroblast may originate from a later stage in the nucleation history (Gaidies et al., *subm.a*).

Because inclusions of allanite in Grt I of rock sample 31F03 and 35F03 are subhedral to euhedral in shape and lack evidence of significant alteration, a primary origin of the respective mineral grains can be considered. Furthermore, since allanite is observed throughout the entire volume of Grt I but not in Grt II, we suggest allanite formation during growth of Grt I.

Allanite, which possibly was not enclosed with the overgrowing garnet but was part of the rock matrix, may be subjected to subsequent overprint and dissolution. The monazite clusters, which are frequently observed in the rock matrix and in Grt II of sample 35F03 [Fig. 5.4(a-d)],

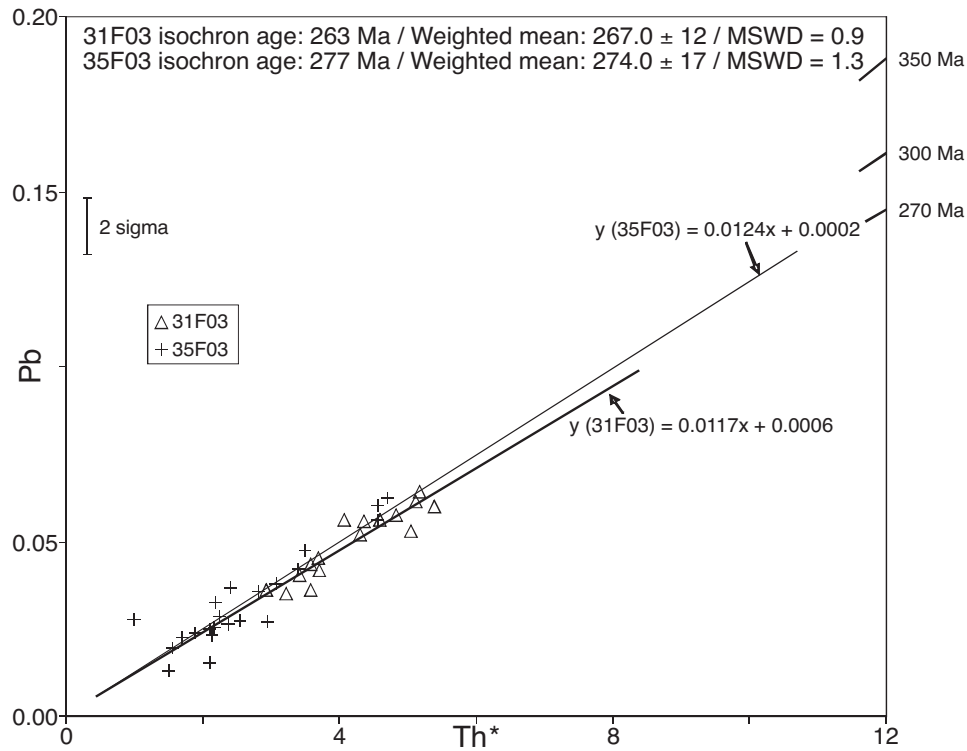


Figure 5.15 – Th* vs. Pb diagram after Suzuki et al. (1991) showing isochron slopes, the corresponding isochron ages and weighted mean ages computed for monazite of the rock samples from the Rappold Complex. Weighted mean ages have been calculated with the software Isoplot/Ex (Ludwig, 2001).

may be interpreted as pseudomorphs after such allanite grains (e.g. Wing et al., 2003; Krenn and Finger, 2007). Their high contents of REE support this hypothesis.

Wing et al. (2003) relate the stability of allanite and monazite in pelitic schists to the CaO content of the bulk rock composition. In that respect it is important to note that chemical fractionation associated with garnet growth may remarkably influence the effective Ca-activity of the bulk rock system. As chemical fractionation is strongly controlled by the garnet-forming P - T - t trajectory, this has to be considered to determine the thermodynamically relevant Ca-activity. In the study presented here, growth of Grt I in rock sample 35F03 significantly reduces the effective Ca-activity during metamorphism. This is indicated by the remarkable reduction of the stability field of plagioclase (Figs 5.10, 5.14) during growth of garnet from P - T point (1) to point (2) in Fig. 5.13.

Since geochronological information on the growth of Grt I are yet unknown, the age of this garnet forming metamorphic event can only indirectly be estimated. The P - T path required

to produce the chemical composition of Grt I [P - T point (1) to point (2) in Fig. 5.13] strongly suggests a Barrow-type metamorphic evolution during Grt I formation. Such a geothermal history is assumed for the Variscan metamorphic event in the Austroalpine crystalline basement (e.g. Tollmann, 1977). We therefore propose formation of Grt I with allanite inclusions during the Carboniferous.

Mineral inclusions of ilmenite, muscovite, and chloritoid are observed in Grt I and are considered as parts of the garnet-bearing equilibrium assemblages [Fig. 5.12(b)]. In addition, our garnet growth modelling reproduces the concurrent growth of Grt I and staurolite and suggests progressive formation of staurolite subsequent to Grt I formation. The discrepancy between observed and calculated X_{grs} content in the central portions of Grt I may be explained by phase relations with allanite/epidote, which – due to the lack of the respective thermodynamic data – could not be considered in our simulations.

From garnet growth modelling it is likely that biotite did not concurrently grow with Grt I at a P - T trajectory similar to the one predicted for the formation of Grt I in rock sample 35F03 [Fig. 5.12(b)]. In conjunction with a possible dichotomy between allanite and monazite (Spear and Pyle, 2002; Wing et al., 2003), this may confirm the assumption that the few clusters of monazite associated with quartz, \pm muscovite, \pm biotite, \pm plagioclase along cracks in Grt I of sample 35F03 [Fig. 5.4(d)] are not related to growth of Grt I and allanite but rather present a younger mineral assemblage.

Since all monazite grains in clusters of rock sample 35F03 are of Permian age, allanite dissolution and pseudomorphism of monazite after allanite possibly occurred during the Permian. From the textural setting, the Y chemistry, the Barrow-type P - T path typical for Variscan metamorphism, and a possible dichotomy of allanite and monazite in the rock samples from the Rappold Complex, we suggest the formation of Permian monazite subsequent to the growth of Grt I.

To simulate the geothermal history during Permian metamorphism, we have chosen a P - T - t path that may reflect the possible HT/LP metamorphic event in the Austroalpine basement and accounts for the results obtained by Gaidies et al. (subm.b) for the Permian metamorphic evolution of metapelites from the Wölz Complex (Fig. 5.13). As a result of chemical fractionation during growth of Grt I and the associated shrinkage of the garnet stability field, in our simulations garnet does not grow during the Permian. In such a case, monazite would be the only relic mineral phase of Permian metamorphism in the Rappold Complex.

Frequently, the formation of monazite at the expense of allanite is linked to the prograde

growth of staurolite at the expense of garnet during lower amphibolite facies conditions (e.g. Wing et al., 2003; Smith and Barreiro, 1990; Kohn and Malloy, 2004). However, based on textural and mass balance considerations, Yang and Pattison (2006) suggest that the major phase relations at the lower limit of the stability field of staurolite can not be attributed responsible for the formation of monazite in allanite-bearing rocks from the Black Hills, South Dakota. Yang and Pattison (2006) propose that the discontinuous breakdown of allanite triggers the formation of monazite and, hence, monazite ages may rather correspond to monazite forming reactions at the expense of allanite then to the resorption of garnet.

The high contents of Y in monazite of rock sample 31F03 from the Rappold Complex compared with the available Y bulk rock budget (Table 5.2) as well as the low Y contents in allanite inclusions and the lack of xenotime in Grt I point to an additional phase besides allanite as precursor for monazite formation in sample 31F03. Since Y strongly partitions into garnet during growth compared with other major minerals and due to its high modal abundance in metapelites of the Rappold Complex, garnet may serve as potential Y source for monazite formation. In that respect, the period of garnet instability between P - T points (2) and (3) in Fig. 5.13 may reflect stages of garnet resorption and significant Y liberation at elevated T conditions during the Permian. The comparatively high Y content in monazite of rock sample 31F03 compared with monazite of sample 35F03 may directly result from increased influences of garnet resorption in the respective rock sample (compare X-ray maps in Figs 5.6 and 5.7).

In our model, the influence of garnet resorption on major equilibrium phase relations is not considered. In principle, garnet resorption shifts the lower limit of the garnet stability field to lower T - P conditions. In cases, where resorption of garnet may have a remarkable influence on effective bulk rock composition, the lower limit of the garnet stability may be moved such that the P - T - t path of the Permian metamorphic event intersects the garnet stability field. For the complex polymetamorphic evolution considered in the calculations presented here, this would lead to garnet formation during the Permian as well.

The complex chemical composition of garnet in rock sample 31F03 (Figs 5.1, 5.6) may reflect several stages of periodic garnet resorption and growth during the Permian. It is interesting to note that monazite in the respective rock sample forms randomly distributed individual grains in contrast to the pseudomorphous monazite clusters in rock sample 35F03, which was less intensely resorbed.

In accordance to Tomkins and Pattison (2007), we attribute the various textures of Permian monazite in rock samples 31F03 and 35F03 to different transport rates of LREE through the rock

matrix. Tomkins and Pattison (2007) argue for enhanced fluxes of LREE due to the dehydration of the rock matrix related to prograde garnet growth at the expense of hydrous phases such as biotite and chlorite. Monazite formation, which is not related to garnet growth, may occur in a dehydrated rock matrix with sluggish LREE transport. This may explain the cluster-like appearance of monazite in rock sample 35F03.

The most significant difference between the calculated and observed garnet chemical composition is the typical X_{grs} annulus perceived in rock samples from the Rappold Complex, which could not be reproduced numerically. This feature together with a concomitant decrease in X_{alm} and X_{prp} (Figs 5.1, 5.2, 5.6, 5.7, and 5.8) mark the transition between Grt I and Grt II. From the textural relationship between Grt II and the main foliation of the rock matrix, which was formed during Eo-Alpine metamorphism in the Cretaceous, it can be inferred that both were formed during the same metamorphic event.

The numerous indications of Grt I resorption prior to Grt II formation indicate that the X_{grs} annulus in Grt II may result from an increase of the Ca-activity of the rock matrix through garnet resorption. The increased Ca-activity may have stabilised plagioclase rather than allanite during the Permian geothermal event. At the elevated P conditions during the Eo-Alpine metamorphic event (third metamorphic event in Fig. 5.13) Ca preferentially partitions into garnet compared with plagioclase. It is interesting to note that the increase in X_{grs} is larger in rock sample 31F03 than in sample 35F03 and that sample 31F03 possibly underwent comparatively more significant stages of dissolution. In addition, the high contents of Y in monazite of rock sample 31F03 may indirectly reflect a higher level of garnet resorption.

Monazite with irregular shape and surrounding apatite-allanite-epidote coronas have firstly been described by Finger et al. (1998) in a granitoid lithology at amphibolite facies conditions. They interpret such a texture as evidence for the growth of the corona at the expense of monazite and noticed that monazite crystals armoured by minerals with low intracrystalline diffusion coefficients like garnet were prevented from breakdown and corona development.

Because allanite-apatite coronas around monazite are restricted to the rock matrix, Grt II in the rock samples from the Rappold Complex evidently grew prior to corona formation. From the results of the garnet growth simulation in conjunction with the textural relation between Grt II and the Cretaceous main foliation of the rock samples, we suggest the corona formation along the retrograde branch of the Eo-Alpine P - T - t trajectory. The irregularly distributed domains with heterogeneous chemical composition within individual allanite grains of the rock matrix confirm the secondary origin of allanite, possible as pseudomorph after monazite. The formation

of allanite may be triggered by resorption of Grt II.

The P - T conditions obtained for the thermal maximum during Eo-Alpine metamorphism perfectly match the estimates derived by Bernhard and Hoinkes (1999) through garnet-biotite thermometry and rutile-ilmenite equilibria. However, it is important to note that the required P - T path for Eo-Alpine metamorphism in the Rappold Complex obtained from our calculations (third metamorphic cycle in Fig. 5.13) essentially differs from the geothermal history during the Cretaceous proposed for the Wölz Complex (Gaidies et al., *subm.b*).

Whereas for the underlying Wölz Complex a clockwise P - T path during the Cretaceous is determined by Gaidies et al. (*subm.b*), this study points to an anticlockwise P - T path in the Rappold Complex. In addition, the onset of Eo-Alpine metamorphism in the Rappold Complex is placed to conditions of $\sim 520^\circ\text{C}$ and 4 kbar, which is ~ 3 kbar lower than expected for Eo-Alpine metamorphism in the Wölz Complex.

The wart-like texture of Grt II in metapelites of the Rappold Complex may be explained by sluggish material transport through the rock matrix. Due to the complex polymetamorphic history prior to Grt II formation, the rock is likely to have been significantly dehydrated. In such a case, material transport may be slow, thus controlling the garnet growth rate and morphology. As a result, the sites of garnet nucleation and growth may be confined to the sites of precursor location and a wart-like texture rather than concentric garnet shells may be formed. Concurrent growth of garnet and micas such as biotite and phengite during retrograde conditions may increase the influence of material transport on garnet morphology.

As for garnet growth modelling with the THERIA_G model (Gaidies et al., *subm.a*) the rock matrix has to be considered thermodynamical homogenous, significant dehydration during polymetamorphism in the Rappold Complex may explain the apparent discrepancy between the geothermal histories determined for the Eo-Alpine metamorphic event in the Rappold and Wölz Complexes.

5.7 Conclusions

Permian metamorphism in the Rappold Complex is documented by Th-U-Pb microprobe ages of monazite in garnet-bearing metapelites. They confirm the increased geothermal gradient suggested by geochronological investigations of garnet in metapegmatites from the Rappold Complex (Schuster and Thöni, 1996; Schuster et al., 2001).

From the coupling of garnet growth modelling with monazite geochronology and the investigation of the textural and compositional relations between the major and accessory mineral phases two additional metamorphic cycles besides the Permian metamorphic event can be distinguished.

Due to abundant growth of garnet along a Barrow-type P - T path in the course of Variscan metamorphism, the stability field of garnet significantly decreased and shifted to higher P - T conditions. Garnet growth during this metamorphic event was related to allanite formation.

As a result of the reduced size of the garnet stability field, garnet growth during the Permian HT/LP event may only have occurred in rock samples, which – prior to growth – underwent significant garnet resorption. In that respect, isolated and randomly distributed monazite grains of Permian age may indicate garnet growth during the Permian.

Rock samples, which were not subject to significant garnet resorption do not contain Permian garnet growth increments and can be used for P - T - t path reconstruction. In such rock samples, pseudomorphous monazite clusters after allanite have been observed.

Since information on the kinetics of garnet resorption are scarce, the interplay between garnet dissolution and re-growth during the Permian can not be considered in our simulations. For the thermal maximum of the Permian metamorphic event, conditions of ~ 625 °C are suggested.

Synkinematic growth of an additional garnet generation with the rock matrix occurred during the Eo-Alpine metamorphic event in the Cretaceous. The corresponding P - T path is marked with a maximum in P and T of ~ 9.5 kbar and ~ 645 °C. At such conditions, thin overgrowths on the pre-existing garnet porphyroblasts were formed. Due to progressive dehydration of the matrix in the course of the three different metamorphic cycles, the growth of the Eo-Alpine garnet generation may have been transport controlled giving rise to its wart-like texture.

5.8 Acknowledgements

We are grateful to W. Tschudin for the sample preparation and thank E. Reusser for the help with the EPMA of garnet. The contribution and expertise of R. Schuster in terms of the regional geological framework is gratefully acknowledged.

Chapter 6

Overall conclusions

From the investigation of bulk rock chemistries and compositions of zoned metamorphic garnet porphyroblasts estimates for the P - T conditions that prevailed at the incipient stages of garnet growth as well as for P - T - t trajectories representative for garnet growth during pre-Eo-Alpine and Eo-Alpine metamorphic events in the Austroalpine basement can be deduced.

With the development of the software program THERIA_G a powerful tool is created, the combined application of which with Th-U-Pb microprobe dating of monazite allows to unravel essential parts of the polymetamorphic evolution of the Austroalpine basement from the investigation of garnet chemical zoning.

For the Variscan metamorphic event, which is documented by the formation of a first garnet generation with allanite inclusions in the Rappold Complex, a Barrow-type P - T path is obtained. The oldest garnet growth phase of rocks from the Wölz Complex grew during the Permian at isobaric conditions of ~ 4 kbar. From the investigation of polyphase garnet porphyroblasts of the Rappold Complex a thermal maximum of $\sim 625^\circ\text{C}$ is derived for the Permian metamorphic event.

Whereas during the Permian garnet abundantly grew in the Wölz Complex it only grew in metapelites of the Rappold Complex, which experienced significant resorption of the pre-existing Carboniferous garnet generation. Garnet growth during the Eo-Alpine metamorphic event is noticed in all rock samples investigated in this thesis. Eo-Alpine metamorphism in the Wölz Complex reached a thermal maximum of $\sim 625^\circ\text{C}$ and a maximum pressure of ~ 10.5 kbar. Rocks of the Rappold Complex underwent a thermal maximum of $\sim 645^\circ\text{C}$ and peak pressure conditions of ~ 9.5 kbar.

Based on the investigation of garnet chemical zoning with THERIA_G it can clearly be

demonstrated that garnet chemical composition may be influenced by chemical fractionation between garnet and the rock matrix during garnet growth, intracrystalline diffusion in garnet, and the nucleation history. Since the radial growth rate of garnet is exceedingly large for the first growth increments of garnet in a given volume of rock, over which thermodynamic equilibrium is attained, the external conditions do not significantly change and the garnet core compositions are rather homogeneous. However, for garnet that originates from later stages in the nucleation history, increased chemical gradients can be assumed in the garnet core, which are prone to secondary modification by diffusional relaxation. Furthermore, changes in the chemical gradients of garnet-forming components can be related to modifications of the garnet-bearing metamorphic assemblages during garnet formation.

The full potential of garnet growth modelling with THERIA.G can only be exploited, if detailed information on the size and frequency distribution of garnet crystals in a given volume of rock is given and the garnet chemical composition of each size class is known. In such a case, the investigation of the largest crystals may result in information on the P - T path of metamorphism. The analysis of garnet grains that nucleated late in the geothermal history may provide well-founded estimates for the temporal aspects of prograde metamorphism. In addition, the approach developed in this thesis to simulate the formation of garnet populations may be used to test models for the kinetics of garnet nucleation and growth.

Appendix A

Appendix to Chapter 2

The Appendix to Chapter 2 comprises the EPMA dataset and the bulk-rock compositions, which are part of the supplementary material of the study by Gaidies et al. (2006). The complete material – including the P – T phase diagram sections with areas of isopleth intersection as well as the database file, one solution-model file, and one input-file used with PERPLEX – are available online alongside the article at: <http://www.blackwell-synergy.com/doi/suppl/10.1111/j.1525-1314.2006.00648.x> and can be found on the enclosed CD.

A.1 EPMA dataset and bulk-rock compositions

Table A.1 – EPMA dataset showing the garnet core compositions.

Sample	10F03	11F03	16F03	19F03	24F03	28F03	29F03A	31F03	32F03
SiO ₂	36.02	35.79	37.01	37.03	36.71	37.95	37.08	38.48	37.59
Al ₂ O ₃	21.64	19.96	19.17	20.40	19.57	20.13	20.88	20.04	20.51
FeO	32.56	33.58	27.64	29.19	31.91	33.07	33.39	30.69	31.53
MnO	4.19	5.17	8.01	6.57	3.58	1.66	6.94	6.30	5.58
MgO	2.43	1.59	1.50	1.76	2.08	1.86	1.54	1.26	2.41
CaO	3.80	5.17	4.88	4.78	4.92	5.93	2.00	5.32	2.72
Total	100.64	98.04	98.21	99.73	98.77	100.60	101.83	102.09	100.34
Oxygen	24	24	24	24	24	24	24	24	24
Si	5.81	5.97	6.11	6.01	6.03	6.09	5.96	6.12	6.05
Al	4.11	3.93	3.73	3.90	3.79	3.80	3.96	3.76	3.89
Fe ²⁺	4.39	4.69	3.82	3.96	4.38	4.44	4.49	4.08	4.25
Mn	0.57	0.73	1.12	0.90	0.50	0.23	0.95	0.85	0.76
Mg	0.58	0.40	0.37	0.43	0.51	0.45	0.37	0.30	0.58
Ca	0.66	0.35	0.86	0.83	0.87	1.02	0.34	0.91	0.47
Fe/(Fe+Mg)	0.88	0.92	0.91	0.90	0.90	0.91	0.92	0.93	0.88
X _{alm}	0.71	0.76	0.62	0.65	0.70	0.72	0.73	0.67	0.70
X _{prp}	0.09	0.06	0.06	0.07	0.08	0.07	0.06	0.05	0.10
X _{grs}	0.11	0.06	0.14	0.14	0.14	0.17	0.06	0.15	0.08
X _{sps}	0.09	0.12	0.18	0.15	0.08	0.04	0.15	0.14	0.13

Table A.1 – Cont'd.

Sample	33F03	37F03	39F03	40F03-1	40F03-2	41F03	42F03	43F03	44F03
SiO ₂	37.16	36.70	36.00	37.14	35.38	37.52	36.79	37.35	36.47
Al ₂ O ₃	19.01	19.94	20.10	20.55	19.59	18.47	20.62	20.12	17.94
FeO	28.23	30.85	32.06	34.38	31.95	30.00	28.38	33.88	33.10
MnO	9.20	4.80	6.92	5.20	6.86	4.01	9.38	5.67	4.71
MgO	0.91	1.21	1.39	1.58	1.37	1.11	1.12	1.51	1.21
CaO	5.20	7.29	2.70	2.42	3.55	8.05	3.47	2.13	5.29
Total	99.71	100.79	99.17	101.27	98.70	99.16	99.76	100.66	98.72
Oxygen	24	24	24	24	24	24	24	24	24
Si	6.10	5.95	5.95	5.99	5.91	6.15	6.00	6.06	6.09
Al	3.68	3.81	3.92	3.91	3.85	3.57	3.97	3.85	3.53
Fe ²⁺	3.87	4.18	4.43	4.64	4.46	4.11	3.87	4.60	4.62
Mn	1.28	0.66	0.97	0.71	0.97	0.56	1.30	0.78	0.67
Mg	0.22	0.29	0.34	0.38	0.34	0.27	0.27	0.36	0.30
Ca	0.91	1.27	0.47	0.42	0.64	1.41	0.61	0.37	0.95
Fe/(Fe+Mg)	0.95	0.94	0.93	0.92	0.93	0.94	0.93	0.93	0.94
X _{alm}	0.62	0.65	0.71	0.76	0.70	0.65	0.64	0.75	0.71
X _{prp}	0.04	0.05	0.06	0.06	0.05	0.04	0.05	0.06	0.05
X _{grs}	0.15	0.20	0.08	0.07	0.10	0.22	0.10	0.06	0.15
X _{sps}	0.20	0.10	0.16	0.12	0.15	0.09	0.21	0.13	0.10

Table A.2 – Bulk rock compositions.

Sample	10F03	11F03	16F03	19F03	24F03	28F03	29F03A	31F03	32F03
SiO ₂	45.35	61.95	45.27	45.36	45.42	58.34	64.04	44.52	68.22
TiO ₂	0.94	0.87	0.98	1.49	1.27	1.15	0.83	1.30	0.77
Al ₂ O ₃	22.76	17.66	23.31	27.04	32.23	20.39	18.02	27.78	15.63
Fe ₂ O ₃	8.85	7.12	14.97	11.13	9.43	8.65	7.70	12.41	6.56
MnO	0.15	0.06	0.33	0.14	0.05	0.07	0.10	0.25	0.13
MgO	2.04	1.90	4.34	2.49	0.98	2.42	2.10	3.05	1.98
CaO	4.27	0.43	1.70	2.92	0.43	0.76	0.52	0.92	0.80
Na ₂ O	0.50	0.96	0.88	2.88	1.88	1.40	1.06	1.57	0.43
K ₂ O	4.35	3.62	4.35	2.49	6.14	3.72	3.43	5.24	3.87
H ₂ O	2.99	3.32	4.79	3.46	3.75	2.87	2.68	3.21	1.88
CO ₂	0.14	0.50	0.18	0.04	0.02	0.39	0.34	0.03	0.38
Total	100.30	98.39	101.10	99.44	101.60	100.16	100.82	100.28	100.65

Table A.2 – Cont'd.

Sample	33F03	37F03	39F03	40F03-1	40F03-2	41F03	42F03	43F03	44F03
SiO ₂	59.71	61.41	51.50	56.22	54.21	52.42	59.64	57.37	55.19
TiO ₂	1.06	1.01	1.23	1.07	1.07	0.91	1.01	0.97	1.01
Al ₂ O ₃	19.54	18.24	24.29	22.58	23.73	20.04	21.07	20.87	22.20
Fe ₂ O ₃	9.02	8.58	10.22	9.29	9.03	8.12	8.05	9.57	8.80
MnO	0.55	0.08	0.17	0.14	0.17	0.09	0.15	0.19	0.09
MgO	2.15	2.60	2.16	2.22	2.03	2.42	1.99	2.39	2.32
CaO	1.56	1.02	1.27	0.45	0.81	0.60	0.36	0.64	0.42
Na ₂ O	1.99	1.41	1.47	0.77	0.94	1.37	0.65	1.07	1.03
K ₂ O	2.78	3.39	4.05	4.52	4.79	3.47	5.09	3.67	4.64
H ₂ O	1.67	2.43	3.10	3.08	3.16	3.21	2.58	3.01	3.10
CO ₂	0.15	0.39	0.39	0.04	0.04	0.33	0.45	0.38	0.35
Total	100.18	100.56	99.85	100.38	99.98	100.30	101.04	100.13	99.15

Appendix B

Appendix to Chapter 3

B.1 Solution model of Chl (Chlorite)

Solid solution of chlorite (Chl) is modelled with the four endmembers clinochlore (clin), daphnite (daph), amesite (ames), and Mn-chlorite (Mnchl). Following the solution model proposed by Holland and Powell (1998) extended to Mn-bearing chlorite, on the octahedral sites M_{23} mixing of Mg, Fe, Mn, on M_1 Mg, Fe, Al, Mn, and on the tetrahedral site T_2 mixing of Al and Si is allowed. Al-free chlorite (Afchl) is not included because its calculated concentration for the given bulk rock composition is negligible.

The activities of the endmembers can be expressed as:

$$\begin{aligned}a(\text{clin}) &= 4(x_{Mg}^{M_{23}})^4(x_{Mg}^{M_1})(x_{Al}^{T_2})(x_{Si}^{T_2}) \\a(\text{daph}) &= 4(x_{Fe}^{M_{23}})^4(x_{Fe}^{M_1})(x_{Al}^{T_2})(x_{Si}^{T_2}) \\a(\text{ames}) &= 1(x_{Mg}^{M_{23}})^4(x_{Al}^{M_1})(x_{Al}^{T_2})^2 \\a(\text{Mnchl}) &= 4(x_{Mn}^{M_{23}})^4(x_{Mn}^{M_1})(x_{Al}^{T_2})(x_{Si}^{T_2})\end{aligned}$$

The Margules parameters are:

$$W_{\text{clin-daph}} = 2500 \text{ J}; W_{\text{clin-ames}} = 18000 \text{ J}; W_{\text{ames-daph}} = 13500 \text{ J}$$

Equipartitioning of Mg, Fe, and Mn on the octahedral sites is not assumed.

B.2 Full formalism of the discretized diffusion equation

This section overviews the discretization of the diffusion equation in order to numerically simulate multicomponent diffusional transport in a spherical geometry. The detailed algorithm of discretization is documented in a Maple©-file on the enclosed CD. In addition, the CD contains the complete set of Fortran77 source code files, needed to compile THERIA_G as well as executables for Mac, UNIX, and PC. A MATLAB®-source file for the computation of intragranular diffusion in garnet can be found in Section B.2.1.

For the assumption that D is independent with respect to r , the general diffusion equation for spherical geometries

$$\frac{\partial C}{\partial t} = \frac{\frac{\partial}{\partial r} \left(r^2 D \left(\frac{\partial C}{\partial r} \right) \right)}{r^2} \quad (\text{B.1})$$

can be written as

$$\frac{\partial C}{\partial t} = D \left(\frac{\partial^2 C}{\partial r^2} + \frac{2}{r} \frac{\partial C}{\partial r} \right) \quad (\text{B.2})$$

(Crank, 1975). Boundary and initial conditions sufficient to guarantee a unique solution are

$$\begin{aligned} C(0, t) &= f_0(t), \\ C(L, t) &= f_L(t), \text{ and} \\ C(r, 0) &= g(r), \end{aligned}$$

where the solution is obtained for the region $0 \leq r \leq L$, $0 \leq t \leq T$. T could be infinity. If the spatial part of the computational space/time (r/t) grid superimposed on this region is considered irregular, the first derivative of C with respect to r can be expressed as

$$\frac{\partial C}{\partial r} = \frac{\frac{(C_{n+1}-C_n)\Delta r_1}{\Delta r_2} + \frac{(C_n-C_{n-1})\Delta r_2}{\Delta r_1}}{\Delta r_2 + \Delta r_1}, \quad (\text{B.3})$$

where the subscripts refer to a position n on the spatial grid and Δr_1 and Δr_2 correspond to the spatial steps to the left and to the right of a specific node n , respectively. The second derivative can be expressed as

$$\frac{\partial^2 C}{\partial r^2} = \frac{\frac{\Delta r_1 \left(C_{n+1} - C_n - \Delta r_2 \left(\frac{\partial C_n}{\partial r} \right) \right)}{(\Delta r_2)^2} + \frac{\Delta r_2 \left(C_{n-1} - C_n + \Delta r_1 \left(\frac{\partial C_n}{\partial r} \right) \right)}{(\Delta r_1)^2}}{\frac{1}{2} \Delta r_2 + \frac{1}{2} \Delta r_1}, \quad (\text{B.4})$$

which after introduction of (B.3) into (B.4) and appropriate rearrangement yields

$$\frac{\partial^2 C}{\partial r^2} = - \frac{2(-C_{n+1}\Delta r_1 + C_n\Delta r_1 + C_n\Delta r_2 - C_{n-1}\Delta r_2)}{\Delta r_1\Delta r_2(\Delta r_1 + \Delta r_2)} \quad (\text{B.5})$$

The first derivative of C with respect to t reads

$$\frac{\partial C}{\partial t} = \frac{C_n^{m+1} - C_n^m}{\Delta t}, \quad (\text{B.6})$$

where the superscripts refer to a position on the time-grid; m stands for the current time, at which the element distribution along the diffusion profile is known (the initial condition); $m + 1$ refers to the future time, at which the compositional profile of garnet is unknown. Thus, the explicitly discretized diffusion equation for spherical geometries takes the form

$$\begin{aligned} \frac{C_n^{m+1} - C_n^m}{\Delta t} &= \frac{2D(-rC_{n+1}^m\Delta r_1 + rC_n^m\Delta r_1 + rC_n^m\Delta r_2 - rC_{n-1}^m\Delta r_2)}{r\Delta r_2\Delta r_1(\Delta r_2 + \Delta r_1)} \\ &+ \frac{2D\left(-C_{n+1}^m(\Delta r_1)^2 + C_n^m(\Delta r_1)^2 - C_n^m(\Delta r_2)^2 + C_{n-1}^m(\Delta r_2)^2\right)}{r\Delta r_2\Delta r_1(\Delta r_2 + \Delta r_1)} \end{aligned} \quad (\text{B.7})$$

The implementation of the Crank-Nicolson scheme (Crank and Nicolson, 1947) results in

$$\begin{aligned} \frac{C_n^{m+1} - C_n^m}{\Delta t} &= \frac{D}{r\Delta r_1\Delta r_2(\Delta r_2 + \Delta r_1)} \\ &\cdot \left(rC_{n+1}^{m+1}\Delta r_1 - rC_n^{m+1}\Delta r_1 - r\Delta r_2C_n^{m+1} + r\Delta r_2C_{n-1}^{m+1} \right. \\ &+ (\Delta r_1)^2 C_{n+1}^{m+1} - (\Delta r_1)^2 C_n^{m+1} + (\Delta r_2)^2 C_n^{m+1} - (\Delta r_2)^2 C_{n-1}^{m+1} \\ &+ rC_{n+1}^m\Delta r_1 - rC_n^m\Delta r_1 - r\Delta r_2C_n^m + r\Delta r_2C_{n-1}^m \\ &\left. + (\Delta r_1)^2 C_{n+1}^m - (\Delta r_1)^2 C_n^m + (\Delta r_2)^2 C_n^m - (\Delta r_2)^2 C_{n-1}^m \right) \end{aligned} \quad (\text{B.8})$$

Diffusive flux of three independent components (Mn, Fe, and Mg in THERIA_G) can be expressed in the general form

$$\frac{\partial C_1}{\partial t} = \frac{\frac{\partial}{\partial r}\left(r^2 D_{11}\left(\frac{\partial C_1}{\partial r}\right)\right)}{r^2} + \frac{\frac{\partial}{\partial r}\left(r^2 D_{12}\left(\frac{\partial C_2}{\partial r}\right)\right)}{r^2} + \frac{\frac{\partial}{\partial r}\left(r^2 D_{13}\left(\frac{\partial C_3}{\partial r}\right)\right)}{r^2} \quad (\text{B.9})$$

$$\frac{\partial C_2}{\partial t} = \frac{\frac{\partial}{\partial r} \left(r^2 D_{21} \left(\frac{\partial C_1}{\partial r} \right) \right)}{r^2} + \frac{\frac{\partial}{\partial r} \left(r^2 D_{22} \left(\frac{\partial C_2}{\partial r} \right) \right)}{r^2} + \frac{\frac{\partial}{\partial r} \left(r^2 D_{23} \left(\frac{\partial C_3}{\partial r} \right) \right)}{r^2} \quad (\text{B.10})$$

$$\frac{\partial C_3}{\partial t} = \frac{\frac{\partial}{\partial r} \left(r^2 D_{31} \left(\frac{\partial C_1}{\partial r} \right) \right)}{r^2} + \frac{\frac{\partial}{\partial r} \left(r^2 D_{32} \left(\frac{\partial C_2}{\partial r} \right) \right)}{r^2} + \frac{\frac{\partial}{\partial r} \left(r^2 D_{33} \left(\frac{\partial C_3}{\partial r} \right) \right)}{r^2} \quad (\text{B.11})$$

and for D independent of r

$$\frac{\partial C_1}{\partial t} = D_{11} \left(\frac{\partial^2 C_1}{\partial r^2} + \frac{2 \frac{\partial C_1}{\partial r}}{r} \right) + D_{12} \left(\frac{\partial^2 C_2}{\partial r^2} + \frac{2 \frac{\partial C_2}{\partial r}}{r} \right) + D_{13} \left(\frac{\partial^2 C_3}{\partial r^2} + \frac{2 \frac{\partial C_3}{\partial r}}{r} \right) \quad (\text{B.12})$$

$$\frac{\partial C_2}{\partial t} = D_{21} \left(\frac{\partial^2 C_1}{\partial r^2} + \frac{2 \frac{\partial C_1}{\partial r}}{r} \right) + D_{22} \left(\frac{\partial^2 C_2}{\partial r^2} + \frac{2 \frac{\partial C_2}{\partial r}}{r} \right) + D_{23} \left(\frac{\partial^2 C_3}{\partial r^2} + \frac{2 \frac{\partial C_3}{\partial r}}{r} \right) \quad (\text{B.13})$$

$$\frac{\partial C_3}{\partial t} = D_{31} \left(\frac{\partial^2 C_1}{\partial r^2} + \frac{2 \frac{\partial C_1}{\partial r}}{r} \right) + D_{32} \left(\frac{\partial^2 C_2}{\partial r^2} + \frac{2 \frac{\partial C_2}{\partial r}}{r} \right) + D_{33} \left(\frac{\partial^2 C_3}{\partial r^2} + \frac{2 \frac{\partial C_3}{\partial r}}{r} \right) \quad (\text{B.14})$$

After the application of (B.8) to (B.12)-(B.14) and appropriate rearrangement a matrix equation results:

$$\mathbf{A} \vec{C}^{m+1} = \mathbf{M} \vec{C}^m, \quad (\text{B.15})$$

where

$$\mathbf{A} = \begin{bmatrix} \mathbf{A}_{11} & \mathbf{A}_{12} & \mathbf{A}_{13} \\ \mathbf{A}_{21} & \mathbf{A}_{22} & \mathbf{A}_{23} \\ \mathbf{A}_{31} & \mathbf{A}_{32} & \mathbf{A}_{33} \end{bmatrix}, \quad \mathbf{M} = \begin{bmatrix} \mathbf{M}_{11} & \mathbf{M}_{12} & \mathbf{M}_{13} \\ \mathbf{M}_{21} & \mathbf{M}_{22} & \mathbf{M}_{23} \\ \mathbf{M}_{31} & \mathbf{M}_{32} & \mathbf{M}_{33} \end{bmatrix},$$

$$\vec{C}^{m+1} = \begin{bmatrix} \vec{C}_1^{m+1} \\ \vec{C}_2^{m+1} \\ \vec{C}_3^{m+1} \end{bmatrix}, \quad \vec{C}^m = \begin{bmatrix} \vec{C}_1^m \\ \vec{C}_2^m \\ \vec{C}_3^m \end{bmatrix}.$$

In general, \mathbf{A} and \mathbf{M} consist of several sub-matrices \mathbf{A}_{11} , \mathbf{A}_{12} , \dots as well as \mathbf{M}_{11} , \mathbf{M}_{12} , \dots and \vec{C}^{m+1} and \vec{C}^m are composed of several sub-vectors \vec{C}_1^{m+1} , \vec{C}_2^{m+1} , \dots as well as \vec{C}_1^m , \vec{C}_2^m , \dots , the number of which depends on the number of independent diffusing chemical components. In the following, \mathbf{A}_{11} , \mathbf{A}_{12} , \mathbf{M}_{11} , \mathbf{M}_{12} , and \vec{C}_1^{m+1} are shown exemplarily, whereas the remaining matrices and vectors are composed accordingly:

$$\mathbf{A}_{11} =$$

$$\begin{bmatrix} 1+3D_{11}^{(1)}j & -3D_{11}^{(1)}j & 0 & \dots & 0 \\ lD_{11}^{(2)}((\Delta r_2)^2 - r\Delta r_2) & 1+lD_{11}^{(2)}(r\Delta r_2 + r\Delta r_1 - (\Delta r_2)^2 + (\Delta r_1)^2) & lD_{11}^{(2)}(-(\Delta r_1)^2 - r\Delta r_1) & 0 & 0 \\ 0 & \ddots & \ddots & \ddots & 0 \\ \vdots & 0 & lD_{11}^{(L-1)}(\dots) & 1+lD_{11}^{(L-1)}(\dots) & lD_{11}^{(L-1)}(\dots) \\ 0 & \dots & 0 & -D_{11}^{(L)}p & 1+D_{11}^{(L)}p \end{bmatrix}$$

$$\mathbf{A}_{12} =$$

$$\begin{bmatrix} 3D_{12}^{(1)}j & -3D_{12}^{(1)}j & 0 & \dots & 0 \\ lD_{12}^{(2)}((\Delta r_2)^2 - r\Delta r_2) & lD_{12}^{(2)}(r\Delta r_2 + r\Delta r_1 - (\Delta r_2)^2 + (\Delta r_1)^2) & lD_{12}^{(2)}(-(\Delta r_1)^2 - r\Delta r_1) & 0 & 0 \\ 0 & \ddots & \ddots & \ddots & 0 \\ \vdots & 0 & lD_{11}^{(L-1)}(\dots) & lD_{11}^{(L-1)}(\dots) & lD_{11}^{(L-1)}(\dots) \\ 0 & \dots & 0 & -D_{12}^{(L)}p & D_{12}^{(L)}p \end{bmatrix}$$

$$\mathbf{M}_{11} =$$

$$\begin{bmatrix} 1-3D_{11}^{(1)}j & 3D_{11}^{(1)}j & 0 & \dots & 0 \\ -lD_{11}^{(2)}((\Delta r_2)^2 - r\Delta r_2) & 1-lD_{11}^{(2)}(r\Delta r_2 + r\Delta r_1 - (\Delta r_2)^2 + (\Delta r_1)^2) & -lD_{11}^{(2)}(-(\Delta r_1)^2 - r\Delta r_1) & 0 & 0 \\ 0 & \ddots & \ddots & \ddots & 0 \\ \vdots & 0 & -lD_{11}^{(L-1)}(\dots) & 1-lD_{11}^{(L-1)}(\dots) & -lD_{11}^{(L-1)}(\dots) \\ 0 & \dots & 0 & D_{11}^{(L)}p & 1-D_{11}^{(L)}p \end{bmatrix}$$

$M_{12} =$

$$\begin{bmatrix} -3D_{12}^{(1)j} & 3D_{12}^{(1)j} & 0 & \dots & 0 \\ -lD_{12}^{(2)}((\Delta r_2)^2 - r\Delta r_2) & -lD_{12}^{(2)}(r\Delta r_2 + r\Delta r_1 - (\Delta r_2)^2 + (\Delta r_1)^2) & -lD_{12}^{(2)}(-(\Delta r_1)^2 - r\Delta r_1) & 0 & 0 \\ 0 & \ddots & \ddots & \ddots & 0 \\ \vdots & 0 & -lD_{12}^{(L-1)}(\dots) & -lD_{12}^{(L-1)}(\dots) & -lD_{12}^{(L-1)}(\dots) \\ 0 & \dots & 0 & D_{12}^{(L)p} & -D_{12}^{(L)p} \end{bmatrix}$$

$$\vec{C}_1^{m+1} = \begin{bmatrix} C_{1,n=0}^{m+1} \\ C_{1,n=1}^{m+1} \\ \vdots \\ C_{1,n=L-1}^{m+1} \\ C_{1,n=L}^{m+1} \end{bmatrix}, \quad \text{where } j = \Delta t / (\Delta r_1)^2, \\ p = \Delta t / (\Delta r_2)^2, \text{ and } l = \Delta t / (r\Delta r_2\Delta r_1(\Delta r_2 + \Delta r_1)).$$

\vec{D}_{11} and \vec{D}_{12} are vectors, which are computed according to (3.2) and (3.3). The superscripts linked to D in \mathbf{A}_{11} , \mathbf{A}_{12} , \mathbf{M}_{11} , and \mathbf{M}_{12} reflect their compositional - and, hence - space dependence. The dots used in the above expressions symbolise logical continuations.

In order to close the inner boundary symmetrically, a fictitious node $n_{f1} = -1$ is introduced, which matches node $n = 1$ with respect to its chemical composition and distance to $n = 0$. Hence, at $n = 0$

$$\begin{aligned} \Delta r_1 &= \Delta r_2, \\ C_{i,n-1}^m &= C_{i,n+1}^m, \\ C_{i,n-1}^{m+1} &= C_{i,n+1}^{m+1}. \end{aligned}$$

Whereas the initial condition reflects the initial distribution of element concentrations along the diffusion profile, the outer boundary condition considers the element fluxes across the boundary of the system. If the quantity of a component i that should enter garnet exceeds the size of the respective matrix reservoir, the garnet is closed for diffusional exchange with the matrix. In that case, the outer boundary condition takes the form

$$\frac{\partial C_i}{\partial t} = 0$$

which – as for the inner boundary – is implemented by the introduction of a symmetrical fictitious node $n_{f2} = +1$. This case is exemplified in the matrices given above. If the quantity of i that enters garnet does not exceed its matrix reservoir, the garnet rim composition is fixed by the respective garnet/matrix equilibrium partitioning and, hence, in that case, the outer boundary of garnet is regarded as open.

THERIA_G computes simultaneously the solution of (B.15) for \vec{C}^{m+1} at each time step, Δt , by Gaussian elimination.

B.2.1 MATLAB[®]-source code for the multi-component diffusion module implemented in THERIA_G

This source code calculates the influence of diffusion on Mn-, Fe-, Mg-, and Ca-distribution in garnet of spherical geometry. For the initial condition a step function is used; the outer boundary is closed. As a result, the Mn-distribution for chosen P - T conditions is plotted as a function of time.

```
%-----+
% 3-d diffusion of four components in a sphere using |
% the crank-nicolson-scheme, neumann boundary cond., |
% and a concentration-dependent diffusion-matrix.      |
% The spatial grid is variable.                        |
% at i=0: Cim1=Cip1 and at i=nrhr: Cip1=Cim1          |
% Fred Gaidies, University of Basel, 10/06            |
%-----+
clear;home
TC      = input('Please enter the temperature (degree C). ');
P       = input('Please enter the pressure (kbar). ');
TT      = input('Please enter the total time of diffusion (My). ');
%initial condition:-----
drV     = ones(1,50)*1/10000;
nr      = length(drV);
Mn      = ones(nr,1)*14;Mn(nr/2+1:end)=12;
Fe      = ones(nr,1)*70;Fe(nr/2+1:end)=72;
Mg      = ones(nr,1)*3;Mg(nr/2+1:end)=4;
Ca      = 100-(Mn+Fe+Mg);
%-----+
length  = 0.5*drV(1)+sum(drV(2:end-1))+drV(end)/2;%length of model...
%        (cm), i.e. does not equal the radius
for i=1:nr-1
    X1(i)= drV(1)/2+sum(drV(2:i))+drV(i+1)/2;
end
X       = [0,X1];
```

```

X      = X+drV(1)/2;
CV     = [Mn;Fe;Mg;Ca];
cv     = CV(1:3*nr);
CVinit = CV;
%---mass balance-----
vt     = zeros(1,nr);
for i = 1:nr
    vt(i) = 4/3*pi*(sum(drV(1:i)))^3;
end
for i = 1:nr-1
    vr(i) = vt(i+1)-vt(i);
end
vr     = [vt(1),vr];
for i = 1:nr
    wMn1(i) = CVinit(i)*vr(i);
    wFe1(i) = CVinit(i+nr)*vr(i);
    wMg1(i) = CVinit(i+2*nr)*vr(i);
    wCa1(i) = CVinit(i+3*nr)*vr(i);
end
wMn1t = sum(wMn1);wFe1t = sum(wFe1);
wMg1t = sum(wMg1);wCa1t = sum(wCa1);
%-----
%kinetic parameters from Chakra + Gangu (1992) at fO2 defined by ...
%graphite buffer
DMnzero = 5.1*10^-4; %pre-exponential constant in cm^2/s
AEMn    = 60569;    %activation energy for diffusion at 1 bar in ...
%                cal/mol
AVMn    = 6.0;     %activation volume for diffusion in cm^3/mol
DFezero = 6.4*10^-4;
AEFe    = 65824;
AVFe    = 5.6;
DMgzero = 1.1*10^-3;
AEMg    = 67997;
AVMg    = 5.3;
%=====
TK      = TC+273.15;
RJ      = 8.31451070; %universal gas constant in J/(mol*K)
RCal    = RJ/4.1868; %universal gas constant in cal/(mol*K)
DMntrace = DMnzero*exp((-AEMn-(P-1)*AVMn)/(RCal*TK));
DFetrace = DFezero*exp((-AEFe-(P-1)*AVFe)/(RCal*TK));
DMgtrace = DMgzero*exp((-AEMg-(P-1)*AVMg)/(RCal*TK));
DCatrace = 0.5*DFetrace; %after Loomis (?) and Florence & Spear (1991)
%-----
%calculation of the D-matrix after Lasaga (1979)...
%assuming negligible activity coefficient gradients;
DMnMn = ones(nr,1);DMnFe = ones(nr,1);DMnMg = ones(nr,1);
DFeMn = ones(nr,1);DFeFe = ones(nr,1);DFeMg = ones(nr,1);

```

```

DMgMn = ones(nr,1);DMgFe = ones(nr,1);DMgMg = ones(nr,1);

for i = 1:nr
    denom = CV(i)/100*DMntrace+CV(nr+i)/100 ...
    *DFetrace+CV(2*nr+i)/100*DMgtrace+CV(3*nr+i)/100*DCatrace;
    DMnMn(i,1) = DMntrace*1-((DMntrace*CV(0*nr+i)/100)/denom)* ...
    (DMntrace-DCatrace);
    DMnFe(i,1) = DMntrace*0-((DMntrace*CV(0*nr+i)/100)/denom)* ...
    (DFetrace-DCatrace);
    DMnMg(i,1) = DMntrace*0-((DMntrace*CV(0*nr+i)/100)/denom)* ...
    (DMgtrace-DCatrace);
    DFeMn(i,1) = DFetrace*0-((DFetrace*CV(1*nr+i)/100)/denom)* ...
    (DMntrace-DCatrace);
    DFeFe(i,1) = DFetrace*1-((DFetrace*CV(1*nr+i)/100)/denom)* ...
    (DFetrace-DCatrace);
    DFeMg(i,1) = DFetrace*0-((DFetrace*CV(1*nr+i)/100)/denom)* ...
    (DMgtrace-DCatrace);
    DMgMn(i,1) = DMgtrace*0-((DMgtrace*CV(2*nr+i)/100)/denom)* ...
    (DMntrace-DCatrace);
    DMgFe(i,1) = DMgtrace*0-((DMgtrace*CV(2*nr+i)/100)/denom)* ...
    (DFetrace-DCatrace);
    DMgMg(i,1) = DMgtrace*1-((DMgtrace*CV(2*nr+i)/100)/denom)* ...
    (DMgtrace-DCatrace);
end
%-----
year = 365.25*24*60*60;
K = 0.1*(min(drV))^2/max(DMnMn);%dt is 5-times smaller than ...
% using the stability criterion for explecit schemes
'For appropriate accuracy use a smaller value than the ...
following maximum time step size (in years):',num2str(K/year),
TSS = input('Please enter the time step size (years). ');
dt = year*TSS; %size of timestep in seconds
nt = year*1000000*TT; %timespan in seconds
n = dt/drV(1)^2;
p = dt/drV(end)^2;
%-----
tic
%The equation system: A*cnew=M*cold

MnMnA = zeros(nr,nr); MnMnM = zeros(nr,nr);
MnFeA = zeros(nr,nr); MnFeM = zeros(nr,nr);
MnMgA = zeros(nr,nr); MnMgM = zeros(nr,nr);
FeMnA = zeros(nr,nr); FeMnM = zeros(nr,nr);
FeFeA = zeros(nr,nr); FeFeM = zeros(nr,nr);
FeMgA = zeros(nr,nr); FeMgM = zeros(nr,nr);
MgMnA = zeros(nr,nr); MgMnM = zeros(nr,nr);
MgFeA = zeros(nr,nr); MgFeM = zeros(nr,nr);

```

```

MgMgA = zeros(nr,nr); MgMgM = zeros(nr,nr);

for i = 1:nr-2

    dr1 = drV(i)/2+drV(i+1)/2;
    dr2 = drV(i+1)/2+drV(i+2)/2;
    r    = sum(drV(1:i+1));
    l    = dt/(r*dr2*dr1*(dr2+dr1));

    D11 = DMnMn(i+1); D12 = DMnFe(i+1); D13 = DMnMg(i+1);
    D21 = DFeMn(i+1); D22 = DFeFe(i+1); D23 = DFeMg(i+1);
    D31 = DMgMn(i+1); D32 = DMgFe(i+1); D33 = DMgMg(i+1);

    MnMnA(i+1,i)    = 1*D11*(dr2^2-r*dr2);
    MnMnA(i+1,i+1) = 1+l*D11*(r*dr2+r*dr1-dr2^2+dr1^2);
    MnMnA(i+1,i+2) = 1*D11*(-dr1^2-r*dr1);

    MnMnM(i+1,i)    = -1*D11*(dr2^2-r*dr2);
    MnMnM(i+1,i+1) = 1-l*D11*(r*dr2+r*dr1-dr2^2+dr1^2);
    MnMnM(i+1,i+2) = -1*D11*(-dr1^2-r*dr1);

    MnFeA(i+1,i)    = 1*D12*(dr2^2-r*dr2);
    MnFeA(i+1,i+1) = 1*D12*(r*dr2+r*dr1-dr2^2+dr1^2);
    MnFeA(i+1,i+2) = 1*D12*(-dr1^2-r*dr1);

    MnFeM(i+1,i)    = -1*D12*(dr2^2-r*dr2);
    MnFeM(i+1,i+1) = -1*D12*(r*dr2+r*dr1-dr2^2+dr1^2);
    MnFeM(i+1,i+2) = -1*D12*(-dr1^2-r*dr1);

    MnMgA(i+1,i)    = 1*D13*(dr2^2-r*dr2);
    MnMgA(i+1,i+1) = 1*D13*(r*dr2+r*dr1-dr2^2+dr1^2);
    MnMgA(i+1,i+2) = 1*D13*(-dr1^2-r*dr1);

    MnMgM(i+1,i)    = -1*D13*(dr2^2-r*dr2);
    MnMgM(i+1,i+1) = -1*D13*(r*dr2+r*dr1-dr2^2+dr1^2);
    MnMgM(i+1,i+2) = -1*D13*(-dr1^2-r*dr1);

    FeMnA(i+1,i)    = 1*D21*(dr2^2-r*dr2);
    FeMnA(i+1,i+1) = 1*D21*(r*dr2+r*dr1-dr2^2+dr1^2);
    FeMnA(i+1,i+2) = 1*D21*(-dr1^2-r*dr1);

    FeMnM(i+1,i)    = -1*D21*(dr2^2-r*dr2);
    FeMnM(i+1,i+1) = -1*D21*(r*dr2+r*dr1-dr2^2+dr1^2);
    FeMnM(i+1,i+2) = -1*D21*(-dr1^2-r*dr1);

    FeFeA(i+1,i)    = 1*D22*(dr2^2-r*dr2);
    FeFeA(i+1,i+1) = 1+l*D22*(r*dr2+r*dr1-dr2^2+dr1^2);

```

```

FeFeA(i+1,i+2) = 1*D22*(-dr1^2-r*dr1);

FeFeM(i+1,i)   = -1*D22*(dr2^2-r*dr2);
FeFeM(i+1,i+1) = 1-1*D22*(r*dr2+r*dr1-dr2^2+dr1^2);
FeFeM(i+1,i+2) = -1*D22*(-dr1^2-r*dr1);

FeMgA(i+1,i)   = 1*D23*(dr2^2-r*dr2);
FeMgA(i+1,i+1) = 1*D23*(r*dr2+r*dr1-dr2^2+dr1^2);
FeMgA(i+1,i+2) = 1*D23*(-dr1^2-r*dr1);

FeMgM(i+1,i)   = -1*D23*(dr2^2-r*dr2);
FeMgM(i+1,i+1) = -1*D23*(r*dr2+r*dr1-dr2^2+dr1^2);
FeMgM(i+1,i+2) = -1*D23*(-dr1^2-r*dr1);

MgMnA(i+1,i)   = 1*D31*(dr2^2-r*dr2);
MgMnA(i+1,i+1) = 1*D31*(r*dr2+r*dr1-dr2^2+dr1^2);
MgMnA(i+1,i+2) = 1*D31*(-dr1^2-r*dr1);

MgMnM(i+1,i)   = -1*D31*(dr2^2-r*dr2);
MgMnM(i+1,i+1) = -1*D31*(r*dr2+r*dr1-dr2^2+dr1^2);
MgMnM(i+1,i+2) = -1*D31*(-dr1^2-r*dr1);

MgFeA(i+1,i)   = 1*D32*(dr2^2-r*dr2);
MgFeA(i+1,i+1) = 1*D32*(r*dr2+r*dr1-dr2^2+dr1^2);
MgFeA(i+1,i+2) = 1*D32*(-dr1^2-r*dr1);

MgFeM(i+1,i)   = -1*D32*(dr2^2-r*dr2);
MgFeM(i+1,i+1) = -1*D32*(r*dr2+r*dr1-dr2^2+dr1^2);
MgFeM(i+1,i+2) = -1*D32*(-dr1^2-r*dr1);

MgMgA(i+1,i)   = 1*D33*(dr2^2-r*dr2);
MgMgA(i+1,i+1) = 1+1*D33*(r*dr2+r*dr1-dr2^2+dr1^2);
MgMgA(i+1,i+2) = 1*D33*(-dr1^2-r*dr1);

MgMgM(i+1,i)   = -1*D33*(dr2^2-r*dr2);
MgMgM(i+1,i+1) = 1-1*D33*(r*dr2+r*dr1-dr2^2+dr1^2);
MgMgM(i+1,i+2) = -1*D33*(-dr1^2-r*dr1);

end
%boundary conditions-----
MnMnA(1,1:2)   = [1+3*DMnMn(1)*n -3*DMnMn(1)*n];
MnMnA(nr,nr-1:nr) = [-DMnMn(nr)*p 1+DMnMn(nr)*p];
MnMnM(1,1:2)   = [1-3*DMnMn(1)*n 3*DMnMn(1)*n];
MnMnM(nr,nr-1:nr) = [DMnMn(nr)*p 1-DMnMn(nr)*p];

MnFeA(1,1:2)   = [3*DMnFe(1)*n -3*DMnFe(1)*n];
MnFeA(nr,nr-1:nr) = [-DMnFe(nr)*p DMnFe(nr)*p];

```

```

MnFeM(1,1:2) = [-3*DMnFe(1)*n 3*DMnFe(1)*n];
MnFeM(nr,nr-1:nr) = [DMnFe(nr)*p -DMnFe(nr)*p];

MnMgA(1,1:2) = [3*DMnMg(1)*n -3*DMnMg(1)*n];
MnMgA(nr,nr-1:nr) = [-DMnMg(nr)*p DMnMg(nr)*p];
MnMgM(1,1:2) = [-3*DMnMg(1)*n 3*DMnMg(1)*n];
MnMgM(nr,nr-1:nr) = [DMnMg(nr)*p -DMnMg(nr)*p];

FeMnA(1,1:2) = [3*DFeMn(1)*n -3*DFeMn(1)*n];
FeMnA(nr,nr-1:nr) = [-DFeMn(nr)*p DFeMn(nr)*p];
FeMnM(1,1:2) = [-3*DFeMn(1)*n 3*DFeMn(1)*n];
FeMnM(nr,nr-1:nr) = [DFeMn(nr)*p -DFeMn(nr)*p];

FeFeA(1,1:2) = [1+3*DFeFe(1)*n -3*DFeFe(1)*n];
FeFeA(nr,nr-1:nr) = [-DFeFe(nr)*p 1+DFeFe(nr)*p];
FeFeM(1,1:2) = [1-3*DFeFe(1)*n 3*DFeFe(1)*n];
FeFeM(nr,nr-1:nr) = [DFeFe(nr)*p 1-DFeFe(nr)*p];

FeMgA(1,1:2) = [3*DFeMg(1)*n -3*DFeMg(1)*n];
FeMgA(nr,nr-1:nr) = [-DFeMg(nr)*p DFeMg(nr)*p];
FeMgM(1,1:2) = [-3*DFeMg(1)*n 3*DFeMg(1)*n];
FeMgM(nr,nr-1:nr) = [DFeMg(nr)*p -DFeMg(nr)*p];

MgMnA(1,1:2) = [3*DMgMn(1)*n -3*DMgMn(1)*n];
MgMnA(nr,nr-1:nr) = [-DMgMn(nr)*p DMgMn(nr)*p];
MgMnM(1,1:2) = [-3*DMgMn(1)*n 3*DMgMn(1)*n];
MgMnM(nr,nr-1:nr) = [DMgMn(nr)*p -DMgMn(nr)*p];

MgFeA(1,1:2) = [3*DMgFe(1)*n -3*DMgFe(1)*n];
MgFeA(nr,nr-1:nr) = [-DMgFe(nr)*p DMgFe(nr)*p];
MgFeM(1,1:2) = [-3*DMgFe(1)*n 3*DMgFe(1)*n];
MgFeM(nr,nr-1:nr) = [DMgFe(nr)*p -DMgFe(nr)*p];

MgMgA(1,1:2) = [1+3*DMgMg(1)*n -3*DMgMg(1)*n];
MgMgA(nr,nr-1:nr) = [-DMgMg(nr)*p 1+DMgMg(nr)*p];
MgMgM(1,1:2) = [1-3*DMgMg(1)*n 3*DMgMg(1)*n];
MgMgM(nr,nr-1:nr) = [DMgMg(nr)*p 1-DMgMg(nr)*p];
%-----
A = sparse([MnMnA,MnFeA,MnMgA;FeMnA,FeFeA,FeMgA;MgMnA,MgFeA,MgMgA]);
M = sparse([MnMnM,MnFeM,MnMgM;FeMnM,FeFeM,FeMgM;MgMnM,MgFeM,MgMgM]);
%=====
%time loop
figure(2);clf;hold on;grid on;
plot(X,CVinit(1:max(size(Mn))),'-g'); %initial condition in green
soll = ones(1,nr)*wMn1t/sum(vr);
plot(X,soll,'-r'); %final condition in red
for tstep = 0:dt:nt

```

```

Rhs = M*cv;
cv = A\Rhs;
cMn = cv(1:nr);cFe = cv(nr+1:2*nr);
cMg = cv(2*nr+1:3*nr);cCa = 100-cMn-cFe-cMg;
CV = [cv;cCa];
if mod(tstep,year*500000)==0
    plot(X,cv(1:nr));axis([0 sum(drV) min(Mn) max(Mn)]);
    drawnow;
end
xlabel('Radius [cm]');
ylabel('Concentration of Mn');
plot(X,soll,'-r');plot(X,CVinit(1:max(size(Mn))),'-g')
%=====
%UPDATE of A and M
DMnMn = ones(nr,1);DMnFe = ones(nr,1);DMnMg = ones(nr,1);
DFeMn = ones(nr,1);DFeFe = ones(nr,1);DFeMg = ones(nr,1);
DMgMn = ones(nr,1);DMgFe = ones(nr,1);DMgMg = ones(nr,1);
for i = 1:nr
    denom = CV(i)/100*DMntrace+CV(nr+i)/100 ...
    *DFetrace+CV(2*nr+i)/100*DMgtrace+CV(3*nr+i)/100*DCatrace;
    DMnMn(i,1) = DMntrace*1-((DMntrace*CV(0*nr+i)/100)/denom)* ...
    (DMntrace-DCatrace);
    DMnFe(i,1) = DMntrace*0-((DMntrace*CV(0*nr+i)/100)/denom)* ...
    (DFetrace-DCatrace);
    DMnMg(i,1) = DMntrace*0-((DMntrace*CV(0*nr+i)/100)/denom)* ...
    (DMgtrace-DCatrace);
    DFeMn(i,1) = DFetrace*0-((DFetrace*CV(1*nr+i)/100)/denom)* ...
    (DMntrace-DCatrace);
    DFeFe(i,1) = DFetrace*1-((DFetrace*CV(1*nr+i)/100)/denom)* ...
    (DFetrace-DCatrace);
    DFeMg(i,1) = DFetrace*0-((DFetrace*CV(1*nr+i)/100)/denom)* ...
    (DMgtrace-DCatrace);
    DMgMn(i,1) = DMgtrace*0-((DMgtrace*CV(2*nr+i)/100)/denom)* ...
    (DMntrace-DCatrace);
    DMgFe(i,1) = DMgtrace*0-((DMgtrace*CV(2*nr+i)/100)/denom)* ...
    (DFetrace-DCatrace);
    DMgMg(i,1) = DMgtrace*1-((DMgtrace*CV(2*nr+i)/100)/denom)* ...
    (DMgtrace-DCatrace);
end
%=====
MnMnA = zeros(nr,nr); MnMnM = zeros(nr,nr);
MnFeA = zeros(nr,nr); MnFeM = zeros(nr,nr);
MnMgA = zeros(nr,nr); MnMgM = zeros(nr,nr);
FeMnA = zeros(nr,nr); FeMnM = zeros(nr,nr);
FeFeA = zeros(nr,nr); FeFeM = zeros(nr,nr);
FeMgA = zeros(nr,nr); FeMgM = zeros(nr,nr);
MgMnA = zeros(nr,nr); MgMnM = zeros(nr,nr);

```

```

MgFeA = zeros(nr,nr); MgFeM = zeros(nr,nr);
MgMgA = zeros(nr,nr); MgMgM = zeros(nr,nr);

for i = 1:nr-2

    dr1 = drV(i)/2+drV(i+1)/2;
    dr2 = drV(i+1)/2+drV(i+2)/2;
    r    = sum(drV(1:i+1));
    l    = dt/(r*dr2*dr1*(dr2+dr1));

    D11 = DMnMn(i+1); D12 = DMnFe(i+1); D13 = DMnMg(i+1);
    D21 = DFeMn(i+1); D22 = DFeFe(i+1); D23 = DFeMg(i+1);
    D31 = DMgMn(i+1); D32 = DMgFe(i+1); D33 = DMgMg(i+1);

    MnMnA(i+1,i)    = 1*D11*(dr2^2-r*dr2);
    MnMnA(i+1,i+1) = 1+1*D11*(r*dr2+r*dr1-dr2^2+dr1^2);
    MnMnA(i+1,i+2) = 1*D11*(-dr1^2-r*dr1);

    MnMnM(i+1,i)    = -1*D11*(dr2^2-r*dr2);
    MnMnM(i+1,i+1) = 1-1*D11*(r*dr2+r*dr1-dr2^2+dr1^2);
    MnMnM(i+1,i+2) = -1*D11*(-dr1^2-r*dr1);

    MnFeA(i+1,i)    = 1*D12*(dr2^2-r*dr2);
    MnFeA(i+1,i+1) = 1*D12*(r*dr2+r*dr1-dr2^2+dr1^2);
    MnFeA(i+1,i+2) = 1*D12*(-dr1^2-r*dr1);

    MnFeM(i+1,i)    = -1*D12*(dr2^2-r*dr2);
    MnFeM(i+1,i+1) = -1*D12*(r*dr2+r*dr1-dr2^2+dr1^2);
    MnFeM(i+1,i+2) = -1*D12*(-dr1^2-r*dr1);

    MnMgA(i+1,i)    = 1*D13*(dr2^2-r*dr2);
    MnMgA(i+1,i+1) = 1*D13*(r*dr2+r*dr1-dr2^2+dr1^2);
    MnMgA(i+1,i+2) = 1*D13*(-dr1^2-r*dr1);

    MnMgM(i+1,i)    = -1*D13*(dr2^2-r*dr2);
    MnMgM(i+1,i+1) = -1*D13*(r*dr2+r*dr1-dr2^2+dr1^2);
    MnMgM(i+1,i+2) = -1*D13*(-dr1^2-r*dr1);

    FeMnA(i+1,i)    = 1*D21*(dr2^2-r*dr2);
    FeMnA(i+1,i+1) = 1*D21*(r*dr2+r*dr1-dr2^2+dr1^2);
    FeMnA(i+1,i+2) = 1*D21*(-dr1^2-r*dr1);

    FeMnM(i+1,i)    = -1*D21*(dr2^2-r*dr2);
    FeMnM(i+1,i+1) = -1*D21*(r*dr2+r*dr1-dr2^2+dr1^2);
    FeMnM(i+1,i+2) = -1*D21*(-dr1^2-r*dr1);

    FeFeA(i+1,i)    = 1*D22*(dr2^2-r*dr2);

```



```

FeFeA(i+1,i+1) = 1+l*D22*(r*dr2+r*dr1-dr2^2+dr1^2);
FeFeA(i+1,i+2) = 1*D22*(-dr1^2-r*dr1);

FeFeM(i+1,i) = -1*D22*(dr2^2-r*dr2);
FeFeM(i+1,i+1) = 1-1*D22*(r*dr2+r*dr1-dr2^2+dr1^2);
FeFeM(i+1,i+2) = -1*D22*(-dr1^2-r*dr1);

FeMgA(i+1,i) = 1*D23*(dr2^2-r*dr2);
FeMgA(i+1,i+1) = 1*D23*(r*dr2+r*dr1-dr2^2+dr1^2);
FeMgA(i+1,i+2) = 1*D23*(-dr1^2-r*dr1);

FeMgM(i+1,i) = -1*D23*(dr2^2-r*dr2);
FeMgM(i+1,i+1) = -1*D23*(r*dr2+r*dr1-dr2^2+dr1^2);
FeMgM(i+1,i+2) = -1*D23*(-dr1^2-r*dr1);

MgMnA(i+1,i) = 1*D31*(dr2^2-r*dr2);
MgMnA(i+1,i+1) = 1*D31*(r*dr2+r*dr1-dr2^2+dr1^2);
MgMnA(i+1,i+2) = 1*D31*(-dr1^2-r*dr1);

MgMnM(i+1,i) = -1*D31*(dr2^2-r*dr2);
MgMnM(i+1,i+1) = -1*D31*(r*dr2+r*dr1-dr2^2+dr1^2);
MgMnM(i+1,i+2) = -1*D31*(-dr1^2-r*dr1);

MgFeA(i+1,i) = 1*D32*(dr2^2-r*dr2);
MgFeA(i+1,i+1) = 1*D32*(r*dr2+r*dr1-dr2^2+dr1^2);
MgFeA(i+1,i+2) = 1*D32*(-dr1^2-r*dr1);

MgFeM(i+1,i) = -1*D32*(dr2^2-r*dr2);
MgFeM(i+1,i+1) = -1*D32*(r*dr2+r*dr1-dr2^2+dr1^2);
MgFeM(i+1,i+2) = -1*D32*(-dr1^2-r*dr1);

MgMgA(i+1,i) = 1*D33*(dr2^2-r*dr2);
MgMgA(i+1,i+1) = 1+1*D33*(r*dr2+r*dr1-dr2^2+dr1^2);
MgMgA(i+1,i+2) = 1*D33*(-dr1^2-r*dr1);

MgMgM(i+1,i) = -1*D33*(dr2^2-r*dr2);
MgMgM(i+1,i+1) = 1-1*D33*(r*dr2+r*dr1-dr2^2+dr1^2);
MgMgM(i+1,i+2) = -1*D33*(-dr1^2-r*dr1);

end
%boundary conditions-----
MnMnA(1,1:2) = [1+3*DMnMn(1)*n -3*DMnMn(1)*n];
MnMnA(nr,nr-1:nr) = [-DMnMn(nr)*p 1+DMnMn(nr)*p];
MnMnM(1,1:2) = [1-3*DMnMn(1)*n 3*DMnMn(1)*n];
MnMnM(nr,nr-1:nr) = [DMnMn(nr)*p 1-DMnMn(nr)*p];

MnFeA(1,1:2) = [3*DMnFe(1)*n -3*DMnFe(1)*n];

```

```

MnFeA(nr,nr-1:nr) = [-DMnFe(nr)*p DMnFe(nr)*p];
MnFeM(1,1:2)      = [-3*DMnFe(1)*n 3*DMnFe(1)*n];
MnFeM(nr,nr-1:nr) = [DMnFe(nr)*p -DMnFe(nr)*p];

MnMgA(1,1:2)      = [3*DMnMg(1)*n -3*DMnMg(1)*n];
MnMgA(nr,nr-1:nr) = [-DMnMg(nr)*p DMnMg(nr)*p];
MnMgM(1,1:2)      = [-3*DMnMg(1)*n 3*DMnMg(1)*n];
MnMgM(nr,nr-1:nr) = [DMnMg(nr)*p -DMnMg(nr)*p];

FeMnA(1,1:2)      = [3*DFeMn(1)*n -3*DFeMn(1)*n];
FeMnA(nr,nr-1:nr) = [-DFeMn(nr)*p DFeMn(nr)*p];
FeMnM(1,1:2)      = [-3*DFeMn(1)*n 3*DFeMn(1)*n];
FeMnM(nr,nr-1:nr) = [DFeMn(nr)*p -DFeMn(nr)*p];

FeFeA(1,1:2)      = [1+3*DFeFe(1)*n -3*DFeFe(1)*n];
FeFeA(nr,nr-1:nr) = [-DFeFe(nr)*p 1+DFeFe(nr)*p];
FeFeM(1,1:2)      = [1-3*DFeFe(1)*n 3*DFeFe(1)*n];
FeFeM(nr,nr-1:nr) = [DFeFe(nr)*p 1-DFeFe(nr)*p];

FeMgA(1,1:2)      = [3*DFeMg(1)*n -3*DFeMg(1)*n];
FeMgA(nr,nr-1:nr) = [-DFeMg(nr)*p DFeMg(nr)*p];
FeMgM(1,1:2)      = [-3*DFeMg(1)*n 3*DFeMg(1)*n];
FeMgM(nr,nr-1:nr) = [DFeMg(nr)*p -DFeMg(nr)*p];

MgMnA(1,1:2)      = [3*DMgMn(1)*n -3*DMgMn(1)*n];
MgMnA(nr,nr-1:nr) = [-DMgMn(nr)*p DMgMn(nr)*p];
MgMnM(1,1:2)      = [-3*DMgMn(1)*n 3*DMgMn(1)*n];
MgMnM(nr,nr-1:nr) = [DMgMn(nr)*p -DMgMn(nr)*p];

MgFeA(1,1:2)      = [3*DMgFe(1)*n -3*DMgFe(1)*n];
MgFeA(nr,nr-1:nr) = [-DMgFe(nr)*p DMgFe(nr)*p];
MgFeM(1,1:2)      = [-3*DMgFe(1)*n 3*DMgFe(1)*n];
MgFeM(nr,nr-1:nr) = [DMgFe(nr)*p -DMgFe(nr)*p];

MgMgA(1,1:2)      = [1+3*DMgMg(1)*n -3*DMgMg(1)*n];
MgMgA(nr,nr-1:nr) = [-DMgMg(nr)*p 1+DMgMg(nr)*p];
MgMgM(1,1:2)      = [1-3*DMgMg(1)*n 3*DMgMg(1)*n];
MgMgM(nr,nr-1:nr) = [DMgMg(nr)*p 1-DMgMg(nr)*p];
%-----
A = sparse([MnMnA,MnFeA,MnMgA;FeMnA,FeFeA,FeMgA;MgMnA,MgFeA,MgMgA]);
M = sparse([MnMnM,MnFeM,MnMgM;FeMnM,FeFeM,FeMgM;MgMnM,MgFeM,MgMgM]);
%-----
end
% mass-balance-----
for i = 1:nr
    wMn2(i) = CV(i)*vr(i);
    wFe2(i) = CV(i+nr)*vr(i);

```

```
wMg2(i) = CV(i+2*nr)*vr(i);
wCa2(i) = CV(i+3*nr)*vr(i);
end
wMn2t = sum(wMn2);wFe2t = sum(wFe2);
wMg2t = sum(wMg2);wCa2t = sum(wCa2);
home
'Mn(final)-Mn(initial):',num2str(wMn2t-wMn1t),
'Fe(final)-Fe(initial):',num2str(wFe2t-wFe1t),
'Mg(final)-Mg(initial):',num2str(wMg2t-wMg1t),
'Ca(final)-Ca(initial):',num2str(wCa2t-wCa1t),
'total flux:',num2str((wMn2t+wFe2t+wMg2t+wCa2t)- ...
(wMn1t+wFe1t+wMg1t+wCa1t)),
toc
```


Appendix C

Appendix to Chapter 4

C.1 *P-T-t* paths A*, B, C, and A** used for garnet growth simulation

Table C.1 – *P-T-t* path A*.

T (°C)	P (bar)	t (My)
457.855	3883.035	0.000
535.395	3794.420	25.847
591.640	3712.592	44.595
595.308	3704.845	45.817
597.229	3704.845	46.458
598.976	3720.340	47.040
599.719	3784.672	47.288
598.474	3872.263	47.703
596.400	3901.460	48.394
592.667	3911.192	49.638
481.958	4053.478	86.541
451.219	4061.225	96.788
408.905	4058.442	150.000
474.265	6053.144	193.573
528.831	7550.000	194.119
570.288	8350.000	194.534
596.311	9623.377	194.794
607.493	10220.779	194.906
612.400	10360.000	194.955
618.213	10246.753	195.013
622.248	9909.091	195.053
623.458	9415.584	195.065
622.248	8766.234	195.078
619.827	8116.883	195.102
602.882	6870.130	195.271
402.450	3071.429	197.276

Table C.2 – *P-T-t* path B.

T (°C)	P (bar)	t (My)
457.855	3883.035	0.000
535.395	3794.420	25.847
641.640	3712.592	61.262
645.308	3704.845	62.484
647.229	3704.845	63.125
648.976	3720.340	63.707
649.719	3784.672	63.954
648.474	3872.263	64.369
646.400	3901.460	65.061
642.667	3911.192	66.305
481.958	4053.478	119.875
451.219	4061.225	130.121
408.905	4058.442	150.000
474.265	6053.144	193.573
528.831	7550.000	194.119
570.288	8350.000	194.534
596.311	9623.377	194.794
607.493	10220.779	194.906
612.400	10360.000	194.955
618.213	10246.753	195.013
622.248	9909.091	195.053
623.458	9415.584	195.065
622.248	8766.234	195.078
619.827	8116.883	195.102
602.882	6870.130	195.271
402.450	3071.429	197.276

Table C.3 – *P-T-t* path C.

T (°C)	P (bar)	t (My)
457.855	3883.035	0.000
535.395	3794.420	25.847
666.640	3712.592	69.595
670.308	3704.845	70.817
672.229	3704.845	71.458
673.976	3720.340	72.040
674.719	3784.672	72.288
673.474	3872.263	72.703
671.400	3901.460	73.394
667.667	3911.192	74.638
481.958	4053.478	136.541
451.219	4061.225	146.788
408.905	4058.442	150.000
474.265	6053.144	193.573
528.831	7550.000	194.119
570.288	8350.000	194.534
596.311	9623.377	194.794
607.493	10220.779	194.906
612.400	10360.000	194.955
618.213	10246.753	195.013
622.248	9909.091	195.053
623.458	9415.584	195.065
622.248	8766.234	195.078
619.827	8116.883	195.102
602.882	6870.130	195.271
402.450	3071.429	197.276

Table C.4 – *P-T-t* path A**.

T (°C)	P (bar)	t (My)
457.855	3883.035	0.000
535.395	3794.420	77.540
591.640	3712.592	133.785
595.308	3704.845	137.452
597.229	3704.845	139.374
598.976	3720.340	141.120
599.719	3784.672	141.863
598.474	3872.263	143.108
596.400	3901.460	145.182
592.667	3911.192	148.915
481.958	4053.478	149.706
451.219	4061.225	149.925
408.905	4058.442	150.000
474.265	6053.144	193.573
528.831	7550.000	194.119
570.288	8350.000	194.534
596.311	9623.377	194.794
607.493	10220.779	194.906
612.400	10360.000	194.955
618.213	10246.753	195.013
622.248	9909.091	195.053
623.458	9415.584	195.065
622.248	8766.234	195.078
619.827	8116.883	195.102
602.882	6870.130	195.271
402.450	3071.429	197.276

Bibliography

- Abart, R., Martinelli, W., 1991. Variszische und alpidische Entwicklungsgeschichte des Wölzer Kristallins (Steiermark, Österreich). *Mitteilungen der Gesellschaft der Geologie- und Bergbaustudenten in Österreich* 37, 1–14.
- Atherton, M. P., 1968. The variation in garnet, biotite, and chlorite composition in medium grade pelitic rocks from the Dalradian, Scotland, with particular reference to the zonation in garnet. *Contributions to Mineralogy and Petrology* 18, 347–361.
- Ayres, M., Vance, D., 1997. A comparative study of diffusion profiles in Himalayan and Dalradian garnets: constraints on diffusion data and the relative duration of the metamorphic events. *Contributions to Mineralogy and Petrology* 128, 66–80.
- Baldwin, J. A., Powell, R., Brown, M., Moraes, R., Fuck, R. A., 2005. Modelling of mineral equilibria in ultrahigh-temperature metamorphic rocks from the Anápolis-Itaçu Complex, central Brazil. *Journal of Metamorphic Geology* 23, 511–531.
- Berman, R. G., 1988. Internally-consistent thermodynamic data for minerals in the system $\text{Na}_2\text{O}-\text{K}_2\text{O}-\text{CaO}-\text{FeO}-\text{Fe}_2\text{O}_3-\text{Al}_2\text{O}_3-\text{SiO}_2-\text{TiO}_2-\text{H}_2\text{O}-\text{CO}_2$. *Journal of Petrology* 29, 445–552.
- Bernhard, F., Hoinkes, G., 1999. Polyphase micaschists of the central Wölzer Tauern, Styria, Austria. *Berichte der Deutschen Mineralogischen Gesellschaft, Beiheft zum European Journal of Mineralogy* 11, 32.
- Carlson, W. D., 1989. The significance of intergranular diffusion to the mechanism and kinetics of porphyroblast crystallization. *Contributions to Mineralogy and Petrology* 103, 1–24.
- Carlson, W. D., 1991. Competitive diffusion-controlled growth of porphyroblasts. *Mineralogical Magazine* 55, 317–330.

- Carlson, W. D., 2002. Scales of disequilibrium and rates of equilibration during metamorphism. *American Mineralogist* 87, 185–204.
- Cashman, K. V., Ferry, J. M., 1988. Crystal size distribution (CSD) in rocks and the kinetics and dynamics of crystallization. III. Metamorphic crystallization. *Contributions to Mineralogy and Petrology* 99, 401–415.
- Chakraborty, S., Ganguly, J., 1992. Cation diffusion in aluminosilicate garnets: experimental determination in spessartine-almandine diffusion couples, evaluation of effective binary, diffusion coefficients, and applications. *Contributions to Mineralogy and Petrology* 111, 74–86.
- Cherniak, D. J., Watson, E. B., Grove, M., Harrison, T. M., 2004. Pb diffusion in monazite: a combined RBS/SIMS study. *Geochimica et Cosmochimica Acta* 68, 829–840.
- Chernoff, C. B., Carlson, W. D., 1997. Disequilibrium for Ca during growth of pelitic garnet. *Journal of Metamorphic Geology* 15, 421–438.
- Christian, J. W., 1975. *The theory of transformations in metals and alloys: Part 1 - Equilibrium and general kinetic theory*. Pergamon Press, Oxford.
- Cocherie, A., Mezeme, E. B., Legendre, O., Fanning, C. M., Faure, M., Rossi, P., 2005. Electron-microprobe dating as a tool for determining the closure of Th-U-Pb systems in migmatic monazites. *American Mineralogist* 90, 607–618.
- Connolly, J. A. D., 1990. Multivariable phase diagrams: An algorithm based on generalized thermodynamics. *American Journal of Science* 290, 666–718.
- Connolly, J. A. D., 2005. Computation of phase equilibria by linear programming: A tool for geodynamic modeling and its application to subduction zone decarbonation. *Earth and Planetary Science Letters* 236, 524–541.
- Connolly, J. A. D., Cesare, B., 1993. C-O-H-S fluid composition and oxygen fugacity in graphitic metapelites. *Journal of Metamorphic Geology* 11, 368–378.
- Connolly, J. A. D., Petrini, K., 2002. An automated strategy for calculation of phase diagram sections and retrieval of rock properties as a function of physical conditions. *Journal of Metamorphic Geology* 20, 697–708.
- Crank, J., 1975. *The Mathematics of Diffusion*. Clarendon Press, Oxford.

- Crank, J., Nicolson, P., 1947. A practical method for numerical evaluation of solutions of partial differential equations of the heat-conduction type. *Proceedings of the Cambridge Philosophical Society* 43, 50–67.
- Cygan, R. T., Lasaga, A. C., 1982. Crystal growth and formation of chemical zoning in garnets. *Contributions to Mineralogy and Petrology* 79, 187–200.
- de Capitani, C., 1994. Gleichgewichts-Phasendiagramme: Theorie und Software. *Berichte der Deutschen Mineralogischen Gesellschaft, Beiheft zum European Journal of Mineralogy* 6, 48.
- de Capitani, C., Brown, T. H., 1987. The computation of chemical equilibrium in complex systems containing non-ideal solutions. *Geochimica et Cosmochimica Acta* 51, 2639–2652.
- Dohmen, R., Chakraborty, S., 2003. Mechanism and kinetics of element and isotopic exchange mediated by a fluid phase. *American Mineralogist* 88, 1251–1270.
- Evans, G., Blackledge, J., Yardley, P., 1999. Numerical methods for partial differential equations. Springer undergraduate mathematics series. Springer, London.
- Evans, T. P., 2004. A method for calculating effective bulk composition modification due to crystal fractionation in garnet-bearing schist: implications for isopleth thermobarometry. *Journal of Metamorphic Geology* 22, 547–557.
- Faryad, S. W., Chakraborty, S., 2005. Duration of Eo-Alpine metamorphic events obtained from multicomponent diffusion modeling of garnet: a case study from the Eastern Alps. *Contributions to Mineralogy and Petrology* 150, 306–318.
- Faryad, S. W., Hoinkes, G., 2003. *P-T* gradient of Eo-Alpine metamorphism within the Austroalpine basement units east of the Tauern Window (Austria). *Mineralogy and Petrology* 77, 129–159.
- Feenstra, A., 1996. An EMP and TEM - AEM study of margarite, muscovite and paragonite in polymetamorphic metabauxites of Naxos Cyclades (Greece) and the implications of fine-scale mica interlayering and multiple mica generations. *Journal of Petrology* 37, 201–233.
- Finger, F., Broska, I., Roberts, M. P., Schermaier, A., 1998. Replacement of primary monazite by apatite-allanite-epidote coronas in an amphibolite facies granite gneiss from the eastern Alps. *American Mineralogist* 83, 248–258.

- Florence, F. P., Spear, F. S., 1991. Effects of diffusional modification of garnet growth zoning on P - T path calculations. *Contributions to Mineralogy and Petrology* 107, 487–500.
- Florence, F. P., Spear, F. S., 1995. Intergranular diffusion kinetics of Fe and Mg during retrograde metamorphism of a pelitic gneiss from the Adirondack Mountains. *Earth and Planetary Science Letters* 134, 329–340.
- Frank, W., Esterlus, E., Frey, I., Jung, G., Krohe, A., Weber, J., 1982. Die Entwicklungsgeschichte von Stub- und Koralmkristallin und die Beziehung zum Grazer Paläozoikum. *Jb. Hochschulschwerpunkt S15*, 263–293.
- Franz, G., Hinrichsen, T., Wannemacher, E., 1977. Determination of the miscibility gap on the solid solution series paragonite-margarite by means of infrared spectroscopy. *Contributions to Mineralogy and Petrology* 59, 307–316.
- Froitzheim, N., Schmid, S. M., Frey, M., 1996. Mesozoic paleogeography and the timing of eclogite-facies metamorphism in the Alps: a working hypothesis. *Eclogae Geologicae Helvetiae* 89, 81–110.
- Gaidies, F., Abart, R., de Capitani, C., Schuster, R., Connolly, J. A. D., Reusser, E., 2006. Characterization of polymetamorphism in the Austroalpine basement east of the Tauern Window using garnet isopleth thermobarometry. *Journal of Metamorphic Geology* 24, 451–475.
- Gaidies, F., de Capitani, C., Abart, R., subm.a. THERIA_G: A software program to numerically model prograde garnet growth.
- Gaidies, F., de Capitani, C., Abart, R., Schuster, R., subm.b. Prograde garnet growth along complex P - T - t paths: Results from numerical experiments on polyphase garnet from the Wölz Complex (Austroalpine Basement).
- Gottschalk, M., 1997. Internally consistent thermodynamic data for rock-forming minerals in the system SiO_2 - TiO_2 - Al_2O_3 - CaO - MgO - FeO - K_2O - Na_2O - H_2O - CO_2 . *European Journal of Mineralogy* 9, 175–223.
- Griffen, D. T., 1981. Synthetic Fe/Zn staurolites and the ionic radius of $^{IV}\text{Zn}^{2+}$. *American Mineralogist* 66, 932–937.

- Habler, G., Thöni, M., 2001. Preservation of Permo-Triassic low-pressure assemblages in the Cretaceous high-pressure metamorphic Saualpe crystalline basement (Eastern Alps, Austria). *Journal of Metamorphic Geology* 19, 679–697.
- Hauzenberger, C. A., Robl, J., Stuwe, K., 2005. Garnet zoning in high pressure granulite-facies metapelites, Mozambique belt, SE-Kenya: constraints on the cooling history. *European Journal of Mineralogy* 17, 43–55.
- Hejl, E., 1984. Geochronologische und petrologische Beiträge zur Gesteinsmetamorphose der Schladminger Tauern. *Mitteilungen der Gesellschaft der Geologie- und Bergbaustudenten in Österreich* 30/31, 289–318.
- Hejl, E., 1998. Über die känozoische Abkühlung und Denudation der Zentralalpen östlich der Hohen Tauern - eine Apatit-Spaltspurenanalyse. *Mitteilungen der Österreichischen Geologischen Gesellschaft* 89, 179–199.
- Hoinkes, G., Koller, F., Rantisch, G., Dachs, E., Hoek, V., Neubauer, F., Schuster, R., 1999. Alpine metamorphism of the Eastern Alps. *Schweizerische Mineralogische und Petrographische Mitteilungen* 79, 155–181.
- Holland, T. J. B., Baker, J. M., Powell, R., 1998. Mixing properties and activity-composition relationships of chlorites in the system MgO-FeO-Al₂O₃-SiO₂-H₂O. *European Journal of Mineralogy* 10, 395–406.
- Holland, T. J. B., Powell, R., 1998. An internally consistent thermodynamic data set for phases of petrological interest. *Journal of Metamorphic Geology* 16, 309–343.
- Hollister, L. S., 1966. Garnet zoning: an interpretation based on the Rayleigh fractionation model. *Science* 154, 1647–1651.
- Inui, M., Toriumi, M., 2004. A theoretical study on the formation of growth zoning in garnet consuming chlorite. *Journal of Petrology* 45 (7), 1369–1392.
- Jercinovic, M. J., William, M. L., 2005. Analytical perils (and progress) in electron microprobe trace element analysis to geochronology: background acquisition, interferences, and beam irradiation effects. *American Mineralogist* 90, 526–546.

- Keller, L. M., Abart, R., Wirth, R., Schmid, D. W., Kunze, K., 2006. Enhanced mass transfer through short-circuit diffusion: Growth of garnet reaction rims at eclogite facies conditions. *American Mineralogist* 91, 1024–1038.
- Keller, L. M., Hauzenberger, C. A., Abart, R., 2007. Diffusion along interphase boundaries and its effect on retrograde zoning patterns of metamorphic minerals. *Contributions to Mineralogy and Petrology* (DOI 10.1007/s00410-007-0188-6).
- Kim, H. S., Bell, T. H., 2005. Combining compositional zoning and foliation intersection axes (FIAs) in garnet to quantitatively determine early *P-T-t* paths in multiply deformed and metamorphosed schists: north central Massachusetts, USA. *Contributions to Mineralogy and Petrology* 149, 141–163.
- Kleemann, U., Reinhardt, J., 1994. Garnet-biotite thermometry revisited: the effect of Al^{VI} and Ti in biotite. *European Journal of Mineralogy* 6, 925–941.
- Kohn, M. J., Malloy, M. A., 2004. Formation of monazite via prograde metamorphic reactions among common silicates: Implications for age determinations. *Geochimica et Cosmochimica Acta* 68, 101–113.
- Koroknai, B., Neubauer, F., Genser, J., Topa, D., 1999. Metamorphic and tectonic evolution of Austroalpine units at the western margin of the Gurktal nappe complex, Eastern Alps. *Schweizerische Mineralogische und Petrographische Mitteilungen* 79, 277–295.
- Koziol, A. M., Newton, R. C., 1988. Redetermination of the anorthite breakdown reaction and improvement of the plagioclase-garnet-Al₂SiO₅-quartz geobarometer. *American Mineralogist* 73, 216–223.
- Koziol, A. M., Newton, R. C., 1989. Grossular activity-composition relationships in ternary garnets determined by reversed displaced-equilibrium experiments. *Contributions to Mineralogy and Petrology* 103, 423–433.
- Krenn, E., Finger, F., 2004. Metamorphic formation of Sr-apatite and Sr-bearing monazite in a high-pressure rock from the Bohemian Massif. *American Mineralogist* 89, 1323–1329.
- Krenn, E., Finger, F., 2007. Formation of monazite and rhabdophane at the expense of allanite during Alpine low temperature retrogression of metapelitic basement rocks from Crete, Greece: Microprobe data and geochronological implications. *Lithos* 95, 130–147.

- Kretz, R., 1964. Analysis of equilibrium in garnet-biotite-sillimanite gneisses from Quebec. *Journal of Petrology* 5, 1–20.
- Kretz, R., 1966. Grain size distribution for certain metamorphic minerals in relation to nucleation and growth. *Journal of Geology* 75, 147–173.
- Kretz, R., 1974. Some models for the rate of crystallization of garnet in metamorphic rocks. *Lithos* 7, 123–131.
- Kretz, R., 1993. A garnet population in Yellowknife schist, Canada. *Journal of Metamorphic Geology* 11, 101–120.
- Lasaga, A. C., 1979. Multicomponent exchange and diffusion in silicates. *Geochimica et Cosmochimica Acta* 43, 455–469.
- Loomis, T., 1982. Numerical simulation of the disequilibrium growth of garnet in chlorite-bearing aluminous pelitic rocks. *Canadian Mineralogist* 20, 411–423.
- Loomis, T., Ganguly, J., Elphick, S., 1985. Experimental determinations of cation diffusivities in aluminosilicate garnets. II. Multicomponent simulation and tracer diffusion coefficients. *Contributions to Mineralogy and Petrology* 90, 45–51.
- Ludwig, K. R., 2001. Isoplot/Ex, Version 2.49e. A geochronological toolkit for Microsoft Excel. Berkeley Geochronological Center Special Publications 1a.
- Mahar, E. M., Baker, J. M., Powell, R., Holland, T. J. B., Howell, N., 1997. The effect of Mn on mineral stability in metapelites. *Journal of Metamorphic Geology* 15, 223–238.
- Mandl, G., 2000. The Alpine sector of the Tethyan shelf - Examples of Triassic to Jurassic sedimentation and deformation from the Northern Calcareous Alps. *Mitteilungen der Österreichischen Geologischen Gesellschaft* 92, 61–77.
- Menard, T., Spear, F. S., 1993. Metamorphism of calcic pelitic schists, Stafford Dome, Vermont: compositional zoning and reaction history. *Journal of Petrology* 34, 977–1005.
- Miller, C. L., Thöni, M., 1997. Eo-Alpine eclogitisation of Permian MORB-type gabbros in the Koralpe (Eastern Alps, Austria): new geochronological, geochemical and petrological data. *Chemical Geology* 137, 283–310.

- Miller, C. L., Thöni, M., Konzett, J., Kurz, W., Schuster, R., 2005. Eclogites from the Koralpe and Saualpe type-localities, Eastern Alps, Austria. *Mitteilungen der Österreichischen Mineralogischen Gesellschaft* 150, 227–263.
- Montel, J.-M., Foret, S., Veschambre, M., Nicollet, C., Provost, A., 1996. Electron microprobe dating of monazite. *Chemical Geology* 131, 37–53.
- Montel, J.-M., Kornprobst, J., Vielzeuf, D., 2000. Preservation of old U-Th-Pb ages in shielded monazite: example from the Beni Bousera Hercynian kinzigites (Morocco). *Journal of Metamorphic Geology* 18, 335–342.
- Newton, R. C., Charlu, T. V., Kleppa, O. J., 1980. Thermochemistry of the high structural state plagioclases. *Geochimica et Cosmochimica Acta* 44, 933–941.
- Onsager, L., 1945. Theories and problems of liquid diffusion. *Annals of the New York Academy of Sciences* 46, 241–265.
- Oxburgh, E. R., 1992. Heterogeneous lithospheric stretching in the early history of orogenic belts. In: Hsü, K. (Ed.), *Mountain building processes*. Academic Press, London, pp. 85–93.
- Parrish, R. R., 1990. U-Pb dating of monazite and its application to geological problems. *Canadian Journal of Earth Sciences* 27, 1431–1450.
- Powell, R., Holland, T. J. B., 1993. An internally consistent dataset with uncertainties and correlations: 3. Applications to geobarometry, worked examples and a computer program. *Journal of Metamorphic Geology* 6, 173–204.
- Powell, R., Holland, T. J. B., 1999. Relating formulations of the thermodynamics of mineral solid solutions: Activity modeling of pyroxenes, amphiboles, and micas. *American Mineralogist* 84, 1–14.
- Proyer, A., Dachs, E., 2000. Contrasting parageneses in mica schists of the Hohe Tauern, caused by manganese and zinc. *Mineralogy and Petrology* 69, 197–212.
- Schmid, S. M., Fügenschuh, B., Kissling, E., Schuster, R., 2004. Tectonic map and overall architecture of the Alpine orogen. *Eclogae Geologicae Helvetiae* 97, 93–117.
- Schuster, R., Frank, W., 1999. Metamorphic evolution of the Austroalpine units east of the Tauern Window: indications for Jurassic strike slip tectonics. *Mitteilungen der Gesellschaft der Geologie- und Bergbaustudenten in Österreich* 42, 37–58.

- Schuster, R., Koller, F., Hoeck, V., Hoinkes, G., Bousquet, R., 2004. Explanatory notes to the map: Metamorphic structure of the Alps - Metamorphic evolution of the Eastern Alps. *Mitteilungen der Österreichischen Mineralogischen Gesellschaft* 149, 175–199.
- Schuster, R., Scharbert, S., Abart, R., Frank, W., 2001. Permo-Triassic extension and related HT/LP metamorphism in the Austroalpine - Southalpine realm. *Mitteilungen der Gesellschaft der Geologie- und Bergbaustudenten in Österreich* 45, 111–141.
- Schuster, R., Thöni, M., 1996. Permian garnets: indication for a regional Permian metamorphism in the southern part of the Austroalpine basement units. *Mitteilungen der Gesellschaft der Geologie- und Bergbaustudenten in Österreich* 141, 219–221.
- Shaw, D. M., 1956. Geochemistry of pelitic rocks. Part III: Major elements and general geochemistry. *Geological Society of America Bulletin* 67, 919–934.
- Smith, H. A., Barreiro, B., 1990. Monazite U-Pb dating of staurolite grade metamorphism in pelitic schists. *Contributions to Mineralogy and Petrology* 105, 602–615.
- Smith, H. A., Giletti, B. J., 1997. Lead diffusion in monazite. *Geochimica et Cosmochimica Acta* 61, 1047–1055.
- Sölva, H., Thöni, M., Grasemann, B., Linner, M., 2001. Emplacement of Eo-Alpine high-pressure rocks in the Austroalpine Ötztal complex (Texel group, Italy/Austria). *Geochimica et Cosmochimica Acta* 14, 345–360.
- Spear, F. S., 1988. Metamorphic fractional crystallization and internal metasomatism by diffusional homogenization of zoned garnets. *Contributions to Mineralogy and Petrology* 99, 507–517.
- Spear, F. S., 1993. *Metamorphic Phase Equilibria and Pressure-Temperature-Time Paths*. Mineralogical Society of America Monograph. Mineralogical Society of America, Washington, D.C.
- Spear, F. S., Daniel, C. G., 1998. Three-dimensional imaging of garnet porphyroblast sizes and chemical zoning: nucleation and growth history in the garnet zone. *Geological Materials Research* 1, 1–44.
- Spear, F. S., Daniel, C. G., 2001. Diffusion control of garnet growth, Harpswell Neck, Maine, USA. *Journal of Metamorphic Geology* 19, 179–195.

- Spear, F. S., Florence, F. P., 1992. Thermobarometry in granulites: pitfalls and new approaches. *Precambrian Research* 55, 209–241.
- Spear, F. S., Kohn, M. J., Florence, F. P., Menard, T., 1991a. A model for garnet and plagioclase growth in pelitic schists: implications for thermobarometry and *P-T* path determinations. *Journal of Metamorphic Geology* 8, 683–696.
- Spear, F. S., Peacock, S. M., Kohn, M. J., Florence, F. P., Menard, T., 1991b. Computer programs for petrologic *P-T-t* path calculations. *American Mineralogist* 76, 2009–2012.
- Spear, F. S., Pyle, J. M., 2002. Apatite, monazite, and xenotime in metamorphic rocks. *Reviews in Mineralogy and Geochemistry* 48, 293–335.
- Stowell, H. H., Menard, T., Ridgway, C. K., 1996. Ca-metasomatism and chemical zonation of garnet in contact-metamorphic aureoles, Juneau Gold Belt, southern Alaska. *Canadian Mineralogist* 34, 1195–1209.
- Stowell, H. H., Taylor, D. L., Tinkham, D. L., Goldberg, S. A., Ouderkirk, K. A., 2001. Contact metamorphic *P-T-t* paths from Sm-Nd garnet ages, phase equilibria modelling and thermobarometry: garnet ledge, south-eastern Alaska, USA. *Journal of Metamorphic Geology* 19, 645–660.
- Suzuki, K., Adachi, M., Tanaka, T., 1991. Middle Precambrian provenance of Jurassic sandstone in the Mino Terrane, central Japan: Th-U-total Pb evidence from an electron microprobe monazite study. *Sedimentary Geology* 75, 141–147.
- Symmes, G. H., Ferry, J. M., 1991. Evidence from mineral assemblages for infiltration of pelitic schists by aqueous fluids during metamorphism. *Contributions to Mineralogy and Petrology* 108, 419–438.
- Thompson, J. B., 1957. The graphical analysis of mineral assemblages in pelitic schists. *American Mineralogist* 42, 842–858.
- Thöni, M., 2002. Sm-Nd isotope systematics in garnet from different lithologies (Eastern Alps): age results, and an evaluation of potential problems for garnet Sm-Nd chronometry. *Chemical Geology* 185, 255–281.
- Thöni, M., 2006. Dating eclogite-facies metamorphism in the Eastern Alps - approaches, results, interpretations: a review. *Mineralogy and Petrology* 88, 123–148.

- Thöni, M., Miller, C. L., 2000. Permo-Triassic pegmatites in the eo-Alpine eclogite-facies Koralpe complex, Austria: age and magma source constraints from mineral chemical, Rb-Sr and Sm-Nd isotope data. *Schweizerische Mineralogische und Petrographische Mitteilungen* 80, 169–186.
- Tollmann, A., 1977. *Geologie von Österreich. Band 1.* Deuticke, Wien.
- Tollmann, A., 1985. *Geologie von Österreich. Band 2. Ausserzentralalpiner Anteil.* Deuticke, Wien.
- Tomkins, H. S., Pattison, D., 2007. Accessory phase petrogenesis in relation to major phase assemblages in pelites from the Nelson contact aureole, southern British Columbia. *Journal of Metamorphic Geology* 25, 401–421.
- Tracy, R. J., Robinson, P., Thompson, A. B., 1976. Garnet composition and zoning in the determination of temperature and pressure of metamorphism, central Massachusetts. *American Mineralogist* 61, 762–775.
- Vance, D., Holland, T., 1993. A detailed isotopic and petrological study of a single garnet from the Gassetts Schist, Vermont. *Contributions to Mineralogy and Petrology* 114, 101–118.
- Vance, D., Mahar, E., 1998. Pressure-temperature paths from *P-T* pseudosections and zoned garnets: potential, limitations and examples from the Zaskar Himalaya, NW India. *Contributions to Mineralogy and Petrology* 132, 225–245.
- Vielzeuf, D., Baronnet, A., Perchuk, A. L., Laporte, D., Baker, M. B., 2007. Calcium diffusivity in alumino-silicate garnets: an experimental and ATEM study. *Contributions to Mineralogy and Petrology* DOI 10.1007/s00410-007-0184-x.
- Wei, C. J., Powell, R., 2003. Phase relations in high-pressure metapelites in the system KF-MASH (K_2O -FeO-MgO- Al_2O_3 - SiO_2 - H_2O) with application to natural rocks. *Contributions to Mineralogy and Petrology* 145, 301–315.
- White, R. W., Powell, R., Holland, H. D., Worley, B., 2000. The effect of TiO_2 and Fe_2O_3 on metapelitic assemblages at greenschist and amphibolite facies conditions: mineral equilibria calculations in the system K_2O -FeO-MgO- Al_2O_3 - SiO_2 - H_2O - TiO_2 - Fe_2O_3 . *Journal of Metamorphic Geology* 18, 497–511.

- White, R. W., Powell, R., Phillips, G. N., 2003. A mineral equilibria study of the hydrothermal alteration in mafic greenschist facies rocks at Kalgoorlie, Western Australia. *Journal of Metamorphic Geology* 21, 455–468.
- Wing, B. A., Ferry, J. M., Harrison, T. M., 2003. Prograde destruction and formation of monazite and allanite during contact and regional metamorphism of pelites: petrology and geochronology. *Contributions to Mineralogy and Petrology* 145, 228–250.
- Yang, P., Pattison, D., 2006. Genesis of monazite and Y zoning in garnet from the Black Hills, South Dakota. *Lithos* 88, 233–253.
- Zeh, A., 2001. Inference of a detailed P - T path from P - T pseudosections using metapelitic rocks of variable composition from a single outcrop, Shackleton Rang, Antarctica. *Journal of Metamorphic Geology* 19, 329–350.
- Zeh, A., 2006. Calculation of garnet fractionation in metamorphic rocks, with application to a flat-top, Y-rich garnet population from the Ruhla Crystalline Complex, Central Germany. *Journal of Petrology* 47, 2335–2356.
- Zeh, A., Holness, M. B., 2003. The effect of reaction overstep on garnet microtextures in metapelitic rocks on the Ilesha Schist Belt, SW Nigeria. *Journal of Petrology* 44, 967–994.
- Zeh, A., Klemd, R., Buhlmann, S., Barton, J. M., 2004. Pro- and retrograde P - T evolution of granulites from the Beit Bridge Complex (Limpopo Belt, South Africa): constraints from quantitative phase diagrams and geotectonic implications. *Journal of Metamorphic Geology* 22, 79–95.

CURRICULUM VITAE

Prepared June 11, 2007

Fred Gaidies

Born 29. Dec. 1975, Rostock, Germany
German citizen
Two children

Professional Address:

Department of Geosciences
Institute of Mineralogy and Petrography
University of Basel
Bernoullistrasse 30
CH-4056 Basel, Switzerland
phone: 4056 061 267 3628
fred.gaidies@unibas.ch

Home Address:

Schlesienstrasse 3
D-79395 Neuenburg, Germany
phone: 0049 179 128 4205

Education:

2003 – present	PhD	Geosciences, University of Basel, Switzerland
1996 – 2003	Diploma	Geosciences, TU Berlin and GFZ Potsdam, Germany
1994	High School Exam	Jugenddorf-Christophorusschule, Rostock, Germany

Employment:

2003 – 2006 Assistant for XRF at the Institute of Mineralogy and Petrography, University of Basel, Switzerland.

1998 – 2001 Student assistant in Sedimentology and Quaternary Geology (Prof. J. H. Schroeder) and Historical Geology and Palaeontology (Prof. Dr. B. D. Erdtmann) at the Technical University of Berlin, Germany.

2000 – 2001 Student assistant at GASAG, Gas Works of Berlin Inc., Germany.

1999 Student assistant at Arcturus Mine, Independence Gold Mining, Arcturus, Zimbabwe.

Courses Taught:

2003 – 2006 Various teaching assistance at the Department of Geosciences, University of Basel on XRF – analysis.